University of Tasmania

FINAL RESEARCH REPORT

AUGUST 1988

CONTROLS ON GOLD AND SILVER GRADES IN VOLCANOGENIC SULPHIDE DEPOSITS

(AMIRA PROJECT 84/P210)

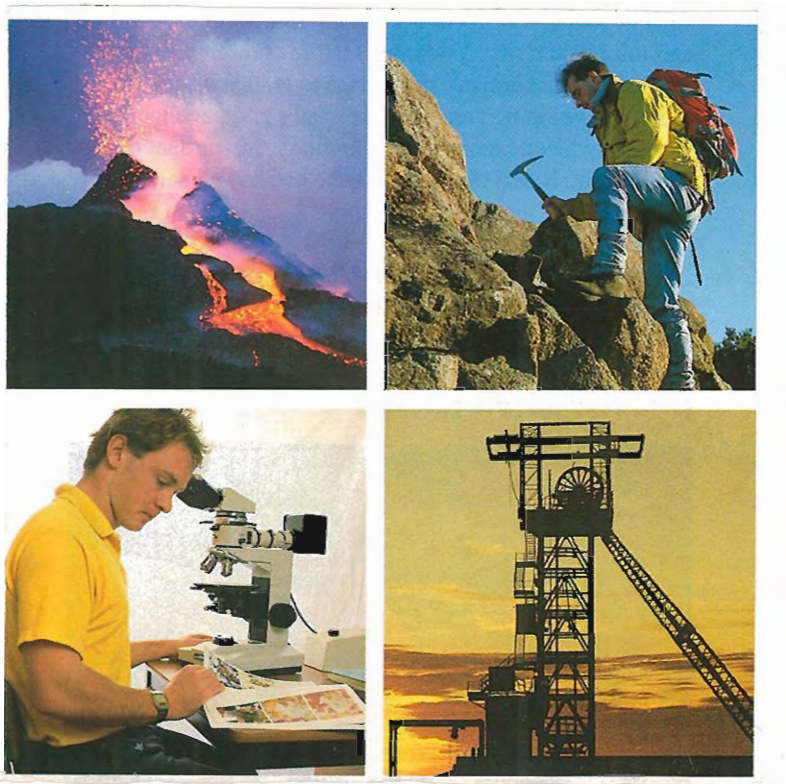

The critical chain of events : **Volcanic Processes, Exploration and Research...** lead to **New Mining Ventures**

CONTENTS

ATTENDANCE LIST FOR FINAL RESEARCH MEETING

24TH AUGUST, 1988

UNIVERSITY COUNCIL ROOM

Aberfoyle Limited	E. Dronseika D. Jack R. Paterson D. Wallace
The Broken Hill Proprietary Co. Limited	A. Wilde
Billiton Australia	D. Hall
BP Minerals Australia	C. Laughton
Department of Mines/Tasmania	R. Bottrill K. Corbett D. Duncan G. Green R. Hargreaves J. Pemberton J. Taheri M. Vicary
EZ/NBH	Geoff Iliff Ian Mathison
Pancontinental Mining Limited	K. Airas M. Jones
Placer	P. Ellis
RGC Exploration	J. Angus L. Newnham
AMIRA	J.D. Bailey
University of Tasmania	Sharon Adrichem David Archer Tony Crawford Greg Jenkins David Huston Ross Large Joe Stolz Khin Zaw

INTRODUCTION

Restatement of Aims

To investigate the geological and geochemical controls on the distribution of precious metals within volcanic hosted massive sulphide deposits, with the objective of developing exploration models useful for the discovery of further precious metal-rich deposits.

Progress 1985-1988

'This is the fourth and final report on the results of this research project. Our progress and results this year have been very satisfying and I can confidently report that we have achieved the aims and objectives outlined in our original proposal at the commencement of this project in 1985. During the three years of this research program we have made major advances in our understanding of the controls on precious metals in volcanogenic hydrothermal systems, which have application in the future exploration and mining of volcanogenic gold, silver and base metal deposits.

In particular, the following has been achieved:

1. Detailed documentation of the geology, mineralogy and zonation of precious metals within a number of Australian massive sulphide deposits (Rosebery, Que River and Hercules in Tasmania, Balcooma and Mt. Chalmers in Queensland, and Scuddles and Teutonic Bore in Western Australia) has led to the recognition of two major gold associations; the Au-Zn (-Pb-Ag-ba) association and the Au-Cu association. Compilation of a tonnage-grade data base for similar precious metal-rich volcanogenic deposits in Japan and the Canadian Archean has confirmed these two associations.

2. Research into the chemistry of gold transport and deposition has led to the development of a geologic-thermodynamic model which can account for (and predict) the concentration and location of gold within volcanogenic systems under a variety of hydrothermal solution conditions. This model has major implications for gold transport and deposition in other geological environments (eg. epithermal or porphyry systems).

3. Geochemical studies of the Cambrian volcanics which comprise the Mt. Read Volcanic archave increased our understanding of the volcanic processes involved, their relationship to the tectonic setting and the interplay between volcanic processes, hydrothermal processes, alteration and mineralisation.

4. Research into the primary gold content of the Cambrian volcanics and sediments of western Tasmania has identified the probable source rocks for gold. This work has significant exploration implications.

5. A series of exploration models for gold-bearing volcanogenic deposits have been developed which facilitate the transfer of research technology developed in this program to mining company sponsors.

Acknowledgements

I would like to thank the sponsors to this AMIRA project for their continued financial support and encouragement; Aberfoyle, Billiton, B.H.P., B.P., C.E.C., C.S.R., E.Z./North B.H., Goldfields Exploration, Pancontinental and Tasmanian Department of Mines.

Those company geologists who provided access and assistance in our study of their deposits and prospects are particularly thanked; David Wallace, Rod Patterson and Ed Dronseika (Aberfoyle), David Hall (Billiton), Chris Laughton (B.P.), Peter Legge, Geoff Iliff, Terry Lees (E.Z.), Bob Hall, Ken Harvey (C.E.C.) and John Angus, Fergus Fitzgerald, Paul Roberts (Goldfields). Assistance provided throughout the project by Jeff Bailey from AMIRA is also gratefully appreciated.

Fruitful discussions and liaison with a number of Mines Department personnel, particularly Keith Corbett, Geoff Green, Tony Brown and David Duncan have contributed significantly to this project.

My special thanks go to the present and past members of the AMIRA research team at the University of Tasmania; Sharon Adrichem, Stewart Capp, Tony Crawford, Ian Gordon, Steven Hunns, David Huston, Greg Jenkins, Peter McGoldrick, John Pemberton, Peter Ruxton, Joe Stolz and Khin Zaw, all of whom contributed to make this a very successful research project. Important contributions by support staff in the Geology Department, including Phil Robinson who runs our analytical lab, Simon Stevens in the thin and polished section lab and Karyl Whelan and Julie Beattie in the secretarial section are greatly appreciated. June Pongratz deserves special acknowledgement for her expertise at drafting and the quality presentation and layout of this report.

Ross Large,

Project Leader.

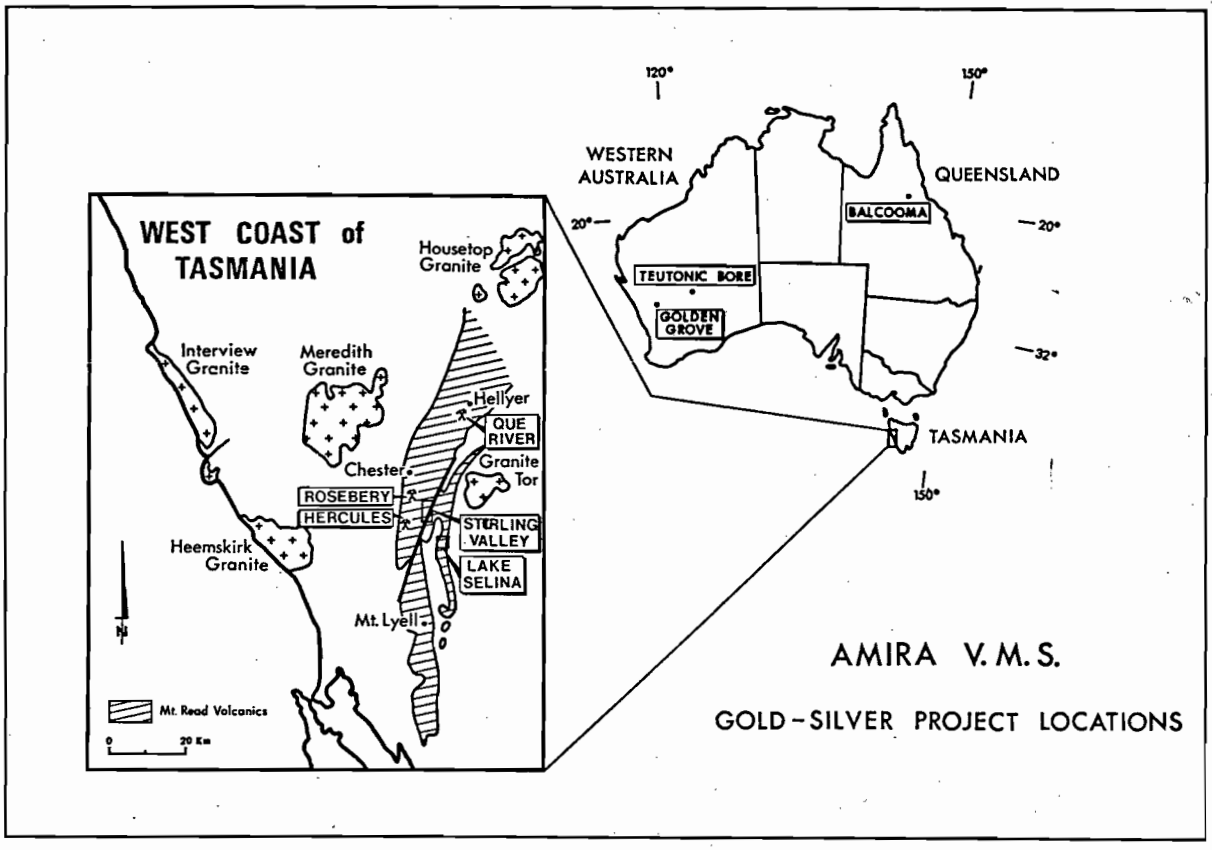
WEST COAST of TASMANIA
Housetop Granite
Interview Granite
Meredith Granite
Hellyer
QUE RIVER
Granite Tor
Chester
ROSEBERY
HERCULES
STERLING VALLEY
LAKE SELINA
Heemskirk Granite
Mt. Lyell
Mt. Read Volcanics
0 20 Km
120°
150°
WESTERN AUSTRALIA
QUEENSLAND
BALCOOMA
20°
TEUTONIC BORE
GOLDEN GROVE
32°
TASMANIA
150°
AMIRA V.M.S.
GOLD-SILVER PROJECT LOCATIONS

TABLE 1 : Tonnage - grade data for Australian VMS deposits.

DEPOSITS	AGE	M.TONNES	Cu %	Pb %	Zn %	Ag ppm	Au ppm
WESTERN TASMANIA							
•ROSEBERY	Cambrian	19.4	0.74	5	16.2	155	2.9
•HERCULES	"	2.6	0.42	5.2	16.7	159	2.7
•QUE RIVER - PQ Lens	"	2.1	0.45	9.2	16.2	241	4.4
- P North	"	0.4	0.43	6.5	10.8	189	2.9
- S Lens	"	0.6	1.5	2.2	6	63	0.3
•HELLYER	"	19	0.4	7	13	160	2.3
Mt.LYELL - The Blow	"	5.6	1.3	N.R.	N.R.	61	2
- West Lyell	"	58.3	0.72	0.01	0.04	2	0.24
- Prince Lyell	"	17.4	1.2	0.01	0.04	3	0.38
- North Lyell	"	4.8	5.3	N.R.	N.R.	33	0.39
WESTERN AUSTRALIA							
•GOSSAN HILL - Cu	Archean	15	3.4	0.05	0.1	14	0.1
- Zn	"	1.7	0.4	1.6	14	87	2.2
•SCUDDLES - Massive ore	"	18.6	0.81	0.68	9.5	78	1.2
- Stringer	"	7.5	2.1	0.1	0.6	12	0.3
•TEUTONIC BORE - Massive ore	"	1.4	4.2	1.2	16.4	203	0.2
- Stringer	"	0.75	2.4	0.1	1.9	52	0.2
KOONGIE PARK	L. Proterozoic	1	2	1	11	10	N.R.
QUEENSLAND							
THALANGA	Cambrian	7.5	3	3	9	83	0.52
LIONTOWN	"	2	1	2	10	100	2
Mt.MORGAN	Devonian	50	0.72	0.05	0.1	6	4.75
CONJUBOY	Palaeozoic	1	1.5	4	8	50	0.5
•BALCOOMA - Cu	L. Palaeozoic	3.5	3	N.R.	N.R.	N.R.	N.R.
- Zn	"	0.5	0.6	5.3	11.3	64	0.4
•Mt.CHALMERS - Massive ore	L. Permian	3.2	1.8	0.1	0.7	11	1.8
- West lode	"	0.4	1.7	1	3.5	42	3
N.S.W.							
WOODLAWN - Complex ore	Silurian	6.3	1.7	5.5	14.4	89	N.R
- Stockwork ore	"	3.7	1.9				
CAPTAINS FLAT	"	4.2	0.7	6	10	56	1.7
VICTORIA							
BENAMBRA - Wilga	Silurian	4.6	3.6	N.R.	5.8	32.2	N.R.
- Currawong	"	9.5	1.6	0.9	4.3	38	1.3

• - Deposits being studied in this AMIRA Project.

N.R. - No reliable data available.

SUMMARY OF RESEARCH FINDINGS

Gold in F(J) Lens of Rosebery, J(K)-P Lens of Hercules and the South Hercs Deposit, Tasmania

Khin Zaw

At depth in the southern end of the Rosebery mine, the Cambrian Pb-Zn massive sulphide lenses (FJ lens) have been replaced by pyrrhotite-pyrite ± magnetite ± tourmaline assemblages due to fluids emanating from a Devonian granite. Pyrrhotite-pyrite zones in the F(J) lens carry high gold grades (up to 29 g/t Au), whereas the magnetite and tourmaline rich zones carry low gold (<5 g/t). The Devonian metasomatism has led to recrystallization of the primary Cambrian gold, resulting in a significant increase in average gold and electrum grain sizes. Preliminary fluid inclusion studies indicate that the Devonian replacement fluids were CO_2-bearing brines. Studies on the FeS content of sphalerite have provided information on the depth of mineralisation and the fS_2 conditions during gold mineralisation.

The Hercules J(K)-P lens is a highly deformed massive sulphide which contains significant gold mineralisation (>5 g/t) in the hangingwall Pb-Zn zone, with subordinate gold in the footwall disseminated to massive pyrite-chalcopyrite zone. The South Hercs deposit, which lies 1 km along strike from the Hercules VMS, is a carbonate altered disseminated to semi-massive sulphide deposit containing high gold and silver but low base metals (2.1 g/t Au, 139 g/t Ag and 4.6% Zn + Pb). Small massive sulphide lenses and related siliceous stringer and disseminated zones contain erratic gold grades, however the best gold (>10 g/t) is largely confined to a massive colloform pyrite ± barite zone at the top of the ore lens. Zones of later carbonate alteration cut across the ore zones but are devoid of gold, silver or base metals.

Paragenesis and Fluid Inclusions in the Que River Footwall Precious Metal Zone, Tasmania

Greg Jenkins

Gold and silver enrichment occurs in the footwall of the PQ massive sulphide lens adjacent to the major sulphide stringer zone. The Au-Ag zone is related to minor lead-zinc mineralisation and low temperature K-feldspar (adularia) alteration, silicification and late stage sericite. Preliminary studies indicate that the paragenetic sequence of the zone is

1. early sphalerite-galena-tetrahedrite-pyrite
2. sphalerite-Kfeldspar (white alteration)
3. pyrite-quartz veins
4. carbonate-barite cavity fill.

Two generations of fluid inclusions have been recognised in quartz from stage 3. The majority of inclusions are secondary in origin and probably related to Devonian deformation. Studies on the primary inclusions will proceed over the next six months, and should provide evidence on the chemical process involved in the formation of the footwall precious metal zone.

Sulphur Isotope Studies at Que River

Peter McGoldrick

Sulphur isotope data from Que River indicate that the end-member (most primitive) mineralising fluid had a d34S value of about +5 ‰. A fluid with this signature could evolve directly by cooling a magmatic fluid formed in equilibrium with a melt having $\delta^{34}S$ of ~0‰. Alternatively, if heated (250-350°C) seawater leached magmatic sulphides and small amounts of seawater-derived anhydrite from intermediate volcanics a fluid with $\delta^{34}S$ of ~+5 would be produced.

The heavy S in many samples from the stringer zone at Que River indicates the $\delta^{34}S$ fluid became much heavier as the primitive fluid moved through the stringer zone. Seawater S was the source of this heavy S and by the time barite was precipitating fluid $\delta^{34}S$ may have approximated Cambrian seawater $\delta^{34}S$ (+30 ‰).

Final Report - Balcooma Prospect - Northern Queensland

David Huston

In the Balcooma deposit, gold has a strong association with copper in both copper-rich and zinc-lead-rich massive sulphide. In copper-rich mineralisation gold also has a strong association with bismuth. Mineralogically, gold occurs as 1-10 μm electrum grains in association with chalcopyrite, bismuth minerals and galena. The low gold grades at Balcooma are attributable to either: (1) an intermediate pH of the mineralising fluids at or near the switchover from gold thio-complexes to gold chloro-complexes, or (2) low oxygen fugacity of the mineralising fluids.

Silver occurs as a trace element (~140 ppm) in chalcopyrite in copper-rich mineralisation while it occurs as a trace element in galena (~1200 ppm) in zinc-lead mineralisation.

Gold Fineness in Volcanogenic Massive Sulphide Deposits

David Huston and Khin Zaw

Studies on undeformed massive sulphide deposits indicate
a) gold occurs as electrum principally in association with chalcopyrite in Cu-Au zones.
b) gold occurs locked in arsenopyrite or pyrite in massive Zn-Pb-Ag zones of zinc-rich ores.
c) gold occurs as electrum in association with other sulphides in baritic zones overlying zinc-rich ores.

Moderate deformation associated with moderate strain rates at low temperature may expel gold from the host mineral and deposit it as coarse electrum associated with base metal sulphides. At high metamorphic grades, diffusion will control the growth of electrum. As the size of an electrum grain will be controlled by the amount of gold available in the region of diffusion surrounding the growing grain, the grade of the ore may also control grain growth. Deposits of higher gold grade should have coarser electrum given similar post-depositional deformation and metamorphism. This same argument may also be applied to undeformed deposits of the copper-gold association where the grain size of electrum should be controlled by the amount of gold in the mineralising fluid.

In practical terms, gold recoveries should be higher in deposits of the copper-gold association. Baritic ores may have better recoveries than sphalerite-galena-pyrite ores in undeformed deposits of the zinc-lead-silver-gold association. Deformation of moderate strain rates will produce better recoveries. In deformed and metamorphosed ores, deposits of higher grade should have higher recoveries than deposits of lower grade.

The Source of Gold in the Western Tasmania VMS Deposit

Joe Stolz and Ross Large

The primary unaltered calcalkaline andesite, dacite and rhyolite volcanics in the Mt. Read Volcanics average between 0.9 and 1.3 ppb gold, which is comparable with the gold contents of modern volcanics of similar composition. However, the high-Ti basalts of the Crimson Creek Formation are anomalously enriched in gold containing up to 23 ppb. These flood basalts, which are the products of early Cambrian rifting, probably underlie the Mt. Read Volcanics and represent a possible source for gold, which has been leached and concentrated in the VMS deposits in the middle to late Cambrian.

The closely comparable Au abundances in the Mount Read Volcanics and modern volcanics of similar composition, together with strong positive correlations between Au and platinum group element (Pd, Pt) concentrations for the basaltic rocks suggests that there has been little loss or redistribution of Au from the volcanics during Devonian greenschist facies metamorphism.

The anomalous gold in the Crimson Creek basalts also indicates the potential for shear-related lode Au mineralisation within or at the margins of the Crimson Creek equivalent lava sequences. Likely exploration targets include the extensive early Cambrian basalt-andesite sequences south of Macquarie Harbour (the Mainwaring Group) and in the Smithton Trough (Smithton Basalts).

Gold Distribution and Genesis in Australian Volcanogenic Massive Sulphide Deposits, and Significance for Gold Transport Models

Ross Large, David Huston, Peter McGoldrick, Peter Ruxton and Garry McArthur

Volcanogenic massive sulfide deposits in Australia exhibit a range in average gold content from 0.2 ppm to 4.75 ppm Au, with an overall mean of 1.6 ppm. The Mount Morgan Cu-Au deposit in Eastern Queensland had been the major producer (237.5 tonnes of Au), followed by the deposits in the Mt. Read Volcanics of Western Tasmania (Rosebery, Hercules, Que River, Hellyer and Mt. Lyell) which together have a pre-mining resource of 156.3 tonnes of Au.

Two distinct spacial and mineralogical associations of gold mineralisation have been defined for the Eastern Australian VMS deposits.

1. A gold-zinc association (with lead, silver and barite) which typically occurs throughout the massive and layered ores with gold and barite concentrated toward the stratigraphic hanging wall of the deposit.
2. A gold-copper association which typically occurs in the footwall stringer and lower massive zones of some deposits, particularly those with a high Cu/Zn ratio.

This bipartite gold association observed in the Eastern Australian deposits is also displayed in other VMS provinces, such as the Kuroko district (Japan) and the Canadian Archean.

Thermodynamic studies on the controls of gold transport and deposition indicate that the two gold associations described above may relate directly to the gold transporting mechanism. The footwall gold-copper association reflects gold transport as the $AuCl_2^-$ complex by high temperature (>300°C), low pH (<4.5) moderate to high fO_2 and high salinity fluids (>seawater). The hanging wall gold-zinc association reflects gold transport as the $Au(HS)_2^-$ complex by lower temperature (200-250°C), moderate pH (4.5-6) and moderate fO_2 fluids. A process of gold refining, where cooling hydrothermal solutions leach gold (plus zinc and lead) from the lower parts of the sulfide body and reprecipitate the gold at the top of the body, associated with dropping temperature and increasing SO_4/H_2S ratio, is proposed as the mechanism which leads to gold enrichment at the top of zinc-rich deposits. This process is common in barite-rich Palaeozoic deposits but rare in Archean deposits, due to lower SO_4/H_2S fluid ratios in the latter.

By analogy with massive sulfides, other deposits which exhibit a gold-copper association, such as porphyry related gold-copper ores, acid-sulfate epithermal deposits, and Proterozoic magnetite-gold deposits, are considered to form by the transport and deposition of gold from chloride complexes.

Exploration Implications of the Chemical Model for Gold Deposition in Volcanogenic Massive Sulphide Systems

David Huston

An understanding of the processes that control the transport and deposition of gold in volcanogenic massive sulfide deposits helps in defining targets within the systems that form the deposit. Chemical modelling indicates that pH and temperature are the primary controls on gold grades in these systems. Extreme pH either alkaline (>5) or acid (<4) in the depositing hydrothermal fluids promotes the formation of gold-rich massive sulfide deposits. Conversely, fluids of intermediate pH (4-5) will produce deposits of intermediate or low gold tenor. Temperature has a lesser affect on the potential gold grades, but it affects the likely association and possibly the metallurgical recovery of the gold. Gold-rich deposits of the copper-gold association form from higher temperature fluids (>300°C) of low pH, while gold-rich deposits of the zinc-lead-silver-gold association form from low temperature fluids (<300°C) of high pH. Conditions that may promote extreme pH's in the fluids include unusual lithologies in the footwall leaching zone or a magmatic input into the mineralising system.

Due to differences in the mechanism of precipitation, gold and base metals do not necessarily precipitate together. Because of this characteristic, the following environments may produce gold-rich deposits in volcanogenic systems external to the massive sulfide: (1) epigenetic mineralization near the base of the footwall leaching zone where gold complexing switches over from a chloro-complex to a thio-complex, (2) the very edges of footwall alteration zones in porous rocks where seawater in the rocks interacts with upwelling hydrothermal fluids, (3) pyritic cherts at the top or along the edges of the massive sulfide mound, and (4) exhalative cherts associated with Archean massive sulfides external to the ore-forming environment.

Exploration Models for Gold-bearing Deposits in the Mount Read Volcanics, Western Tasmania

Ross Large

Five distinct styles of gold mineralisation have been defined within submarine volcanic settings such as the Mt. Read Volcanics (MRV).

- sea floor Zn-Au (Pb-Ag-Cu-Ba) polymetallic massive sulphides (eg. Rosebery, Que River, Hellyer)
- sea floor Cu-Au massive sulphides and associated stockworks (eg. Mt. Chalmers)
- Footwall Au-base metal-adularia veins and disseminated stockwork systems (eg. Que River PMZ)
- Deep level Cu-Au-pyrite-chlorite disseminated and stockwork zones (eg. Mt. Lyell)
- magnetite-hematite-pyrite ± Cu ± Au vein replacement systems associated with granitic intrusives (eg. Jukes Pty., Lake Selina).

The key factors contributing to the gold-zinc-silver-rich nature of deposits in the Mt. Read Volcanics are considered to be:

- *Tectonic Environment* - the Central Volcanic Complex (CVC) has developed as a series of coalescing volcanic centres along a narrow rift structure. High heat flow associated with rifting developed long-lived convective hydrothermal systems.
- *Source Rocks* - the Cambrian volcanics represent an adequate source for gold and base metals. Anomously high gold values in the Crimson Creek high-Ti basalts (stratigraphically below the CVC) may have been a significant factor.
- *Chemistry of fluids* - the hydrothermal fluids were buffered by the volcanics to allow maximum transport of gold and base metal complexes. Switchover of gold transport from $AuCl_2^-$ to $Au(HS)_2^-$ within the developing sulphide mounds provided a mechanism for gold-zinc refining and upgrading of the outer and upper zones of the orebodies.

Many of the volcanic centres in the CVC show a bimodal suite with mineralisation concentrated at the contact between one suite and the other (eg. rhyolite-dacite, andesite-dacite or andesite-basalt contacts). The Tyndal Group represents a graben fill sequence of epiclastics and volcanics overlying the CVC. Significant mineralisation (eg. Henty Prospect) is concentrated along the conformable or faulted contact between the Tyndal Group and the CVC. Intrusion of Cambrian granites and granitic porphyries along the eastern margin of the Mount Read Volcanics was probably the final phase of magmatic activity in the Cambrian. A complex series of alteration zones are related to the granitic intrusives (pink K-feldspar-hematite → chlorite-magnetite → pyrite-sericite) which are outlined by a semi-continuous belt of magnetic anomalies extending from Mt. Darwin to the Murchison Gorge. Minor Au-Cu prospects are located within some of the magnetic zones.

Post-deformation, Late Devonian gold mineralisation associated with granite emplacement is confined along the Henty Fault and other major faults. Evidence to date suggests the possibility of an early phase of Cambrian mineralisation focused along the Henty Fault (when it acted as one of the major rift faults) followed by a later overprint of Devonian mineralisation related to granite intrusion.

GOLD IN F(J) LENS OF ROSEBERY, J(K)-P LENS OF HERCULES AND THE SOUTH HERCS DEPOSIT: INTERPLAY OF CAMBRIAN AND DEVONIAN MINERALISATION

Khin Zaw

INTRODUCTION

In this report, the precious metal distribution and zonation within F(J) lens of the Rosebery south-end orebodies, J(K)-P lens of the Hercules mine and the recently discovered South Hercs deposit will be presented. Textural and geochemical characteristics of Au mineralogy and associated sulphide assembalges will also be reported together with the results of a preliminary fluid inclusion study.

SUMMARY AND CONCLUSIONS

1. The F(J) lens of Rosebery, J(K)-P lens of Hercules and the South Hercs deposit show distinct mineral zonation. Gold (up to 29 g/t) occurs in the pyrrhotite-pyrite zone of the F(J) lens of Rosebery where Fe-S-O replacement of Devonian origin is superimposed on the primary sulphide lenses of Cambrian age.

2. At the J(K)-P lens of Hercules, a highly deformed massive sulphide deposit of Cambrian age, contains significant gold mineralisation (>5 g/t) in the hangingwall sphalerite-galena ± pyrite zone with a subordinate concentration of gold (about 3 g/t) in the footwall disseminated to massive pyrite-chalcopyrite zone.

3. The South Hercs deposit which lies 1 km along strike from the Hercules deposit, is a carbonate altered disseminated to semi-massive sulphide deposit with gold (>10 g/t) mostly confined to the colloform pyrite ± barite zone at the top of the ore lens.

4. Sphalerite geobarometer studies on the F(J) lens at Rosebery indicate that Devonian replacement mineralisation occurred at an estimated depth of 8.0 ± 0.5 km. Initial investigation indicates that FeS mole % in sphalerites and Au grades at the north-end (A and B lens) of Rosebery give a sympathetic relation suggesting gold transport and deposition by $Au(HS)_2^-$ complexes in the Cambrian exhalative lenses. However, no clear trend was recorded in the F(J) lens of Devonian origin at the south-end of Rosebery.

5. Preliminary fluid inclusion studies demonstrate that the hydrothermal fluid associated with the Devonian replacement zone was a CO_2-bearing brine which was expelled from the Devonian granitoid intrusion below the Rosebery orebody. The presence of Cambrian exhalative fluids have yet to be recognised in fluid inclusions.

BACKGROUND

Both Rosebery and Hercules deposits are classic examples of deformed stratiform polymetallic massive sulphide deposits of volcanogenic type (e. g. Green *et al.*, 1981; Lees *et al.*, 1988 in press). A trangressive zone of biotite-magnetite-pyrrhotite-tourmaline assemblages of Devonian origin replacing the Cambrian sulphide lenses was recently reported at the south-end of Rosebery mine (Solomon *et al.*, 1987; Khin Zaw, 1987a). The South Hercs deposit lies a kilometer south along strike from the Hercules massive sulphide deposit and is regarded as a sulphide impregnated Au/Ag deposit.

METHOD

The author worked at the Rosebery mine site from December 1986 to February 1987 on the F(J) lens of Rosebery and from February 1988 to April 1988 studying the Hercules and south Hercs deposits. Mineralogical zonation and ore metal distribution (Zn, Cu, Ag, Au and Fe) was investigated at the mine-site by plotting the geological information and assay data along the diamond drill holes using the "Prime" computer and "Surpac" software system. Representative DDH samples were collected with particular emphasis on the Au distribution and later detailed mineragraphic studies and microprobe analyses were carried out.

GEOLOGICAL RELATIONSHIPS

F(J) Lens of Rosebery Mine

A comprehensive account of geological setting of the Rosebery deposit has been given by recent workers (e.g. Brathwaite, 1974; Green *et al.*, 1981; Lees *et al.*, 1988 in press) and will not be repeated here. A trangressive zone of Fe-S-O replacement assemblages of Devonian origin superimposed on the primary sulphide lenses of Cambrian age was documented at the south-end of Rosebery mine (Solomon *et al.*, 1987; Khin Zaw, 1987a). Detailed gelogical setting, textural and geochemical characteristics of the replacement assemblages were reported in the last AMIRA report (Khin Zaw, 1987a).

J(K)-P Lens of Hercules Mine

The geology and mineralisation of the Hercules mine area have previously been discussed by Hall *et al.* (1965) and Burton (1975) and very recently by Lees (1987) and Lees *et al.*, (1988 in press). The stratigraphic sequence is similar to Rosebery, the significant difference being a coarse, silicified volcanic breccia immediately underlying most of the host rocks. Folding in the Hercules mine area has produced open folds with steeply east-dipping axial plane cleavage and the ore lenses are oriented parallel to this cleavage.

The Hercules orebody consists of numerous small lenses in the order of 100m x 100m x 10m which are generally joined at some point to a neighbouring lens. The ore lenses contain a variety of textures from massive high grade ore to spotty ore, the latter is composed of porphyroblastic sulphides, comprising porphyroblasts or streaks of sphalerite of up to 10 mm across, rimmed by firstly galena with minor chalcopyrite, then a sericite or chlorite selvage (Lees, 1987).

South Hercs Deposit

The South Hercs deposit is a stringery to disseminated, sulphide impregnated Au/Ag zone located just south of old Hercules mine (Fig. 1). As it is a newly discovered deposit which will be mined in near future, a brief account of the deposit history and geology will be reported below.

Previous Investigation

Although base and precious metal mineralisation was noted by early prospectors in the south Hercs area, no particular exploration efforts were attempted until 1945. Electrolytic Zinc Company acquired the mining leases in the area in 1920, and drilled a series of holes near the Au-rich M lode, one of the southernmost Pb-Zn lenses of the old Hercules mine workings, but no further work was continued. Diamond drilling was resumed in 1973-74 and several holes drilled in 1974 intersected the stringery Pb-Zn and minor Au/Ag mineralisation.

The recent increase in precious metal prices led to renewed exploration activity at the South Hercs area in the early 1980's. Drilling up to June 1987 gave probable ore reserves of 700,000 tonnes grading 1.7% Pb, 2.9% Zn, 0.1% Cu, 139 g/t Ag and 2.11 g/t Au (Geoff Illiff, pers. comm., 1988).

Geological setting

The general geology of the south Hercs deposit was briefly given by Lees (1988). The stratigraphic sequence of the south Hercs area is essentially similar to that of the Hercules mine area as it is the southern extension of the same mineralised horizon. The footwall of the deposit consists of a variety of strongly altered, tuffaceous rocks ranging from fine-grained tuff to silicified volcanic lithic breccia.

The host rock is also essentially similar to that of the Rosebery and Hercules Mines and consists of grey, fine-grained, siliceous, tuffaceous rocks varying to sericitic feldspar phyric tuff. The hangingwall rock immediately overlying the host rock contains a significant sedimentary component of grey shales, poorly bedded siltstones and lithic wackes. The shale dominated sequence is followed by massive epiclastics of dacitic to andesitic composition.

The cleavage/bedding relationships at the south Hercs deposit give a distinct discontinuity. The bedding in the sediments strikes 010° dipping 45°-50°E whereas cleavage varies between strikes of 170° and 005° and invariably dips steeper than the bedding at 65°-70°E. A fault zone has been observed in the footwall of the northern part of the deposit (5700-5800mN) comprising a shear zone often with pug zones and/or quartz veins. Its strike is parallel to the stratigraphy. South of the main deposit, the host rocks and sediments are offset about 100 m to the west by an apparent cross fault. An E-W shearing component was also recognised by recent structural mapping in the south Hercs area by Aerden (per. comm., 1988).

Mineralisation and alteration

The mineralisation at the South Hercs depsits is essentially composed of stringer to semi-massive base metal sulphides with subordinate Au/Ag grades. Thin lenses to semi-massive sphalerite-galena±pyrite occurs in the silicified host rock with or without stringers and disseminated sulphide. This zone has variable Au/Ag distribution and forms a blanket followed above by massive pyrite±barite with significantly higher Au

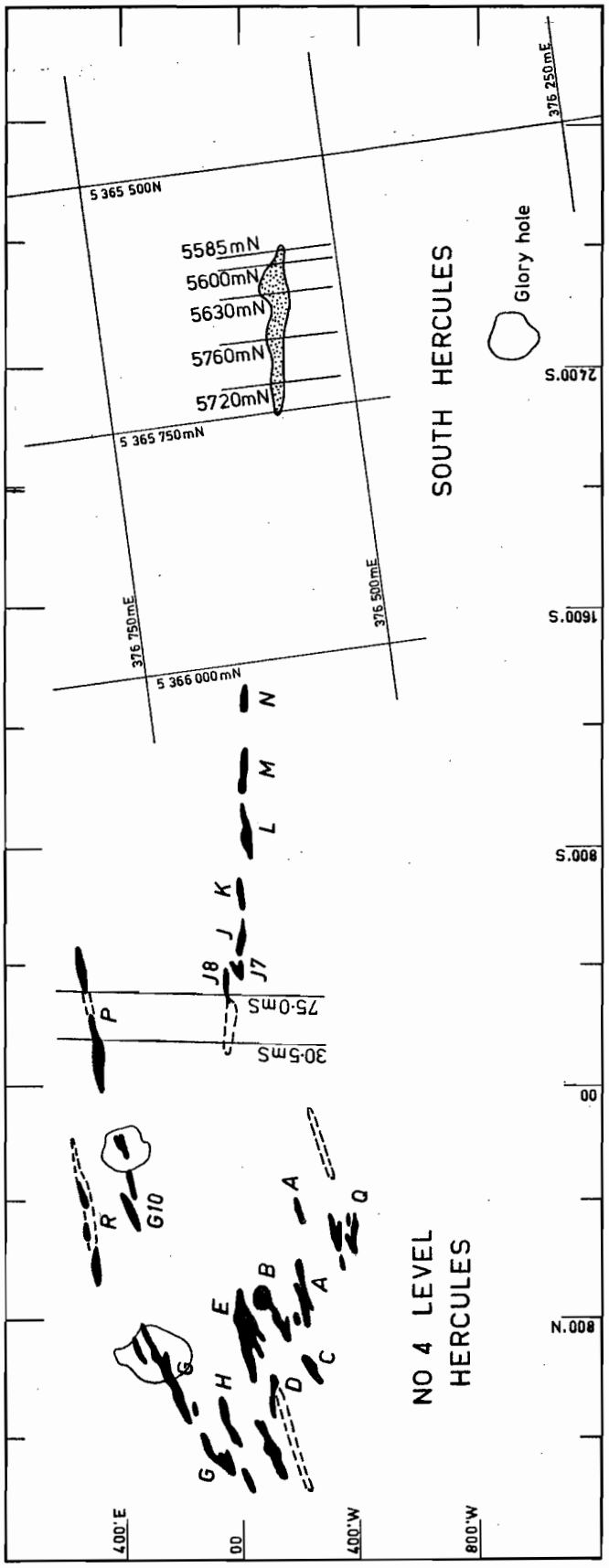

Fig. 1. Map showing location of Hercules ore lenses together with South Hercs deposit. The dashed outlines of the ore lenses indicate projection to the No. 4 Level of the Hercules mine.

grades. Irregular and patchy quartz-pink carbonate veins with coarse-grained, recrystallised, yellowish sphalerite and galena are observed in the ore zone and these veins may contain thin networks of tetrahedrite veinlets with elevated Ag values (e. g. H1142 @ 38.5 m, 5600mN). Sometimes Ag values may attain 2000 g/t.

The above mineralisation is associated with a spectacular pervasive carbonate alteration assemblage ranging from bleby and cherty to massive carbonates (see below). Other major alteration types are silicification and quartz-sericite alteration in the footwall volcanic tuff and breccia. Intense quartz-sericite alteration results in a quartz schist texture in the footwall volcanics.

ORE MINERAL ZONATION

Zonation at F(J) lens of Rosebery Mine

In the last AMIRA report, Khin Zaw (1987a) described the spatial and zonal distribution of Fe-S-O assemblages of Devonian origin superimposed on the primary Cambrian exhalative sulphide lenses at F(J) lens and documented the three different replacement zones:

3. Tourmaline-quartz±magnetite zone
2. Pyrrhotite-pyrite zone and
1. Magnetite (hematite)-biotite±chalcopyrite zone

Figures 2-4 show E-W cross-sections (270mS, 280mS, and 300mS) for geology and mineralogical zonation of the F(J) lens with contoured Au distribution in Figs. 5-7.

The magnetite (hematite)-biotite zone is mostly confined to the lower levels of the mine particularly below 17 levels. Magnetite extensively replaces massive pyrite lenses and magnetite itself occurs as massive bodies where replacement was complete. Hematite is also noted in association with magnetite and in places hematite alone is found replacing pyrite. In the footwall, chlorite is alterted to biotite and recrystallised chalcopyrite is present in high concentration. Unusual replacement assemblages such as garnet-biotite-helvite-tourmaline are also present in this zone. Thin quartz-carbonate-fluorite veins of up to 3cm across are also noted cutting the magnetite-biotite assemblages.

A massive pyrrhotite-pyrite zone replacing the primary sphalerite and galena sulphide lenses is also well exposed in the F(J) lens between 16 and 17 Levels. It varies from pyrrhotite-dominant to pyrite-dominant (Solomon *et al.*, 1987) with or without tourmaline and magnetite. The tourmaline-quartz zone occurs enveloping and immediately lying above the massive pyrrhotite-pyrite bodies and cross-cuts the host rocks and other sulphide lenses. Patches of pyrrhotite, pyrite and magnetite (hematite) with chlorite, fluorite and carbonate are also found in association with tourmaline-quartz assemblages.

Zonation at J(K)-P lens of Hercules Mine

No Devonian granitoid-related Fe-S-O replacement assemblages were recognised at the Hercules mine but the ore zone appears to have been strongly affected by Devonian metamorphism as evidenced by the porphyroblastic texture of the ore. The ore lenses are zoned as in the case of primary syngenetic lenses of the Rosebery deposits as described by Huston and Large (1988 in press) for A and B lens of the north-end of the Rosebery deposit.

Figures 8 shows mineralogical zonation of the J(K) and P lenses on section 34.80mS between 15 and 16 levels at Hercules and Au distribution is contoured in Fig. 9. As in the case of the Rosebery deposit, the following zonation can be recognised at the Hercules mine:

4. Carbonate±barite zone
3. Spotty sphalerite-galena±pyrite zone
2. Massive sphalerite-galena±pyrite zone
1. Massive to disseminated pyrite zone (with up to 4 % chalcopyrite)

Massive to disseminated pyrite zone with chalcopyrite forms at the base of the lenses and is followed by a massive to spotty sphalerite-galena±pyrite zone and then gives way to a carbonate±barite zone at the top of the lenses. The only difference from Rosebery is the spotty and porphyroblastic nature of the ore assemblages in the primary Pb-Zn sulphide horizon at Hercules suggesting more deformation and metamorphism than the Rosebery ores.

Zonation at South Hercs Deposit

Figures 10-11 show mineralogical zonation of the south Hercs deposit on E-W cross-sections (5600mN, 5630mN, 5700mN) and gold distribution is shown in Figs. 12-13. Mineralogical zonation at the south Hercs deposit can be essentially classified into two major types by carbonate alteration and stringer to semi-massive mineralisation. Three different sub-zones for each major type can be divided as below:

I. Carbonate altered zone (no gold or silver)

3. Bleby carbonate sub-zone
2. Massive carbonate sub-zone
1. Cherty carbonate sub-zone

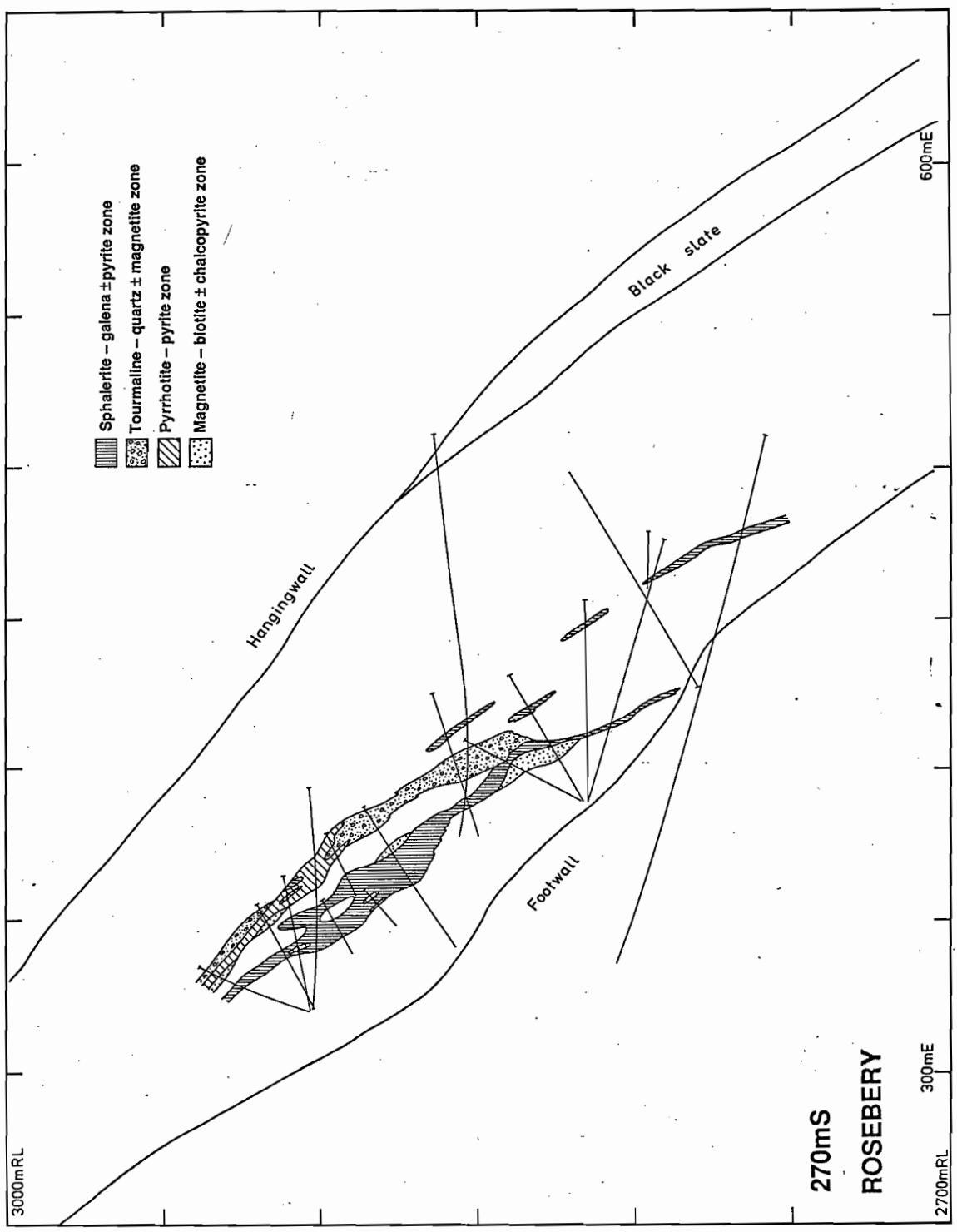

Fig. 2 Geology and mineral zonation of 270mS section, F(J) lens of the south-end of Rosebery.

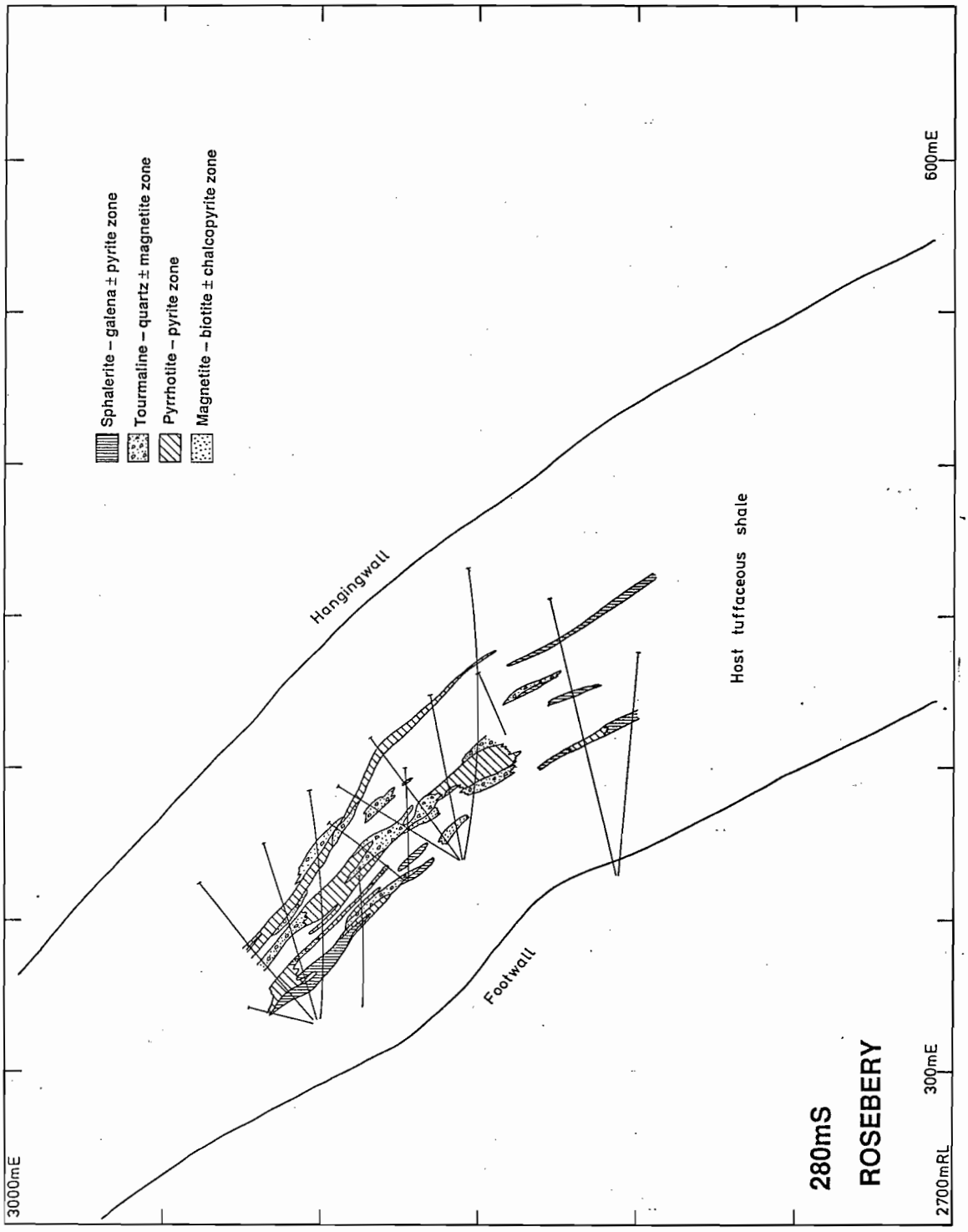

Fig. 3 Geology and mineral zonation of 280mS section, F(J) lens of the south-end of Rosebery.

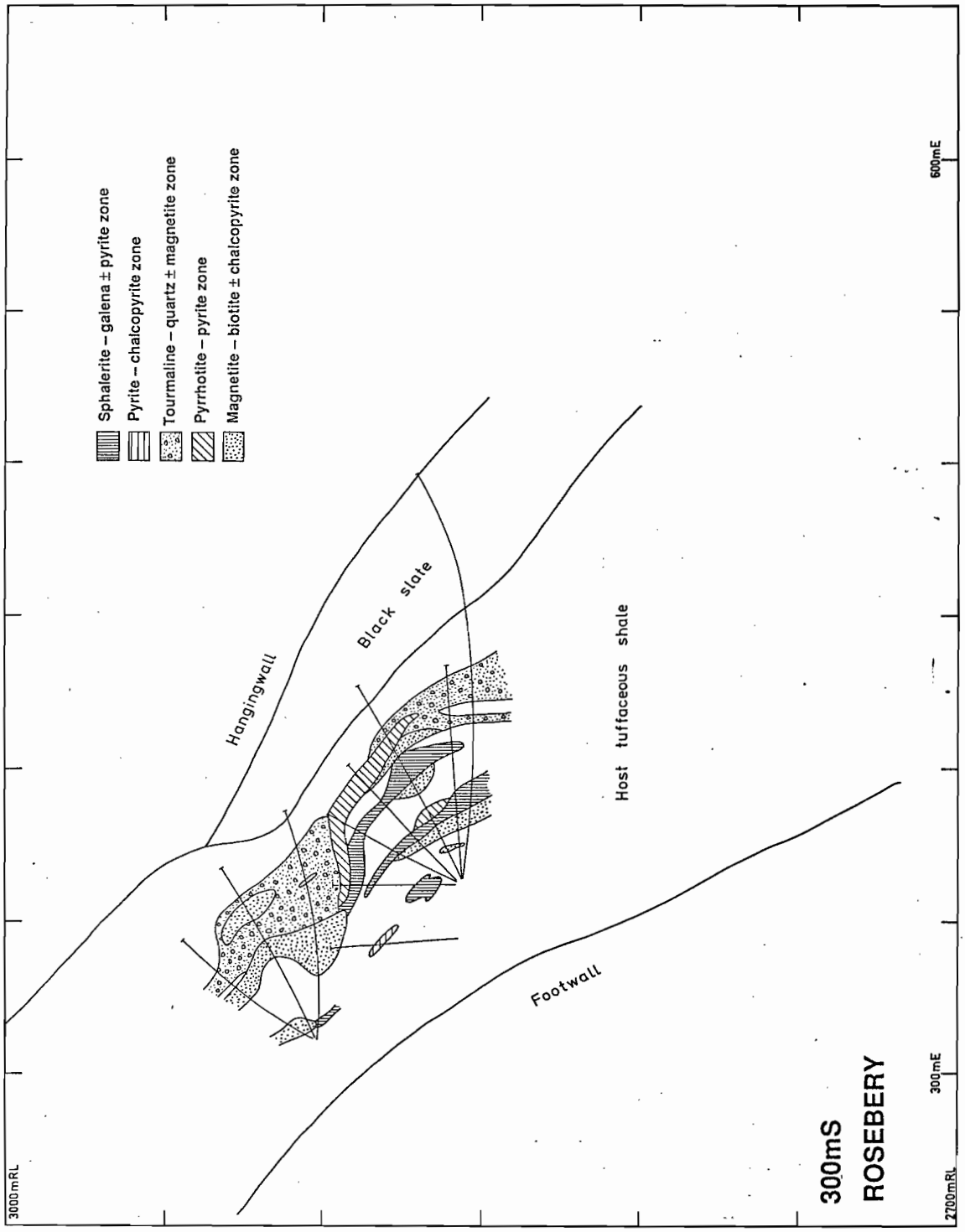

Fig. 4 Geology and mineral zonation of 300mS section, F(J) lens of the south-end of Rosebery.

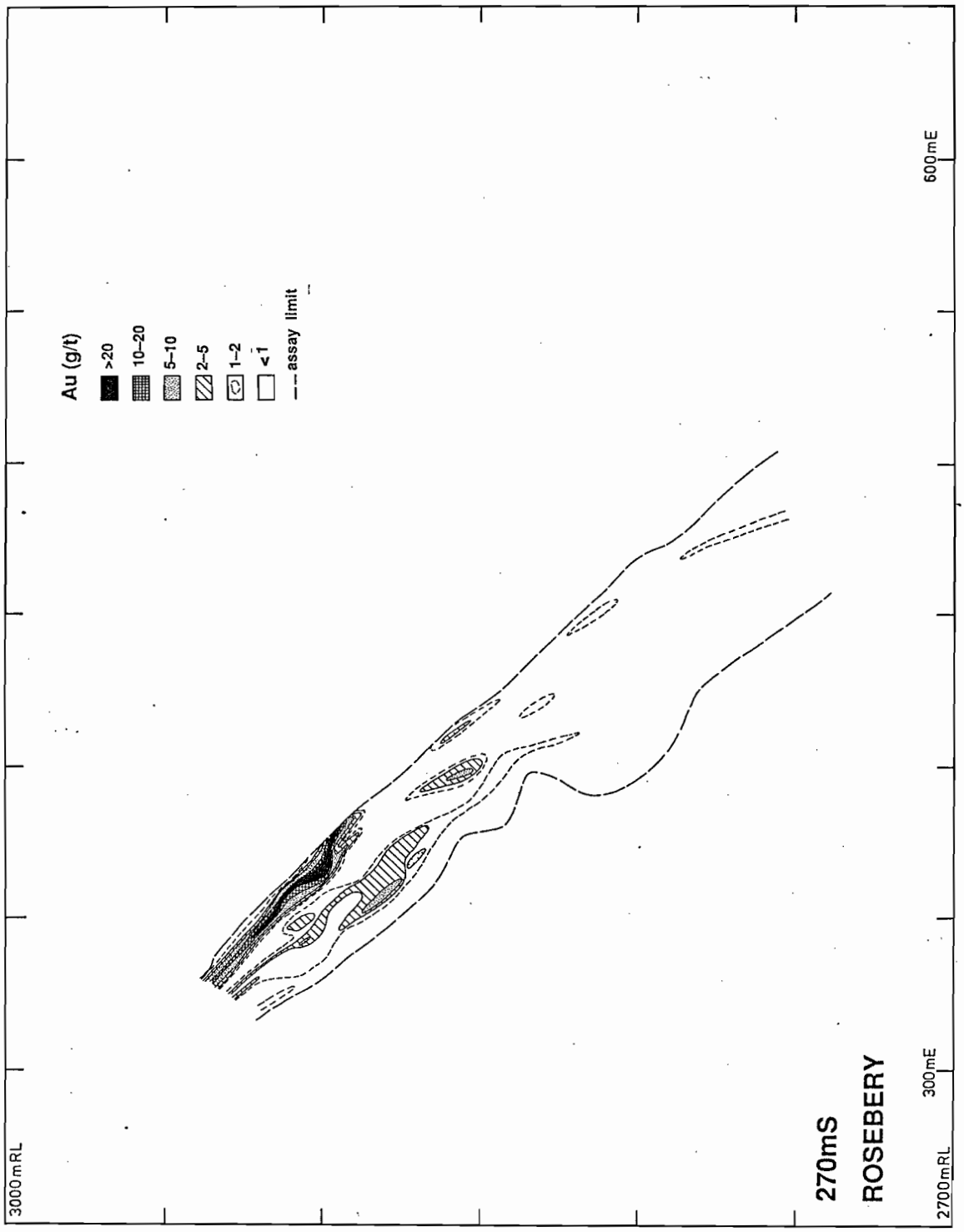

Fig. 5 Distribution of gold on 270mS section, F(J) lens of the south-end of Rosebery.

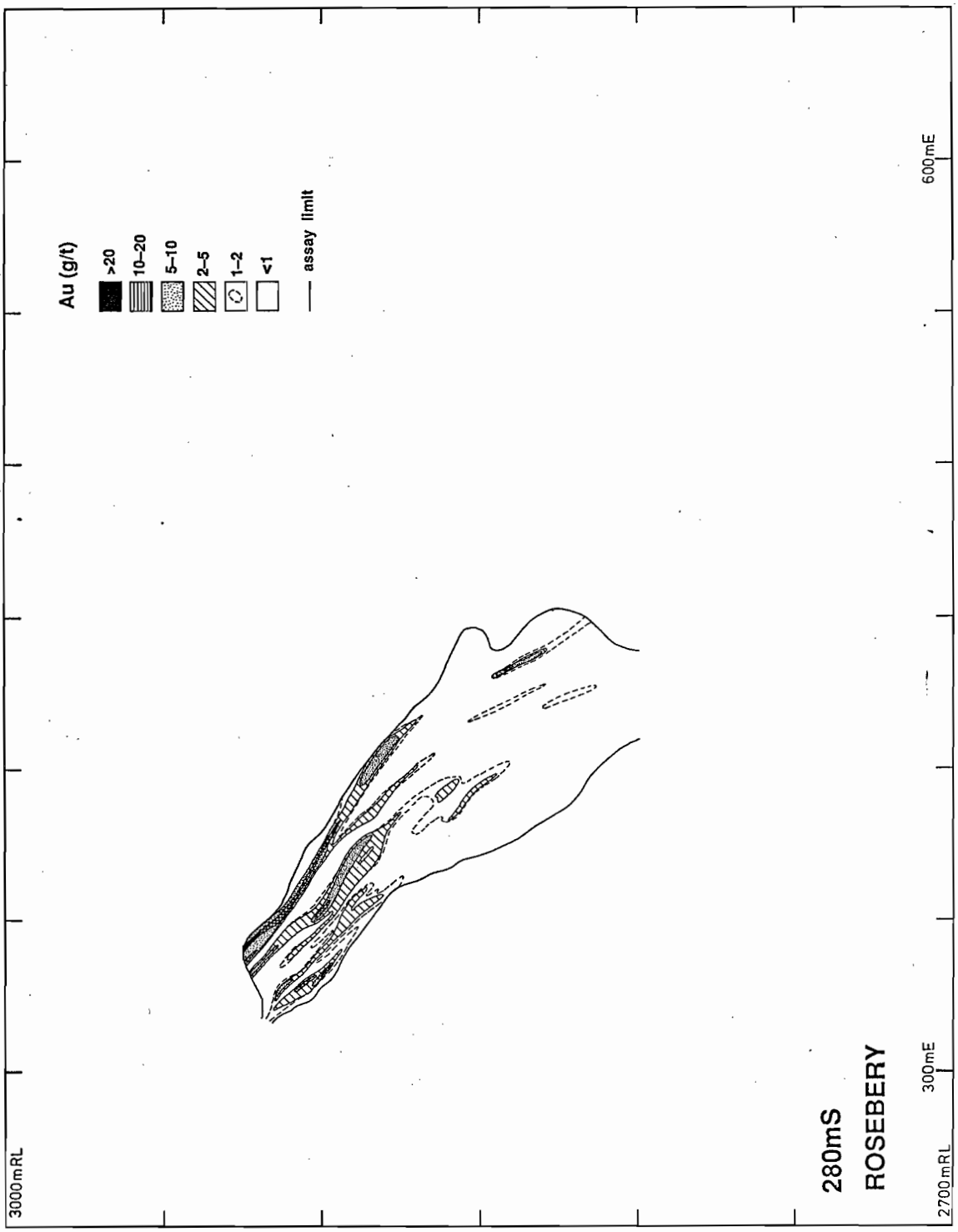

Fig. 6 Distribution of gold on 280mS section, F(J) lens of the south-end of Rosebery.

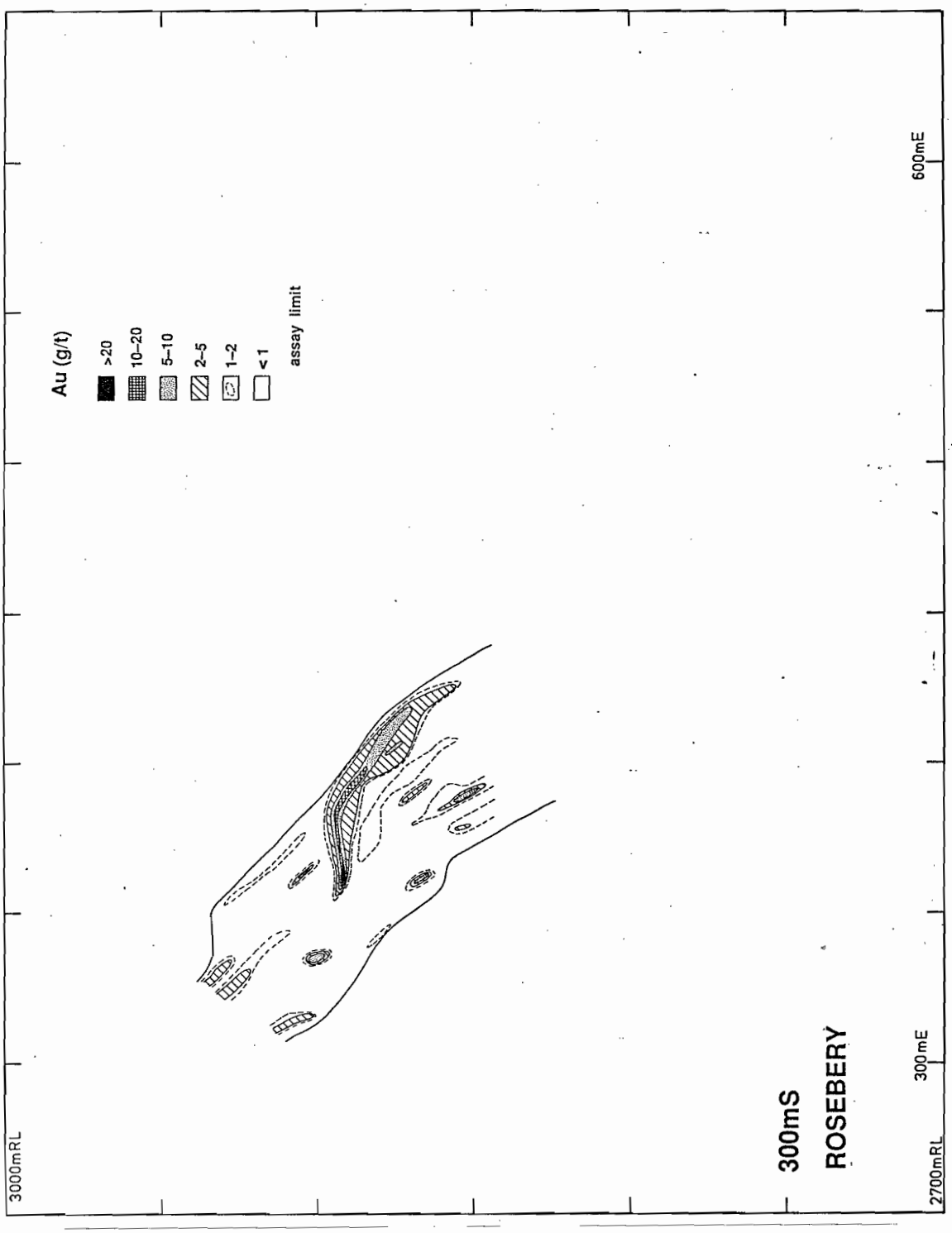

Fig. 7 Distribution of gold on 300mS section, F(J) lens of the south-end of Rosebery.

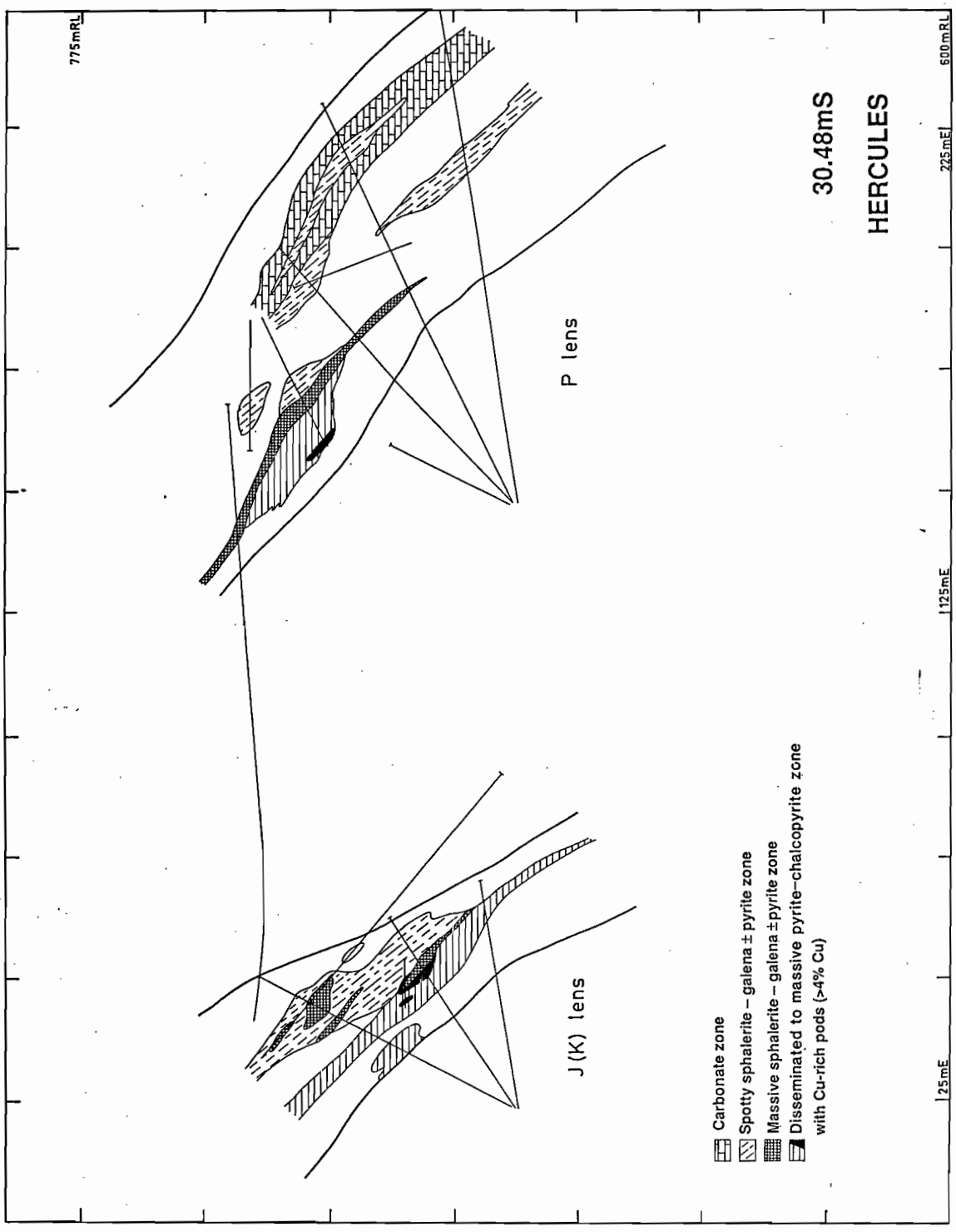

Fig. 8 Geology and mineral zonation of 30.48mS section, J(K)-P lens of Hercules.

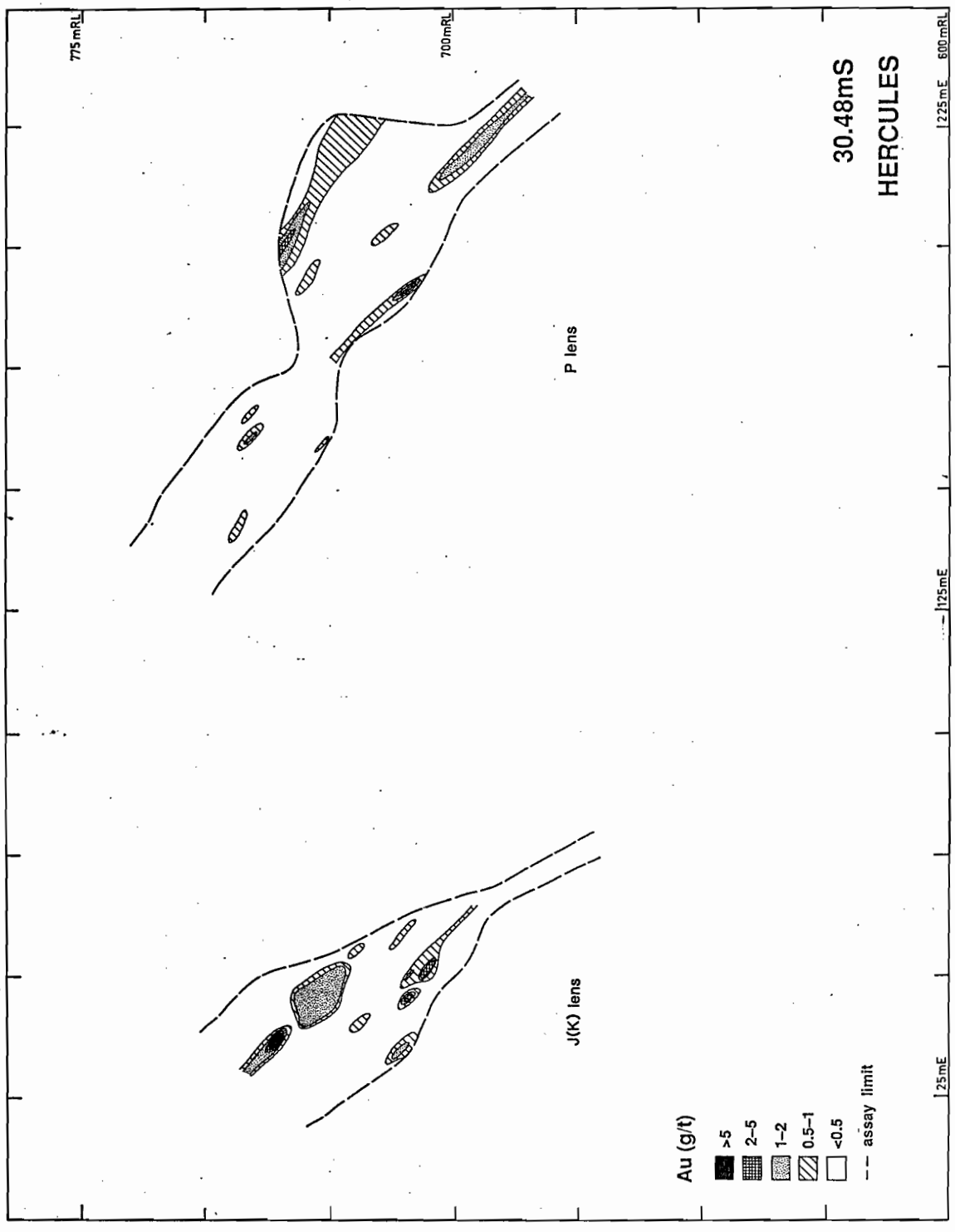

Fig. 9 Distribution of gold on 30.48mS section, J(K)-P lens of Hercules.

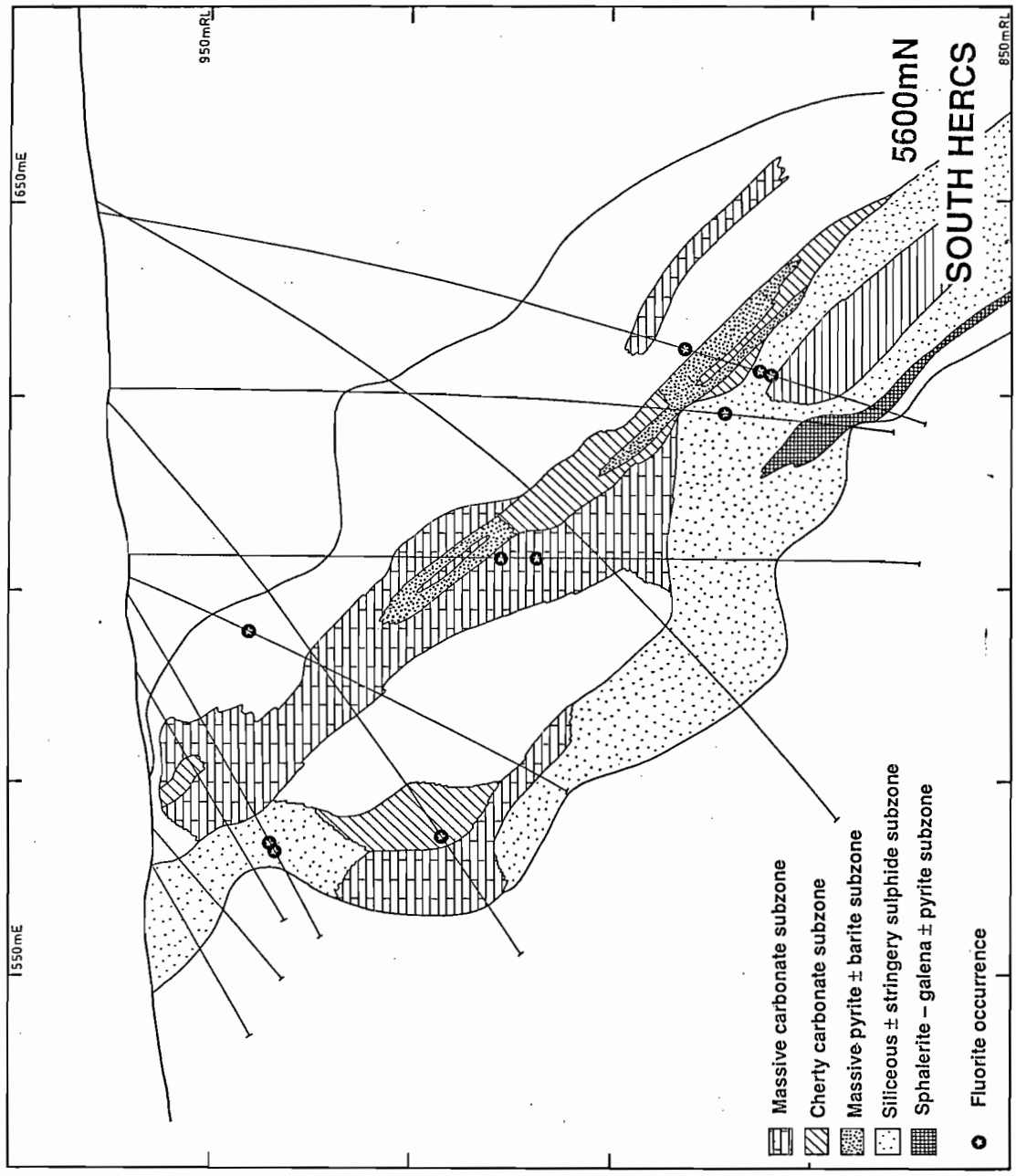

Fig. 10 Geology and mineral zonation of 5600mN section, South Hercs deposit.

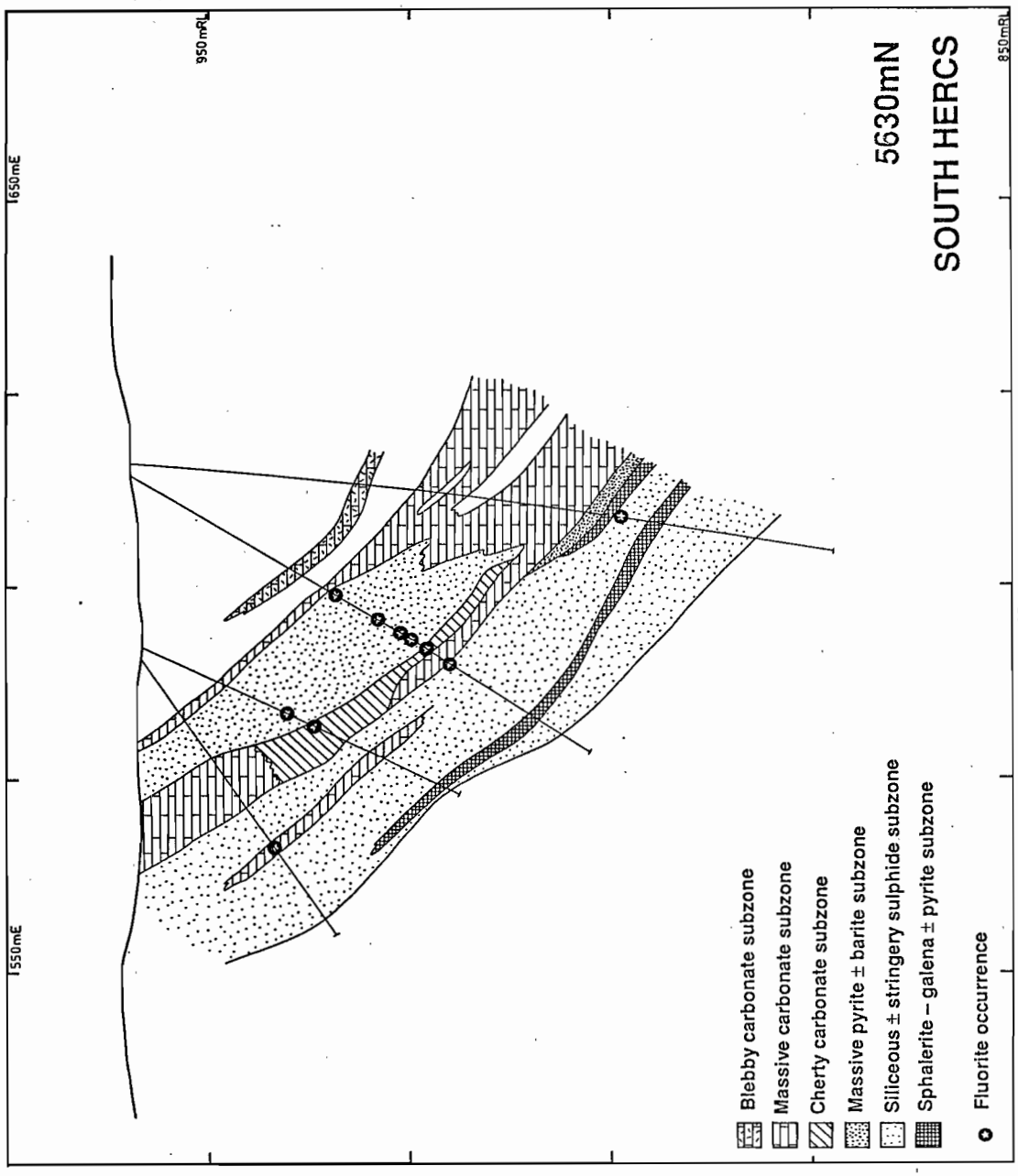

Fig. 11 Geology and mineral zonation of 5630mN section, South Hercs deposit.

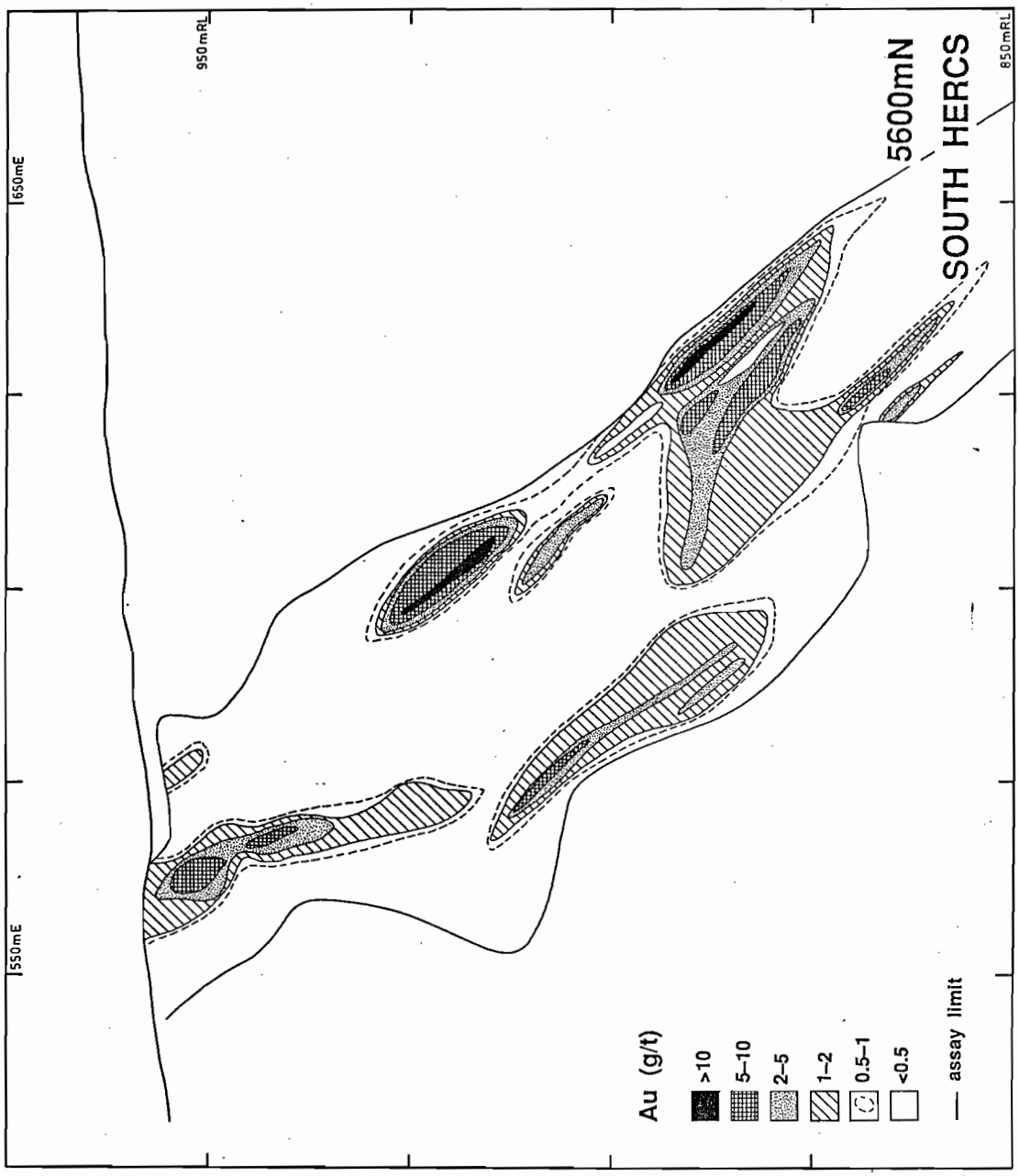

Fig. 12 Distribution of gold on 5600mN section, South Hercs deposit.

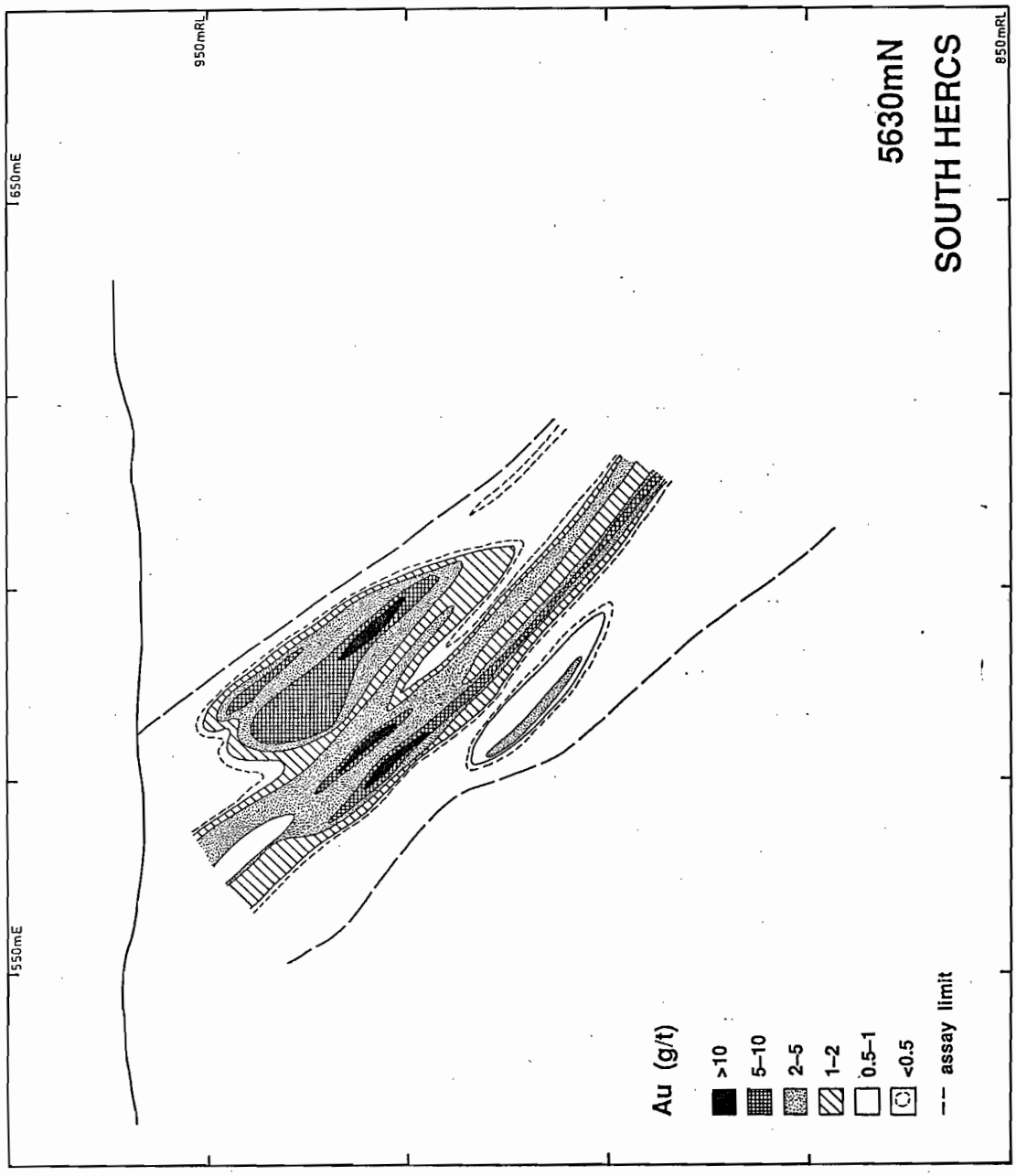

Fig. 13 Distribution of gold on 5630mN section, South Hercs deposit.

II. Mineralised sulphide zone (variable gold and silver)

3. Massive pyrite±barite sub-zone
2. Siliceous±stringe sulphide sub-zone
1. Sphalerite-galena±pyrite sub-zone

As mentioned previously carbonate alteration at the south Hercs deposit is the most spectacular alteration type and gives a significant textural variation. Lees (1988) reported different styles of carbonate textures from bladed, fireworks, pods, cannonballs through spots, spheroids or oolites to recrystallised, tightly packed massive carbonates, but no genetic relation was given.

Although most of the carbonates at South Hercs appear to be recrystallised and secondary, the fine-grained oolitic, sometimes zoned spheroids are suggestive of a primary, syngenetic origin. Oolitic carbonate spots are apparrently recrystallised into larger, botryoidal cannonball aggregates, and may be colasced into tightly packed spheroids to massive carbonates. A complete gradation of carbonate textures can be seen in many drill holes. In addition, late fracture-filling quartz-carbonate±fluorite veins of 10cm across (e. g. H1108 @ 29.5 m) are not uncommon and cross-cut the recrystallised massive carbonates. These late quartz-carbonate±fluorite veins grade into quartz-fluorite to fluorite gash veins.

In this investigation, the carbonate altered zone was subdivided into three carbonate sub-zones of bleby, massive and cherty assemblages. The bleby cabonate sub-zone occurs at the topmost part of the ore zone and is mostly confined to the hangingwall. Arsenopyrite is noted in the bleby carbonate sub-zone well up in the hangingwall siltstone unit (e. g. H1128 @ 31.50m, 5670mN).

The massive carbonate sub-zone occurs below the bleby carbonate sub-zone and sometimes as a lateral equivalent of the massive pyrite±barite sub-zone. The massive carbonate sub-zone may contain abundant cannonball to colasced carbonate spheriods. The cherty carbonate sub-zone is similar to the massive carbonate sub-zone but more massive, finer grained and cherty in appearence, and contains cryptocrystalline silica. Both carbonate sub-zones are seen to wrap around the massive pyrite±barite sub-zone.

The mineralised sulphide zone was subdivided into three sub-zones. The massive pyrite±barite sub-zone contains significant Au grades and mostly occurs at the top of the ore lens. This sub-zone is characterised by compact massive pyrite (e.g. H1142 @ 44.3m, 22 g/t Au, 5600mN) and colloform aggregates of pyrite intermixed with chert (e. g. H1117 @ 24.3m). The barite in this sub-zone is remarkably bladed in prismatic grains of up to 1cm across, which appear to be pseudomorphs after anhydrite (e. g. H1145 @ 62.3m, 5670mN). The colloform pyrite grains may join together and give a prismatic , bladed texture like barite crystals (e. g. H1145 @ 70.3m, 5670mN).

The massive pyrite±barite sub-zone contain silica but very little other base metal sulphides. In places shearing has been noted and fine- to medium-grained, pyrite framboids in the silica-rich zone sometimes become streched by the deformation (e. g. H1114 @ 39.8m, 5630mN). The massive pyrite±barite sub-zone is comparable in texture, composition and Au enrichment with the distal pyrite zone of the Rosebery mine (Huston and Large, 1986) which contains appreciable gold values. The massive colloform pyrite-silica zone at the top of the Heyller massive sulphide deposit (McArthur, 1986) is texturally very similar to the massive pyrite±barite sub-zone at South Hercs deposit. The author also noted that Au is also enriched in the pyrite-silica cap of the Heyller deposits (e. g. HL 228 @ 50.3m, 6.0 g/t, 10670mN).

The siliceous±stringer sulphide sub-zone is essentially a silicified and sericitic tuff with disseminated to stringer Pb-Zn mineralisation. This sub-zone varies in texture from a siliceous tuff with disseminated sulphides to sericitic tuff with elongated blotches or blebs of sphalerite rimmed by sericite (e. g. H1118 @ 33.0m, 5630mN). The size of the sericite-rimmed sphalerites ranges from 2 mm to more than 1 cm across. The sphalerite in this sub-zone may accompany chalcopyrite and recrystallised galena.

The massive sphalerite-galena±pyrite sub-zone forms as thin lenses. This zone is sometimes spotty in texture. It mostly occurs below the carbonate and massive pyrite±barite sub-zones and it may contain a subordinate amount of gold.

GOLD MINERALISATION AND DISTRIBUTION

F(J) Lens of Rosebery Mine

In the F(J) lens of the Rosebery south-end orebodies, it was demonstrated in the last AMIRA report (August, 1987) that the trangressive magnetite-biotite replacement zone generally contains low Au grade (<5 g/t) whereas elevated Au grades (up to 29 g/t) are noted in the pyrrhotite-pyrite zones (see Figs. 5-7). The tourmaline-quartz zone gave generally low Au grades (<3 g/t) which are erratic in distribution. The primary Pb-Zn sulphide lenses contain considerable Au values but generally less than 15 g/t.

J(K)-P Lens of Hercules Mine

Two major association of gold mineralisation is noted at the J(K)-P lens of the Hercules mine. A significant gold mineralisation (>5 g/t) occurs in the massive sphalerite-galena±pyrite zone enclosed within

the porphyroblastic, spotty sulphide zone. This gold association is confined to the top of the ore zone (see Fig. 9)

A subordinate concentration of Au (3.4 g/t) is also noted in the disseminated to massive pyrite-chalcopyrite zone (>4 % Cu) at the base of the J(K)-P lens. The porphyroblastic, spotty sulphide zone and carbonate± barite zone is largely lack in gold mineralisation but the carbonate±barite zone at the top of the lens may contain minor gold.

South Hercs Deposit

Although the gold mineralisation at the south Hercs deposit is patchy and not uniformly distributed, gold is notably enriched in the massive framboidal pyrite±barite sub-zone at the top of the ore lens (e. g. 5600mN) (see Figs 12-13). The highest gold contour (>10 g/t) is largely confined to the massive pyrite±barite sub-zone. The massive sphalerite-galena±pyrite and the siliceous, stringer sulphide sub-zones locally may attain more than 10 g/t Au (e. g. 5630mN), but the gold mineralisation in these sub-zones is generally patchy and erratic.

In contrast, the carbonate zones are virtually absent of gold mineralisation and contain Au (<1 g/t). The occurrences of the fluorite±quartz gashy veins which are of possible Devonian origin are plotted on the geological cross-sections to examine the relationships betweeen gold mineralisation and the fluorite occurrences. No systematic variation was recognised and no correlation with elevated Au grades and the occurrence of fluorite was observed. Arsenic appears to be enriched in the upper part of the ore zone with assay values of up to 11% As recorded in the massive pyrite±barite sub-zone at H1142 @ 44.3m, 5600mN where 22 g/t Au was also recorded. But assay data for As are not sufficient to examine Au-As relationships and distribution of arsenopyrite with gold minerlisation is yet to be studied.

MINERALOGY AND GEOCHEMISTRY OF GOLD MINERALISATION

In this study, mineralogical and geochemical characteristics of the F(J) lens of Rosebery will be presented. Although the F(J) lens of the south-end orebody has the highest gold content of all the sulphide lenses at the Rosebery mine, little study has been done for the mineralogical, textural and geochemical characteristics of gold ore in the lens. Previous mineragraphic studies (Stillwell, 1934; Williams, 1960; Brathwaite, 1969, 1974; Green, 1983; Huston and Large, 1986,1987; Huston and Large, 1988 in press) were also concentrated on the other lenses. Huston and Large (1986, 1987) and Huston and Large (1988 in press) recognised six different style of gold mineralization at the A and B lenses of the north-end orebody (in order of significance):

(1) in massive sphalerite-galena-pyrite ore
(2) in massive barite mineralisation
(3) in the upper parts of pyrite-chalcopyrite pods
(4) in distal pyrite mineralization (at the edges of sphalerite-galena-pyrite mineralisation and in the overlying host rock
(5) in footwall mineralisation (poorly understood) and
(6) in remoblised quartz-carbonate veins

At the north-end orebodies, mineralogically gold occurs as electrum associated dominantly with pyrite and, to a lesser extent, tetrahedrite, and locally with galena and chalcopyrite in cracks. Gold also occurs as an unusual association of bismuthinite-bismuth-gold-maldonite at the northern end of 'E' lens (Huston and Large, 1986, 1987; Huston and Large, 1988 in press). Green (1983) and Brathwaite (1974) noted free gold in pyrite-chalcopyrite ore.

At the F(J) lens of south-end, gold is predominantly observed in the pyrrhotite and pyrite ore. Large *et al.*, (1988 in press) reported that gold in the southern ore lenses occurs as microscopic spherical inclusions (mean diameter 10-40 μm) in the marginal areas of pyrite grains and to a lesser extent chalcopyrite, with some gold (often in association with chalcopyrite) as thin films filling microfractures in pyrite and pyrrhotite. In this study, samples mostly from the F(J) lens were studied and the following different modes of gold occurrences are observed;

(1) in pyrite as inclusions (as reported by Large *et al.*, 1988 in press)
(2) in microfractures in euhedral pyrite grains (as reported by Large *et al.*, 1988 in press)
(3) in pyrrhotite as individual grains
(4) in chalcopyrite veins cutting pyrrhotite
(5) in association with chalcopyrite

Minute grains of gold (~10 μm) as electrum commonly intergrown with or without chalcopyrite is found in a large recrystallised pyrite euhedra (see Fig. 14A) as noted by previous workers at the north-end and postulated to be a primary syngenetic occurrence. Gold is sometimes intimately associated with pyrrhotite veinlets cutting the euhedral pyrite grains suggesting gold is mobilised out of pyrite grains and re-precipitated in the pyrrhotite veinlets during Devonian metasomatic recrystallisation. Such remobilised gold grains (see Fig. 14B) sometimes attain a grain size up to (100 μm) in massive pyrrhotite (sample R3034-7 at 100.5 feet on section 270mS) during recrystallisation.

Gold grains also occur in the chalcopyrite veins cutting massive pyrrhotite bodies and these recrystallised

veins are related to the Devonian event. Gold in a distinct and spectacular association with copper occurs in the F(J) lens (see Fig. 14C). Some gold grains (in sample R3024-3C at 137 feet on section 220mS) attain an unusually large size of 150 μm x 100 μm across probably related to the Devonian recrystallisation. This distinct gold-copper association indicates a similar behavior and complexing medium in the environment of Devonian replacement. Although no bismuthinite-gold-maldonite association was noted in the F(J) lens, native bismuth grains were commonly noted in the pyrrhotite and in the cracks in the pyrite.

The grain size distribution indicates a mode of 6.3-25 μm for the north-end where the primary syngenetic gold association is dominant whereas a mode 25-40 μm is observed for the south-end where remobilised and recrystallised gold is abundant (see Huston and Khin Zaw, 1988 in this AMIRA report). Thus remobilised gold grains appear to be coarser in grain size and suggest an efficient recovery of gold in the F(J) lens.

The fineness (1000Au/Au+Ag wt %) values of the electrum grains in the F(J) lens of the south-end of Rosebery and those of the north-end (A & B) lens of the Rosebery mine are discussed in detail by Huston and Khin Zaw, 1988 in this AMIRA report). Briefly in the north-end, the fineness of gold grains in the distal pyrite mineralisation varies from 650-950 whereas the fineness of those gold grains in the barite mineralisation gives a range of 550-750.

The electrum grains in the remobilised veinlets give a fineness range of 550-650 and those in the bismuthinite veins yielded a fineness of 900. In the south-end, the gold grains in the pyrite euhedra of primary syngenetic origin gave a fineness of 450 and the fineness of the recrystallised gold grains in the pyrrhotite ranges from 450 to 650 whereas the gold grains in assciation with chalcopyrite yielded a fineness of 500-750.

In view of the fineness of gold grains in terms of Cambrian vs. Devonian, the primary syngenetic gold association of the entire Rosebery deposit give a fineness range of 350-650 whereas the recrystallised association of possible Devonian origin yielded a fineness range of 450-950. Thus the fineness of gold mineralisation at the Rosebery mine appears to have been increased during the Devonian recrystallisation.

Huston and Khin Zaw (1988 in this AMIRA report) demostrate that Au and Ag show distinct zonation in the electrum of the F(J) lens of the south-end orebody. Ag is enriched at the rim and Au is concentrated towards the core zone. This zoning of electrum (Au) grains combined with the rather coarse-grained texture of these grains and associated replacement iron assemblages can be attributed to the recrystallisation during the Devonian metasomatic event.

COMPOSITIONAL VARIATION OF SPHALERITES

In recent years, there has been considerable interest in the use of the FeS content of sphalerites as a geobarometer, and also as a geochemical tool to decipher conditions of deposition in hydrothermal and metamorphic environments. In this investigation, compostional variation of sphalerites from the F(J) lens of the Rosebery mine, J(K) and P lens of Hercules mine and the south Hercs deposit were determined (1) to provide pressure (depth) estimates at the time of Fe-S-O replacement during Devonian at the Rosebery mine, and (2) to deduce the control of a_{FeS} in relation to Au remobilisation and deposition.

Sphalerite Geobarometer

Since initial thermodynamic calculation made by Barton and Toulmin (1966) and later confirmed through experimental studies in the Fe-Zn-S system by Scott and Barnes (1971), and Scott (1973, 1976), it is now known that the FeS content of sphalerite is a function of activity of FeS (a_{FeS}) in the system, itself controlled by the activity of sulphur (a_S) , a widely variable parameter in assemblages involving iron sulphides.

It has also been demonstrated that the FeS content in sphalerite coexiting with hexagonal pyrrhotite and pyrite is pressure dependent. This variation of FeS content in sphalerite as a function of pressure is also independent of temperature over a considerable range 300°-550°C and has given rise to the concept of the sphalerite geobarometer.

Textural Variation of Sphalerites

The sphalerites from Rosebery, Hercules and the south Hercs deposits display a wide variety in colour, grain size and texture. The sphalerites from the F(J) lens of the Rosebery mine where overprinted by Devonian granitoid-related metasomatism appear to have a more variable in texture. In the F(J) lens, the sphalerites in the pyrrhotite-pyrite assemblages are more massive, coarse-grained and dark brown in colour whereas the sphalerites in the magnetite-biotite and quartz-tourmaline assemblages are semi-massive to cm-size patches and blebs and yellowish brown in colour.

Some sphalerites in the F(J) lens are also markedly zoned from Fe-poor core (2.16 mole % FeS) to Fe-rich rim (14.78 mole % FeS). The Fe-rich layer is in contact with other iron sulphides. This zoning probably occurs due to the outward diffusion of FeS in sphalerites as suggested by Barton and Skinner (1979) and the zonning of sphalerites in the F(J) lens can be related to the recrystallisation during Devonian metasomatism. The textural relationship of sphalerites at the south Herc

Fig. 14. ***A****. Chalcopyrite-electrum inclusion in pyrite grain, py=pyrite, cp=chalcopyrite, po=pyrrhotite, sp=sphalerite and unlettered=gangue. Sample No. DDH R3492-17 @ 118' (36.2m), section 280mS, horizontal bar is 100 μm.* ***B****. Isolated electrum (Au) grain in the pyrrhotite. cp=chalcopyrite, po=pyrrhotite, Au=gold and unlettered black patches are polishing marks.Sample No. DDH R3034-7 @100.5' (30.8m), section 270mS, horizontal bar is 100 μm.* ***C****. Electrum and chalcopyrite intergrowth in pyrrhotite. cp=chalcopyrite, po=pyrrhotite, Au=electrum, cr=crosite? qtz=quartz and black striations are polishing marks. Sample No. DDH R3024-3C @ 137' (42m), section 220mS, horizontal bar is 100 μm.* ***D****. Sphalerite and pyrrhotite inclusion in pyrite grain, sp=sphalerite, po=pyrhotite, py=pyrite and unlettered patches are polishing marks. Sample No. DDH R3023-2 @ 133' (40.8m), section 270mS, horizontal bar is 100 μm.*

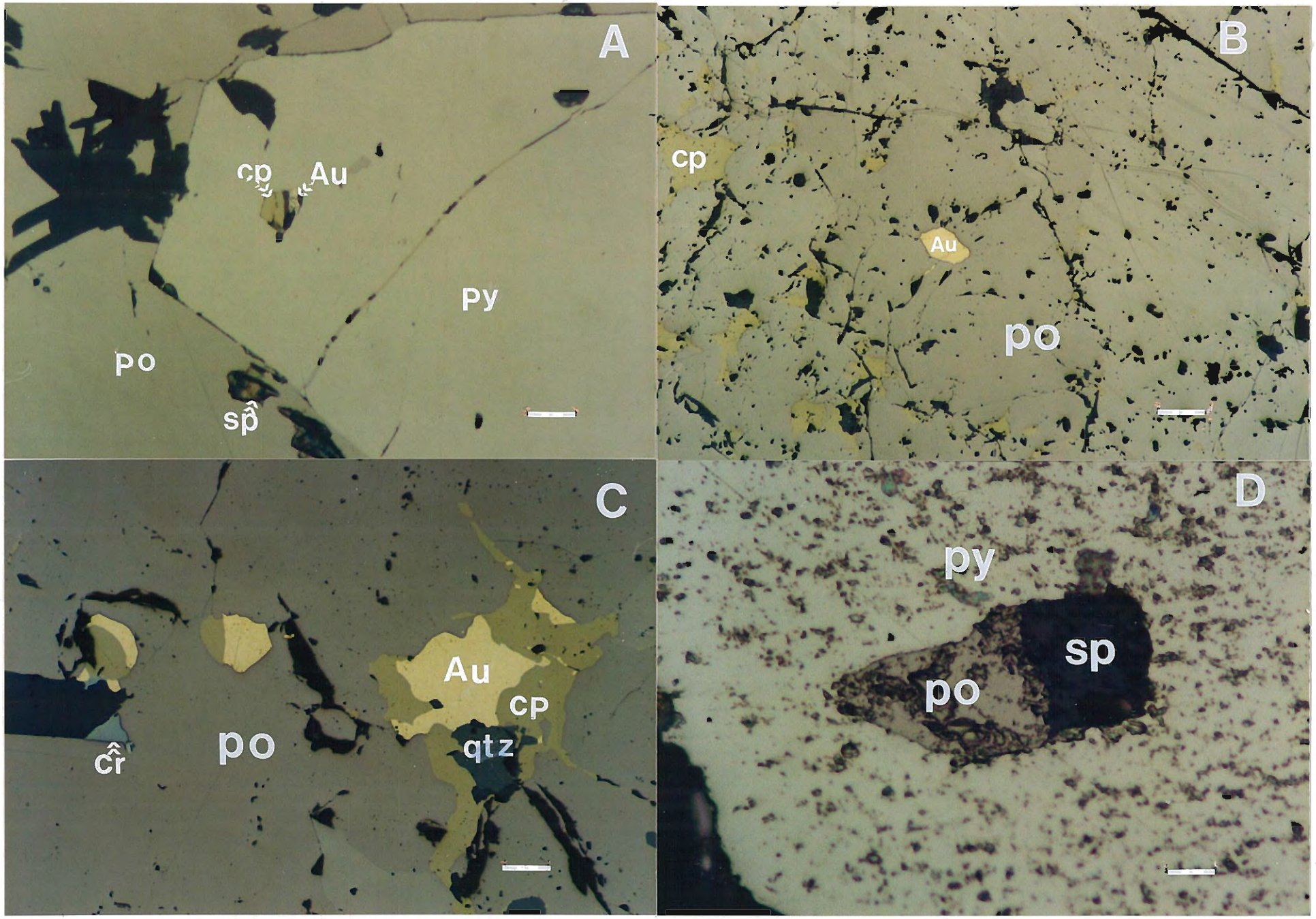
A
cp
Au
py
po
sp
B
cp
Au
po
C
Au
cp
qtz
po
cr
D
py
sp
po

deposit is similar to those of the F(J) lens of Rosebery but zonning of sphalerites is rarely seen.

In contrast, sphalerites from Hercules and north-end of Rosebery (A & B lens) appear to be more homogeneous presumably preserving the original annealed texture as they show very little variation in Fe content across the grain. Chalcopyrite disease in the sphalerites is much less common than those from the the F(J) lens. In addition to these sphalerites types, coarse-grained, light yellow sphalerites with recrystallised galena cubes with or without chalcopyrites are also commonly found in the irregular quartz-carbonate veins of Devonian origin which show cross-cutting features in the Rosebery, Hercules and the south Hercs ore zones.

Analytical Methods

The FeS content of sphalerites was determined using a JOEL electron microprobe with an operating voltage of 20 kV and a beam current of about ~3 μm. Each grain was analysed at least 2-5 spots and the results averaged. Concentration of other minor elements (Mn, Co, Cd and Cu) were also determined. Although minor amounts of Mn, Cd and Cu in the sphalerites was noted, no Co was detected. The results of the microprobe analyses of sphalerites for different textural varieties are shown in Table 1.

FeS content and Geobarometric Implications

The sphalerite geobarometer has received wide application for sphalerites from hydrothermal environments such as skarn deposits (e. g. Khin Zaw, 1976), nickel deposits, western Australia (Groves *et al.*, 1975) and from metamorphosed massive sulphide deposits which include deposits from the Snow Lake area, Manitoba (Bristol, 1974), Quemont mine, Noranda, Quebec (Lusk *et al.*, 1975), Sullivan (Ethier *et al.*, 1976), Broken Hill, New South Wales (Scott *et al.*, 1977), Ruttan mine, Lynn Lake, Manitoba (Bristol, 1979), Calloway mine, Ducktown, Tennessee (Ringler, 1979) and several others (see Scott, 1976).

Recently the sphalerite geobarometer was applied for VMS deposits in the Swedish Caledonides and U.S. Appalachian by Hutchison and Scott (1980) and later Sundblad *et al.*, (1984) did more detailed work on the Swedish Caledonides deposits. A sphalerite geobarometric study was also made on the McPhun's Cairns stratiform sulphide deposit, Scotland (Willan and Hall, 1980) and recently Mole (1983) studied sphalerite composition in relation to deposition and metamorphism of the Foss stratiform Ba-Zn-Pb deposit, Aberfeldy, Scotland. Metamorphic petrologists also used disseminated sphalerite bearing assemblages in metamorphic belts as an indicator of metamorphic pressure (Dewitt and Essene, 1974; Brown *et al.*, 1978).

Although FeS content of sphalerite as a geobarometer was extensively applied as mentioned above, the outcome gave variable results and some workers questioned the applicability of the barometer. The pressure derived from the results of sphalerite barometric studies are variable and often suggest pressures which are greater than those indicated by the silicate mineralogy of the adjacent rocks. The most controvertial issue for the reliability of the sphalerite barometer is the postdepositional changes or retrograde changes in the composition of sphalerites although sphalerite is one of the more refractory sulphide minerals.

Scott (1983) pointed out that the problem arises due to the cooling rate of the particular sulphide assemblages in the hydrothermal system or in the metamorphic environments. Scott (1983, p. 429) also mentioned that sphalerite geobarometer was successfully applied for hydrothermal system such as skarns (Shimizu and Shimazaki, 1981) and vein deposits (e. g. Hudson Bay Mountain area; Hutchison and Scott, 1981) in which cooling was reasonably fast, but metamorphosed deposits which have cooled more slowly show evidence of retrogade changes in sphalerite composition particularly in Cu-rich environments. The resulting sphalerites are considerably depleted in FeS (higher in pressure estimates) relative to that expected from P and T of metamorphism.

Scott (1983) suggested that to avoid this problem attending retrogression, sphalerite inclusions, and particularly those accompanying pyrrhotite that are totally encapsulated in pyrite (e. g. see Fig. 14D) should be sought and analysed. Presumably, such poikiloblastic inclusions were equilibrated during peak pressure (depth) regimes. They display the necessary buffer assemblages and would have been protected from later hydrothermal retrograde reaction by inert encapsulating pyrite.

The following criteria must be met to use FeS content of sphalerites as a geobarometer (Scott and Barnes, 1971; Scott, 1973, 1976).

1) Sphalerites must have equilibrated with pyrite and hexagonal pyrrhotite. Both iron sulphides must be preferably in mutual contact with sphalerites.
2) Temperature of sphalerite deposition also needs to be roughly estimated and has to be above 274°C which corresponds to the inversion temperature of hexagonal to monoclinic pyrrhotite.
3) Precise microprobe analyses of sphalerites are required, as ±0.5 mole % uncertainty corresponds to ±400-500 bars.

The pyrrhotite in the F(J) lens are found to be mixtures of hexagonal and monoclinic pyrrhotite as evidenced by the microprobe analyses (yet to be

Table 1 Compositional variation of sphalerites, F(J) lens, Rosebery.

Sample No./ Section	grain No.	spot No.	Zn wt%	Fe wt%	Mn wt%	Cu wt%	Cd wt%	S wt%	Total wt%	Fe mole %	Mn mole %	Cu mole %	Cd mole %	Au grades g/t	Associated sulphides/oxides /silicates
R3024-2/	1	5	63.61	1.74	0.00	0.35	0.05	33.28	99.05	3.09	0.00	0.45	0.04	13.80	sp-cp-ga
220mS	2	3	63.35	1.45	0.45	0.00	0.16	33.42	99.09	2.58	2.44	0.00	0.13	13.80	isolated sp grain
	3	5	62.77	1.82	0.00	0.34	0.11	32.79	97.88	3.27	0.00	0.44	0.09	13.80	sp-cp
	4	3	63.98	1.10	0.11	0.00	0.35	32.92	98.33	1.96	0.62	0.00	0.29	13.80	sp-cp-ga
average	4	16	63.43	1.53	0.14	0.17	0.17	33.10	98.59	2.72	0.77	0.22	0.14	13.80	sp-cp-ga
R3024-3A	1	3	63.7	1.31	0.13	0.00	0.20	33.01	98.46	2.35	0.70	0.00	0.16	10.30	sp-mag-tourm
220mS	2	4	60.64	5.91	0.22	0.10	0.12	33.56	100.56	10.18	1.01	0.13	0.09	10.30	sp-mag-tourm
average	2	7	62.17	3.61	0.17	0.05	0.16	33.28	99.51	6.26	0.85	0.06	0.13	10.30	sp-mag-tourm
R3024-3C	1	2	61.32	4.32	0.16	0.00	0.16	33.59	99.53	7.58	0.77	0.00	0.13	10.30	isolated sp in qtz
220mS	2	2	56.08	9.21	0.00	0.00	0.00	33.59	98.89	16.12	0.00	0.00	0.00	10.30	sp-po-py (in contact)
	3	4	57.00	8.32	0.00	0.00	0.00	33.70	99.10	14.59	0.00	0.00	0.00	10.30	sp-po-py (not in contact)
	4	2	60.70	4.79	0.15	0.00	0.14	33.52	99.30	8.42	0.69	0.00	0.11	10.30	isolated sp in qtz
	5	3	55.94	9.75	0.05	0.13	0.22	33.32	99.58	16.87	0.20	0.16	0.17	10.30	sp locked in po-py
average	5	13	58.21	7.28	0.07	0.03	0.10	33.54	99.28	12.72	0.33	0.03	0.08	10.30	sp-po-py-qtz
R3023-2	1	4	54.28	8.60	0.00	1.27	0.00	33.32	97.46	15.33	0.00	1.61	0.00	6.30	sp-cp-py
270mS	2	12	56.07	9.10	0.04	0.30	0.00	34.03	99.61	15.88	0.16	0.38	0.00	6.30	sp-cp-py
	3	4	64.68	2.80	0.07	0.00	0.00	34.54	101.32	4.82	0.36	0.00	0.00	6.30	sp locked in py
	4	3	58.55	8.15	0.00	0.02	0.09	34.11	100.99	14.00	0.00	0.02	0.07	6.30	sp in contact with py
	5	3	55.51	9.22	0.00	0.00	0.00	34.88	99.60	16.28	0.00	0.00	0.00	6.30	sp in contact with po-py
	6	3	56.31	9.57	0.05	0.00	0.08	33.91	100.00	16.57	0.20	0.00	0.06	6.30	sp locked in bet po-py gr
	7	5	56.39	9.15	0.00	0.08	0.00	33.96	99.58	15.94	0.00	0.10	0.00	6.30	sp in contact with po-py
	8	3	57.94	8.53	0.00	0.00	0.00	34.61	101.08	14.69	0.00	0.00	0.00	6.30	sp-py
	9	3	55.11	9.50	0.00	0.47	0.00	33.55	98.63	16.67	0.00	0.60	0.00	6.30	sp locked in bet po-py gr
	10	3	56.65	8.66	0.19	0.00	0.00	33.64	99.42	15.13	0.77	0.00	0.00	6.30	sp-py
	11	2	57.08	8.58	0.00	0.00	0.00	34.48	100.20	14.96	0.00	0.00	0.00	6.30	sp-cp-po-py
	12	5	55.44	8.87	0.00	0.12	0.00	33.04	97.46	15.74	0.00	0.15	0.00	6.30	sp-py
	13	4	54.06	9.48	0.00	1.71	0.06	33.95	99.33	16.57	0.00	2.11	0.05	6.30	sp-cp-po-py
	14	5	55.63	9.55	0.00	0.56	0.00	33.63	99.35	16.60	0.00	0.70	0.00	6.30	sp locked in bet po-py gr
average	14	59	56.69	8.55	0.02	0.32	0.02	33.97	99.57	14.94	0.11	0.41	0.01	6.30	sp-po-cp-py
R3023-8/	1	5	60.72	5.16	0.08	0.00	0.18	33.15	99.28	9.02	0.38	0.00	0.14	26.20	unknown texture
270mS	2	2	57.93	8.53	0.10	0.00	0.15	33.57	97.34	14.66	0.41	0.00	0.12	26.20	sp-po-py-mag
	3	2	61.55	4.10	0.08	0.00	0.10	33.19	99.16	7.22	0.40	0.00	0.08	26.20	unknown texture
	4	2	59.76	4.23	0.06	0.00	0.21	32.41	96.52	7.63	0.30	0.00	0.17	26.20	unknown texture
	5	2	54.86	8.22	0.00	0.24	0.22	33.80	97.39	14.84	0.00	0.31	0.17	26.20	sp-po-py-mag
	6	3	60.60	6.74	0.00	0.00	0.00	33.01	100.34	11.51	0.00	0.00	0.00	26.20	unknown texture
average	6	16	59.24	6.16	0.05	0.04	0.14	33.19	98.33	10.81	0.25	0.05	0.11	26.20	sp-po-py-mag
R3492-3B/	1	3	63.42	3.02	0.23	0.00	0.00	33.29	99.96	5.26	1.19	0.00	0.00	22.00	sp-cp-py-ga
280mS	2	2	63.99	2.93	0.16	0.00	0.29	33.54	100.36	5.06	0.82	0.00	0.23	22.00	sp-cp-py-ga
average	2	5	63.71	2.98	0.20	0.00	0.14	33.41	100.16	5.16	1.00	0.00	0.11	22.00	sp-cp-py-ga
R3033-29/	1	3	61.61	3.57	0.18	0.00	0.13	33.70	99.18	6.33	0.88	0.00	0.10	9.30	isolated sp in qtz
300mS	2	3	60.60	4.24	0.11	0.00	0.21	33.75	98.91	7.55	0.53	0.00	0.17	9.30	isolated sp in qtz
	3	3	57.47	8.18	0.00	0.06	0.09	33.76	99.56	14.26	0.00	0.08	0.07	9.30	sp-po-py (not in contact)
average	3	9	59.89	5.33	0.10	0.02	0.14	33.74	99.22	9.38	0.47	0.03	0.11	9.30	sp-py-po-qtz

confirmed by magnetic colloid methods and X-ray diffraction). Microprobe analyses of pyrrhotite gave a range of X_{FeS} from 50.05 to 46.12. It is also assumed that hexagonal pyrrhotite in the early replacement zones within the F(J) lens has transformed into monoclinic pyrrhotite by cooling during the late quartz-tourmaline veining. A recent preliminary fluid inclusion study of inclusions in helvite in the early Fe-S-O replacement assembalges gives minimum homogenisation temperature of about 300°C.

Although sphalerites from the Rosebery-Hercules area have suffered greenschist facies regional metamorphism along with the host rocks, no po-py association was noted with the annealed sphalerites. Therefore it was not possible to use the FeS content of sphalerites as a meaningful pressure estimate during regional metamorphism. However, sphalerites associated with po-py in the F(J) lens of the Devonian replacement zone which presumably formed a few million years after the metamorphism provide an opportunity to apply

the sphalerite geobarometer.

In this study, the FeS mole % of sphalerites strictly encapsulated in pyrite with pyrrhotite (see Fig. 14D) or mutual contact assemblages in the F(J) lens were used to determine the pressure (depth) estimates during the replacement event. To avoid the interference by copper, the spalerite grains which contain >0.5 wt % copper were not considered in this study. Hutchison and Scott (1981) recommended against the use of sphalerite grains with chalcopyrite inclusions, since Cu appears to affect the equilibration of sphalerite grains. It was also noted that the smaller the grains the less variation in FeS content in sphalerites and more depleted in Cu content.

The frequency distribution of the mole % FeS in sphalerites of differing textural associations and iron assemblages in the F(J) len of the Rosebery south-end orebody is shown in Fig. 15. The FeS mole % in sphalerites coexisting with or without cp/po/py/ga (not in mutual contact) gave a variable range from 1.96-17.03 mole % FeS. The sphalerites encapsulated in pyrite, but without pyrrhotite, yielded 4.82-15.13 mole % FeS whereas the sphalerite inclusions encapsulated in pyrite along with pyrrhotite or small sphalerite grains in mutual contact with po-py gave a restricted range of 16.12-16.87 mole % FeS.

The CdS mole % in sphalerites from the F(J) lens ranges from 0.00 to 0.29 whereas the sphalerites from the other lenses yielded a range of 0.00-0.38 mole % CdS. The MnS mole % in the sphalerites varies from 0.00 to 1.01 except one grain with 2.44 mole % MnS. The sphalerites from the other lenses (A, B, C, D, G, and H lens) gave a range of 0.00-1.25 mole % MnS. These minor elements do not affect the sphalerite geobarometer. On the basis of cell volume data, Scott and Barnes (1971) considered that these minor elements in concentration up to several wt % beyond those normally found, should not affect the geobarometer. Experiments on the system Zn-Cd-Fe-S by Scott (1973, p. 470) also indicated no change in phase relations with several CdS wt % in the sphalerites.

The FeS mole % vs. CdS mole % and MnS mole % in sphalerites from the F(J) lens and the other lenses of the Rosebery mine are shown in Figs. 16-17, but no recognisable trend was noted, although CdS and MnS content of the sphalerites in the F(J) lens gave more variation and a wider range than those from the other lenses suggesting possible redistribution of these minor elements during Devonian recrystallisation.

The above mole % FeS in sphalerites with po-py assemblages was used to calculate the pressure by applying the following regression equation given by Hutchison and Scott (1981):

$$P = 42.30\text{-}32.10 \log \text{mole \% FeS}$$

Hence, this average mole % FeS is equivalent to 3.0±0.5 kb for the reequilibration of sphalerites in the F(J) lens. Assuming an average rock density of 2.65 gm/cm^3, this pressure estimate would correspond to a depth of 8.0±0.5 km.

Green *et al.* (1981) estimated a depth of 6 km to 8 km during Devonian metamorphism by stratigraphic reconstruction. Although many uncertainties can be encountered in such reconstructions such as facies changes, unconformities, a lack of knowledge concerning the proportion of rock units eroded prior to the Devonian granitoid intrusion, and the actual thickness of folded Cambrian rocks in the mine area, it provided an optimum depth estimate. The depth estimate determined here by using the FeS mole % in the sphalerites in the F(J) lens is consistent with this. Recent geophysical gravity modelling also suggests that the depth of the Devonian granitoid intrusion at about 6 km NW of Rosebery is approximated to be 7.5 km (Dave Acher, per. comm., 1988).

Figure 18 shows the histogram of FeS mole % of sphalerites from the F(J) lens of the Devonian replacement zone and the other lenses (A, B, D, G, H lens). As shown in the Fig. 18, the FeS mole % in sphalerites for the entire Rosebery deposit gave a bimodal distribution. A mode of 16.0 mole % FeS was noted for the F(J) lens where Devonian metasomatism prevailed whereas a mode of 4.0 mole % FeS was found for the other lenses. This suggests that the primary exhalative minerlisation at Rosebery has suffered at least two periods of post-depositional re-equilibration viz. 1) possible annealing of the primary sulphides at the time of metamorphism and 2) metasomatism related to low level granitoid intrusion. This bimodal distribution of sphalerites is not in keeping with the formation of Rosebery ore deposit as a replacement, epigenetic deposit for which a unimodel and more constrained distribution of FeS mole % in sphalerites would be expected.

a_{FeS} vs Au Deposition

The FeS content of sphalerite is dependent on temperature, pressure and the activity of FeS (a_{FeS}) in the system, the latter itself is controlled by by activity of sulphur (a_S). Thus variation in the FeS content in the sphalerites reflects the changes in these parameters of a hydrothermal system, and it can provide a recorder for the physical and chemical characteristics of the environment of ore deposition and related post-depositional history.

The changing temperature and chemistry of mineralising solutions has left a delicate record in the growth-zoned sphalerites of vein and Mississippi-Valley type deposits (Mclimans *et al.*, 1980). Sequential trends of sphalerite composition have been found from sedimentary exhalative deposit such as Sullivan (Campbell and Ethier, 1983) and Mole (1983)

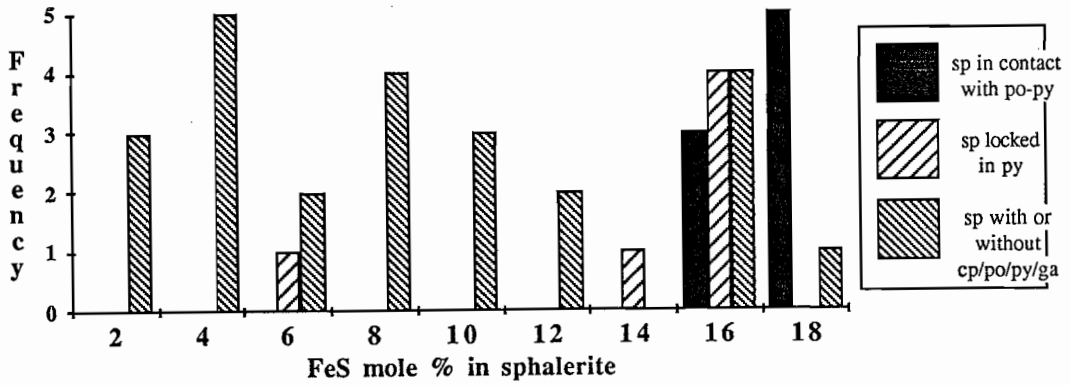

Fig. 15. Frequency distribution diagram for the FeS mole % in sphalerites from the different textural associations in the F(J) lens, Rosebery.

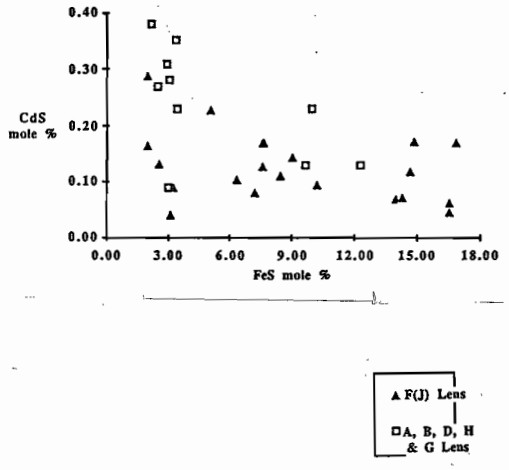

Fig. 16. Plot of FeS mole % vs. CdS mole % in sphalerites in different ore lenses, Rosebery.

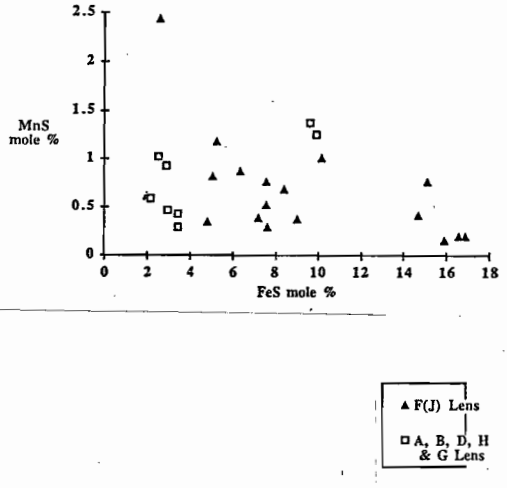

Fig. 17. Plot of FeS mole % vs. MnS mole % in sphalerites in different ore lenses, Rosebery.

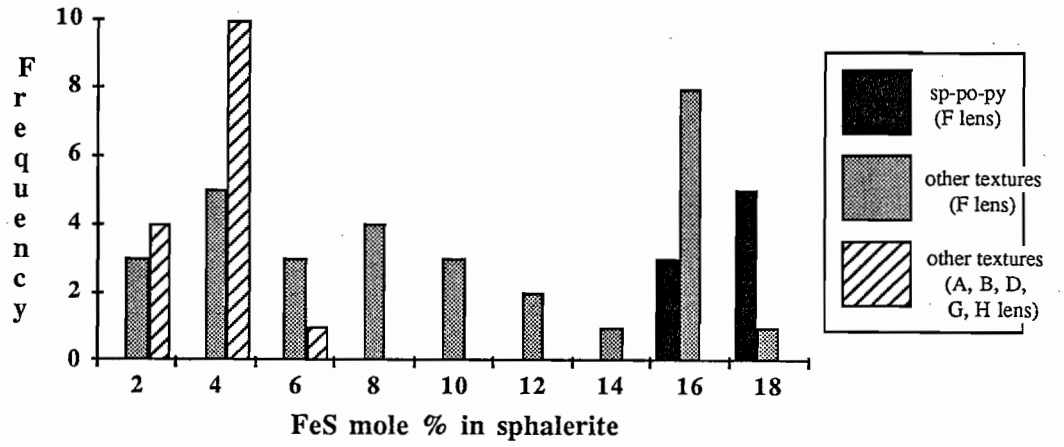

Fig. 18. Frequency distribution diagram for the FeS mole % in sphalerites from the F(J) lens in comparison with those of the other lenses (A, B, D, G, H lens), Rosebery.

considered that at the Foss stratiform Ba-Pb-Zn deposit, Aberfeldy, Scotland, Fe-rich sphalerites were deposited from the metallifierous brines in the vent and the Fe-poor sphalerites were formed from a cooler, exhaled brines on the sea floor away from vent.

Urabe (1974) ascribed that the decrease in FeS content of the sphalerites with stratigraphic height in the Kuroko deposits as largely due to declining temperature from the stockwork to the top of the stratiform ore. But these changes may also be related to changes in total sulphur concentration and oxygen fugacity during mixing of the ore solutions with seawaters. Green *et al.* (1981) also noted at the Rosebery deposit that FeS content of the sphalerites is decreased parallel with the decrease on the Fe/Fe+Mg+Mn ratios of chlorites and increase in $\partial^{34}S$ value from the stratigraphic bottom to the top.

Sphalerite compositional variations in sulphide ore of the Norwegian Caledonides was also studied to provide changes in (a_S) during ore formation and metamorphism (Craig *et al.*, 1984). The variation of FeS content in sphalerites from the modern seafloor hydrothermal vents at 21°N on the East Pacific Rise is also attributed to periodic changes in (a_S) during sphalerite deposition (Styrt *et al.*, 1981; Hekinian *et al.*, 1980; Scott, 1983).

More importantly Hannington and Scott (1988 in press) recently used FeS content of sphalerites as a petrologic indicator for the sulfidation and oxidation state of the gold mineralisation in the volcanogenic massive sulphide system. Hannington and Scott (1988 in press) showed that average FeS content of sphalerites in the volcanogenic deposits (Noranda, Kuroko and modern seafloor deposits) has a strong correlation with Au grades of the deposits viz. the lower the FeS content of the sphalerites, the higher the Au grades. This trend was also true for a group of deposits within a single mining district (e. g. Kuroko deposits). Hannington and Scott (1988 in press) attributed this correlation to changes in temperature and activity of sulphur (a_S) or a_{FeS} which also controls the gold deposition. To the exploration geologists these simple indicators can be used as a guide for targeting the Au-rich massive sulphide system.

In this investigation, the compositonal variation of sphalerites in the samples with known Au grades from the north-end (A & B lens) and the F(J) lens of the south-end of the Rosebery deposit have been plotted in Figs. 19-20. FeS mole % of at least 2-5 sphalerites grains in each sample were averaged and plotted against Au grades. The recrystallised, light yellow coloured sphalerites in the cross-cutting quartz-carbonate veins were not considered in this study.

A vague correlation between the mole % FeS in the sphalerites and the Au grades is suggested in the north-end of the Rosebery orebody (see Fig. 19) as in the case of the modern seafloor VMS deposits and the relatively undeformed Kuroko deposits described by Hannington and Scott (1988 in press). The sphalerites in the Au-bearing samples from the barite mineralisation gave the lowest FeS mole % (1.33) with the highest Au grade (38.3 g/t) whereas the sphalerites with the highest FeS mole % (10.62) gave the lowest Au grade (2.1 g/t).

The underlying Pb-Zn mineralisation yielded the higher FeS mole % in sphalerites with lower Au grades and the barite minerlisation at the top contains lower FeS mole % in sphalerites with higher Au grades. The

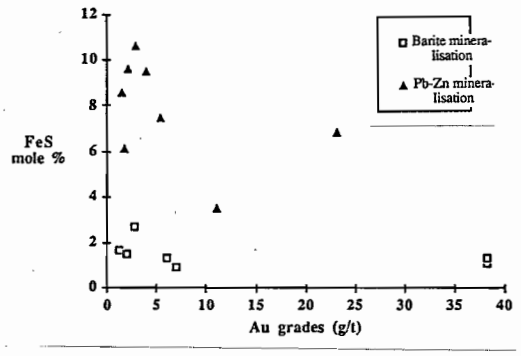

Fig. 19. Plot of FeS mole % in sphalerite vs. Au grades (g/t) in the A and B lens of north-end of Rosebery.

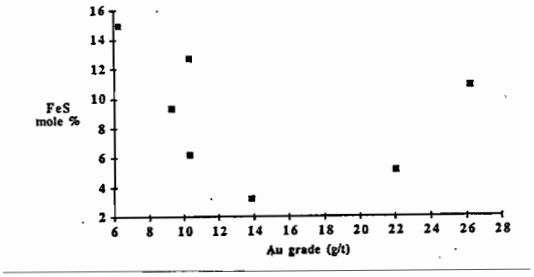

Fig. 20. Plot of FeS mole % in sphalerite vs. Au grades (g/t) in the F(J) lens of the south-end of Rosebery.

correlation of the FeS mole % in the sphalerites and the Au grades supports the transport and deposition of gold in the Pb-Zn ore at Rosebery from bisulphide complexes as proposed by Huston and Large (1986, 1987). The solubility of $Au(HS)_2^-$ is dependent on the activity of sulphur (a_S) which also control the FeS mole % in sphalerites.

The FeS mole % in the sphalerites from the F(J) lens of the south-end orebody gives no clear trend with Au grades (Fig. 20). This suggests that the general trend between the FeS mole % in the sphalerites and the Au grades for the primary exhalative mineralisation at Rosebery was preserved even though affected by later regional metamorphism at the north-end. However, Devonian granitoid-related metasomatism at the south-end possibly destroyed the FeS mole % vs. gold relationships in the F(J) lens. In addition, the gold in the F(J) lens has remobilised and recrystallised along with copper possibly as chloride complexes resulting in no correlation between the FeS mole % and the gold mineralisation as the gold deposition was no longer controlled by the activity of sulphur (a_S).

FLUID INCLUSION STUDY

In this report, preliminary results of the ongoing fluid inclusion study will be presented. No previous fluid inclusion study has been undertaken at Rosebery. This study was carried out with the aim of understanding the thermal aspects of the ore deposition and, to infer the physical and chemical characteristics of gold mineralisation and mobilisation with special emphasis on the F(J) lens of the south-end of Rosebery.

Method of Study

The French Chaixmeca heating/freezing stage was used in this study. The general method, procedure and calibration of the stage and heating/freezing experiments was reported elsewhere (e. g. Khin Zaw, 1984) and the methodology of the CO_2 bearing inclusions are applied as reported by Khin Zaw (1987b). For freezing runs, those very large inclusions with good visibility were studied. The precision and accuracy of the filling temperature measurements are better than ±1°C for heating and ±0.3°C for freezing.

Classification of Inclusion Types

The fluid inclusions in different minerals at the Rosebery mine can be essentially classified into the following major types based on the phases observable in the inclusions at room temperature:

Type I: Two-phase, solitary, liquid and vapour inclusions with no appreciable CO_2

Type II: CO_2-H_2O mixed inclusions which may contain unidentified daughter mineral phases; type II can be subdivided into two types: A) as trails and B) as clusters

Type III: Multiphase inclusions which contain CO_2-liquid, H_2O-liquid and vapour with or without unidentified daughter minerals.

Type IV: Two-phase, liquid-rich inclusions with variable liquid and vapour ratio.

Fluid inclusions were also classified in a temporal sense as primary, secondary and pseudosecondary relative to the time of trapping as defined by Roedder (1984). The fluid inclusion characteristics in different minerals from the Rosebery deposit are shown in Fig. 21. All types of inclusions are found in quartz as quartz occurs in different generations and provide as a best mineral recording the different fluid compositions existed throughout the entire geological history of the deposit.

*Fig. 21. **A**. Two-phase, liquid and vapour type I inclusion in quartz, horizontal is 10 μm. **B**. Negative-shaped mixed CO_2-H_2O type II inclusion with two unknown daughter minerals (D) in helvite, horizontal bar is 10 μm. **C**. CO_2-liquid bearing type III inclusion in fluorite, horizontal bar is 10 μm. **D**. CO_2-liquid bearing type III inclusion with two unknown daughter minerals (D) in fluorite, horizontal bar is 10 μm.*

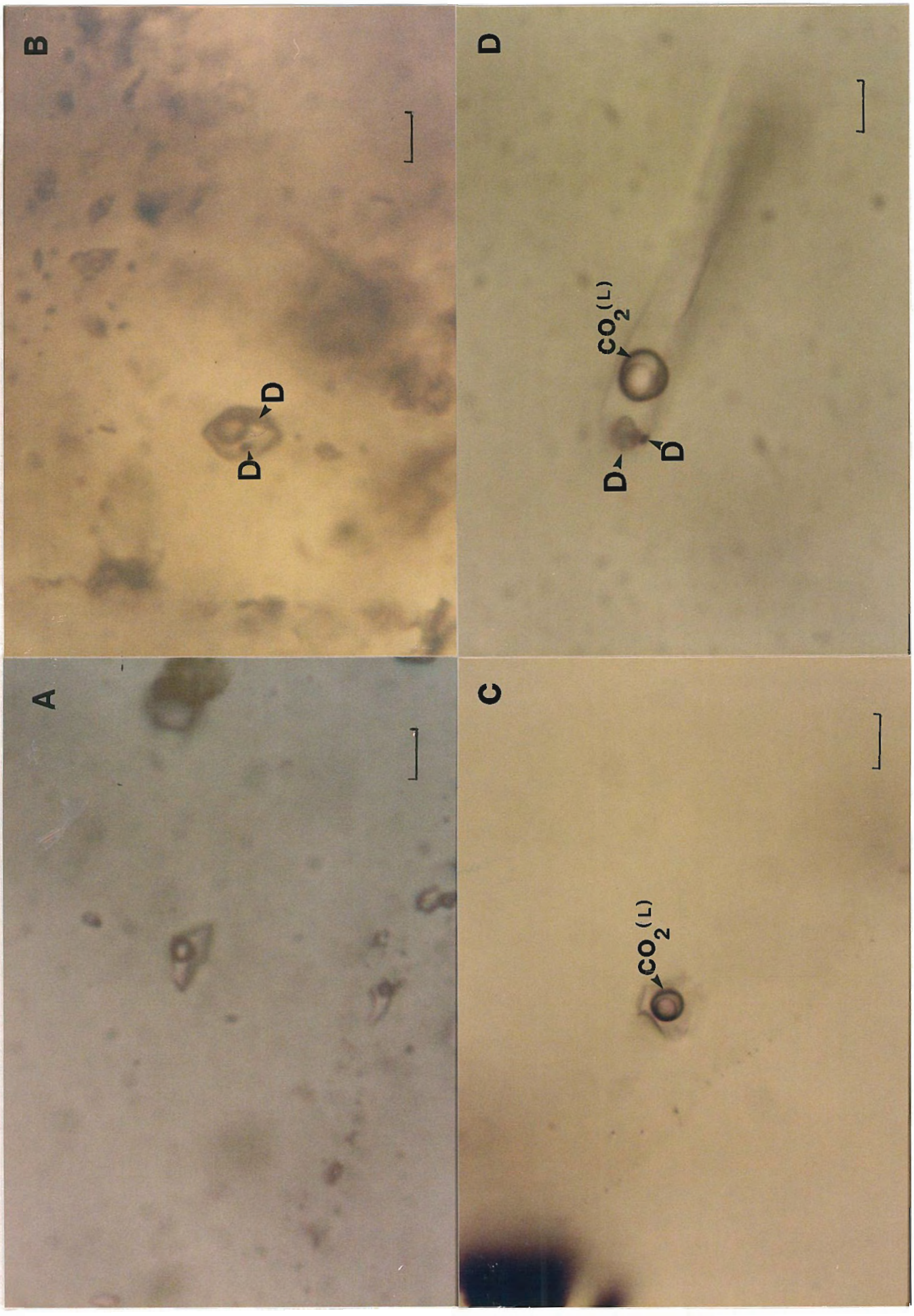
A
B
D
D
C
CO_2 (L)
D
CO_2 (L)
D
D

Type I Inclusions

The type I two-phase, solitary, liquid and vapour inclusions are commonly found in the quartz (Fig. 21A). The type I inclusions appear to be the earliest inclusions type as they are isolated, sometimes negative in shape and away from healed fractures and cross-cut by other inclusion types. The type I and type II mixed CO_2-H_2O inclusions are seen in a quartz sample collected from the footwall of G lens, 17 Level. The quartz is associated with sulphides (sphalerite, galena and chalcopyrite) and carbonates as shown in the Fig. 22 and the solitary type I inclusions are found surrounded by trails of type II inclusions. The type I inclusions are also found in the quartz from the quartz±carbonate veins in the Cu-rich chloritic footwall. Barite samples collected from the H lens also contain type I inclusions but the genetic relation between the inclusions in the quatrz and barite is not solved yet.

Type II Inclusions

Type II inclusions are CO_2-H_2O mixed inclusions and the most abundant inclusion type at the Rosebery mine. Helvite from the biotite-magnetite±chalcopyrite zone of Devonian origin contains type II inclusions with unidentified daughter minerals (see Fig. 21B). Type II inclusions are found as clusters and also as trails. They show positive evidence of the presence of CO_2 as an appreciable amount. The quatrz in the quartz± carbonate veins in the chloritic footwall of the orebody and quartz from all the replacement zones contains type II inclusions.

The recrystallised, yellowish sphalerites associated with galena cubes in the cross-cutting late quartz± carbonate veins may contain trails of type II inclusions along healed fractures suggesting a secondary origin. NaCl crystals as a daughter phase were identified by microscopy in the fluid inclusions in the quartz from the biotite-magnetite zone of the F(J) lens but other daughter phases are not known yet.

Type III Inclusions

Type III inclusions contain CO_2-liquid, H_2O-liquid and vapour and are commonly found in the fluorite associated with tourmaline in the late quartz-tourmaline veins (Fig. 21C). These inclusions sometimes contain unidentified daughter minerals (see Fig. 23D). Type III inclusions are rarely found in the quartz from the other replacement zones. CO_2 liquid in the type III inclusions homogenised into the gas phase.

Type IV Inclusions

Type IV inclusions are two-phase, liquid-rich inclusions and found in all minerals studied. Their irregular shape with variable liquid and vapour ratio positively indicates a secondary origin and they are found cross-cutting all other inclusions types. The randomly distributed array of these secondary type IV inclusions and their textural features also suggest post- or syn-deformational shearing during their emplacement and these type IV inclusions are probably recrystallised from other earlier inclusion types during deformation.

Homogenisation Temperatures

Preliminary heating data are shown in Fig. 23A. Type I inclusions in quartz give a filling temperature range of 206.8°C-250°C with an exception of one inclusion (295.5°C). Type II inclusions mostly decrepitated as the internal pressure of CO_2 increases very rapidly during heating experiments. Homogenistion temperature of the inclusions in quartz varies from 279°C (decrepitated) to 320°C whereas the type II inclusions in helvite gave a filling temperature range of 326°C-330°C. Type I inclusions give a mode of 240°C whereas a mode of 340°C was recorded for the type II inclusions (see Fig. 23A). The $ThCO2_{(L-V)-V}$ of the type III inclusions gave a filling temperature range of 13.9°C-27.0°C with a mode of 22.0°C (Fig. 23B).

Salinity Data

Preliminary results of salinity data are shown in Fig. 23C. the salinity of the type I inclusions in quartz from the biotite-magnetite zone gave 7.3 NaCl equiv. wt %. As the type II mixed CO_2-H_2O inclusions show evidence of chalthration, the decomposition temperature of the chalthrate (T_e) was used for the salinity data. The type II inclusions gave a range of salinity 16.2-18.9 NaCl equiv. wt %. The type II inclusions which contain NaCl daughter minerals yielded 29-37.3 NaCl equiv. wt %.

Discussion

This preliminary fluid inclusions study indicates that the hydrothermal fluids associated with Devonian replacement was CO_2 bearing brines. This composition is comparable with Devonian granitoid intrusions below the Rosebery orebody. Trend or changes of the fluid composition with time are yet to be studied.

Preliminary studies also indicate that no fluids which can be unequivocally ascribed to the Cambrian exhalative fluids was observed. However, it is tempting to deduce that the early type I fluid inclusions with filling temperatures of ≥240°C and salinity < 10 NaCl

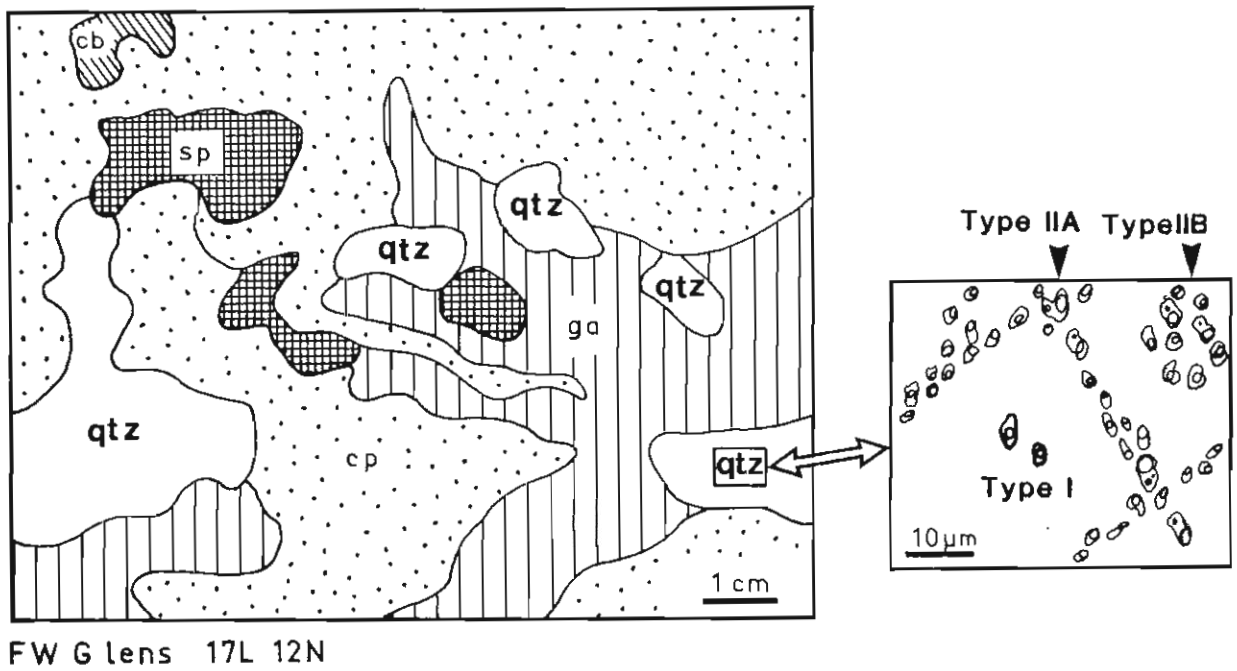

Fig. 22. A sketch showing textural details of type I, and type IIA and type IIB inclusions in quartz from the footwall of G lens, Rosebery. Note that type I inclusions are surrounded by trails of type IIA inclusions.

equiv. wt % with no appreciable CO_2 may represent primary exhalative fluids that have survived the Devonian recrystallisation. Ripley and Ohmoto (1977) demonstrated that primary exhalative fluids was recognisable in fluid inclusions from the strongly metamorphosed Raul mine, Peru.

ACKNOWLEDGEMENTS

The author would like to thank Dr. Ross Large for reading the report. The author is indebted to R. Large and D. Huston for stimulating discussions. Special thanks are due to geologists at the Rosebery mine: G. Iliff, J. Farquar, I. Gordon, and I. Matheson for logistical supports and June Pongratz for drafting the diagrams.

REFERENCES

Barton, P.B., Jr., and Toulmin, P. III, 1966, Phase relations involving sphalerite in the Fe-Zn-S system: ECON. GEOL., v. 61, p.815-849.

Barton, P. B., and Skinner, B. J., 1979, *in* Barnes, H. L., ed., *Geochemistry of hydrothermal ore deposits* , 2nd ed., New York, John Wiley & Sons. p. 278-403.

Brathwaite, R. L., 1969, The geology of the Rosebery ore deposits: Unpub. Ph. D. thesis, University of Tasmania.

Brathwaite, R. L., 1974. The Geology and origin of the Rosebery ore deposit, Tasmania: ECON. GEOL., v. 69, p. 1086-1101.

Bristol, C. C., 1974, Sphalerite geobarometry of some metamorphosed orebodies in the Flin Flon and Snow Lake districts, Manitoba: Canadian Mineralogist v. 12, p. 308-315.

Bristol, C. C., 1979, Application of sphalerite geobarometry to ores from the Ruttan Mine: ECON. GEOL., v. 74, p. 1496-1503.

Brown, P. E., Essene, E. J., and Kelly, W. C., 1978, Sphalerite geobarometry in the Balmat-Edwards district, NewYork: Am. Mineralogist, v. 63, p.250-257.

Burton, C. C. L., 1975, Rosebery, Hercules and Mt. Farrell mines *in* Knight, C. L., ed., *Economic geology of Australia and Papua New Guinea, I. Metals* : Melbourne, Australian Inst. Mining Metallurgy, Mon. 5, p. 619-626.

Campbell, F. A., Ethier, V. G., 1983, Environment of deposition of the Sullivan orebody: Mineral. Deposita, v. 18, p. 39-55.

Craig, J. R., Ljokjell, P., and Vokes, F. M., 1984, Sphalerite compositional variations in sulphide ores of the Norwegian Caledonides: ECON. GEOL., v. 79, p. 1727-1735.

DeWitt, D. B., Essene, E. J., 1974, Sphalerite geobarometry applied to Grenville marbles (abstr.)., Geol. Soc. America Abstr. with Programs 6, p. 709-971.

Ethier, V. G., Campbell, F. A., Both, R. A., and Krouse, H. R., 1976, Geological setting of the Sullivan orebody and estimates of temperature and pressure of metamorphism:

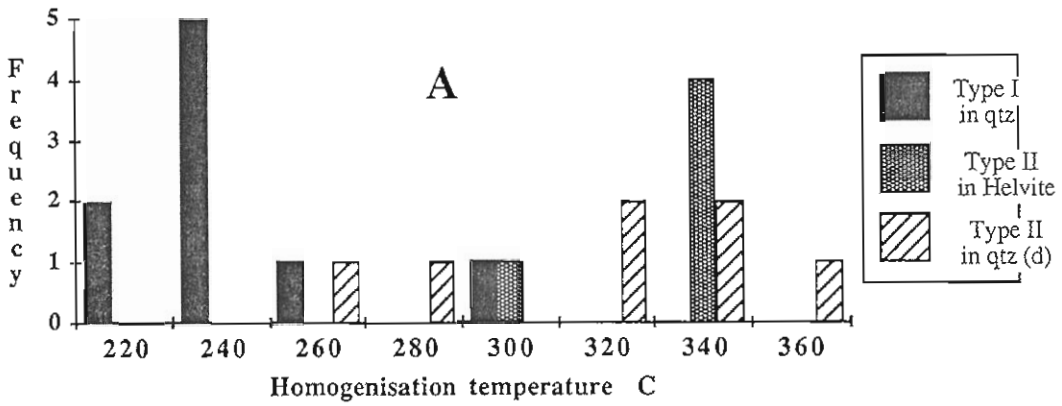

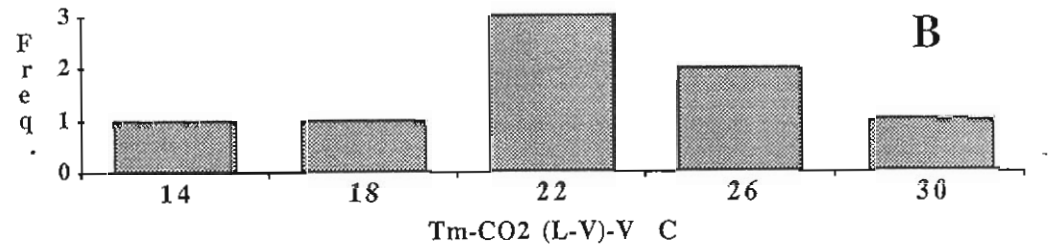

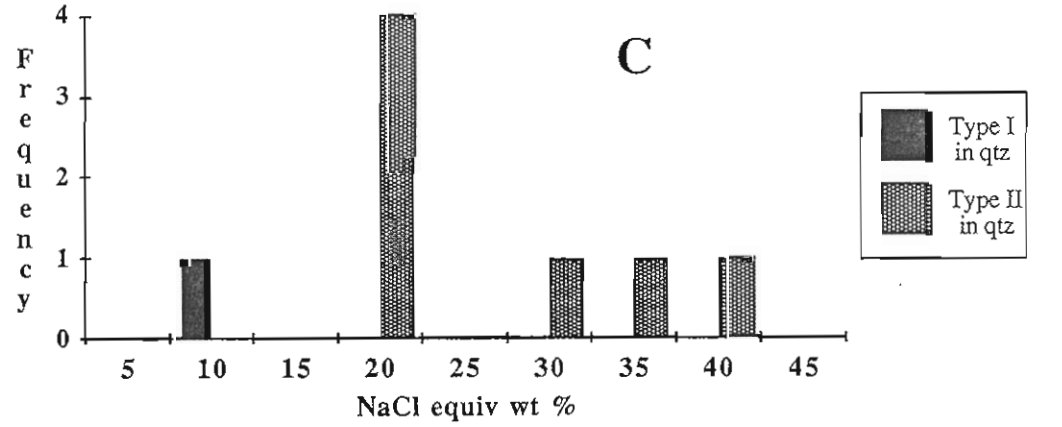

Fig. 23. A. Frequency distribution of homogenisation temperature of type I and type II inclusions, F(J) lens, Rosebery, (d)=decrepitated. B. Frequency distribution of homogenisation temperature of CO_2-liquid $_{(L-V)-V}$ in the CO_2-liquid bearing type III inclusions, F(J), Rosebery. C. Frequency-salinity distribution of type I and type II inclusions, F(J) lens, Rosebery.

ECON. GEOL., v. 71, p. 1570-1588.

Green, G. R., Solomon, M., and Walshe, J. L., 1981, The formation of the volcanic-hosted massive sulfide deposit at Rosebery, Tasmania: ECON. GEOL., v. 76, p. 304-338.

Green, G. R., 1983. The geological setting and formation of the Rosebery volcanic-hosted massive sulphide orebody, Tasmania: Unpub. Ph. D. thesis, University of Tasmania.

Groves, D. I., Binns, R. A., Barrett, F. M., and McQueen, K. G., 1976, Application of sphalerite geobarometry and sulfur isotope geothermometry to ores of the Quemont Mine, Noranda, Quebec: ECON. GEOL ., v. 71, p. 949-963.

Hall, G., Cottle, V. M., Rosenhein, P. B., McGhie, R. R., and Druett, J. G., 1965, Lead-zinc ore deposits of Read-Rosebery in *Geology of Australian ore deposits* , ed., J. McAndrew, p. 485-489 (8th Commonwealth Mining and Metallurgical Congress: Melbourne; and the Australian Institute of Mining and Metallurgy: Melbourne).

Hannington, M. D., and Scott, S. D., 1988 in press, Sulfidation equilibria as guides to gold mineralisation in volcanogenic massive sulphides: manuscript submitted to ECON. GEOL.

Hekinian, R., Fevrier, M., Bischoff, J. L., Picot, P., and Shanks W. C., 1980, Sulphide deposits from East Pacific Rise near 21° N, Science: v.207, p. 1433-1444.

Huston, D. L., and Large, R. R., 1986, The distribution, mineralogy and geochemistry of precious metals in the north-end orebody, Rosebery Mine, Tasmania: manuscript submitted to Electrolytic Zinc Company of Australasia Company.

Huston, D. L., and Large, R. R., 1987, Precious metals in the Rosebery North-end orebody, Tasmania, Australia *in The Geological structure, Mineralisation and Economic of the Pacific Rim*, pp 199-203, Proceeding of Pacific Rim Congress 1987, Gold coast, Australia.

Huston, D. L., and Large, R. R., 1988 in press, The distribution, mineralogy and geochemistry of precious metals in the north-end orebody, Rosebery Mine, Tasmania, manuscript submitted to ECON. GEOL.

Huston, D. L., and Khin Zaw, Controls on the fineness and grain size of electrum in volcanogenic massive sulphide deposits: AMIRA Report, August, 1988.

Hutchison, M. N., and Scott, S.D., 1980, Sphalerite geobarometry applied to metamorphosed sulfide ores of the Swedish Caledonides and U.S. Appalachians: Norges Geol. Unders sokelse, no. 360 , p. 59-71.

Hutchison, M. N., and Scott, S.D., 1981, Sphalerite geobarometry in the Cu-Fe-Zn-S system: ECON. GEOL ., v. 76, p. 143-153.

Khin Zaw, 1976, The CanTung E-zone orebody, Tungsten, Northwest Territories: A major scheelite skarn deposit: Unpub. M. Sc. thesis, Queen's University, Kingston, Ontario.

Khin Zaw, 1984, Geology and geothermometry of vein-type W-Sn deposits at Pennaichaung and Yetkanzintaung propects, Tavoy township, Tenasserim Division, Southern Burma: Mineral. Deposita, v. 19, p. 138-144.

Khin Zaw, 1987a, Progress report on F lens metal zonation, Rosebery Mine: AMIRA Report, August 1987, p. 46-69.

Khin Zaw, 1987b, A preliminary fluid inclusion study on Tennant Creek deposit in Geology and Geochemistry of Gold-Copper Iron Oxide Systems Vol. 2, Tennant Creek Workshop, July 1987, University of Tasmania.

Large, R. R., Huston, D. L., McGoldrick, P., McArthur, G., Wallace, D., Carswell, J., Purvis, G., Creelman, B., and Ramsden, T., 1988 in press, Gold in western Tasmania, Manuscript submitted to Australian Institute of Mining and Metallurgy, Bicentennial Volume.

Lees, T., 1987, Geology and Mineralization of Rosebery-Hercules area, Tasmania, Unpub. M.Sc. thesis, Univ. of Tasmania.

Lees, T., 1988, The South Hercules ore deposit: Unpub. Report to Electrolytic Zinc Company of Australasia.

Lees, T., Khin Zaw, Large, R. R., Huston, D. L., 1988 in press, Economic geology of the Rosebery-Hercules area, western Tasmania, Aust. I. M. M. Spec. volume 13.

Lusk, J., Campbell, F. A., and Krouse, H. R., 1975, Application of sphalerite geobarometry and sulfur isotope geothermometry to ores of the Quemont mine, Noranda, Quebec: ECON. GEOL., v.70, p. 1070-1083.

McArthur. G. J., 1986. The Hellyer massive sulphide deposit, *in* Large, R. R., (ed), *The Mount Read Volcanics and Associated Ore Deposits* : symposium, Burnie, November, 1986, Programme with abstract, p. 11-20.

McLimans, R. K., Barnes, H. L., and Ohmoto, H., 1980, Sphalerite stratigraphy of the Upper Mississippi Valley zinc-lead District, Southwest Wisconsin: ECON. GEOL., v. 75, p. 351-361.

Mole, N. R., 1983, Sphalerite composition in relation to deposition and metamorphism of the Foss stratiform Ba-Zn-Pb deposit, Aberfeldy, Scotland: Mineral. mag., v. 47, p. 487-500.

Ringler, R. W., 1979, Sphalerite geobarometry of the Calloway Mine, Ductown, Tennessee: ECON. GEOL., v. 74, p. 937-942.

Ripley, E. M., and Ohmoto, H., 1977, Mineralogic, sulphur isotope, and fluid inclusion studies of the stratabound copper deposits at rhe Raul Mine, Peru: ECON. GEOL., v. 72, p. 1017-1041.

Roedder, E., 1984, Fluid Inclusion: Mineral. Soc. Amer. Reviews in Mineralogy 12, 644p.

Scott, S. D., 1973, Experimental calibration of the sphaletite geobarometer: ECON. GEOL., v.68, p.466-474.

Scott, S. D., 1976, Application of the sphalerite geobarometer to regionally metamorphosed terrains: Am. Mineralogist, v.61, p.661-670.

Scott, S. D., 1983, Chemical behaviour of sphalerite and arsenopyrite in hydrothermal and metamorphic environment: Mineral. mag., v. 47, p.427-435.

Scott, S. D., and Barnes, H. L., 1971, Sphalerite geothermometry and geobaromertry: ECON. GEOL., v. 66, p. 653-669.

Scott, S. D., Both, R. A., and Kissin, S. A., 1977, Sulphide petrology of the Broken Hill region, New South Wales: ECON. GEOL., v. 72, p. 1410-1425.

Shimizu, M., and Shimazaki, H., 1981, Application of the sphalerite geobarometer to some skarn-type ore deposit: Mineral. Deposita, v. 16, p. 45-50.

Stillwell, F. L., 1934. Observations on the lead-zinc ore at Rosebery, Tamania, Aust. I. M. M. Proc. No. 94: p. 43-67.

Styrt, M. M., Brackmann, A. J., Holland, H. D., Clark, B. C., Pisutha-Arnold, V., Eldridge, C. S., and Ohmoto, H., 1981, Earth Planet. Sci. Lett., v. 53, p. 382-390.

Solomon, M., Vokes, F. M., and Walshe, J. L., 1987, Chemical remobilization of volcanic-hosted sulfide deposits at Rosebery and Mt. Lyell, Tasmania: Ore Geology Reviews, v. 2, p. 173-190.

Sundblad, K., Zachrisson, E., Smeds, S.-A.,Berglund, and Alinder, C., 1984, Sphalerite geobarometry and arsenopyrite geothermometry applied to metamorphosed sulphide ores in the Swedish Caledonides: ECON. GEOL., v. 79, p. 1660-1668.

Urabe, T., 1974. Iron content of aphalerite coexisting with pyrite from some Kuroko deposits: Soc. Mining Geologists Japan. Spec. Issue 6, p. 377-384.

Willan, R. C. R., and Hall, A. J., 1980, Sphalerite geobarometry and trace-element studies on stratiform sulphide from McPhun's Cairn, Loch Fyne, Argyll, Scotland: Trans. Inst. Min. Metall., section B, v. 89, p. B31-B41.

Williams, K.L., 1960. Some less common minerals in the Rosebery and Hercules zinc-lead ores, Aust. I.M.M. Proc., No. 196: p. 51-60.

PARAGENESIS AND FLUID INCLUSIONS IN THE QUE RIVER FOOTWALL PRECIOUS METAL ZONE

Gregory W. Jenkins

INTRODUCTION

The precious metal zone (PMZ) at Que River is a zone of low grade galena-sphalerite--pyrite stringer mineralisation which contains anomalously high quantities of gold relative to base metals when compared to other areas of stringer mineralisation and to much of the massive sulphide ore. Barium, arsenic and antimony are also enriched in the PMZ (McGoldrick & Large, 1987). The PMZ occurs in the eastern footwall to PQ ore lens, in the northern parts of the mine.

Results presented in the previous report by McGoldrick & Large (1987) are summarized below.

1. The PMZ is best developed in a coarse pyritic polymict andesitic volcaniclastic with patches of distinctive white alteration.

2. The PMZ is part of the alteration zone about the hydrothermal system which produced the orebodies, occurring as distal parts of the Cu/ Pb-Zn/ Pb-Zn-Ag-Au-As-Sb zonation.

3.) The gold-bearing stringers are best developed in the more porous and permeable volcaniclastics.

4. Gold is not directly hosted by the white alteration.

5. The white alteration is a mixture of sphalerite and sericitized K feldspar.

6. The increase in $\partial^{34}S$ values from massive ore to the PMZ can be explained by variations in physico-chemical conditions of sulphide precipitation, or by increased mixing of seawater and hydrothermal fluid away from the main vent.

7. Gold precipitation was not necessarily caused by boiling, but the possibility should not be excluded.

This report briefly examines the mineralogy and paragenesis at Que River with a view to determining which fluid inclusions in which minerals will yield meaningful values of fluid composition and temperature, in order to further define the conditions of gold transport and precipitation.

SUMMARY AND CONCLUSIONS

1. A recognisable paragenetic sequence exists in the PMZ in spite of metamorphic overprinting. This sequence can be used to determine the time of formation of fluid inclusions of hydrothermal origin. The inclusions can then be used to determine conditions in and about the orebodies, stringers and PMZ.

2. Fluid inclusions of metamorphic origin may be easily distinguished from those of hydrothermal origin.

3. Quartz is the host mineral to fluid inclusions of hydrothermal origin which are most likely to give meaningful results. The effects of deformation during metamorphism have been taken up by microfracturing of the quartz grains with trapping of recognisable secondary inclusions, rather than by ductile deformation of the quartz which could have altered the original inclusions. No fluid inclusions of undoubted hydrothermal origin have been observed in sphalerite. The presence of very fine grained sphalerite in K feldspar in areas of white alteration makes the K feldspar too cloudy for accurate measurements to be made on any inclusions it may contain.

4. It is desirable, but not essential, to know the pressure of the fluids at the time of inclusion trapping, in order to apply the necessary correction to the measured homogenization temperatures. It is not necessary to know the pressure if only relative temperatures across the hydrothermal system are required.

5. The possibility that boiling occurred remains open, but it will be difficult to prove boiling unless the depth of water at the time of hydrothermal activity is known accurately.

COMMENTS ON WHITE ALTERATION

The white colour is simply due to reflection and dispersion of light from the boundaries of sphalerite grains up to 10 μm in size surrounded by K feldspar. The K feldspar is extensively sericitized, but the sericite is not responsible for the white appearance. It is most likely that the sphalerite and its surrounding K feldspar formed at the same time.

PARAGENESIS

A paragenetic sequence is recognisable from textural features of the PMZ stringers in spite of metamorphic effects. The textural features of galena will not be discussed because of the fact that its ductility under metamorphic conditions would have produced gross changes in its original textures. Paragenetic stages relevant to the PMZ were as follows:

(1) Precipitation of pyrite, sphalerite and, presumably, galena and tetrahedrite.

(2) Coprecipitation of sphalerite and K feldspar to produce white alteration.

Sphalerite and white alteration are crosscut by later veins. It is uncertain whether the coarser sphalerite and the sphalerite/K feldspar intergrowths were produced synchronously. The fact that white alteration patches sometimes appear to emanate from veins supports the idea that the white alteration postdates the coarse sphalerite.

(3) Several episodes of pyrite±quartz veining occurred next. The earliest veins are characterized by fine grained (≈10-50 μm) quartz and pyrite, and later veins by coarser grainsizes (≈50-500 μm). Frequently, the quartz grains in veins are subhedral to euhedral and prismatic in shape, and have inclusions of varying types outlining planes of growth; these quartz crystals are interpreted as having grown into open cavities which would have been channels for hydrothermal solutions.

The earlier veins sometimes contain sphalerite in addition to pyrite and quartz.

Areas of white alteration which are crosscut by veins sometimes display silicification extending into and partly replacing them with 50-100 μm quartz grains occurring along hemispherical surfaces. This produces a thrombolitic, or clotted, texture visible in hand specimen.

During all the episodes of pyrite±quartz veining, earlier clear to mauve sphalerite was progressively replaced. The parts of sphalerite grains near the boundaries with other minerals have a darker mauve colour grading to black at the very edges of the sphalerite grains; this is due to 0.1 μm inclusions of an unidentified mineral, which increases in concentration towards the outer boundaries of the sphalerite grains. The minute inclusions also occur about microfractures which extend into the sphalerite. It is likely that the solid inclusions are a form of chalcopyrite disease caused by chalcopyrite exsolution during sphalerite replacement. A similar texture in sphalerite from a Kuroko deposit is described by Barton (1978).

(4) In the final stages of hydrothermal activity, carbonate and barite filled the remaining cavities.

It is not yet known with certainty at what stage, or stages, gold was precipitated, but it is most likely that it is associated with at least some of the pyrite±quartz veining. It will be necessary to define the mineralogical associations of the gold in order to confirm this.

METAMORPHIC OVERPRINT

Metamorphism to prehnite-pumpellyite facies (Whitford, 1984) during Devonian time produced the following effects:

(1) Recrystallization of some of the sphalerite, to produce sphalerite with an amber colour. Higher iron content produced patches of darker amber to opaque sphalerite. The clear to mauve sphalerite does not show these effects, implying that at least some of it was not recrystallized.

(2) The galena, being ductile under high pressure, was rearranged texturally.

(3) Pervasive microfracturing of the more brittle minerals occurred. Microfractures occur within grains and extend across grain boundaries. Most of the quartz was fractured rather than undergoing ductile deformation.

(4) Most of the pyrite was recrystallized to produce coarse euhedral grains.

(5) Some of the quartz was recrystallized, becoming clear and free of inclusions. This quartz is usually strained, displaying undulose extinction.

(6) Phyllosilicates in areas of higher stress were realigned to a preferred orientation. Most of the sericite of hydrothermal origin was probably affected in some way by the metamorphism, even though no preferred orientation is visible in most places.

FLUID INCLUSIONS

The aim of studying fluid inclusions in this system is to deduce temperatures, pressures and compositions of the fluids in various parts of the system at certain times, particularly during gold precipitation. It is also desirable to determine whether any boiling occurred.

In order to derive meaningful results from fluid inclusion studies, it is obviously necessary to distinguish between fluid inclusions formed at different times. In the present case, it is particularly important to recognise and ignore the fluid inclusions produced as a result of metamorphism. Such fluid inclusions, unfortunately, are preserved in far greater abundance than those produced by the hydrothermal processes. However, it is possible

to recognise fluid inclusions of metamorphic origin by the following characteristics:
(1) They are usually 10 μm or less in size.
(2) They have a high (≈90:10) liquid:vapour ratio, i.e. the vapour bubble is small.
(3) They occur in surfaces, sometimes planar, of fluid inclusions which crosscut the growth planes of the minerals and usually extend across grain boundaries. In quartz, the surfaces containing inclusions are usually slightly curved due to the conchoidal fracture of the mineral.

Preliminary temperature measurements were made on a few of these inclusions from section 7700N in the PMZ. Homogenization temperatures were in the range of 145° to 191°C (Fig.1). Application of a correction for 2 kb pressure (within the range of prehnite-pumpellyite metamorphism) gives temperatures of inclusion formation and trapping of 300° to 350°C (Roedder, 1984, fig. 9-6), also within the range of prehnite-pumpellyite metamorphism. This supports a metamorphic origin for the inclusions.

Fluid inclusions in quartz which will give usable results, that is, those inclusions trapped during hydrothermal activity, have the following characteristics:
(1) They have a lower liquid:vapour ratio than inclusions of metamorphic origin.
(2) They are isolated rather than occurring in large numbers along recognisable surfaces.
Alternatively, they occur as planes of small inclusions trapped along recognisable growth planes of quartz crystals, particularly coarse euhedral quartz, or they are trapped at the bases of quartz overgrowths.

No measurements have been made on the relatively scarce inclusions of hydrothermal origin, pending the arrival of more modern and accurate measuring equipment. Homogenization temperatures are expected to differ markedly from those of metamorphic inclusions, as the liquid:vapour ratios of the hydrothermal fluid inclusions are lower.

Because of the recrystallization of much of the sphalerite during metamorphism, and because of its tendency to fracture readily along cleavage planes, no inclusions of definite hydrothermal origin have been observed at this stage. Fluid inclusions in barite have not yet been examined. A few fluid inclusions occur in the K feldspar of the white alteration, but the opacity induced by the fine grained sphalerite makes it impossible to measure their characteristics at different temperatures.

When the mineralogical associations of gold have been defined, the fluid inclusions in coprecipitated vein quartz will be examined to determine temperature differences across the orebodies and PMZ.

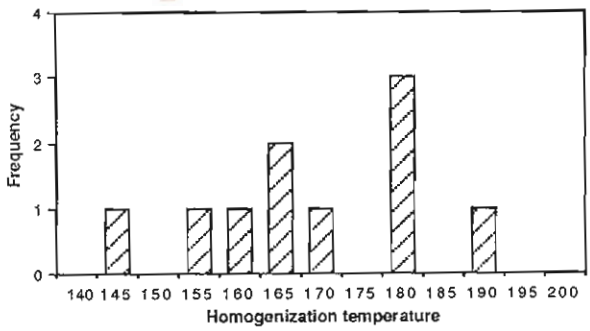

Figure 1 Temperatures of homogenization of fluid inclusions of metamorphic origin in vein quartz from the precious metal zone at Que River.

PRESSURE CORRECTIONS

The temperature of homogenization of a fluid inclusion does not necessarily correspond to the temperature at which it was formed, due to the effects of pressure; it is necessary to apply a correction to compensate for this. Measurements of fluid inclusion behaviour at low temperatures can give enough information to deduce the salinity, and hence density, of an inclusion. Combining this information with the homogenization temperature of the inclusion defines a straight line in the P-T plane (Roedder, 1984). If the pressure at the time of trapping of the inclusion is known, the temperature at that time can be defined. That is, an independent geobarometer or geothermometer is required to exactly define the conditions of inclusion trapping. If this is not possible, the temperature of formation can only be absolutely defined within certain limits.

This will not present problems for the present study where only relative temperatures across the orebodies and alteration halo are required, assuming no major variations (more than several tens of bars) in pressure within the system.

As the hydrothermal vents discharged to the sea floor, it is probable that the pressure in the system was not much higher than the water pressure at the sea floor. However, if the water depth was 10 km, or about the depth of present day oceanic trenches, the pressure at the sea floor would have been approximately 1kb, necessitating a substantial (several tens of °C or more) positive correction to the homogenization temperatures of fluid inclusions formed in the sea floor hydrothermal

system. It is most likely, although not proved, that the water depth was considerably less; Corbett & Solomon (1988) suggest that parts of the Mt. Read Volcanics may have erupted subaerially, in which case nearby water depths were unlikely to have been much more than one or two kilometres. The pressure correction needed in this situation, and the possible errors, are much more reasonable.

BOILING IN THE PRECIOUS METAL ZONE

The possibility that boiling in the PMZ may have caused gold precipitation can be investigated using fluid inclusions. Two indicators of boiling are available.

In the first situation, which is rarely observed in nature, but proves boiling beyond doubt, liquid-rich and vapour-rich inclusions which can be shown to have formed at the same time homogenize to liquid and vapour respectively at the same temperature. This proves the coexistence of a liquid phase and a vapour phase, caused by boiling, at the time of trapping of the inclusions (Roedder, 1984).

The second way to prove boiling using fluid inclusions is to demonstrate that the pressure and temperature at the time of inclusion trapping were such that boiling must have occurred, using P-T data for boiling such as presented by Haas (1971). For this, an independent geothermometer or geobarometer, or an accurate estimate of water depth assuming a hydrothermal system at about sea floor water pressure, is needed. None of these is available at present.

Liquid-rich and vapour-rich inclusions of the same generation have been observed in a few grains of quartz. Measurement of their homogenization characteristics will determine whether this is due to boiling, or simply to necking down of larger inclusions.

REFERENCES

Barton, P.B. (1978). Some ore textures involving sphalerite from the Furutabe Mine, Akita Prefecture, Japan. *Mining Geol.*, 28, 293-300.

Corbett, K.D., & Solomon, M. (1988). Cambrian volcanism and mineral deposits. *in* Burrett, C., & Martin, E. (eds.) *The geology and mineral resources of Tasmania*. Geol. Soc. Aust., Tas. Div., Special Publication (in press).

Haas, J.L. (Jr.) (1971) The effect of salinity on the maximum thermal gradient of a hydrothermal system at hydrostatic pressure. *Econ. Geol.*, 66, 940-946.

McGoldrick, P.J., & Large, R.R. (1987) Final report on the footwall precious metal zone, Que River. AMIRA Project 84/P210, *Controls on gold and silver grades in volcanogenic massive sulphide deposits*. 2nd Annual Report, 9-45.

Roedder, E. (1984) Fluid inclusions. Mineralogical Society of America, *Reviews in Mineralogy*, 12, 644pp.

Whitford, D.J. (1984) Geochemistry of alteration of the Que River orebodies." *in* Baillie, P.W., & Collins, P.L.F. (eds.) *Mineral exploration and tectonic processes in Tasmania*. Geol. Soc. Aust., Tas. Div., Symposium, Burnie, 57-58.

SULPHUR ISOTOPE STUDIES AT QUE RIVER

Peter McGoldrick

INTRODUCTION

Variations in the S isotopic signature of sulphide and sulphate minerals in an ore deposit may provide information about
1) the temperature at which the mineralisation formed
2) the source(s) of S in the deposit
3) the chemical conditions of, and mechanisms for ore deposition (Ohmoto and Rye, 1979).

Sulphur isotopic analyses of over 90 mineral separates from samples from the Que River deposit are presented here. Pyrites comprise the bulk of the data, but 13 base metal sulphide and eight barite separates were also analysed. The results have important implications for the ultimate source of S in the mineralsing fluid and the evolution of this fluid in the immediate ore-forming environment (ie. massive sulphide mound and underlying stringer zone).

RESULTS

Isotopic analyses for Que River mineral separates are presented in Table 1 and displayed on Fig. 1. Individual samples number 21 from the massive sulphide bodies, 25 from 'normal' stringer (the 'footwall' of PQ lens on 7550N section), 14 from the stringer zone to the west of P north lens and 16 from the Precious Metal Zone stringer. Samples of pyrite from stringer veins deep below the massive sulphide lenses, and sulphides from the fuchsite-carbonate breccia and dacite overlying the massive sulphide were also analysed.

The samples from the massive ores show the narrowest range of $\delta^{34}S$ values (18 of 20 sulphide separates between 5.3 and 8.9 ‰). 'Normal' and 'western' stringer sulphides range from 6.0 to 11.7 ‰ (33 out of 35 separates). Precious Metal Zone stringer sulphides have $\delta^{34}S$ values between 7.8 and 17.0 ‰. The separates from the dacite and fuchsite-carbonate breccia and, to a lesser extent, the deep stringer, have a much wider range of $\delta^{34}S$ values and will not be discussed further here. Eight barite separates have $\delta^{34}S$ of between 36.2 and 45.2 ‰.

DISCUSSION

In theory, the equilibrium fractionation of S between co-existing sulphide minerals is a powerful geothermometer. In practise, difficulties in proving equilibrium co-precipitation and/or obtaining pure mineral separates of the minerals of interest make the utility of S isotopes as indicators of the temperature of formation of mineralisation somewhat limited. No attempt to derive temperatures from the Que River data was made.

In contrast, the observed trend from lightest S in the massive ores to heavier S (and with a wider range) in stringer samples from the stratigraphic footwall of the massive ores has important implications for the origin of S in the deposit and the physio-chemical evolution of the mineralising fluid.

Sulphur Source

Equilibrium fractionation of S in pyrite relative to S in H_2S in a hydrothermal fluid above ~250°C is ≤+1‰ (Ohmoto and Rye, 1979). Therefore, at Que River the measured $\delta^{34}S$ values in pyrite will be within 1 ‰ of the $\delta^{34}S$ value of H_2S in their parent hydrothermal fluid (under equilibrium conditions at temperatures above about 250°C). Because pyrite from the massive ores displays a limited spread in $\delta^{34}S$ and has the lightest S in the Que River deposit, this S isotopic signature is thought to best approximate the $\delta^{34}S$ H_2S of the primitive (ie. least evolved) mineralising fluid. The presence of heavier S in sulphides from the stringer zone indicate that fluid $\delta^{34}S$ H_2S became heavier in response to processes operating at or near to the site of the footwall stringer zone (see below).

Given that the lightest pyrite S in the massive ores averages about +6 ‰ then +5 ‰ is a good estimate of the $\delta^{34}S$ H_2S of the primitive Que River mineralising fluid.

Before discussing the possible source for a 250°-350°C fluid with a $\delta^{34}S$ H_2S signature of +5 ‰ some discussion of magmatic S isotope variations is necessary. The $\delta^{34}S$ values of fresh mafic to ultramafic rocks and their primary sulphide minerals generally range from -1 to +2 ‰ (Ohmoto and Rye,1979; Sakai et al., 1984). The average values for acid igneous rocks, as well as the crust is 0 ± 3 ‰. These are essentially identical to

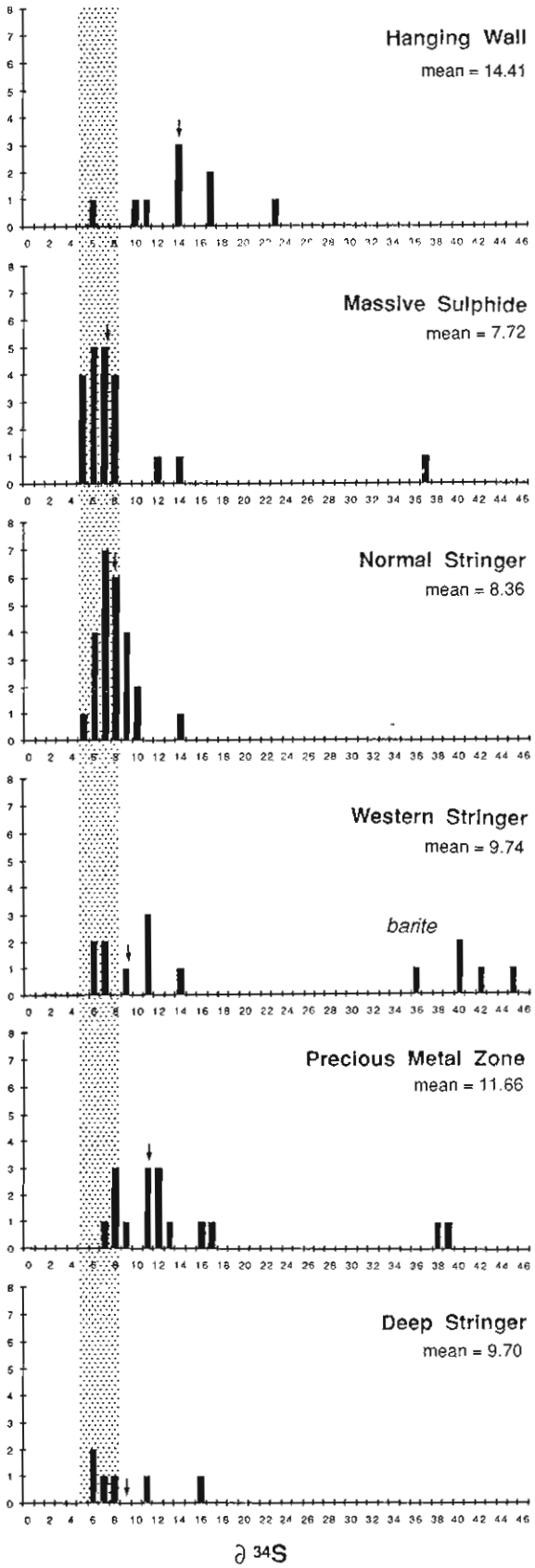

Figure 1 Frequency histograms showing $\delta^{34}S$ data from Que River. The stippling shows the main range for the massive sulphide. Mean values (arrows) are for sulphide samples only and do not include barite values.

those of mantle rocks. Thus it is likely that the volcanics beneath the Que River deposits had a primary S isotope signature of about zero and hence magmatic S leached by convecting solutions during water-rock interaction could not be the *only* S source for the primitive mineralising fluid.

Two possible explanations for this heavy S are:
1) an aqueous magmatic fluid provided some or all of the S in the primitive mineralising solution; *or*
2) a component of S with a heavy S isotopic signature was mixed with magmatic S during leaching of the underlying rocks; (seawater sulphate, or anhydrite precipitated from seawater would have been the source for this heavy S).

For magmatic fluids from basic magmas the $\delta^{34}S$ fluid = δ^{34} H_2S = ~$\delta^{34}S$ melt, while for intermediate and acid melts the fluid $\delta^{34}S$ may be up to ~3 ‰ heavier than the melt (Ohmoto and Rye, 1979, Fig. 10.6). During cooling of a magmatic fluid redox changes may cause fractionation between $\delta^{34}S$ H_2S and $\delta^{34}S$ fluid and produce $\delta^{34}S$ H_2S of upto about 7 ‰ heavier than the original magmatic signature. Hence cooled magmatic fluid could have been the primitive mineralising fluid at Que River. It should be noted however that magmatic solutions cannot produce solutions with $\delta^{34}S$ H_2S of much greater than 7 ‰ under normal redox conditions (Ohmoto and Rye, 1979, Fig. 10.7), hence cooled magmatic solutions could not have been the only S source in Que River mineralisation with $\delta^{34}S_i$ values ≥ ~8 ‰.

The alternative explanation for a heavy S signature in the primitive mineralising fluid is that small amounts of seawater sulphate were quantitatively reduced and mixed with magmatic S leached from rocks beneath the site of the Que River deposit during hot seawater-rock interaction. Although cool seawater contains large amounts of dissolved sulphate with a heavy S signature the retrograde solubility of anhydrite means that all this heavy S is removed from seawater at temperatures well below the 250-350°C temperature range necessary for seawater to form a pregnant hydrothermal solution. Hence, the heavy S source for the primitive fluid is probably previously precipitated anhydrite. Recent work (Shanks and Seyfried, 1987; Woodruff and Shanks, 1988) provides evidence that this process is responsible for the heavy S enrichment in some 'black smoker' vent fluids (cf. S in MORBs).

Fluid Evolution in the Ore-forming System

The presence of a wide range of $\delta^{34}S$ values in the stringer zone beneath the massive ore, and the observation that this S is heavier than S in the massive ores indicates that $\delta^{34}S$ H_2S in the mineralising fluid must have been evolving in both time and space to

Table 1 : Sulphur isotope data from Que River (all analyses conducted at the Central Science Lab University of Tasmania)

Dacites and fuchsite-carbonate altered breccia (hangingwall)

Sample#	Section	DDH	Depth (m)	Type	∂34Scdt
502722	7700	QR483	86.2	vein pyrite from dacite wedge	23.44
87-502691	7725	QR499	112.6	pyrite from dacite wedge	17.34
87-502688	7725	QR502	98.8	pyrite from dacite wedge	14.00
87-502679	7725	QR567	104.7	pyrite from western dacite	10.46
87-502669	7725	QR601	53.6	pyrite from fs-car bx	11.79
87-502669	7725	QR601	53.6	pyrite from fs-car bx	17.20
87-502669	7725	QR601	53.6	pyrite from fs-car bx	14.41
87-502669	7725	QR601	53.6	pyrite from fs-car bx	14.55
502735	7700	QR557	50.2	sphalerite from fs-car altd bx	6.51

Massive sulphide

Sample #	Section	DDH	Depth (m)	Type	d34Scdt
502962	7550	QR311	36.8	pyrite band in bms	6.82
502984	7550	QR405	61.6	f.g. sp-rich bms	5.43
502985	7550	QR277	80.0	sp>ga>py bms	5.34
502915A	7550	QR277	78.3	sp>ga>py bms	5.73
502915B	7550	QR277	78.3	pyrite in bms	6.28
502915C	7550	QR277	78.3	colloform pyrite in bms	6.29
502916A	7550	QR277	82.2	coarse pyrite in bms	12.76
502916B	7550	QR277	82.2	f.g. sp-rich bms	5.64
87-502665	7725	QR601	44.6	pyrite	7.81
87-502666	7725	QR601	48.2	pyrite	8.61
502702	7700	QR783	89.3	pyrite from Pnth posn (or W of)	7.52
87-502678	7725	QR567	83.1	pyrite from Pnorth position	14.93
87-502678	7725	QR567	83.1	sphalerite from Pnorth position	7.11
87-502676	7725	QR567	69.7	pyrite from W of P north	6.41
87-502676	7725	QR567	69.7	sphalerite from W of P north	8.46
87-502676	7725	QR567	69.7	pyrite from W of P north	6.93
502760	7300	QR004	146.7	pyrite from east of S lens	7.86
502765	7425	QR670	69.0	pyrite from S lens	8.92
502767	7425	QR670	84.6	pyrite from west of S lens	7.41
502856	7500	QR 720	4.1	pyrite from S lens	8.10
502702	7700	QR783	89.3	barite from Pnth posn (or W of)	37.32

Normal stringer sulphide

Sample#	Section	DDH	Depth (m)	Type	∂34Scdt
502902	7550	QR276	17.3	pyrite	9.47
502903A	7550	QR276	76.3	vein margin pyrite	9.03
502903B	7550	QR276	76.3	vein pyrite	7.42
502903C	7550	QR276	76.3	vein galena	9.41
502904A	7550	QR276	81.3	vein margin pyrite	8.66
502904B	7550	QR276	81.3	vein sphalerite	6.47
502904C	7550	QR276	81.3	vein centre sphalerite	8.50
502908A	7550	QR278	56.8	pyrite	9.52
502908B	7550	QR278	56.8	sphalerite	6.52
502906	7550	QR278	43.3	pyrite	7.79
502914A	7550	QR277	62.5	coarse pyrite	6.67
502914B	7550	QR277	62.5	fine pyrite	10.30
502911A	7550	QR278	79.0	coarse vein pyrite	14.54
502911B	7550	QR278	79.0	disseminated pyrite	8.90
502912	7550	QR277	40.5	pyrite	8.52

Table 1 : Sulphur isotope data from Que River (all analyses conducted at the Central Science Lab University of Tasmania)

Sample#	Section	DDH	Depth (m)	Type	∂34Scdt
502926	7550	QR312	25.8	massive pyrite	7.07
502927	7550	QR312	28.5	massive pyrite	6.37
502929A	7550	QR312	34.0	coarse pure pyrite	7.42
502929B	7550	QR312	34.0	coarse pyrite	7.09
502988	7550	QR311	26.8	massive pyrite	8.42
502958A	7550	QR311	4.0	vein margin pyrite	10.94
502958B	7550	QR311	4.0	vein sphalerite/galena (4:1)	7.92
502981A	7550	QR405	31.1	pyrite	8.51
502981B	7550	QR405	31.1	pyrite	7.38

Western stringer sulphides

Sample#	Section	DDH	Depth (m)	Type	∂34Scdt
502711	7700	QR492	141.3	pyrite from W of Pnorth	7.53
502714	7700	QR483	143.7	coarse pyrite from W of Pnorth	7.51
87-502689	7725	QR502	144.4	pyrite from mineralized vc	11.78
87-502687	7725	QR605	73.7	pyrite "balls" from vc	11.08
87-502677	7725	QR567	75.5	pyrite	6.78
87-502677	7725	QR567	75.5	sphalerite	6.80
87-502693	7725	QR499	150.1	pyrite	11.78
87-502692	7725	QR499	136.0	pyrite	9.40
87-502724	7800	QR793	80.9	pyrite	14.95
87-502724	7800	QR793	80.9	barite	45.21
502743	7700	QR557	109.3	barite	42.18
502732	7700	QR483	176.0	massive barite	40.03
87-502693	7725	QR499	150.1	barite	36.18
87-502689	7725	QR502	144.4	barite from mineralized vc	40.55

Precious metal zone sulphides

Sample #	Section	DDH	Depth (m)	Type	∂34Scdt
502687	7700	QR783	2.40	disseminated pyrite	11.92
502689	7700	QR783	5.75	pyrite	17.04
502692	7700	QR783	36.10	pyrite	13.82
502700	7700	QR783	80.90	pyrite	16.54
502681	7700	QR632	67.50	pyrite	7.75
87-502696	7725	QR604	15.50	pyrite	12.17
87-502697	7725	QR604	75.00	pyrite (W of fold axis?)	8.59
87-502703	7725	QR801	15.80	pyrite	8.88
87-502705	7725	QR801	34.80	pyrite	12.76
87-502706	7725	QR801	35.40	pyrite	11.95
87-502709	7725	QR801	65.10	pyrite	8.30
87-502698	7725	QR740	10.00	pyrite	12.80
87-502694	7725	QR703	36.80	pyrite	11.67
18-4-86-3	7730	5250	8 level	diss. pyrite (u/g sample)	9.06
87-502698	7725	QR740	10.00	barite	38.24
87-502694	7725	QR703	36.80	barite	39.72

Deep stringer sulphide

Sample#	Section	DDH	Depth (m)	Type	∂34Scdt
502654A	7525	QR87	450.2	pyrite	6.24
502654B	7525	QR87	450.2	pyrite	8.71
502655	7525	QR87	473.0	pyrite	16.94
502656	7525	QR87	490.0	pyrite	6.79
502645	7537.5	QR35	313.6	pyrite stringer in ?andesite	7.82
87-502712	7725	QR801	87.9	pyrite from deep below PMZ	11.69

heavier values. Under equilibrium conditions at temperatures of around 250-300°C this could only happen if significant proportions of heavy seawater S were incorporated in the ore-forming fluid.

The heaviest S in stringer pyrite is from the Precious Metal Zone where $\delta^{34}S$ py ranges up to 17 ‰. Under reducing conditions ($H_2S >> SO_4^=$ in solution) fluid $\delta^{34}S$ is comparable to $\delta^{34}S$ H_2S and metal sulphide S isotope signatures will be similar to fluid $\delta^{34}S$. Hence H_2S dominant fluids could have $\delta^{34}S$ fluid as low as ~16 ‰ and still precipitate sulphide with $\delta^{34}S$ of 17 ‰. However, as solution conditions become more oxidised ($SO_4^=$ ~≥H_2S) then much heavier fluid S is required for equilibrium precipitation of metal sulphides with heavy $\delta^{34}S$.

Barite from the stringer zone has very heavy S (+36 to +42) ‰), which is much heavier than Cambrian seawater sulphate (~+30 ‰; Kaplan, 1975). This suggests that by the time the mineralising fluids became oxidised enough to precipitate barite that the fluid S had become dominated by S with a seawater isotopic signature.

Equilibrium fractionation between sulphate and sulphide at 250°C is about 22 ‰ (Ohmoto and Rye, 1979, Fig. 10.5). Hence sulphide minerals formed in equilibrium with barite having $\delta^{34}S$ of +39 ‰ should have $\delta^{34}S$ of +17 ‰ (c.f. the heaviest S in Precious Metal Zone pyrites!).

CONCLUSIONS

Sulphur isotope data from Que River indicate:

1) The end-member (most primitive) mineralising fluid had a $\delta^{34}S$ value of about +5 ‰.
2) A fluid with this signature could evolve directly by cooling a magmatic fluid formed in equilibrium with a melt having $\delta^{34}S$ of ~0 ‰.
3) Alternatively, if heated (250-350°C) seawater leached magmatic sulphides and small amounts of seawater-derived anhydrite from intermediate volcanics a fluid with $\delta^{34}S$ of ~+5 would be produced.
4) The heavy S in many samples from the stringer zone at Que River indicates the $\delta^{34}S$ fluid became much heavier as the primitive fluid moved through the stringer zone.
5) Seawater S was the source of this heavy S and by the time barite was precipitating fluid $\delta^{34}S$ may have approximated Cambrian seawater $\delta^{34}S$ (+30 ‰).

Figure 2 summarises the possible sources and evolution of S in the Que River mineralisation.

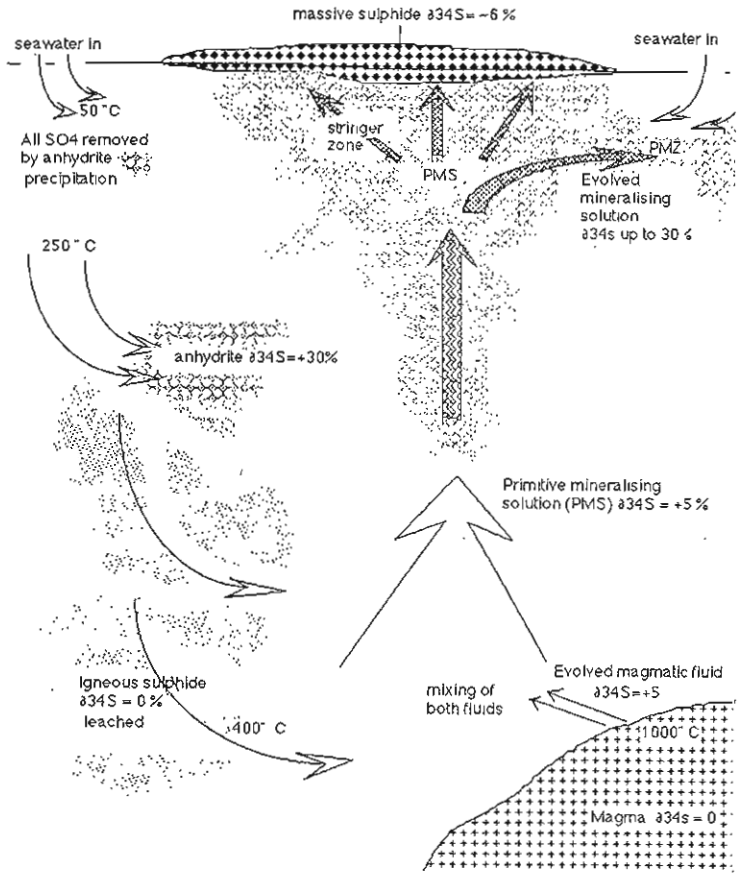

Figure 2 Diagrammatic sketch to indicate the possible sources of sulphur and isotope evolution in the Que River hydrothermal system.

REFERENCES

Kaplan, I.R. (1975) Stable isotopes as a guide to biogeochemical processes. *Royal Soc. London Proc.*, B189, 183-211.

Ohmoto, H., & Rye, R.O. (1979) Isotopes of sulfur and carbon *in* Geochemistry of hydrothermal ore deposits (Barnes, H.L., ed.) Wiley, New York, 509-567.

Sakai, H., Des Marais, D.J., Ueda, A., & Moore, J.G. (1984) Concentrations and isotope ratios of carbon, nitrogen and sulfur in ocean-floor basalts. *Geochim. Cosmochim. Acta*, *48*(12), 2433-2441.

Shanks, W.C.,III, & Seyfried, W.E.,Jr. (1987) Stable isotope studies of vent fluids and chimney minerals, southern Juan de Fuca Ridge: sodium metasomatism and seawater sulfate reduction. *in* Special section on The southern Juan de Fuca Ridge; hydrothermal fluids, sulfides and geophysical studies. *J. Geophys. Res.*, B, 92(11), 11387-11399.

Woodruff, L.G. & Shanks, W.C.,III (1988) Sulfur isotope study of chimney minerals and vent fluids from 21°N, East Pacific Rise: Hydrothermal sulfur sources and disequilibrium sulfate reduction. *J. Geophys. Res.*, B, 93(5), 4562-4572.

FINAL REPORT—BALCOOMA PROSPECT, NORTHERN QUEENSLAND

David L. Huston

INTRODUCTION

This section briefly summarises the previous AMIRA studies at Balcooma (Huston, 1986a, 1986b and 1987) and then concentrates on the distribution and occurrence of gold and silver in the massive sulphide.

SUMMARY

1. In the Balcooma deposit, gold has a strong association with copper in both copper-rich and zinc-lead-rich massive sulphide. In copper-rich mineralisation gold also has a strong association with bismuth. Mineralogically, gold occurs as 1-10 μm electrum grains in association with chalcopyrite, bismuth minerals and galena. The low gold grades at Balcooma are attributable to either: (1) an intermediate pH of the mineralising fluids at or near the swithchover from gold thio-complexes to gold chloro-complexes, or (2) low oxygen fugacity of the mineralising fluids.

2 Silver occurs as a trace element (~140 ppm) in chalcopyrite in copper-rich mineralisation while it occurs as a trace element in galena (~1200 ppm) in zinc-lead-rich mineralisation.

SUMMARY OF PREVIOUS STUDIES

Huston (1986) initially suggested the existance of multiple ore horizons at Balcooma. This has since been confirmed by detailed studies of structure and stratigraphy (Huston, 1987a and 1987b). The latest interpretation requires the presence of four–two major and two minor–ore-bearing horizons within a strongly deformed metapelite lens that lies in a sequence dominated by metagraywackes. The results of last year's drilling support the interpretation as two discrete alteration pipes or zones are recognized down section from the two major mineralised horizons (Fig. 1). Sulphur isotope data also indicates that pyrite grains from the lower zinc-lead horizon have slightly heavier sulphur (average $\partial^{34}S$ = 10.7 ‰) than those from the copper horizon (average $\partial^{34}S$ = 9.7 ‰). These data also support the interpretation that the two bodies of mineralisation lie at different stratigraphic horizons.

Studies of metal associations using company assay data (Huston, 1987) clearly show that gold is associated with copper throughout the prospect, whereas silver has two quite different associations: in copper-rich mineralisation it is associated with copper, but in zinc-lead-rich mineralisation it is assocaited with lead. The present report will extend these observations by describing the distribution and mineral associations of gold and silver in the massive ores.

METAL DISTRIBUTION IN THE MASSIVE ORES

Figures 2 and 3 illustrate the relationships between gold, silver, copper, lead and zinc for massive pyrite-chalcopyrite and massive pyrite-sphalerite-galena, respectively. Gold correlates best with copper in both types of mineralisation, but the correlation in massive pyrite-chalcopyrite is better than that in massive pyrite-sphalerite-galena.

Figures 4b and 4c illustrate this observation in the massive pyrite-chalcopyrite lens on section 8900mN. Gold and copper highs occur together within the lens; outside the massive lens both copper and gold grades fall dramatically which indicates that very little gold has been mobilised outside of the massive sulfide. Most of the higher (to 2000 ppm) lead (and, by inference, zinc) values also occur in the massive sulphide lens (Fig. 4d). This accounts for a lower, but still significant, correlation between gold and zinc in massive pyrite-chalcopyrite. In addition to the strong correlation with copper, gold also displays a strong correlation with bismuth in copper-rich mineralisation (Fig. 5).

Gold and copper also have a weak, but statistically significant, correlation in massive pyrite-sphalerite-galena mineralisation. In contrast, gold and zinc do not have a statistically significant correlation (Fig. 3). This correlation differs greatly from the observations made at Rosebery (Huston & Large, 1986) and Que River (Large & McGoldrick, 1986) where zinc and gold are strongly correlated in zinc-rich ore. Rather, the characteristic distribution of gold in both zinc-lead-rich and copper-rich mineralisation at Balcooma is more similar to the copper-gold association seen at the Archaean Scuddles deposit (Ruxton, 1987).

Silver has quite contrasting associations between the two types of massive sulphide. In massive pyrite-

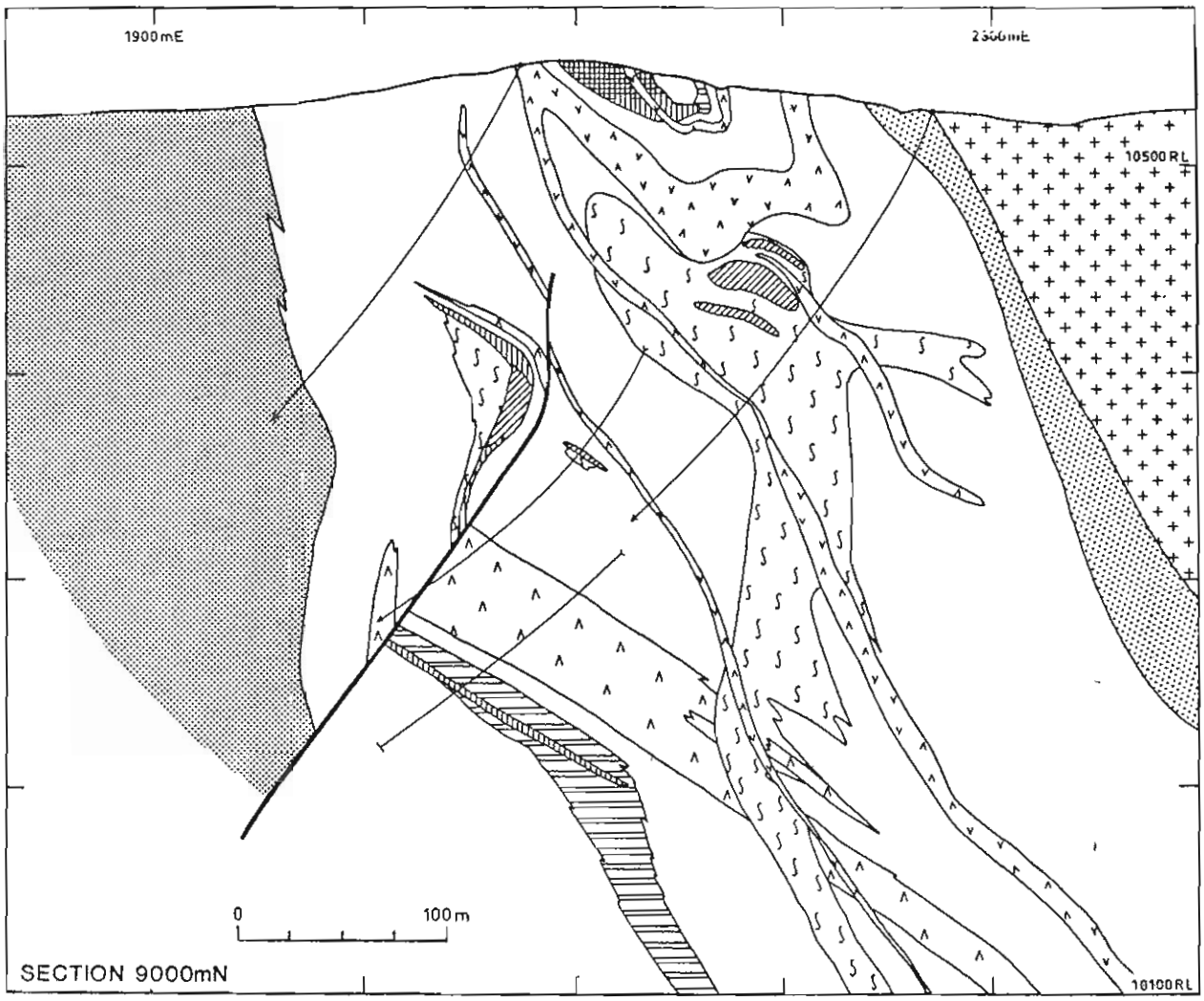

Figure 1 Geology of section 9000mN, Balcooma prospect.

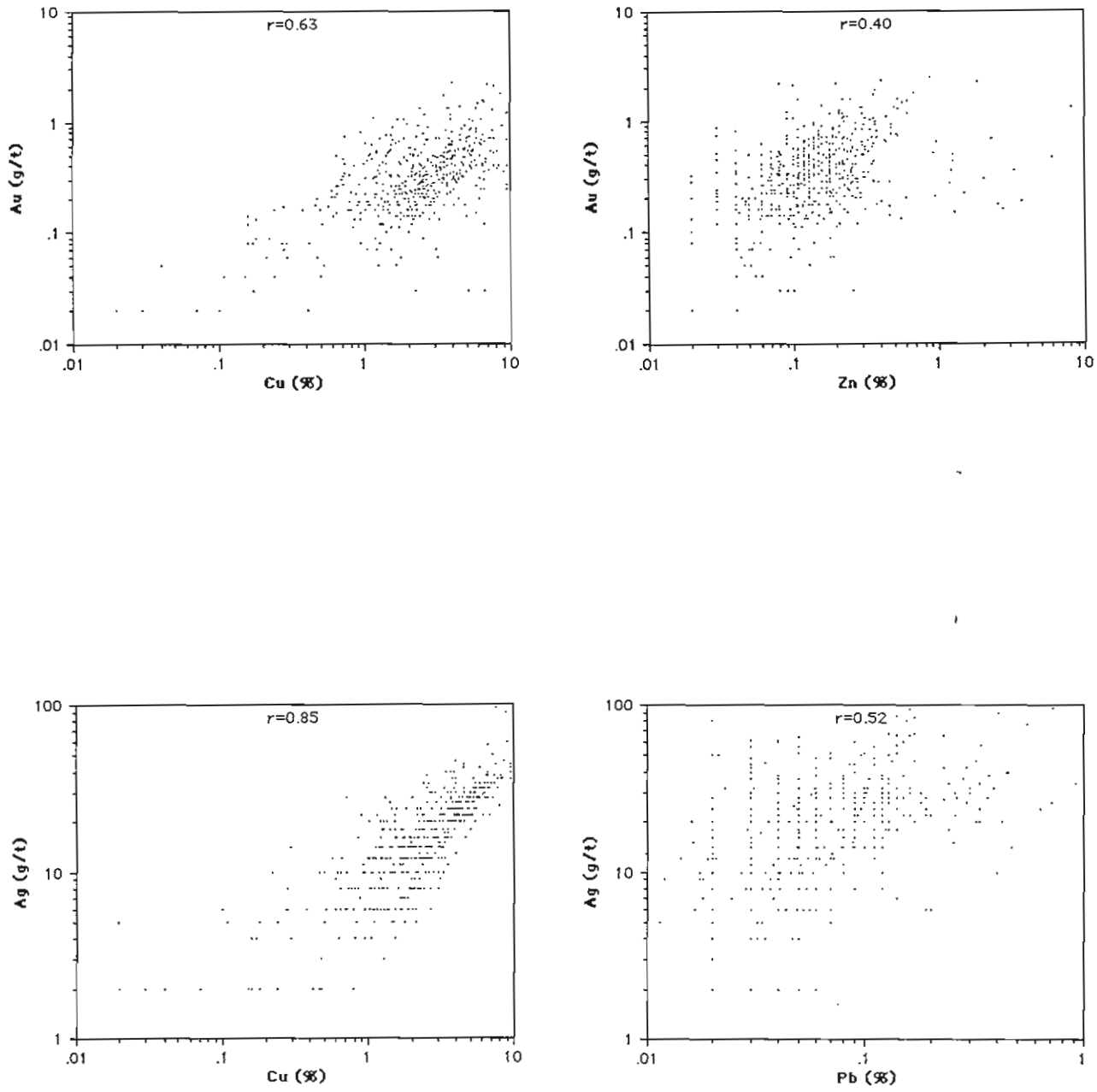

Figure 2 Relationships between base metals, gold and silver in massive pyrite-chalcopyrite mineralisation.

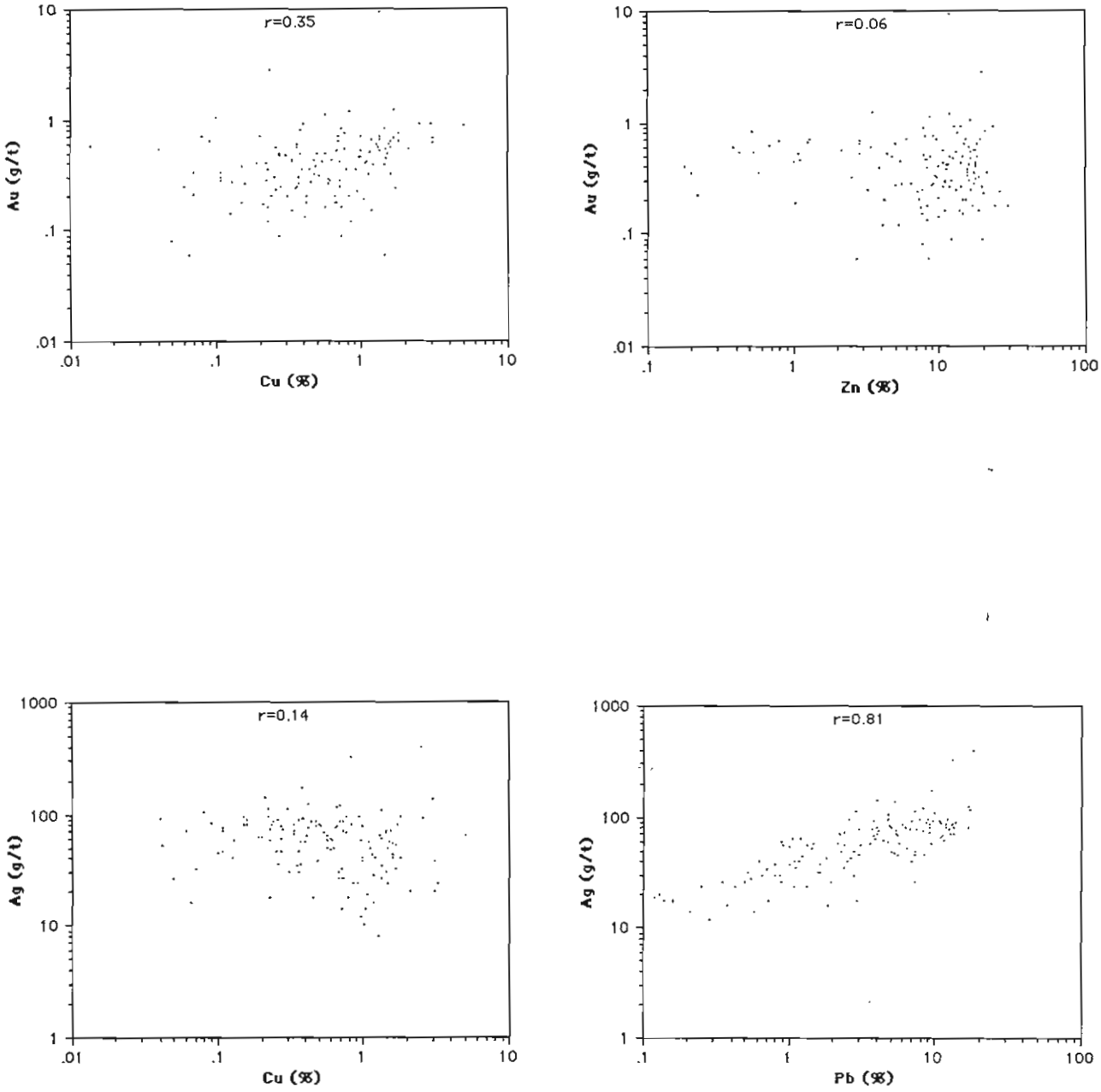

Figure 3 Relationships between base metals, gold and silver in massive pyrite-sphalerite-galena mineralisation.

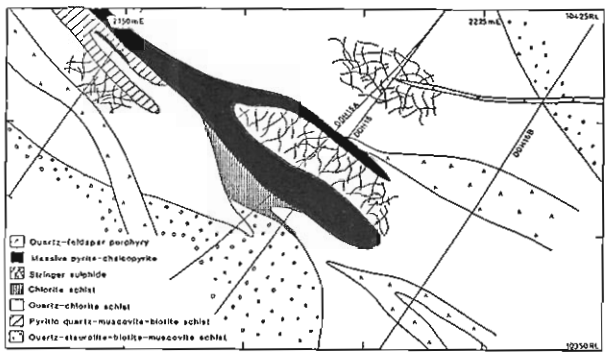

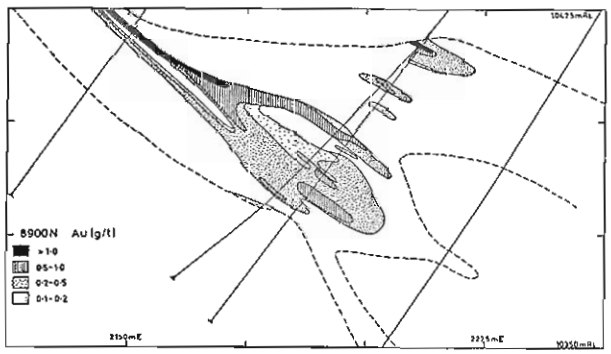

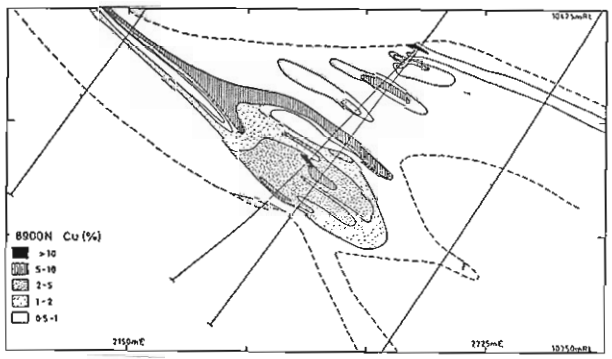

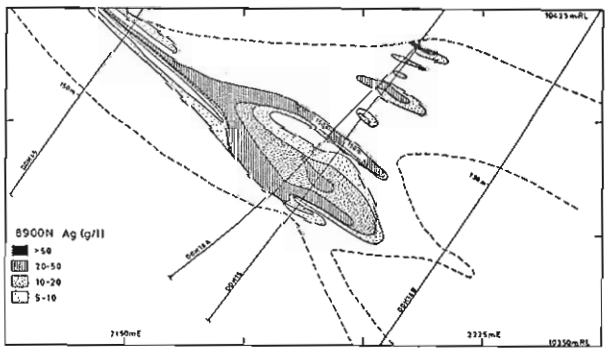

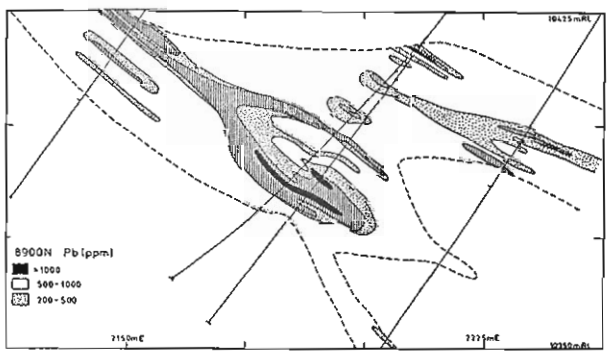

Figure 4 Geology and the distribution of gold, copper, silver and lead from section 8900mN.

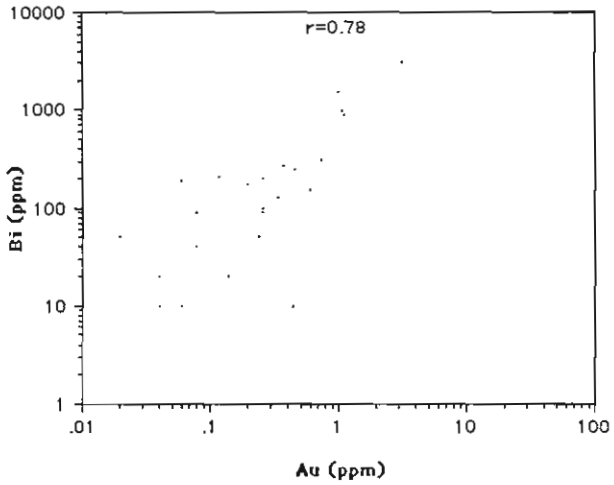

Figure 5 Scattergram showing the correlation between gold and bismuth in copper-rich mineralisation.

chalcopyrite silver has a strong correlation to copper whereas in massive pyrite-sphalerite-galena silver has a strong association with lead. The silver-lead association is typical of most massive sulphide deposits (Amcoff, 1984), but the siver-copper association is much less common (e.g. Millenbach; Knuckey *et al.*, 1982). The distribution of silver on section 8900 mN corresponds to copper, and it is restricted to the massive pyrite-chalcopyrite lens.

MINERAL ASSOCIATIONS OF GOLD AND SILVER

Results from metal distribution studies indicate that gold has a moderate to strong association with copper in both copper-rich mineralisation and zinc-lead-rich mineralisation, and that it has a strong correlation to bismuth in at least copper-rich mineralisation. Silver correlates strongly with copper in copper-rich mineralisation, but it has a strong association with lead in zinc-lead-rich mineralisation. These general observations hold also in mineral to mineral realtionships.

Gold

Patterson (1981) first noted electrum at Balcooma. In sample RA8011 he observed 1-10 μm electrum grains in association with chalcopyrite and bismuth minerals. Examination of that specimen by the author yielded a 3 μm x 4.5 μm electrum grain in a sulphide pool containing chalcopyrite, native bismuth, galena and a Bi-Te-S mineral with a rough microprobe analysis approximating gruenlingite (Bi_4TeS_3,). Examination of additional polished thin sections from Balcooma resulted in twelve addition grains in seven occurrences from three sections.

Sample 16A-135.9 contains a single 2 μm x 2 μm electrum grain in a chalcopyrite-pyrrhotite veinlet that cuts a strongly fractured pyrite porphyroblast. Minor bismuthinite and a Bi-Te-S mineral are also present in the veinlet. This sample, RA8011 and 42-62.7 all come from copper-rich mineralisation. Section 42-62.7 contains three electrum grains from two separate occurrences. Two electrum grains (4 μm x 6 μm and 5 μm x 5 μm) occur with native bismuth in a galena-bismuthinite pool which is surrounded by chalcopyrite, whereas the third, and largest, grain (5 μm x 12 μm) occurs with bismuthinite in an inclusion within late, spongy pyrite. In most occurrences from copper-rich mineralisation, electrum has a strong association with chalcopyrite and bismuth minerals which confirms the association of gold with copper and bismuth noted in metal distribution studies.

Only one electrum-bearing sample, 12-132.7, came from massive pyrite-sphalerite-galena mineralisation. It contains a total of eight electrum grains scattered between four separate occurrences. In the first occurrence, five electrum grains, which range in size from 1 μm x 1 μm to 3 μm x 9 μm, sit in a chalcopyrite-galena veinlet that cuts an embayed pyrite porphyroblast. The porphyroblast is embayed and the veinlet is truncated by sphalerite. In the second occurrence, a 1 μm x 1.5 μm electrum grain is present in another chalcopyrite veinlet that cuts a pyrite porphyroblast. Electrum also has two other occurrences where single grains (0.2 μm x 0.7 μm and 5 μm x 7 μm) occur in galena-chalcopyrite±quartz veinlets that cut pyrite. The occurrence of electrum in veins within pyrite is similar to the occurrence of electrum in massive sphalrite-galena-pyrite ore at Rosebery (Huston & Large, 1986), however the association with chalcopyrite at Balcooma is dissimilar. The association of electrum with chalcopyrite-bearing veinlets confirms the copper-gold association noted even in zinc-lead-rich mineralisation at Balcooma.

The average grain dimension for all the electrum grains observed at Balcooma is less than 10 μm, which is smaller than the average dimension of electrum at Rosebery (Huston & Large, 1986) and at Mt. Chalmers (Huston & Khin Zaw, this volume). As electrum from copper-rich mineralisation is associated with chalcopyrite and bismuth minerals, the recovery of gold from Balcooma might be expected to be higher than at Rosebery where much of the gold is locked in pyrite grains (Henley & Steveson, 1978; and Huston & Large, 1986). Gold recovery from zinc-lead-rich mineralisation may be similar to Rosebery, however, as in this style of mineralisation electrum has a grossly similar occurrence to Rosebery.

Electrum fineness at Balcooma has a relatively

limited range between 670 and 790 which is similar to other deposits of the copper-gold association (Huston & Khin Zaw, this volume).

Silver

No silver-rich minerals have been noted at Balcooma by Patterson (1981) or in this study. These results indicate that silver must occur as a minor component in other phases. In zinc-lead-rich mineralisation, the strong association between silver and lead suggests that silver occurs in argentiferous galena. Galena from Balcooma often contains minute inclusions of native bismuth which indicate that it is bismuth-rich. Amcoff (1984) has suggested that the presence of bismuth allows more silver into the galena lattice as a paired substitution. This best explains the occurrence of silver in galena. A separtate test would be to examine the relationship between silver and bismuth in lead-rich mineralisation, but this is not possible due to lack of data. Using the average concentration of silver and lead from mssive zinc-lead-rich mineralisation, the average silver content in galena is 1200 ppm.

In copper-rich mineralisation, silver has a very strong correlation with copper. Due to this strong correlation and as galena only occurs in trace amounts, the most likely host for silver is chalcopyrite. Using the results from assay data and the Cu versus Ag scattergram, the average content of silver in chalcopyrite is 140 ppm (Huston, 1987). As the correlation between copper and silver is remarkably consistent, this content should be rather constant.

CONCLUSIONS

The Balcooma prospect is an example of a gold-poor massive sulphide deposit of the copper-gold assocaition. The deposit is unlike most Phanerozoic deposits in that barite has not been observed and large quantities of pyrrhotite and magnetite are present. These characteristics are more typical of Archaean deposits. The strong copper-gold association and weak to non-existant zinc-gold association are similar to the associations of gold present at the Archean Scuddles deposit.

Gold chloro-complexes probably transported the gold that was deposited (Huston & Large, in press). Transport of gold as a thio-complex may also have occurred, but this gold may not have been precipitated. The lack of barite in the mineralisation indicates that the oxidation of H_2S required to precipitate the thio-complexed gold may not have occurred at Balcooma. This requires locally reduced seawater during the time of deposition in analogy to Archaean deposits (cf. Large, 1977). Such conditions may have occurred if Balcooma formed in a restricted basin.

At least two factors may have caused the low gold grades at Balcooma: (1) a fluid pH near that of the switchover in gold complexing, or (2) a low oxygen fugacity in the mineralising fluid. Both factors are unconstrained due to the intensity of metamorphism in the Balcooma metamorphics.

The silver distribution at Balcooma seems to be controlled by two factors: (1) the amount of silver taken up in the chalcopyrite lattice, and (2) the extent of paired substitution of silver with bismuth in galena. The physicochemical controls on these processes have yet to be understood fully.

REFERENCES

Amcoff, O., 1984, Distibution of silver in massive sulphide ores: *Mineralium Deposita*, v. 19, p.63-69.

Huston, D.L., 1986a, Balcooma area, Queensland, project outline, *in* Controls on gold and silver grades in volcanogenic sulphide deposits (84/P210), April 1986 progress report: Unpub. AMIRA report, University of Tasmania, p. 27-28.

Huston, D.L., 1986b, A preliminary description of the stratigraphy and structure of the Balcooma prospect, northern Queensland, *in* Controls on gold and silver grades in volcanogenic sulphide deposits (84/P210), November 1986 progress report: Unpub. AMIRA report, University of Tasmania, p. 84-89.

Huston, D.L., 1987, Balcooma prospect, northern Queensland, *in* Controls on gold and silver grades in volcanogenic sulphide deposits (84/P210), August '1987 progress report: Unpub. AMIRA report, University of Tasmania, p. 150-168.

Huston, D.L., and Large, R.R., 1986, The distribution, mineralogy and geochemisty of precious metals in the north-end orebody, Rosebery Mine, Tasmania: Unpub. report, University of Tasmania, 132 p.

Huston, D.L., and Large, R.R., in press, A chemical model for the concentration of gold in volcanogenic massive sulphide deposits: *Ore Geology Reviews.*

Huston, D.L., and Khin Zaw, this volume, Controls of the fineness and grain size of electrum in volcanogenic massive sulphide deposits.

Knuckey, M.J., Comba, C.D.A., and Riverin, G., 1982, Structure, metal zoning and alteration at the Millenbach deposit, Noranda, Quebec, *in* Hutchinson, R.W., Spence, C.D., and Franklin, J.M., eds., Precambrian sulphide deposits: *Geol. Ass. Can. Special Paper 25*, p. 296-317.

Large, R.R., 1977, Chemical evolution and zonation of massive sulfide deposits in volcanic terrains: *Econ. Geol.*, v. 72, p. 549-572.

Large, R.R., and McGoldrick, 1986, Structure and metal distribution in the PQ-P north lens system, Que River mine, *in* Controls on gold and silver grades in volcanogenic sulphide deposits (84/P210), April 1986 progress report: Unpub. AMIRA report, University of Tasmania, p. 3-17.

Patterson, D.J., 1981, Mineralogical reconnaissance of diamond drill core, Balcooma DDH16, QH14532-15489 (RA8003-8060): Unpub. Mineral Services report 4440, Mt. Isa Mines, 4 p.

Ruxton, P., 1987, Gold-base metal relationships at Scuddles, Western Australia, *in* Controls on gold and silver grades in volcanogenic sulphide deposits (84/P210), August 1987 progress report: Unpub. AMIRA report, University of Tasmania, p. 131-149.

CONTROLS ON THE FINENESS AND GRAIN SIZE OF ELECTRUM IN VOLCANOGENIC MASSIVE SULPHIDE DEPOSITS

David L. Huston and Khin Zaw

INTRODUCTION

The occurrence, grain size and fineness of electrum grains in massive sulphide deposits has implications for both the practical aspect of gold recovery and the theoretical aspect of genetic modelling. Grain size and mineral associations of electrum are the primary controls on metallurgical recovery in complex sulphide ores. Coarse grained gold is more likely to be liberated than fine grained gold which may remain encased in sulphides during grinding. To date this problem has not been addressed widely in the literature. Therefore, the first purpose of this discussion is to describe the occurrence and grain size of electrum in eastern Australian volcanogenic massive sulphide deposits, and to discuss geologic controls on these characteristics.

Several recent papers (Shikazono and Shimizu, 1987; and Rose and Morrison, 1988) have used the chemical composition of electrum in a genetic sense as both a classification of gold-bearing deposits and as an indication of the geochemistry of gold transport. Due to a paucity of data on electrum fineness, these exercises have not been undertaken on volcanogenic massive sulphide deposits in a systematic way. In view of this, the second goal of this paper is to describe the variation in the fineness of electrum among eastern Australian deposits, and to geochemically model the chemistry of gold transport and deposition in these systems.

Publicly available data on the occurrence, grain size and fineness of electrum exists for the following eastern Australian deposits: Que River and Hellyer (Ramsden and Creelman, 1984; and Whitford *et_al.*, 1985), and Rosebery (Huston and Large, 1986 and in press (a)). To this data base, recent studies by the authors have added data from the Rosebery south-end pyrrhotite-pyrite replacement body (c.f. Khin Zaw, this volume), the Balcooma prospect (c.f. Huston, this volume (a)) and the Mt. Chalmers deposit. These five deposits span the entire spectrum of Phanerozoic deposits. Three deposits (Hellyer, Que River, and Rosebery) are of the zinc-lead-silver-gold association of Huston and Large (in press (b)), whereas two deposits (Balcooma and Mt. Chalmers) are of the copper-gold association. Gold grades vary from 0.4 g/t at Balcooma to 3.5 g/t at Que River (Table 1).

The intensity of deformation varies markedly among the studied deposits. The Mt. Chalmers and Hellyer deposits are undeformed or weakly deformed and still retain pristine ore textures (Large and Both, 1980; and McArthur, 1986). The Que River deposit has been deformed into a "W"-shaped fold, and although primary textures have been retained locally, the ores may have a mylonitic fabric on the fold limbs (Large *et al.*, in press). The structure at Rosebery is unresolved although folding (Brathwaite, 1972; and Lees *et al.*, in press) and faulting (R. Berry, pers. com.) may be present. The copper-rich lens of the Balcooma deposit sits in the core of a antiformal syncline, whereas the zinc-lead-rich lens lies on the western limb of this fold (Huston, 1987).

The degree of metamorphism varies from relatively unmetamorphosed at Mt. Chalmers (Large and Both, 1980) to middle amphibolite at Balcooma. The Hellyer and Que River deposits have undergone, pumpellyite-prehnite facies metamorphism, whereas the Rosebery deposit has undergone lower greenschist facies metamorphism (Green *et al.*, 1981). As a group, these five deposits display a large variation in gold grades, metal associations, deformation intensity and metamorphism which should give insight into the geological processes that control electrum grain size and fineness.

SUMMARY

1. Studies of undeformed massive sulphide deposits indicate that gold occurs as electrum in association largely with chalcopyrite in deposits of the copper-gold association. In deposits of the zinc-lead-silver-gold association, gold occurs as a trace element in arsenopyrite or pyrite in sphalerite-galena-pyrite ore. In baritic zones from zinc-lead-silver-gold association deposits, gold may occur as electrum in association with other sulphides as the chemistry of deposition may be different.

2. Moderate deformation associated with moderate strain rates at low temperature may expel gold from the host mineral and deposit it as coarse electrum that may be associated with base metal sulphides.

Table 1. Gold and silver grades from deposits discussed in this report.

Deposit	Silver (g/t)	Gold (g/t)	Atomic Ag/Au ratio
Que River			
PQ lens	241	4.4	100
P-north lens	189	2.9	119
Rosebery	155	2.9	98
Mt. Chalmers			
Main lode	11	1.8	11
West lode	42	3.0	26
Balcooma	20	0.4	91

3. At high metamorphic grades, diffusion will control the growth of electrum. As the size of an electrum grain would be controlled by the amount of gold available in the region of diffusion surrounding the growing grain, the grade of the ore may also control grain growth. Deposits of higher gold grade should have coarser electrum given similar post-depositional deformation and metamorphism. This same argument may also be applied to undeformed deposits of the copper-gold association where the grain size of electrum should be controlled by the amount of gold in the mineralising fluid.

4. In practical terms, gold recoveries should be higher in deposits of the copper-gold association. Baritic ores may have better recoveries than sphalerite-galena-pyrite ores in undeformed deposits of the zinc-lead-silver-gold association. Deformation of moderate strain rates will produce better recoveries. In deformed and metamorphosed ores, deposits of higher grade should have higher recoveries than deposits of lower grade.

5. Chemical modelling predicts the highly variable fineness of electrum in deposits of the zinc-lead-silver-gold association by assuming thiocomplex transport of gold. Analogous modelling on the copper-gold association failed to predict actual variations due to shortcomings in data and assumptions.

DESCRIPTION OF INDIVIDUAL DEPOSITS

Hellyer and Que River

The Hellyer and Que River ores have been extensively studied by the CSIRO (Whitford *et al.*, 1984; and Ramsden and Creelman, 1984). At Hellyer, which is the least deformed massive suphide in the Mt. Read Volcanics, only a single grain of elecrum has been observed despite an very intensive search (McArthur, 1986). Rather, the gold appears to occur in arsenopyrite at a level of some 500 ppm, and to a lesser extent in pyrite (Ramsden and Creelman, 1984). Significantly, Ramsden and Creelman (1984) did not analyse arsenopyrite from the barite zone, presumably because none was observed. This possibility is supported by the sudden drop off in arsenic values from this zone (see Fig. 4, Rasmden and Creelman, 1984). At Hellyer, which must be considered as the undeformed end member of the zinc-lead-silver-gold association, gold occurs principally in arsenopyrite and to a lesser extent in pyrite. However, the occurrence of gold in the barite zone was not conclusively resolved by Ramsden and Creelman (1984).

At Que River, which has been significantly more deformed (Large *et al.*, in press), Whitford *et al.* (1984) have recorded the presence of electrum. They noted three general occurrences: (1) coarse grained (10-400 μm; average 100 μm), rounded electrum grains that occur predominately with galena, and (2) fine grained (<10 μm) grains that occur predominately with pyrite, and (3) intermediate sized (>10 μm) grains that occur at the contacts between pyrite grains and other sulphide minerals. The coarsest grained electrum occurs in base metal sulphides near pyrite (Whitford *et al.*, 1984). The fineness of the electrum grains was found to be highly variable, with a range from 550 to 820 and a mean of 720. Gold was found in pyrite in trace amounts of about 150 ppm (Whitford *et al.*, 1984).

Rosebery

Primary Mineralisation

Huston and Large (1986 and in press (a)) studied the occurrence, grain size and fineness of electrum from the relatively undeformed north-end of Rosebery. The characteristics of electrum were found to vary depending on ore type. In massive pyrite-chalcopyrite, 1-10 μm electrum grains were observed as inclusions in and along cracks in arsenopyrite grains in a crosscutting chalcopyrite veinlet. As only one example of this type of mineralisation was observed, the electrum occurrence may not be considered conclusive.

In massive sphalerite-galena-pyrite mineralisation, electrum is typically very fine grained, with a dominant grain size of about 5 μm although grains up to 45 μm were observed (Fig. 1). The grains are always associated with pyrite, and the majority of the the grains occur in cracks within or along grain boundaries between pyrite grains. As at Que River, electrum from this style of mineralisation has a variable fineness, with a range between 320 and 700. Fine grained electrum tends to have a lower fineness than coarser grains, and the rims of coarser grains tend to be enriched in silver (Fig. 2; R3391-138.25). Silver-rich rims have also been noted in electrum from the Kosaka andShakanai deposits in Japan (Shimazaki, 1974). Brathwaite (1969) noted an occurrence of electrum in a tetrahedrite pool from sphalerite-galena-pyrite ore at Rosebery.

The occurrence and fineness of electrum in Rosebery baritic mineralisation differs markedly from massive sphalerite-galena-pyrite ore. Electrum occurs in association with chalcopyrite and galena, or without sulphide association; it was not observed in association with pyrite. Limited microprobe analyses indicate that this electrum has a limited range in fineness; three of the four grains analysed had finenesses between 730 and 760, which is higher than the range for massive sphalerite-galena-pyrite ore. In this case, the larger grains do not have silver-rich rims. Grain size was found to be quite variable and between 3 μm and 75 μm.

In distal pyrite mineralisation, which is equivalent to the silceous cap at Hellyer (Mac Arthur, 1986), electrum again occurs with pyrite. In the one sample that contains primary colloform textures in pyrite, the electrum occurs interstitially to pyrite grains in association with galena and tetrahedrite. Whereas the variation in grain size is similar to massive sphalerite-galena-pyrite ore, the fineness of electrum is higher and has a narrow range (610-730 if one gold-rich sample is excluded).

In general, the occurrence of syngenetic electrum varies up stratigraphy at Rosebery. Electrum from massive sphalerite-galena-pyrite has a strong association with pyrite and a low, but variable, fineness. Electrum

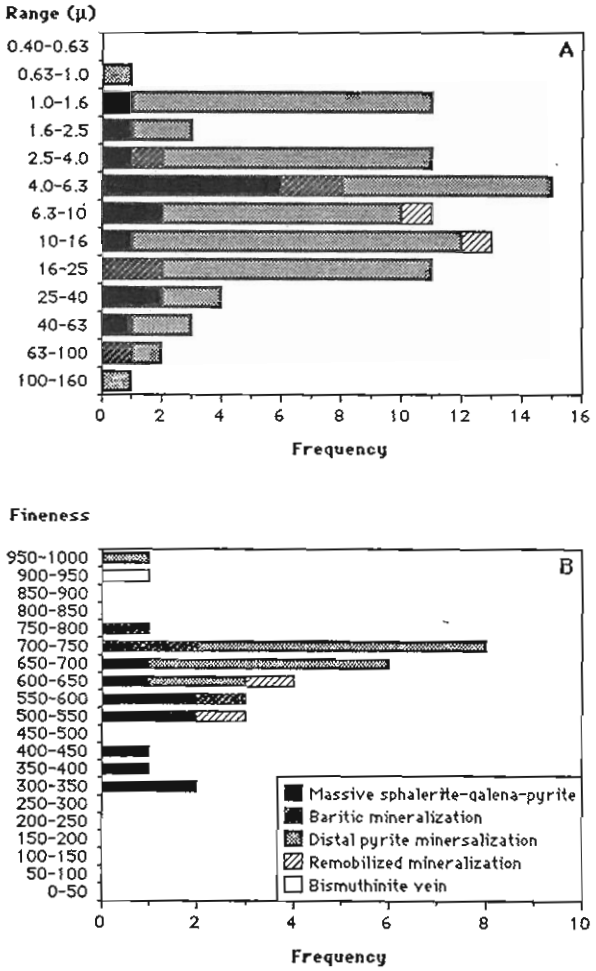

Figure 1 Grain size (a) and fineness (b) of electrum fron the Rosebery north-end.

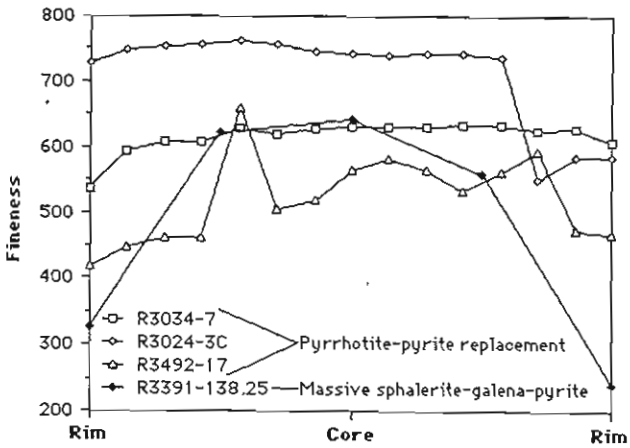

Figure 2 Variation of fineness within electrum grains from the Rosebery deposit.

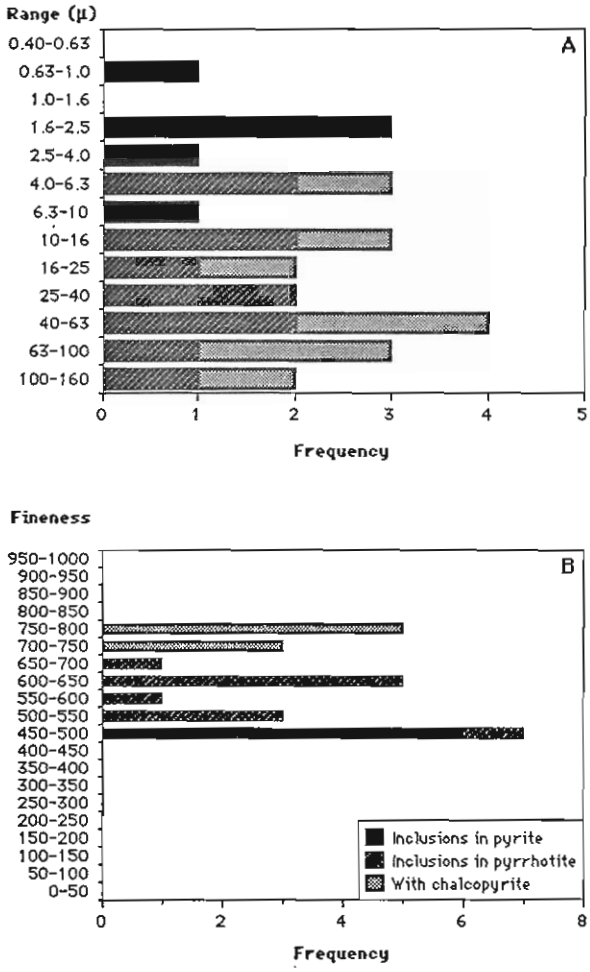

Figure 3 Grain size (a) and fineness (b) of electrum from the pyrrhotite-pyrite replacement body, Rosebery south-end.

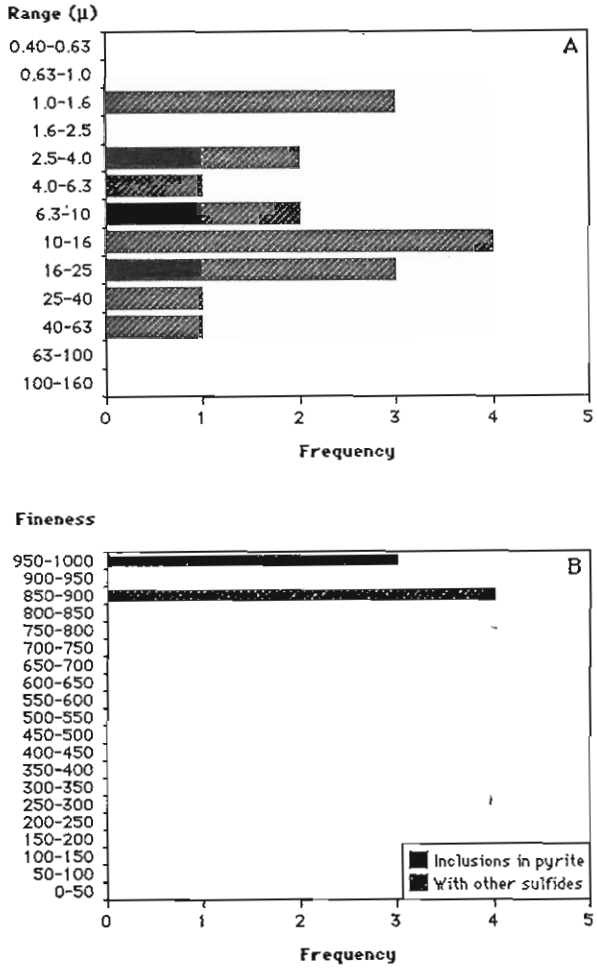

Figure 4 Grain size (a) and fineness (b) of electrum from the Mt Chalmers deposit.

from baritic mineralisation has a variety of occurrences, but does not occur with pyrite, and has a high fineness with a narrow range. Electrum from distal pyrite mineralisation has a strong association with pyrite and a high fineness with a narrow range.

Remobilised Mineralisation

Due to Devonian metamorphism and metasomatism, the Rosebery deposit has undergone various degrees of recrystallisation and remobilisation. The intensity is weakest in the north-end and increases towards the south-end where a crosscutting pyrrhotite-pyrite body has replaced syngenetic massive sulphide (Khin Zaw, this volume).

All of the original mineragraphic studies of Rosebery ores (Stillwell, 1934; Williams, 1960; Brathwaite, 1969; and Green, 1983) noted the occurrence of electrum in recrystallised tetrahedrite. Electrum in remobilised quartz-carbonate veins was also noted by Huston and Large (1986) in association with chalcopyrite. The two grains observed were roughly 10 µm in dimension and had a fineness of 520 and 630, respectively (Fig. 1; Huston and Large, in press (a)). Additionally, 930 fine electrum was also observed in a bismuthinite vein in association with maldonite.

Figure 3 illustrates the variations in the grain size and fineness of electrum from the south-end pyrrhotite-pyrite replacement body, which is a metasomatic replacement of massive sulphide ore associated with Devonian magmatism (Solomon *et al.*, 1987; and Khin Zaw, this volume). The electrum has three distinct occurrences: (1) as inclusions in pyrite, (2) as inclusions in pyrrhotite, and (3) in assocaition with chalcopyrite (Khin Zaw, this volume). Excluding electrum included in pyrite, electrum from this body has a coarser grain size (usually 10-160 μm) and a higher fineness (500-800) than electrum in syngenetic massive sphalerite-galena-pyrite ore from the north-end. These coarse grains also have silver-rich rims (Fig. 2; R3034-7, R3024-3C amd R3492-17).

Electrum included in pyrite has a much finer grain size (<10 μm) and a lower fineness (450-500) than the other two occurrences. As these characteristics and associations are more typical of massive sphalerite-galena-pyrite ore from the north-end, the electrum included in pyrite may be relic syngenetic electrum that has not been affected by the Devonian metasomatism (Khin Zaw, this volume).

Mt. Chalmers

The Mt. Chalmers deposit is an example of an undeformed deposit of the copper-gold association in which primary textures are preserved (Large and Both, 1980; and Huston and Large, in press). This study examined the occurrence of electrum from the extensive University of Tasmania reference collection for Mt. Chalmers (collected by R. Large). Electrum was observed to have two distinct occurrences: (1) as inclusions in pyrite, and (2) in association with other sulphides. In the latter occurrence, electrum was observed in contact with pyrite, galena and sphalerite although the predominant occurrrence was with chalcopyrite. The presence of a Cu-Bi-Pb sulphosalt (probably aikenite ($CuPbBiS_3$)) and native bismuth were also noted in the samples, but not in association with electrum. The grain size of the electrum varied between 1 μm and 60 μm, with most grains between 10 μm and 25 μm (Fig. 4).

Based on a limited number of microprobe analyses, the fineness of the electrum varies between narrow limits. Three electrum grains included in pyrite had finenesses between 970 and 990, whereas four grains associated with other sulphides varied between 850 and 870. None of the grains had silver-rich rims. As other grains of electrum observed in this study had the same colour, the fineness range should be rather narrow.

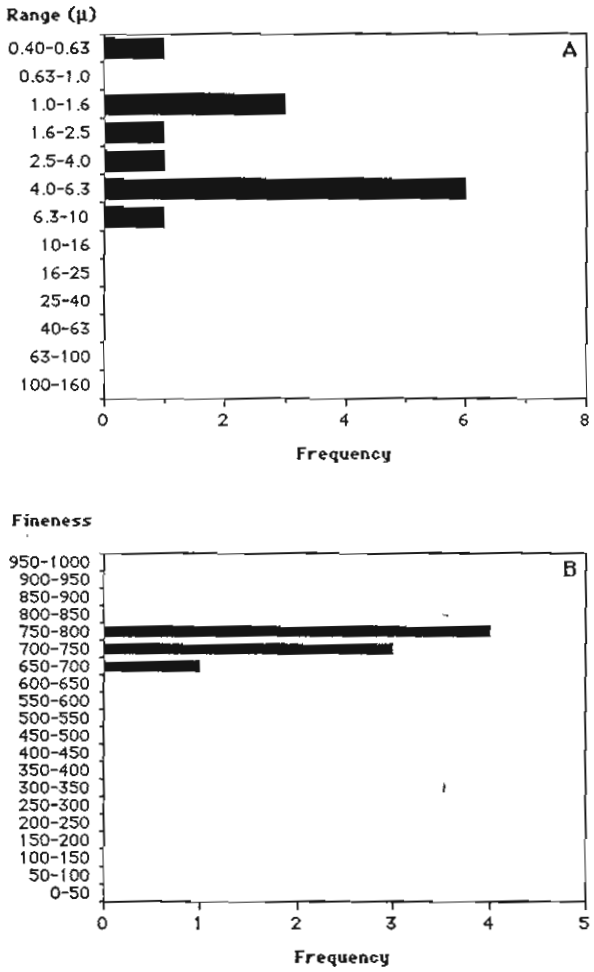

Figure 5 Grain size (a) and fineness (b) of electrum from the Balcooma prospect.

Balcooma

The Balcooma prospect is an example of a strongly deformed and metamorphosed deposit of the copper-gold association (Huston, this volume (a)). The electrum has a strong association with chalcopyrite and bismuth minerals, and a weaker association with galena. Of the five deposits described herein, Balcooma electrum has the smallest grain size: all observed grains were less than 10 μm (Fig. 5). As at Mt. Chalmers, the fineness is high and has narrow limits (670 to 790).

Other Deposits

Outside these deposits, very little other data exist on electrum in volcanogenic massive sulphide deposits. In the Kuroko deposits electrum occurs in upper part of kuroko ore in association with galena, sphalerite and tetrahedrite (Shimazaki, 1974). The composition of electrum from kuroko ore in the Kosaka and Shakanai deposits ranges from 520 to 860 fine, but electrum from oko ore in the Hisaka deposit has a considerably higher fineness of 950-960 (Shimazaki, 1974). In the Nurukawa deposit (Yamada *et al.*, 1987), electrum of tens of microns in diameter was observed in quartz-chalcopyrite veins in keiko and stockwork ores. The electrum was found to vary between 500 and 700 in fineness.

The description of electrum from the Hisaka and Nurukawa deposits is very similar to the Mt. Chalmers and Balcooma prospect: electrum of relatively high fineness associated with chalcopyrite and copper-rich mineralisation. The occurrence of electrum from the Shakanai and Kosaka deposits differs from the Hellyer deposit where gold occurs in arsenopyrite and pyrite, but it is somewhat similar to the occurrence of electrum in the barite zone at Rosebery. Shimazaki (1974) notes that electrum commonly occurs in the upper parts of the kuroko ores and that barite is a gangue mineral in these ores.

Summary of Characteristics

In volcanogenic massive sulphide deposits, gold has two distinct associations: (1) zinc-lead-silver-gold, and (2) copper-gold. The distribution of electrum in the former association has the following characteristics (Ramsden and Creelman, 1984; Whitford *et al.*, 1984; Huston and Large, 1986 and in press (a); and Khin Zaw, this volume):

(1) In pristine deposits, gold in massive sphalerite-galena-pyrite ore occurs as trace elements in either arsenopyrite and/or pyrite.

(2) In deformed ores, the gold occurs as electrum that is commonly associated with pyrite and has a very fine grain size. Electrum may also occur as coarser grains in association with other sulphides.

(3) In massive massive sphalerite-galena-pyrite ore, the recrystallised electrum has a large range in fineness (320 to 820) and coarse grains often have silver-rich rims.

(4) In recrystallised baritic mineralisation, electrum occurs with sulphides other than pyrite or without sulphides. The fineness tends to be higher that the stratigraphically lower massive sphalerite-galena-pyrite. Evidence from Japanese deposits indicate that the pristine association may be similar; the occurrence of gold in the baritic zone at Hellyer was not determined in available CSIRO reports.

(5) In distal pyrite mineralisation electrum has a high fineness of between 610 and 730. The electrum has a strong association with pyrite which, in one case, appears to be primary.

Gold distribution in the copper-gold association has the following characteristics:

(1) Primary electrum occurs in association with chalcopyrite, bismuth minerals, galena and pyrite. This electrum is slightly coarser grained and has a higher fineness (>700) with lower variation than recrystallised electrum in the zinc-lead-silver gold association.

(2) As the grain size of electrum in the strongly deformed and metamorphosed Balcooma prospect is finer than that in the undeformed Mt. Chalmers deposit, recrystallisation does not appear to affect electrum grain size.

GEOLOGIC CONTROLS ON THE OCCURRENCE AND GRAIN SIZE OF ELECTRUM

Three factors may control the occurrence of gold and the grain size of electrum in volcanogenic massive sulphide deposits: (1) primary processes during gold deposition, (2) secondary processes during post-depositional deformation, and (3) the gold tenor of the ores.

Comparison of Hellyer to Mt. Chalmers, indicates a significantly different primary occurrence of gold between deposits of the zinc-lead-silver-gold and the gold-copper associations. In the former association, gold appears to be locked in a submicroscopic state in either arsenopyrite or pyrite, whereas in the latter association, gold occurs as relatively coarse grained electrum grains that are associated with either pyrite or chalcopyrite. These two differing occurrences are the result of two different processes: (1) coprecipitation of gold during the crystallisation of pyrite and arsenopyrite (e.g. Hellyer), and (2) precipitation of gold independent of any particular sulphide (e.g. Mt. Chalmers). These processes are described in greater detail by Huston and Large (in press (b)).

The mechanisms of gold precipitation may differ depending on location in the sulphide mound in deposits of the zinc-lead-silver-gold association. Coprecipitation into arsenopyrite is important in massive sphalerite-galena-pyrite ore at Hellyer, but has not been documented in the baritic zone. In Japan, electrum occurs with galena, sphalerite and tetrahedrite in the upper parts of kuroko ore which also apparently contains barite (Shimazaki, 1974). The Rosebery barite zone also contains electrum free of pyrite. Baritic zones form at the top of the mound where oxygenated seawater mixes with the upwelling hydrothermal fluid. In this

region, precipitation of gold may have been caused by oxidation of H_2S and not by coprecipitation with sulphides, and the gold may occur as electrum free of pyrite (see also Huston, this volume (b)).

Post-depositional deformation and metamorphism also appear to affect the occurrence of gold. Recrystallisation during deformation and metamorphism is controlled by the following factors: (1) strain rate, (2) temperature of deformation, (3) hydrostatic pressure, and (4) solid state diffusion (Hobbs *et al.*, 1976). At low temperature and/or a high strain rate, recrystallisation associated with deformation occurs as grains are flattened and deformation lamellae and bands form (Hobbs *et al.*, 1976). This type of deformation appears to have occurred at Que River and Rosebery. Whitford *et al.* (1984) infer that the coarsest grained electrum occurs in the more deformed parts of the orebody, in association with other "soft" minerals (i.e. galena). Hence, the more deformed limbs of the Que River fold should contain coarser electrum than the less deformed core of the fold. The coarsest grains may occur in moderately deformed zones where a spaced cleavage of galena has formed (c.f. Large *et al.*, in press). As mylonitisation involves grain size reduction (Hobbs *et al.*, 1976), the mylonitic zones present at Que River (Large *et al.*, in press) may not have coarser grained electrum present. By analogy, the coarsest electrum at Rosebery may be found in moderately deformed and recrystallised areas. In less deformed ares such as the core of the Que River fold and the north-end at Rosebery, electrum may not be liberated from enclosing pyrite.

At high temperatures and low strain rates, solid state diffusion becomes important (Hobbs *et al.*, 1976). The Balcooma deposit, which has undergone a high degree of metamorphism and a low strain (i.e. the copper lens occurs in the core of an antiform), has the finest grained electrum. This observation belies the simple premise that more intense metamorphism leads to coarser grained electrum. Some other factor must control the grain size.

Balcooma also contains the lowest gold grade of the deposits studied at 0.4 g/t (Table 1). As solid state diffusion can only occur over a limited distance, the amount of gold in the region of diffusion surrounding the growing electrum grain must control the eventual grain size. As Balcooma has much lower grades than the other deposits described, the amount of gold available to the individual grains is less, and therefore the grain size will be smaller.

Metasomatic replacement has had the effect of significantly increasing the grain size of electrum in the Rosebery south-end pyrrhotite-pyrite replacement body.

Practical Implications

As the association and grain size of electrum must control metallurgical recoveries, the previously discussed geologic parameters should have the following effects on gold recoveries:

(1) Deposits of the copper-gold association should have better recoveries than deposits of the zinc-lead-silver-gold association;

(2) In the zinc-lead-silver-gold association, ore from the the top of the sulphide mound may have better recoveries than ore from the base of the mound, particularly if barite is present;

(3) Moderate deformation and metamorphism may increase recoveries; and

(4) Deposits of higher grade should have better recoveries than deposits of lower grade.

GEOLOGIC CONTROLS ON ELECTRUM FINENESS

Shikazono and Shimuzu (1987) and Rose and Morrison (1988) have recently used the fineness (or other measures of gold content) of electrum as an aid in classifying gold deposits and as a technique to discern the mechanisms of gold transport. The second purpose of this paper is to treat electrum from volcanogenic massive sulphide deposits explicitly in these terms.

The two gold associations in volcanogenic massive sulphide deposits have quite different electrum characteristics. Deposits of the zinc-lead-silver-gold association (e.g. Que River, Rosebery, Kosaka and Shakanai) have a relatively low electrum fineness with a rather large variation in values. On the other hand, electrum from the copper-gold association (e.g. Mt. Chalmers, Balcooma and Nurukawa) has a higher fineness and, more importantly, a much narrower variation in values. Modelling by Huston and Large (in press (b)) indicates that gold in the copper-gold association was transported as a chlorocomplex, whereas gold in the zinc-lead-silver-gold association was transported as a thiocomplex.

Assuming gold transport as a thiocomplex, the fineness of electrum is controlled by the reaction (see also Shikazono and Shimuzu, 1987):

$$Au^0 + AgCl_2^- + 2H_2S = Ag^0 + Au(HS)_2^- + 2H^+ + 2Cl^- \quad \ldots (1)$$

This reaction indicates that $a(Ag^0)/a(Au^0)$ (and hence, electrum fineness) is controlled by $a(AgCl_2^-)/a(Au(HS)_2^-)$, $a(H_2S)$, $a(Cl^-)$, pH and temperature. Even though $a(H_2S)$ and $a(Cl^-)$ might be expected to remain constant in the systems, variations in the other parameters likely will lead to large variations in the resulting fineness. The most striking characteristic of

Table 2. Thermochemical data used in this report.

Reaction	log K_{eq} 200°C	250°C	300°C	350°C
$Ag^0 + Au(HS)^{2-} + 2H^+ + 2Cl^- = Au^0 + AgCl^{2-} + 2H_2S$	6.35	8.16	10.45	——
$Ag^0 + AuCl_2^- = Au^0 + AgCl_2^-$	7.2	6.8	6.6	6.9

Data from Bowers *et al.* (1984), Seward (1973 and 1976), Helgeson (1969) and Barton (1984)

electrum from deposits of the zinc-lead-silver-gold association is the large variation in fineness.

Conversely, for gold chlorocomplex transport, the following reaction controls the fineness of electrum (see also Shikazono and Shimuzu, 1987):

$$Au^0 + AgCl_2^- = Ag^0 + AuCl_2^- \quad \ldots (2)$$

In this case, the electrum fineness is dependant only on $a(AgCl_2^-)/a(AuCl_2^-)$ and temperature. As the temperature of copper-rich ore is restricted to around 300° (c.f. Pisutha-Arnond and Ohmoto, 1983), the fineness variation in this case should be rather restricted.

Henley and Brown (1985) have suggested that silver may occur as a thiocomplex in some systems. This possibility has been investigated by Sugaki *et al.* (1987) who found that at low temperatures (200°C), thiocomplexes dominated over chlorocomplexes in neutral to alkaline fluids of high $a(\Sigma S)$ and low $a(Cl^-)$. As these conditions are unlike conditions in most volcanogenic fluids, silver thiocomplexes are unlikely to have been important.

Using available thermodynamic data (Table 2), the fineness of electrum may be modelled. Fineness may be related to $a(Ag^0)/a(Au^0)$ as follows:

$$\text{Fineness} = 1000Au/(Ag + Au) = 1000AW_{Au}/\{AW_{Ag}[a(Ag^0)/a(Au^0) + AW_{Au}]\} \quad \ldots (3)$$

where AW_i is the atomic weight of element (i). This modelling assumes that the electrum is an ideal solid solution between gold and silver only.

For temperatures greater than 275°C and salinities of around 1 *m*, the species $AgCl_2^-$ predominates among silver species in solution (Seward, 1976); therefore, as a first order approximation the total silver in solution will be assumed to occur as $AgCl_2^-$. As all species in solution have a charge of -1, the activity coefficients are approximately equal, the ratios $a(AgCl_2^-)/a(Au(HS)_2^-)$ and $a(AgCl_2^-)/a(AuCl_2^-)$ approximate the molal ratio $m_{\Sigma Ag}/m_{\Sigma Au}$ in the hydrothermal system.

Due to the efficiency of metal trapping in volcanogenic massive suphide deposits, the ratio $m_{\Sigma Ag}/m_{\Sigma Au}$ should be approximately equal to the atomic ratio Ag/Au in the ores, especially in zinc-lead-rich ores. Table 1 summarises this ratio for the deposits considered. Figure 6 illustrates the variation in electrum fineness against temperature for fluid pH's of 4.5 and 5.5 assuming gold transport as a thiocomplex. These results fit the observed fineness data from deposits of the zinc-lead-silver-gold association very well. Assuming Rosebery conditions (pH = 5.5, $a(H_2S) = 10^{-2.5}$, $a(Cl^-) = 10^0$ and fluid atomic ratio = 100; see also Huston and Large (in press (b))), the calculated fineness for temperatures between 225°C and 275°C (the probable deposition temperature for zinc-lead ore; c.f. Green *et al.*, 1981; and Eldridge *et al.*, 1983) varies between 300 and 850, which fits the observations almost exactly. The calculations also indicate that at higher temperatures and lower pH, the fineness of electrum should increase.

Thermodynamic calculations assuming gold chlorocomplex transport yielded less satisfactory results. Calculations using the assumed conditions yielded a fineness of 1000 in all cases. This result and the consistancy of equilibrium constants with temperature indicates that electrum should have a rather constant, and high, fineness. However, the predicted fineness is much higher than the observed constant. These results may be caused by uncertainties in either the thermochemical data or in the assumptions.

As the existing high temperature data for gold chlorocomplexes is theoretically derived from low temperature data (Helgeson, 1969), a great deal of uncertainty exists in the data. Moreover, the assumption that the atomic ratio Ag/Au of the mineralising fluid equals the ratio in the existing copper-rich ores may be untrue. As silver, lead and zinc are dissolved during the formation of copper-rich ore (e.g. Ohmoto *et al.*, 1983; and Eldridge *et al.*, 1983), the silver to gold ratio in the ores does not reflect the ratio in the mineralising fluids. The true atomic Ag/Au ratio of the fluid should be higher. Finally, the assumption that electrum behaves as an ideal solid solution is not valid for atomic Ag/Au ratios significantly removed from unity. Modelling to account for this non-ideality is currently underway.

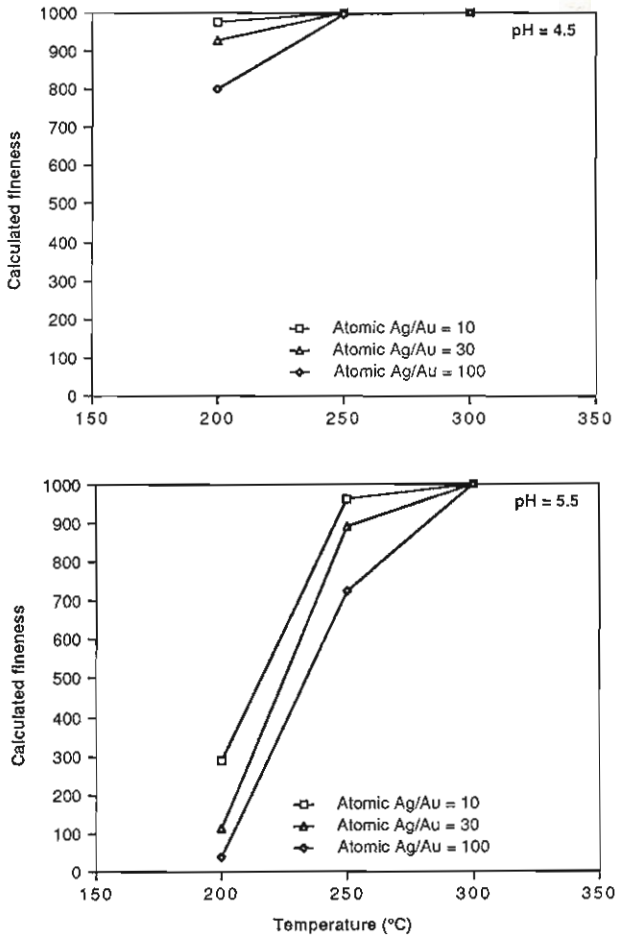

Figure 6 Theoretically predicted variations in the fineness of electrum assuming gold transport as a thiocomplex and silver transport as chlorocomplexes.

These three difficulties in the modelling may account for the differences between the model and reality.

CONCLUSIONS

Predictable geologic processes appear to have controlled the occurrence of gold, and the grain size and fineness of electrum in volcanogenic massive sulphide deposits. Depositional processes appear to control the primary occurrence of gold. In deposits of the zinc-lead-silver-gold association, gold may be locked up in untreatable pyrite and arsenopyrite in the core of the deposit, but towards the top of the deposit, the gold may occur as electrum in association with other base metal sulphides. In deposits of the copper-gold association, gold is more likely to occur as electrum in association with chalcopyrite, so in undeformed ores, deposits of the copper-gold association should have higher recoveries than deposits of the zinc-lead-silver-gold association.

Deformation and metamorphism will tend to coarsen up electrum so recoveries are higher. This enhancement is probably more effective in areas undergoing moderate strain rates, but the formation of mylonites may counteract this effect due to grain size reduction. Deposits that lie in zones of low strain (e.g. closures of folds) may not undergo this upgrading. The grade of the deposit may also limit the size of the electrum grains. As less gold is available to a growing electrum grain in a lower grade deposit, this grain may not coarsen to the extent of a grain in a higher grade deposit.

Deposits of the zinc-lead-silver-gold association have relatively low, but highly variable electrum finenesses. Thermochemical modelling assuming gold transport as a thiocomplex predicts this behaviour. Deposits of the copper-gold association have a higher fineness with a lower variation. Thermodynamic calculations assuming gold chlorocomplexing cannot model the variations in this association due to inadequate thermochemical data and assumptions.

ACKNOWLEDGEMENTS

The authors wish to thank R. Berry, M. Rattenbury and R. Large for discussions relating to this research. S. Stevens is also thanked for providing quick and high quality polished sections.

REFERENCES

Barton, P.B., 1984, Redox reactions in hydrothermal fluids, *in* Henley, R.W., and Truesdall, and Barton, P.B., eds., Fluid-mineral equilibria in hydrothermal systems: *Reviews in Economic Geology*, v. 1, p. 99-114.

Bowers, T.S., Jackson, K.J., and Helgeson, H.C., 1984, Equilibrium activity diagrams: Springer Verlag, Berlin, 397 p.

Brathwaite, R.L., 1969, The geology of the Rosebery ore deposit: Unpub. Ph.D. thesis, Univ. of Tasmania, 218 p.

Brathwaite, R.L., 1972, The structure of the Rosebery ore deposit: *Proc. Aust. Inst. Min. Met.*, v. 241, p. 1-13.

Eldridge, C.S., Barton, P.B., and Ohmoto, H., 1983, Mineral textures and their bearing on formation of the kuroko orebodies, *in* Ohmoto, H. and Skinner, B.J., eds., The kuroko and related volcanogenic massive sulfide deposts: *Econ. Geol. Mon. 5*, p. 241-281.

Green, G.R., 1983, The geologic setting and formation of the Rosebery volcanic-hosted massive sulphide deposit: Unpub. Ph.D. thesis, Univ. of Tasmania, 288 p.

Green, G.R., Solomon, M., and Walshe, J.L, 1981, The formation of the volcanic-hosted massive sulfide ore deposit at Rosebery, Tasmania: *Econ. Geol.*, v. 76, p. 304-338.

Helgeson, H.C., 1969, Thermodynamics of hydrothermal systems at elevated temperatures and pressures: *Amer. J. Sci.*, v. 267, p. 729-804.

Henley, R.W., and Brown, K.L., 1985, A practical guide to the thermodynamics of geothermal fluids and hydrothermal ore deposits, *in* Berger, B.R., and Bethke, P.M., eds., Geologu amd geochemistry of epithermal systems: *Reviews in Economic Geology*, v. 2, p. 25-44.

Hobbs, B.E.,, Means, W.D., and Williams, P.F., 1976, An outline of structrual geology: John Wiley & Sons, New York, 571 p.

Huston, D.L., 1987, Balcooma prospect, northern Queensland, *in* Controls on gold and silver grades in volcanogenic sulphide deposits (84/P210), August 1987 progress report: Unpub. AMIRA report, University of Tasmania, p. 150-168.

Huston, D.L., this volume (a), Final report–Balcooma prospect, northern Queensland.

Huston, D.L., and Large, R.R., 1986, The distribution, mineralogy and geochemisty of precious metals in the north-end orebody, Rosebery Mine, Tasmania: Unpub. report, University of Tasmania, 132 p.

Huston, D.L. and Large, R.R., in press (a), The distribution, mineralogy and geochemistry of gold and silver in the north-end orebody, Rosebery, Tasmania: *Econ. Geol.*

Huston, D.L., and Large, R.R., in press (b), A chemical model for the concentration of gold in volcanogenic massive sulphide deposits: *Ore Geology Reviews.*

Khin Zaw, this volume, Gold in F(J) lens of Rosebery, J(K)-P lens of Hercules and the South Hercs deposit: interplay of Cambrian and Devonian mineralisation.

Large, R.R., 1977, Chemical evolution and zonation of massive sulfide deposits in volcanic terrains: *Econ. Geol.*, v. 72, p. 549-572.

Large, R.R., and Both, R.A., 1980, The volcanogenic sulfide ores at Mount Chalmers, eastern Queensland: *Econ. Geol.*, v. 75, p. 992-1009.

Large, R.R., McGoldrick, P.J., Berry, R.F., and Young, C.H., in press, A tightly folded, gold-rich, massive sulfide deposit: Que River mine, Tasmania: *Econ. Geol.*

Lees, T., Khin Zaw, Large, R.R., and Huston, D.L., in press, Economic geology of the Rosebery-Hercules area: *Aust. Inst. Min. Met. Special Volume 13.*

McArthur, G.J., 1986, The Hellyer massive sulphide deposit (abstract), in Large, R.R., ed., The Mt. Read volcanics and associated ore deposits: Geol. Soc. Aus., Tasmanian Division, p. 11-20.

Ohmoto, H., Mizukami, M., Drummond, S.E., Eldridge, C.S., Pisutha-Arnond, V., and Lenaugh, T.C., 1983, Chemical processes of kuroko formation, *in* Ohmoto, H. and Skinner, B.J., eds., The kuroko and related volcanogenic massive sulfide deposts: *Econ. Geol. Mon. 5*, p. 570-604.

Ramsden, A.R., and Creelman, R.A., 1984, Precious metal mineralogy of Hellyer and Que River ores: CSIRO Restricted Investigation Report 1561R, 27 p.

Rose, W.J., and Morrison, G.W., 1988, Classification of gold deposits using the silver content (fineness) of gold (abstract): Bicentennial Gold '88, Extended abstracts, v. 2, p. 464-468.

Seward, T.M., 1973, Thio complexes of gold and the transport of gold in hydrothermal ore solutions: *Geochim. Cosmochim. Acta*, v. 37, p. 379-399.

Seward, T.M., 1976, The stability of chloride complexes of silver in hydrothermal solutions up to 350°C: *Geochim. Cosmochim. Acta*, v. 40, p. 1329-1341.

Shikazono, N., and Shimizu, M., 1987, The Ag/Au ratio of native gold and electrum and the geochemical environment of gold vein deposits in Japan: *Mineralium Deposits*, v. 22, p. 309-314.

Shimazaki, Y., 1974, Ores of kuroko-type deposits, *in* Ishihara, S., ed., Geology of kuroko deposits: *Min. Geol. Spec. Issue No. 6*, p. 311-322.

Solomon, M., Vokes, F.M, and Walshe, J.L., 1987, Chemical remobilisation of volcanic-hoted sulphide deposits at Rosebery and Mt. Lyell, Tasmania: *Ore Geology Reviews*, v. 2, p. 173-190.

Stillwell, F.L., 1934, Observations on the zinc-lead lode at Rosebery, Tasmania: *Proc. Aust. Inst. Min. Met.*, v. 94, p. 43-67.

Sugaki, A., Scott, S.D., Hayashi, K., and Kitakaze, A., 1987, Ag_2S solubility in sulfide solutions up to 250°C: *Geochemical Journal*, v. 21, p. 291-306.

Whitford, D.J., Creelman, R.A., and Ramsden, A.R., 1984, Petrological, geochemical and mineragraphic studies at Que River and Hellyer: CSIRO Restricted Investigation Report 1544R, 36 p.

Williams, K.L., 1960, Some less common minerals in the Rosebery and Hercules zinc-lead ores: *Proc. Aust. Inst. Min. Met.*, v. 196, p. 51-60.

Yamada, R., Suyama, T., and Ogushi, O., 1987, Gold-bearing siliceous ore of the Nurukawa kuroko deposit, Akita prefecture, Japan: *Mining Geology*, v. 37, p. 109-118 (in Japanese).

THE SOURCE OF THE GOLD IN THE WESTERN TASMANIAN VMS DEPOSITS

Joe Stolz and Ross R. Large

INTRODUCTION

Western Tasmanian volcanogenic massive sulphide (VMS) deposits have significantly higher average Au grades than other VMS deposits from eastern Australia and elsewhere. The aim of this study is to ascertain if these generally higher Au concentrations are a function of enhanced Au abundances in the source rocks leached by the hydrothermal fluids, or if they are the result of some more subtle aspect of the hydrothermal system. In the latter case, variables such as the size of the hydrothermal cell, and the temperature and composition of the hydrothermal fluids (e.g. pH, fO_2, aH_2S, mNaCl) will be important in determining the amount of available Au and base metals to be leached, and their solubility in the fluids (Large, 1987).

The major VMS deposits of western Tasmania are hosted within the Central Volcanic Complex of the Mount Read Volcanics (MRV) or overlying andesites of the Que-Hellyer Sequence (Corbett and Lees, 1987). In the competing tectonic models for the Cambrian development of western Tasmania, the Late-Middle Cambrian andesite-dacite-rhyolite arc-related volcanic association (MRV) was erupted either on to :-

1) Late Proterozoic flood tholeiites and turbidite sediments of the Crimson Creek Formation (Corbett and Lees, 1987; Varne and Foden, 1987; Corbett and Turner, 1988), or

2) on to a basement of overthrust nappes of ultramafic-mafic rocks derived from the forearc of an active arc to the east (Berry and Crawford, 1988; Crawford and Berry, 1988).

The early rift-related volcanics and sediments of the Crimson Creek Formation and the Success Creek Group rest unconformably on Precambrian schists and quartzites typified by the metamorphic rocks of the Tyennan Region.

The possible presence of a thick sequence of mafic-ultramafic rocks beneath the MRV belt is of considerable importance to this study. A compilation of the Au abundance data for volcanic and intrusive rocks of varying composition (Crocket, 1978) indicates that basic and ultrabasic rocks generally have higher Au concentrations (average 3.6 ppb) than intermediate and more silicic volcanics (usually < 2 ppb). Consequently, Crawford (1987) suggested that leaching by hydrothermal fluids of rocks of the Early to Middle Cambrian mafic-ultramafic complexes may have been a critical factor in the development of higher Au concentrations in the Tasmanian VMS deposits.

SUMMARY AND CONCLUSIONS

The major conclusions of this study include :-

1.) The Au concentrations in the least-altered Mount Read Volcanics (average values for the andesites and rhyolites are in the range 0.9-1.3 ppb) are comparable with those of unaltered modern volcanics of similar composition. The ultramafic rocks have significantly lower Au (mean ~ 0.5 ppb) than unaltered peridotite xenoliths, but similar to comparable rocks from ophiolite complexes. High-Mg low-Ti volcanics from the western Tasmanian ultramafic-mafic complexes have similar Au contents (mean ~ 1.6ppb) to Mount Read basalts (i.e. they are not unusually enriched in Au).

2. Relatively high-Ti basalts of the Crimson Creek Formation are the most Au-enriched primary volcanics in the Dundas Trough (up to 23 ppb). These volcanics were probably erupted during the first rifting phase in the trough (Varne and Foden, 1987), and probably form a floor to the Mount Read Volcanic Belt.

3. The closely comparable Au abundances in the Mount Read Volcanics and modern volcanics of similar composition, together with strong positive correlations between Au and platinum group element (Pd, Pt) concentrations for the basaltic rocks suggests that there has been little loss or redistribution of Au from the volcanics during greenschist facies metamorphism.

4. Near-surface alteration by groundwater does, however, result in significant leaching of Au from silicic volcanics, and core samples are therefore preferable for background Au studies.

5. The Crimson Creek basalts represent a suitable source rock to provide the relatively high Au concentrations in the western Tasmanian VMS deposits. However, the

data indicate that the background Au concentrations in the majority of the Mount Read Volcanics are sufficient to produce a 20mt deposit with an average grade of 2.5 g/t Au if the hydrothermal cell is big enough (~60 km^3; Large, 1987).

6. The anomalous Au in the Crimson Creek high-Ti basalts indicates the potential for shear-related lode Au mineralization within or at the margins of the Crimson Creek equivalent lava sequences. Likely exploration targets include the extensive Early Cambrian basalt-andesite sequences south of Macquarie Harbour (the Mainwaring Group), and in the Smithton Trough (Smithton Basalts).

SAMPLING STRATEGY

We have attempted to obtain a representative suite of the least altered examples of potenttial footwall rocks to the major west Tasmanian VMS deposits. This includes:-

1) volcanics and epiclastics from the Central Volcanic Complex and Western Sequence (including the Que-Hellyer Sequence) of the MRV belt,
2) granitic and porphyry intrusions within the MRV pile which appear to be younger than most of the VMS deposits,
3) volcanics and associated cumulates from the mafic-ultramafic complexes,
4) volcanics and associated sediments from the Crimson Creek Formation, and
5) Precambrian metamorphic basement rocks from the Tyennan Block.

A total of 144 samples from these various units have been included in the study. Wherever possible we selected materials from drill holes sited away from mineralization. As this approach severely restricted the range of rock types available, sampling of drill core in the vicinity of VMS deposits was also undertaken paying particular attention to avoid material with evidence of hydrothermal alteration and mineralization. Outcrop sampling (principally from road cutttings) was undertaken to supplement the range of rock types obtained from drill core. Most of the low-Ti basalts, ultramafic and boninite samples are outcrop samples provided by Dr A.V. Brown.

Although most of the core sampling concentrated on the least altered volcanics and associated epiclastics, several drill holes were selected that passed through relatively unaltered volcanics into progressively altered and mineralized material in the stringer zone at Que River, and to a lesser extent, in the more altered rocks at Leech Hill. The object of this was to determine if there was any progressive depletion in Au and base metals towards the stringer zone which might reflect increased hydrothermal leaching from the source rocks approaching a more intense zone of alteration and hence fluid activity.

A complete list of drill holes sampled, sample intervals, descriptions (including photographs of core specimens) and chemical compositions are given in Appendix I. The locations of the outcrop samples and drill hole collars are plotted on the accompanying geological map.

SAMPLE PREPARATION AND ANALYTICAL METHODS

The potentially very low background Au abundances and the irregular distribution of Au which is likey to characterize the volcanics demands careful sampling and handling to avoid contamination and to provide a representative sample. In addition, a sensitive, precise and accurate analytical method is necessary to provide useful data with meaningful variations at the low ppb level.

Most samples were several kg in mass and whole core was used wherever possible. The core logs and core were examined to select representative units and rock types. In general, we attempted to sample > 1m of core over a 10m interval of a particular rock type. Great care was exercised during sampling and handling to avoid contamination. The samples were isolated from jewellery and were thoroughly washed and dried. A small portion of the core was retained as a reference sample and for thin sectioning. The remainder of the material was crushed to < 1cm pieces in the jaw crusher. This was then put through a stainless steel sample splitter to provide a subsample of about 200 g for pulverizing. This was performed in an agate tema all samples except the 15 basalt and ultramafic samples provided by Dr A.V. Brown which had been crushed in a tungsten carbide tema. The major effect of crushing in tungsten carbide and Cr-steel vessels is contamination of W and Cr, respectively. These elements have very sensitive photo-peaks on the neutron activation spectrum and in high concentrations they result in a slight increase in the background, and hence a slight increase in the detection limit of Au. Contamination effects are greatest for quartz-rich rocks, and are considered to have had only a minor effect on the basic and ultrabasic rock samples.

Major elements and all trace elements (except Cu, Zn, Mo and S) were determined by XRF at the University of Tasmania Geology Department except for the 15 mafic-ultramafic samples (numbers beginning with 85-, 48302, and 60919) which were analyzed at the Mines Department of Tasmania. Cu, Zn, Mo and S were determined on all samples by Sheen Analytical Servics (Perth) using a combination of AAS, ICP optical and ICP mass spectrometric techniques. Platinum group element (PGE) data for some samples (identified in

Tables 2-13) are from Brown *et al.* (1988), and the remainder were determined by Sheen Analytical Services using a NiS fire assay ICP-MS tedchnique. Data for concurrently run standards suggest that the accuracy and precision for Pd and Pt are acceptable by this technique.

Au analyses were performed by Nuclear Activation Services (Canada) using a radiochemical neutron activation technique. The method involved irradiation of a 1 g sample for 3 hours, followed by a standard Pb fire assay using 5 mg of Ag as the collector. Gamma-ray spectra for each Ag dore were acquired using high-purity coaxial Ge detectors. The low detection limit of this method (0.1 ppb) is achieved by performing the irradiation prior to the fire assay, thereby eliminating problems with reagent blanks which are a major constraint on other fire assay techniques. The accuracy and precision of the Au analyses were assessed by inclusion of several aliquots of different standards with the sample batches. These standards covered a range of Au concentrations and included some samples with very low Au that had been analyzed by Peter McGoldrick at the University of Melbourne using an even more sensitive radiochemical neutron activation technique. The recommended and measured values for the standards, together with averages and standard deviations are presented in Table 1. These data indicate the technique is accurate over a wide range of concentrations. The repeatability of the analyses indicates an acceptable level of precision and also suggests that there are no severe sampling problems introduced because of the relatively small sample aliquot analyzed (i.e. 1 g).

Table 1 Comparison of recommended and measured Au concentrations for a number of standards

Standard	Measured* Au ppb	Average	Recommended standard value
Gold ore MA-2	1600,3200, 2700,1700	2300 (780)**	1860
Gold ore CH-1	160,240,190, 250,180	204 (39)	240
20451	30,40,24	31.3 (8.1)	31
20459	73,75,74	74 (1)	72
20514	1.5,2.1,1.8	1.8 (0.3)	1.89
20513	0.2,0.6	0.4 (0.28)	0.45
20516	0.1,2.0	1.0 (1)	1.1

* this study ** standard deviation

GEOCHEMISTRY

A detailed geochemical study of the MRV and associated rocks has been presented by Crawford (1986, 1987). The major and trace element data presented here (Tables 2-13) serve to supplement that data base for the Mount Read Volcanics. In addition, the data are useful for identifying different styles of alteration in the suite and for examining correlations between Au abundances and other geochemical parameters.

Volcanic rock names adopted here are based on the same criteria used by Crawford (1987) ; andesites (56-66 wt. % SiO_2), dacites (66-70 wt. % SiO_2), and rhyolites/rhyodacites (>70 wt. % SiO_2). These rock type also have relatively restricted ranges of Ti/Zr values ; basalts (>60-120+), andesites (20-60), dacites (12-20) and rhyolites/rhyodacites (4-12), although there is some overlap between the groups (Large et *al.*, 1986).

Comparison of the analyses presented in this report with those presented by Crawford (1987) indicates a similar range of compositions , although several of the basaltic rocks from this suite have higher loss on ignition values which reflect more extensive alteration (mainly carbonation), confirmed by thin section examination. High-K rhyolitic samples (up to 7% K_2O) from the Jukes-Darwin area also represent extensively altered K-feldspar rich assemblages that apparently were modified by intrusion of Cambrian granitic magmas. In addition to the samples specifically selected to examine the effects of different styles of alteration on Au concentrations, several rhyolite samples with very low Na_2O contents (<0.8 wt %) have been screened from the data set on the basis of excessive alteration. These samples also tend to have elevated concentrations of base metals and sulphur, whereas the abundances of Cu, Pb and Zn in the remaining rock types are generally comparable with values reported by Crawford (1987), and are regarded as background values.

Abundance data for Ni, Cr, V, Sc and Ba have not yet been completed and will be presented in an updated data base at a later date.

GOLD ABUNDANCE DATA

Au concentration data for the various rock types which represent potentially important footwall sequences to the western Tasmanian VMS deposits are presented in Tables 2-13.

Au concentrations in the least altered samples of the MRV display a restricted range of values. Histograms comparing the values of MRV basalts, andesites, dacites and rhyolites with compilations of Au abundance data for unaltered rocks of similar composition are presented in Figs. 1-4. Low-Ti tholeiites, high-Mg andesites and gabbros from the mafic-ultramafic complexes have Au contents which

Table 2 Major and trace element data for volcanics and metasediments from the Que-Hellyer Sequence.

	Basalt MAC10/A	Dacite MAC10/B	Andesite MAC10/C	Andesite MAC10/D	Sandstone MAC10/E	Basalt HL55/A	Basalt HL55/B	Dacite HAT6/A	Andesite HL30/A	Andesite HAT5/A
SiO2	54.03	68.11	62.91	63.37	67.75	53.58	51.13	67.86	64.15	58.49
TiO2	0.86	0.40	0.41	0.60	0.62	0.65	0.48	0.45	0.59	0.45
Al2O3	12.81	15.23	12.97	15.33	13.99	12.85	14.21	16.09	16.43	13.37
Fe2O3	8.60	5.04	6.36	7.27	5.53	9.06	9.11	5.41	6.50	7.73
MnO	0.27	0.12	0.16	0.15	0.09	0.15	0.19	0.09	0.09	0.20
MgO	8.53	1.83	5.63	3.16	2.81	9.87	11.47	1.91	2.80	8.59
CaO	9.94	1.56	6.21	2.95	4.08	9.04	10.76	0.88	2.32	6.59
Na2O	2.11	6.28	3.92	5.05	1.44	2.90	1.52	6.53	6.12	4.18
K2O	2.05	1.29	1.24	1.94	3.59	1.59	0.95	0.67	0.88	0.19
P2O5	0.80	0.14	0.19	0.18	0.12	0.31	0.17	0.10	0.10	0.19
Total	100.00	100.00	100.00	100.00	100.00	100.00	100.00	100.00	100.00	100.00
LOI	7.30	2.29	4.44	3.70	6.05	3.69	6.28	2.12	2.66	6.77
Rb	51	32	41	51	180	27	21	27	25	7
Sr	370	288	271	334	96	559	320	112	188	228
Y	31	36	27	30	33	25	17	30	23	27
Zr	333	228	147	150	170	155	67	158	115	137
Nb	12	15	11	11	19	10	5	11	8	10
Cu	200	9	66	52	63	100	83	6	59	56
Zn	140	260	150	570	97	50	86	100	97	210
Pb	23	58	87	109	44	2	3	4	16	50
Mo	3.5	0.5	1.5	3	4	<0.5	<0.5	1.5	<0.5	1.5
S	1000	<100	600	6200	8500	1100	200	<100	8200	1400
Au (ppb)	3.1	0.7	1.1	2.2	4	0.3	0.8	0.2	4.1	1.4
Pt	3.5									3
Pd	8									7.5
Ti/Zr	15.5	10.5	16.7	24.0	21.9	25.1	42.9	17.1	30.8	19.7
Zr/Y	10.7	6.3	5.4	5.0	5.2	6.2	3.9	5.3	5.0	5.1
Zr/Nb	27.8	15.2	13.4	13.6	8.9	15.5	13.4	14.4	14.4	13.7

	Shale MC1/A	Basalt MC1/B	Rhyolite MC1/C	Basalt MC1/D	Andesite MC2A/A	Sandstone MC2A/B	Basalt MAC1/A	Andesite MAC5/A	Basalt MAC5/B
SiO2	75.72	48.07	71.12	55.00	58.93	72.90	52.89	59.03	54.85
TiO2	0.66	0.59	0.39	1.04	0.51	0.49	0.33	0.52	0.54
Al2O3	13.40	17.96	14.93	16.58	13.69	8.80	12.85	15.65	13.62
Fe2O3	5.03	11.29	4.46	10.27	7.67	5.17	9.83	8.25	9.95
MnO	0.02	0.28	0.09	0.24	0.27	0.14	0.21	0.13	0.31
MgO	2.18	8.95	0.94	4.71	6.69	4.64	10.73	4.89	6.79
CaO	0.02	8.12	0.68	6.47	7.36	6.33	11.58	6.29	10.69
Na2O	<0.2	2.80	5.09	3.57	3.57	<0.2	0.93	4.34	0.98
K2O	2.88	1.39	2.20	1.70	1.08	1.45	1.04	0.68	1.95
P2O5	0.04	0.55	0.08	0.38	0.24	0.10	0.14	0.23	0.32
Total	100.00	100.00	100.00	100.00	100.00	100.00	100.00	100.00	100.00
LOI	5.62	3.63	1.38	2.57	5.69	7.33	15.27	7.11	13.13
Rb	126	33	72	44	25	57	34	25	68
Sr	20	768	187	562	347	40	157	240	123
Y	25	29	36	29	25	24	12	14	19
Zr	130	137	223	142	146	163	42	69	107
Nb	12	10	14	12	12	9	2	4	6
Cu	78	85	6	61	11	170	55	170	110
Zn	59	84	46	230	59	230	190	200	130
Pb	43	5	4	52	209	6	6	12	8
Mo	4.5	<0.5	0.5	1	<0.5	<0.5	<0.5	1.5	0.5
S	16000	100	600	100	1500	500	700	3200	1500
Au (ppb)	5.5	0.6	0.2	1	1.5	1.2	2.4	3.4	2.2
Ti/Zr	30.4	25.8	10.5	43.9	20.9	18.0	47.1	45.2	30.3
Zr/Y	5.2	4.7	6.2	4.9	5.8	6.8	3.5	4.9	5.6
Zr/Nb	10.8	13.7	15.9	11.8	12.2	18.1	21.0	17.3	17.8

Table 3 Major and trace element data for andesitic to rhyolitic volcanics from DDH QR97 and QR1001 adjacent to the Que River deposit.

	Rhyolite QR97/A	Andesite QR97/B	Andesite QR97/C	Andesite QR97/D	Andesite QR97/E	Alt. Andesite QR97/F
SiO2	74.00	66.01	65.92	58.65	73.67	63.04
TiO2	0.31	0.51	0.52	0.61	0.32	0.67
Al2O3	12.70	14.30	14.49	14.90	13.85	17.68
Fe2O3	2.39	5.88	6.24	9.17	2.36	7.49
MnO	0.04	0.12	0.12	0.17	0.04	0.17
MgO	0.35	1.53	1.40	5.68	0.44	3.98
CaO	3.58	6.13	6.01	6.16	3.54	1.98
Na2O	3.07	3.36	3.16	2.67	3.27	0.58
K2O	2.43	2.02	1.84	1.24	2.42	4.25
P2O5	0.07	0.14	0.15	0.15	0.08	0.16
Total	100.00	100.00	100.00	100.00	100.00	100.00
LOI	4.13	7.74	5.99	4.79	5.43	4.95
Rb	73	93	88	31	35	126
Sr	138	104	172	443	214	51
Y	34	31	24	19	20	28
Zr	192	134	106	64	81	125
Nb	13	10	8	3	6	9
Cu	23	96	52	48	34	71
Zn	160	190	60	200	210	160
Pb	11	8	6	41	16	30
Mo	2.0	1.5	1.0	1.0	1.0	1.5
S	<100	<100	<100	<100	<100	30000
Au (ppb)	1.1	1.5	1.5	0.5	0.6	32
Ti/Zr	9.7	22.8	29.4	57.1	23.7	32.1
Zr/Y	5.6	4.3	4.4	3.4	4.1	4.5
Zr/Nb	14.8	13.4	13.3	21.3	13.5	13.9

	Alt. Andesite QR97/G	Alt. Andesite QR97/H	Andesite QR1001/A	Alt. Andesite QR1001/B	Andesite QR1001/C
SiO2	63.96	60.59	63.24	67.28	59.85
TiO2	0.61	0.75	0.61	0.59	0.62
Al2O3	15.33	15.88	15.43	15.07	13.91
Fe2O3	7.96	8.58	7.41	8.79	7.95
MnO	0.51	0.47	0.12	0.21	0.13
MgO	5.97	6.13	3.09	3.79	10.61
CaO	1.35	3.95	3.53	0.80	4.31
Na2O	0.01	0.06	4.49	0.04	1.23
K2O	4.13	3.41	1.92	3.29	1.13
P2O5	0.17	0.18	0.17	0.14	0.20
Total	100.00	100.00	100.00	100.00	100.00
LOI	10.11	9.37	3.71	6.06	9.44
Rb	125	118	55	99	25
Sr	33	29	297	20	66
Y	26	25	28	23	20
Zr	124	115	134	121	104
Nb	10	11	10	8	7
Cu	165	71	12	220	68
Zn	1050	810	86	400	190
Pb	174	341	8	34	7
Mo	1.5	1.5	1.0	2.0	1.0
S	23000	28000	<100	10000	3200
Au (ppb)	11	6.9	3.2	3	2.3
Ti/Zr	29.5	39.1	27.3	29.2	35.7
Zr/Y	4.8	4.6	4.8	5.3	5.2
Zr/Nb	12.4	10.5	13.4	15.1	14.9

Table 4 Major and trace element data for Central Volcanic Sequence rocks from northwest of the Henty Fault. Asterisks denote outcrop samples.

	Dacite PRR/B*	Dacite PRR/C*	Dacite PRR/D*	Dacite PRR/E*	Rhyolite PRR/F*	Rhyolite PRR/G*	Rhyolite PRR/H*	Dacite PRR/I*
SiO2	68.82	68.12	66.99	69.97	73.58	72.70	72.50	68.98
TiO2	0.59	0.60	0.63	0.29	0.25	0.36	0.30	0.48
Al2O3	14.59	14.90	15.90	16.55	13.51	14.46	14.07	14.62
Fe2O3	4.88	5.13	6.40	3.19	2.68	3.09	3.47	4.63
MnO	0.08	0.09	0.17	0.04	0.08	0.07	0.09	0.08
MgO	1.50	1.15	1.35	0.73	0.81	0.54	0.71	1.10
CaO	2.71	3.62	2.18	1.54	1.51	1.70	3.19	3.28
Na2O	5.62	3.73	3.60	3.45	4.78	3.56	2.12	4.06
K2O	1.07	2.52	2.64	4.19	2.77	3.44	3.45	2.65
P2O5	0.13	0.14	0.13	0.04	0.03	0.08	0.07	0.15
Total	100.00	100.00	100.00	100.00	100.00	100.00	100.00	100.00
LOI	1.30	4.20	3.76	2.87	1.68	2.68	4.03	3.79
Rb	32	100	102	157	71	133	146	127
Sr	169	113	107	106	134	113	114	163
Y	35	33	48	49	46	46	22	31
Zr	212	210	238	328	272	268	175	205
Nb	12	12	13	20	17	17	10	11
Cu	26	3	4	1	1	2	2	14
Zn	35	32	31	43	16	34	53	40
Pb	6	4	7	11	4	4	12	9
Mo	<0.5	<0.5	0.5	0.5	<0.5	0.5	<0.5	<0.5
S	<100	300	100	<100	<100	300	100	200
Au (ppb)	<0.1	<0.1	<0.1	0.2	<0.1	0.1	0.4	0.2
Ti/Zr	16.7	17.1	15.9	5.3	5.5	8.1	10.3	14.0
Zr/Y	6.1	6.4	5.0	6.7	5.9	5.8	8.0	6.6
Zr/Nb	17.7	17.5	18.3	16.4	16.0	15.8	17.5	18.6

	Andesite RE1/A	Basalt RE1/B	Andesite RE1/C	Dacite RED87-1/A	Dacite RED87-1/B	Rhyolite RED87-1/C	Rhyolite RED87-1/D	Dacite RED87-1/E
SiO2	59.61	52.63	65.84	69.43	68.96	76.01	73.86	66.71
TiO2	0.84	1.02	0.47	0.48	0.49	0.30	0.29	0.58
Al2O3	16.87	17.36	15.63	14.59	14.53	13.69	13.94	14.84
Fe2O3	9.23	10.33	5.30	4.86	4.98	2.04	4.47	8.00
MnO	0.16	0.21	0.14	0.09	0.07	0.07	0.09	0.18
MgO	1.63	5.94	2.79	1.21	1.19	0.53	1.00	2.00
CaO	4.35	8.30	4.04	3.28	2.71	1.39	1.14	2.13
Na2O	4.17	2.68	2.91	2.37	3.56	2.20	1.93	3.52
K2O	2.80	1.36	2.82	3.57	3.39	3.74	3.22	1.91
P2O5	0.33	0.17	0.06	0.12	0.12	0.02	0.05	0.13
Total	100.00	100.00	100.00	100.00	100.00	100.00	100.00	100.00
LOI	4.41	3.89	4.46	4.14	3.33	2.49	2.65	3.51
Rb	104	42	129	154	115	143	138	87
Sr	152	388	105	113	182	101	43	101
Y	44	28	36	29	30	33	41	33
Zr	166	81	229	203	199	244	262	189
Nb	6	2	13	11	11	15	17	11
Cu	49	55	25	6	4	16	3	4
Zn	115	160	91	94	51	110	36	82
Pb	15	27	7	5	8	5	5	6
Mo	1.0	0.5	<0.5	1.5	<0.5	2.0	1.0	<0.5
S	800	600	1800	900	200	400	600	300
Au (ppb)	1.3	0.9	1.1	2.4	0.5	1	1.1	0.8
Pt		<0.5						
Pd		2						
Ti/Zr	30.3	75.5	12.3	14.2	14.8	7.4	6.6	18.4
Zr/Y	3.8	2.9	6.4	7.0	6.6	6.1	6.4	5.7
Zr/Nb	27.7	40.5	17.6	18.5	18.1	16.3	15.4	17.2

Table 5 Major and trace element data for dacitic to rhyolitic rocks and associated sediments from the Central Volcanic Sequence northwest of the Henty Fault; Rosebery-Hercules area.

	Alt. Rhyolite 71R/A	Shale 71R/B	Rhyolite 71R/C	Rhyolite 80R/A	Dacite 80R/B	Dacite 80R/C	Rhyolite 80R/D
SiO2	75.47	70.34	73.62	73.26	69.22	66.10	74.44
TiO2	0.23	0.88	0.34	0.24	0.50	0.37	0.34
Al2O3	12.48	13.35	14.44	14.70	14.41	17.50	13.80
Fe2O3	7.25	5.94	3.22	2.58	4.39	4.84	2.61
MnO	0.11	0.05	0.07	0.06	0.12	0.09	0.07
MgO	0.89	2.98	0.65	0.59	1.36	1.32	0.65
CaO	0.03	2.73	1.46	1.45	3.39	2.27	2.78
Na2O	0.03	0.50	4.19	1.42	3.60	3.44	3.15
K2O	3.50	3.02	1.95	5.66	2.87	3.98	2.08
P2O5	0.01	0.12	0.05	0.03	0.15	0.07	0.08
Total	100.00	100.00	100.00	100.00	100.00	100.00	100.00
LOI	2.28	6.01	2.00	2.64	4.07	3.73	2.87
Rb	164	136	79	183	108	176	78
Sr	6	97	326	65	207	135	293
Y	40	30	137	45	26	55	29
Zr	202	146	201	284	199	312	193
Nb	14	15	11	18	10	20	10
Cu	10	56	10	16	7	5	6
Zn	63	210	120	20	44	46	87
Pb	5	37	27	4	10	9	14
Mo	0.5	4.5	1.0	2.5	<0.5	1.0	<0.5
S	100	11000	700	300	100	300	400
Au (ppb)	1.1	4.5	0.4	1.5	0.4	1.1	0.4
Tl/Zr	6.8	36.1	10.1	5.1	15.1	7.1	10.6
Zr/Y	5.1	4.9	1.5	6.3	7.7	5.7	6.7
Zr/Nb	14.4	9.7	18.3	15.8	19.9	15.6	19.3

	Shale 80R/E	Rhyolite 85R/A	Shale 85R/B	Rhyolite 85R/C	Dacite BP269/A	Rhyolite BP269/B	Dacite BP269/C
SiO2	68.16	74.34	68.02	73.44	67.52	68.52	68.01
TiO2	0.83	0.28	0.52	0.41	0.70	0.50	0.54
Al2O3	12.65	14.15	14.81	13.50	15.92	15.81	14.64
Fe2O3	8.33	2.01	5.36	3.76	5.01	4.80	4.75
MnO	0.07	0.05	0.11	0.10	0.16	0.05	0.26
MgO	2.41	0.37	1.27	0.81	1.55	2.78	2.01
CaO	4.07	1.08	3.09	1.49	1.93	2.97	3.75
Na2O	0.57	3.46	2.61	3.06	5.81	0.58	3.02
K2O	2.72	4.20	4.07	3.35	1.27	3.90	2.92
P2O5	0.19	0.05	0.13	0.07	0.13	0.10	0.10
Total	100.00	100.00	100.00	100.00	100.00	100.00	100.00
LOI	5.48	2.17	3.82	2.26	3.64	6.50	4.30
Rb	110	151	178	305	56	185	113
Sr	116	131	140	234	242	88	93
Y	31	41	34	48	46	32	33
Zr	132	283	211	243	294	219	154
Nb	13	18	12	13	11	13	9
Cu	86	6	2	51	2	32	32
Zn	170	20	35	22	57	54	72
Pb	93	4	4	6	9	28	32
Mo	4.5	1.5	0.5	2.0	1.0	1.0	9.5
S	25000	100	100	1400	600	5800	1400
Au (ppb)	7.3	0.3	0.2	2.3	0.9	1.5	3.1
Tl/Zr	37.7	5.9	14.8	10.1	14.3	13.7	21.0
Zr/Y	4.3	6.9	6.2	5.1	6.4	6.8	4.7
Zr/Nb	10.2	15.7	17.6	18.7	26.7	16.8	17.1

Table 6 Major and trace element data for andesitic to rhyolitic volcanics from the Central Volcanic Sequence (DP288/A to H955/B), and White Spur Formation (MR1/A to BP273/C) northwest of the Henty Fault; Rosebery-Hercules area.

	Rhyolite DP288/A	Rhyolite DP288/B	Rhyolite DP288/C	Alt. Rhyolite DP288/D	Rhyolite H955/A	Rhyolite H955/B	Dacite MR1/A
SiO2	75.40	73.35	75.13	74.93	71.38	73.57	69.60
TiO2	0.25	0.44	0.28	0.31	0.41	0.36	0.48
Al2O3	12.59	13.93	13.47	13.39	15.19	14.28	14.83
Fe2O3	2.78	3.82	1.93	2.39	2.83	2.39	3.67
MnO	0.09	0.10	0.23	0.18	0.08	0.34	0.08
MgO	0.63	0.83	0.62	1.15	0.79	2.12	0.89
CaO	2.22	2.12	1.20	0.42	1.67	0.46	3.65
Na2O	3.54	2.01	1.80	0.46	3.75	2.26	3.75
K2O	2.43	3.33	5.30	6.71	3.85	4.19	2.92
P2O5	0.06	0.07	0.05	0.06	0.05	0.04	0.12
Total	100.00	100.00	100.00	100.00	100.00	100.00	100.00
LOI	2.62	3.14	2.37	2.02	1.16	2.31	3.21
Rb	90	137	231	323	176	185	133
Sr	103	68	73	48	353	56	252
Y	36	42	35	36	39	33	40
Zr	194	274	231	230	281	246	230
Nb	15	17	14	13	14	12	13
Cu	12	3	11	2	4	3	10
Zn	26	27	180	50	59	77	47
Pb	3	13	47	26	17	7	19
Mo	<0.5	4.5	<0.5	<0.5	1.0	<0.5	0.5
S	700	2700	1300	2700	<100	1900	200
Au (ppb)	0.9	0.7	0.3	7.8	0.8	0.7	0.3
Ti/Zr	7.7	9.6	7.3	8.1	8.7	8.8	12.5
Zr/Y	5.4	6.5	6.6	6.4	7.2	7.5	5.8
Zr/Nb	12.9	16.1	16.5	17.7	20.1	20.5	17.7

	Shale BP272/A	Alt. Andesite BP272/B	Rhyolite BP272/C	Shale BP272/D	Rhyolite BP273/A	Rhyolite BP273/B	Rhyolite BP273/C
SiO2	70.91	62.35	70.71	61.43	74.92	71.09	71.33
TiO2	0.61	0.61	0.66	0.74	0.23	0.46	0.65
Al2O3	12.93	12.56	15.04	11.80	13.00	14.17	16.37
Fe2O3	6.31	6.85	4.92	8.37	3.61	4.09	4.01
MnO	0.12	0.20	0.04	0.18	0.08	0.10	0.06
MgO	1.67	2.38	1.82	5.34	1.81	1.19	2.04
CaO	3.51	11.61	1.64	8.53	0.87	2.39	0.36
Na2O	1.19	0.71	2.15	0.74	2.80	4.36	0.88
K2O	2.54	2.60	2.87	2.66	2.65	2.04	4.21
P2O5	0.21	0.12	0.14	0.19	0.03	0.10	0.09
Total	100.00	100.00	100.00	100.00	100.00	100.00	100.00
LOI	4.46	10.71	3.46	12.24	2.77	3.32	3.27
Rb	137	144	129	121	156	120	228
Sr	150	277	177	333	245	391	61
Y	29	27	28	24	40	34	42
Zr	210	201	286	116	147	181	252
Nb	9	9	14	11	11	10	20
Cu	19	16	79	76	12	7	40
Zn	83	120	70	75	54	37	280
Pb	19	30	17	18	22	13	12
Mo	1.0	2.0	2.5	2.5	0.5	1.5	1.5
S	4000	4300	6000	15000	1100	1000	4300
Au (ppb)	1.1	2.3	4.9	10	1.5	0.9	2
Ti/Zr	17.4	18.2	13.8	38.2	9.4	15.2	15.5
Zr/Y	7.2	7.4	10.2	4.8	3.7	5.3	6.0
Zr/Nb	23.3	22.3	20.4	10.5	13.4	18.1	12.6

Table 7 Major and trace element data for Central Volcanic Sequence rocks from southeast of the Henty Fault; Anthony Road, Leech Hill, Howards Anomaly, West Sedgwick, and adjacent to the South Henty Fault; Bradshaws Road. Asterisks denote outcrop samples.

	Siltstone AR7*	Andesite AR9*	Dacites AR10*	Andesite AR11*	Andesite AR13*	Alt. Rhyolite LH1/A	Alt. Rhyolite LH1/B	Alt. Rhyolite LH1/C	Alt. Rhyolite LH1/D
SiO2	88.60	64.40	69.11	59.96	57.59	69.23	71.64	78.90	73.17
TiO2	0.33	0.73	0.35	0.57	0.52	0.52	0.50	0.32	0.38
Al2O3	5.22	16.76	17.15	15.86	16.96	14.79	14.16	11.81	13.24
Fe2O3	2.01	6.01	3.49	7.87	9.16	5.21	4.77	2.57	5.95
MnO	0.08	0.14	0.04	0.14	0.18	0.11	0.07	0.04	0.12
MgO	1.08	2.21	1.67	4.03	4.92	1.88	1.81	1.31	1.48
CaO	1.02	0.83	0.72	3.19	5.89	3.30	2.84	1.76	2.29
Na2O	0.11	7.93	4.55	5.20	4.22	0.69	0.46	0.28	<0.2
K2O	1.49	0.89	2.78	2.95	0.30	4.09	3.64	2.96	3.26
P2O5	0.05	0.10	0.15	0.22	0.26	0.18	0.12	0.04	0.12
Total	100.00	100.00	100.00	100.00	100.00	100.00	100.00	100.00	100.00
LOI	2.52	1.42	2.04	1.71	4.44	5.88	5.51	4.03	6.41
Rb	56	20	111	73	10	120	113	102	102
Sr	31	257	506	316	1080	70	73	53	70
Y	26	28	36	27	25	34	33	29	30
Zr	282	211	137	178	136	221	212	149	207
Nb	8	12	6	9	7	11	10	16	10
Cu	2	3	12	14	84	11	8	9	120
Zn	15	110	180	120	240	95	64	130	56
Pb	4	27	11	8	16	13	13	29	32
Mo	<0.5	<0.5	<0.5	<0.5	<0.5	1.5	1.0	2.5	0.5
S	200	200	1200	<100	1000	300	1800	700	34000
Au (ppb)	0.4	0.2	0.3	<0.1	0.6	0.8	1.1	1.2	6.2
Tl/Zr	7.0	20.7	15.3	19.2	22.9	14.1	14.1	12.9	11.0
Zr/Y	10.8	7.5	3.8	6.6	5.4	6.5	6.4	5.1	6.9
Zr/Nb	35.3	17.6	22.8	19.8	19.4	20.1	21.2	9.3	20.7

	Alt. Rhyolite HA8/A	Alt. Rhyolite HA8/B	Andesite WS4/A	Basalt BR1/A	Tuff BR1/B	Shale BR1/C	Alt. Rhyolite BR1/D	Basalt BR1/E
SiO2	71.59	72.65	60.01	51.01	76.34	77.30	74.45	53.36
TiO2	0.40	0.36	0.47	0.99	0.37	0.28	0.47	0.93
Al2O3	15.31	14.47	15.78	18.05	13.43	12.56	13.28	16.57
Fe2O3	4.24	5.37	8.01	11.67	3.05	2.27	3.86	9.94
MnO	0.08	0.10	0.13	0.24	0.03	0.03	0.05	0.19
MgO	0.50	0.44	4.85	5.10	1.98	1.38	2.35	6.17
CaO	0.64	0.48	3.27	7.10	0.46	1.54	1.30	8.26
Na2O	0.17	0.30	5.09	4.84	0.13	1.67	0.77	3.31
K2O	6.76	5.72	2.10	0.87	4.14	2.94	3.32	1.13
P2O5	0.32	0.13	0.29	0.13	0.06	0.02	0.16	0.15
Total	100.00	100.00	100.00	100.00	100.00	100.00	100.00	100.00
LOI	3.47	4.04	3.20	4.97	3.13	2.94	3.29	8.76
Rb	179	142	59	33	227	180	188	62
Sr	61	45	465	358	15	116	26	99
Y	19	16	24	25	43	48	42	26
Zr	158	123	134	77	152	151	391	116
Nb	12	10	7	3	18	16	15	3
Cu	230	76	52	150	15	7	11	55
Zn	2000	7400	75	250	96	54	85	370
Pb	418	1330	8	14	27	14	9	22
Mo	1.0	1.5	<0.5	0.5	1.0	0.5	0.5	<0.5
S	29000	38000	200	200	1800	100	500	400
Au (ppb)	16	20	1	0.7	0.4	0.9	<0.1	0.7
Tl/Zr	15.2	17.5	21.0	77.1	14.6	11.1	7.2	48.1
Zr/Y	8.3	7.7	5.6	3.1	3.5	3.1	9.3	4.5
Zr/Nb	13.2	12.3	19.1	25.7	8.4	9.4	26.1	38.7

Table 8 Major and trace element data for rhyolitic rocks from the Central Volcanic Sequence in the Mt Huxley and Jukes-Darwin area.

	Rhyolite HX1/A	Alt. Rhyolite HX1/B	Dacite HX1/C	Rhyolite JD2001/A	Alt. Rhyolite JD2001/B
SiO2	71.75	72.71	69.01	75.99	70.49
TiO2	0.41	0.36	0.50	0.32	0.48
Al2O3	14.85	13.25	14.87	13.24	15.29
Fe2O3	4.07	6.17	5.49	2.64	3.69
MnO	0.06	0.29	0.12	0.07	0.23
MgO	1.20	1.58	2.28	0.45	0.76
CaO	0.43	0.81	1.38	1.33	3.58
Na2O	3.67	0.99	3.49	2.89	0.63
K2O	3.47	3.75	2.75	3.02	4.76
P2O5	0.09	0.09	0.11	0.04	0.08
Total	100.00	100.00	100.00	100.00	100.00
LOI	1.97	3.77	3.43	2.71	5.60
Rb	111	172	108	116	168
Sr	91	36	114	90	96
Y	40	36	27	41	37
Zr	302	279	199	279	261
Nb	13	12	12	15	15
Cu	14	16	8	3	6
Zn	67	420	91	50	140
Pb	4	131	82	9	19
Mo	1.0	2.0	1.0	0.5	<0.5
S	300	2400	1900	100	<100
Au (ppb)	0.6	2.1	0.9	0.4	0.6
Ti/Zr	8.1	7.7	15.1	6.9	11.0
Zr/Y	7.6	7.8	7.4	6.8	7.1
Zr/Nb	23.2	23.3	16.6	18.6	17.4

	Tuff JD2001/C	Alt. Rhyolite JD2001/D	Alt. Rhyolite JD2002/A	Alt. Rhyolite JD2002/B	Alt. Rhyolite JD2002/C
SiO2	72.36	74.68	72.23	72.24	74.46
TiO2	0.34	0.30	0.38	0.53	0.31
Al2O3	12.68	12.98	12.79	13.40	13.13
Fe2O3	9.17	3.34	8.13	5.21	4.21
MnO	0.29	0.08	0.34	0.34	0.11
MgO	0.89	0.38	0.40	1.36	0.47
CaO	0.07	0.06	0.44	2.33	0.05
Na2O	<0.2	<0.2	0.23	<0.2	<0.2
K2O	4.16	8.13	5.01	4.49	7.22
P2O5	0.04	0.04	0.05	0.11	0.04
Total	100.00	100.00	100.00	100.00	100.00
LOI	2.96	1.64	2.38	5.60	1.90
Rb	196	239	193	177	239
Sr	13	72	35	53	37
Y	35	37	38	38	58
Zr	267	267	265	235	276
Nb	13	13	14	11	13
Cu	77	27	10	50	9
Zn	180	49	440	87	42
Pb	9	7	55	10	6
Mo	<0.5	1.0	0.5	1.0	1.5
S	1200	1000	100	4500	1100
Au (ppb)	1.2	0.9	2.6	3.1	0.8
Ti/Zr	7.6	6.7	8.6	13.5	20.9
Zr/Y	7.6	7.2	7.0	6.2	4.8
Zr/Nb	20.5	20.5	18.9	21.4	21.2

Table 9 Major and trace element data for Western Sequence volcanics and epiclastics from southeast of the Henty Fault. Asterisks denote outcrop samples.

	Dacite AR15*	Andesite AR17*	Rhyolite AR18*	Dacite AR19*	Dacite WSP3/A	Rhyolite WSP3/B	Basalt WSP3/C	Andesite WSP3/D
SiO2	68.18	65.28	75.03	69.84	69.31	74.07	49.46	62.73
TiO2	0.61	0.88	0.29	0.69	0.52	0.28	0.76	0.70
Al2O3	15.28	16.41	13.02	16.80	14.20	13.77	16.77	15.57
Fe2O3	5.08	5.83	2.61	3.87	4.61	2.79	10.10	7.02
MnO	0.17	0.11	0.04	0.05	0.09	0.07	0.20	0.10
MgO	1.40	2.16	0.86	1.31	1.47	0.77	6.93	2.87
CaO	3.31	1.44	0.74	0.14	3.00	2.23	9.90	3.16
Na2O	1.73	4.93	3.18	3.36	2.71	2.43	3.44	4.55
K2O	4.09	2.80	3.88	3.86	3.95	3.53	1.83	3.13
P2O5	0.17	0.15	0.04	0.07	0.13	0.06	0.13	0.17
Total	100.00	100.00	100.00	100.00	100.00	100.00	100.00	100.00
LOI	4.95	2.73	1.73	3.20	3.62	3.15	4.06	3.80
Rb	218	102	169	177	143	194	57	108
Sr	54	234	86	325	151	67	376	233
Y	43	38	45	54	30	34	23	34
Zr	278	263	193	311	211	268	64	189
Nb	17	16	16	18	13	16	1	12
Cu	3	4	5	3	10	5	150	37
Zn	45	89	38	130	120	190	180	120
Pb	8	8	7	18	12	44	16	22
Mo	0.5	2.5	1.5	0.5	1.5	<0.5	<0.5	1.5
S	900	600	200	300	800	200	200	9700
Au (ppb)	0.7	0.4	0.6	0.4	0.2	0.8	1.2	1.6
Ti/Zr	13.2	20.1	9.0	13.3	14.8	6.3	71.2	22.2
Zr/Y	6.5	6.9	4.3	5.8	7.0	7.9	2.8	5.6
Zr/Nb	16.4	16.4	12.1	17.3	16.2	16.8	64.0	15.8

Table 10 Major and trace element data for the Murchison Granite, Elliot Bay porphyries, volcanics and sediments from the Cattley Range (CRD86-1) and Crimson Creek Formation (LD86-1/A to 48302).

	Granite LS12/A	Porphyry EB1	Porphyry EB2	Shale CRD86-1/A	Rhyolite CRD86-1/B	Argillite LD86-1/A
SiO2	67.93	75.25	73.20	67.26	73.00	69.63
TiO2	0.44	0.27	0.40	0.90	0.35	0.64
Al2O3	16.09	12.71	13.20	13.67	13.82	13.27
Fe2O3	5.31	2.64	3.73	7.76	4.36	5.12
MnO	0.09	0.04	0.06	0.21	0.26	0.16
MgO	1.82	0.32	0.57	2.53	0.74	2.61
CaO	0.88	1.22	0.95	3.73	2.89	3.16
Na2O	6.66	2.55	2.70	0.28	0.90	2.05
K2O	0.67	4.96	5.12	3.40	3.58	3.15
P2O5	0.11	0.04	0.06	0.25	0.08	0.17
Total	100.00	100.00	100.00	100.00	100.00	100.00
LOI	2.15	0.90	1.14	8.02	5.07	4.47
Rb	153	232	195	131	149	130
Sr	330	85	109	40	29	142
Y	30	40	36	26	47	32
Zr	183	187	298	125	252	193
Nb	11	19	17	12	14	12
Cu	2	18	10	59	7	23
Zn	220	120	42	220	21	81
Pb	28	12	18	41	2	43
Mo	<0.5	3.0	2.5	0.5	<0.5	2.0
S	100	100	<100	2800	<100	<100
Au (ppb)	0.4	0.8	0.4	4	0.5	1.3
Ti/Zr	14.4	8.7	8.0	43.2	8.3	19.9
Zr/Y	6.1	4.7	8.3	4.8	5.4	6.0
Zr/Nb	16.6	9.8	17.5	10.4	18.0	16.1

	Argillite LD86-1/B	Alt. Andesite LD86-1/C	Basalt LD86-1/D	Basalt LD86-1/E	Basalt 85-0014	Basalt 48302
SiO2	68.74	80.52	48.74	48.05	49.54	45.59
TiO2	0.64	0.44	2.58	2.54	3.40	2.57
Al2O3	12.92	8.69	13.19	13.25	14.68	13.36
Fe2O3	5.14	4.82	15.67	16.03	15.02	17.48
MnO	0.12	0.49	0.26	0.25	0.27	0.25
MgO	2.71	1.83	6.22	6.00	5.30	6.28
CaO	4.55	0.41	8.92	10.87	7.93	10.64
Na2O	2.33	0.74	3.17	2.13	3.15	3.33
K2O	2.65	1.97	0.92	0.60	0.19	0.20
P2O5	0.20	0.09	0.31	0.27	0.53	0.30
Total	100.00	100.00	100.00	100.00	100	100
LOI	5.07	2.06	3.32	1.74	1.64	2.3
Rb	98	80	30	18	10	7
Sr	156	62	357	197	200	620
Y	36	17	41	42	59	46
Zr	212	96	172	172	260	162
Nb	12	11	14	15	5	15
Cu	23	47	390	400	11	360
Zn	74	80	150	150	230	130
Pb	20	14	4	3	16	6
Mo	<0.5	<0.5	0.5	0.5	2.0	0.5
S	100	100	600	400	400	800
Au (ppb)	1.7	0.6	10	23	0.1	12
Pt			8	16	0.5	11
Pd			24	31	3	25
Ti/Zr	18.1	27.5	89.9	88.5	78.4	95.1
Zr/Y	5.9	5.6	4.2	4.1	4.4	3.5
Zr/Nb	17.7	8.7	12.3	11.5	52.0	10.8

Table 11 Major and trace element data for high-Mg andesites (HMA), low-Ti tholeiites (LTT) and gabbros from mafic-ultramafic complexes.

	HMA	HMA	LTT	LTT	LTT	Gabbro	Gabbro
	85-0023	85-0028	85-0032	85-0034	60919	85-0107	85-0127
SiO2	55.70	54.12	58.52	62.21	49.78	49.28	50.30
TiO2	0.08	0.04	0.29	0.46	0.25	0.04	0.05
Al2O3	9.14	4.83	13.22	14.00	14.79	13.68	13.71
Fe2O3	10.83	11.18	13.67	10.00	10.64	11.13	11.15
MnO	0.18	0.35	0.13	0.15	0.18	0.20	0.20
MgO	18.60	18.68	4.51	4.99	10.54	12.73	12.36
CaO	5.00	10.26	7.79	4.78	11.77	11.97	10.99
Na2O	0.39	0.22	1.64	3.15	1.45	0.72	1.05
K2O	0.07	0.20	0.19	0.21	0.56	0.11	0.18
P2O5	0.01	0.13	0.04	0.05	0.04	0.14	<0.01
Total	100.00	100.00	100.00	100.00	100.00	100.00	100.00
LOI	8.29	5.10	2.80	8.06	1.71	2.89	1.90
Sc	26	21	47	44		44	
V	97	98	260	230	21	130	
Cr	860	2900	24	139		670	
Ni	687	570	58	70	172	165	
Rb	<4	13	6	6	7	10	6
Sr	10	32	49	64	36	180	140
Y	7	5	8	9	14	4	4
Zr	6	5	8	14	15	<2	<4
Nb	<4	<3	<4	<4	2	<3	<1
Ba	39	49	41	44		22	<1
Cu	70	10	17	75	53	14	18
Zn	84	89	48	84	66	60	68
Pb	14	5	3	9	9	2	<2
Mo	<0.5	<0.5	0.5	<0.5	<0.5	<0.5	<0.5
S	<100	<100	100	200	<100	100	<100
Au (ppb)	0.7	2.9	0.7	2.4	1.5	0.7	2.5
Pd		3	25			18	10
Pt		25	37			64	35
Ti/Zr	79.9	48.0	217.3	197.0	99.9		
Zr/Y	0.9	1.0	1.0	1.6	1.1		
Zr/Nb					7.5		

Table 12 Whole-rock major and trace element data for ultramafic rocks from the Heazlewood Complex (TDH1) and Serpentine Hill. Numbers beginning with 85- and outcrop samples. Analyses 85-0219 and 85-0228 are microprobe analyses of Cr-spinels from chromitite samples.

	Harzburgite TDH1/A	Harzburgite TDH1/B	Dunite TDH1/C	Pyroxenite TDH1/D	Dunite 85-0139
SiO2	43.48	43.36	40.23	53.05	42.14
TiO2	0.05	0.06	0.05	0.05	0.01
Al2O3	1.84	2.95	0.69	4.59	0.09
Fe2O3	10.40	11.21	15.15	7.51	7.73
MnO	0.18	0.17	0.20	0.16	0.10
MgO	43.27	40.88	43.66	26.42	49.89
CaO	0.78	1.35	0.03	8.19	0.02
Na2O	<0.2	<0.2	<0.2	<0.2	0.01
K2O	0.01	0.02	<0.01	0.02	0.01
P2O5	<0.03	<0.03	<0.03	<0.03	0.01
Total	100.00	100.00	100.00	100.00	100.00
LOI	14.58	12.93	14.42	3.25	8.42
Sc					
V					
Cr					1940
Ni					2660
Rb	<2	<2	<2	2	<4
Sr	<2	<2	<2	6	<4
Y	<2	<2	<2	2	<4
Zr	<1	<1	<1	1	<4
Nb	<1	<1	<1	<1	<4
Ba					
Cu	9	7	4	23	2
Zn	69	57	69	57	23
Pb	<2	<2	<2	2	2
Mo	<0.5	<0.5	<0.5	<0.5	1.0
S	100	100	<100	<100	200
Au (ppb)	0.3	0.3	0.3	0.7	0.4

	Dunite 85-0140	Pyroxenite 85-0154	Pyroxenite 85-0155	Chromitite 85-0219*	Chromitite 85-0228*
SiO2	42.66	55.53	53.05		
TiO2	0.02	0.01	0.02	Cr2O3 49.82	50.36
Al2O3	0.10	1.06	3.13	14.55	15.64
Fe2O3	7.50	7.73	8.18	29.40	27.67
MnO	0.10	0.17	0.17	0.55	0.30
MgO	49.53	33.69	32.22	8.98	9.19
CaO	0.02	1.75	3.06		
Na2O	0.04	0.05	0.03		
K2O	0.01	0.01	0.02		
P2O5	0.01	0.01	0.01		
Total	100.00	100.00	100.00	100.35	100.39
LOI	15.80	1.91	3.90		
Sc					
V					
Cr	1758	4862	4605		
Ni	2521	626	724		
Rb	<4	<4	<4		
Sr	<4	<4	4		
Y	<4	<4	<4		
Zr	<4	<4	<4		
Nb	<4	<4	<4		
Ba		<15	<15		
Cu	2	3	3	3	360
Zn	34	52	36	230	130
Pb	2	2	<2	2	7
Mo	<0.5	<0.5	<0.5	1.0	0.5
S	100	<100	<100	<100	<100
Au (ppb)	0.5	0.8	0.3	0.8	0.8
Pd	1	<1	2	5	2
Pt	13	<10	40	47	31

Table 13 Major and trace element data for Precambrian metamorphic rocks.

	Qtz-Musc-Graph Schist	Dolomite	Qtz-Musc-Chl Schist	Quartzite	Garn-Mica Schist	Qtz-Musc-Chl Schist
	PC2	PC3	PC4	PC6	PC10	PC12
SiO2	78.78	6.55	75.96	89.66	80.73	77.07
TiO2	0.61	<0.01	0.33	0.12	0.40	0.83
Al2O3	11.09	0.97	13.07	5.98	9.59	11.25
Fe2O3	3.96	0.16	2.67	0.90	3.59	5.21
MnO	0.03	<0.01	<0.01	0.01	0.05	0.07
MgO	1.90	19.73	1.18	0.81	0.71	1.85
CaO	0.04	29.51	0.18	<0.01	0.97	0.08
Na2O	0.10	0.10	<0.20	<0.20	2.76	0.01
K2O	3.46	0.05	6.52	2.51	1.17	3.55
P2O5	0.04	0.01	0.05	0.01	0.04	0.07
Total	100.00	99.67	100.00	100.00	100.00	100.00
LOI	4.71	42.59	1.85	1.01	0.55	2.73
Rb	108	3	142	57	68	121
Sr	16	64	8	3	61	38
Y	27	2	47	17	36	31
Zr	246	2	271	170	325	311
Nb	13	<1	13	5	12	16
Cu	21	3	3	2	3	26
Zn	62	8	18	<1	35	41
Pb	9	2	7	2	15	4
Mo	1.5	<0.5	0.5	1.5	2.5	0.5
S	7100	<100	<100	<100	<100	<100
Au (ppb)	0.6	0.2	0.2	0.2	0.4	0.5
Ti/Zr	14.9		7.3	4.2	7.4	16.0
Zr/Y	9.1	1.0	5.8	10.0	9.0	10.0
Zr/Nb	18.9		20.8	34.0	27.1	19.4

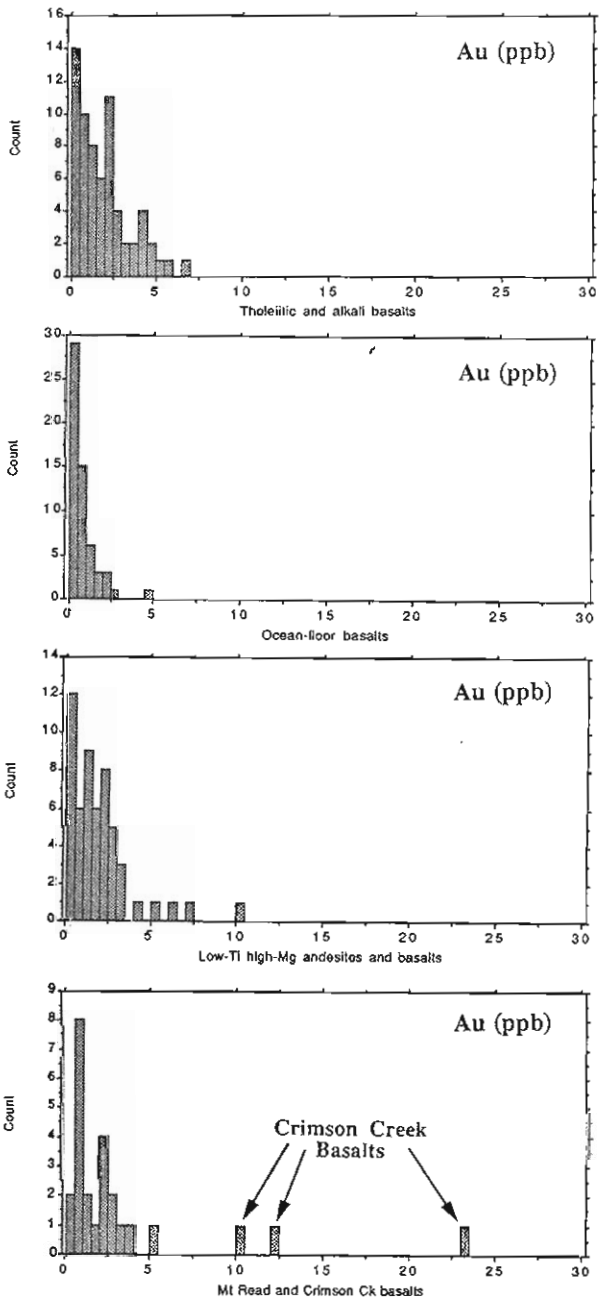

Figure 1 Frequency histograms comparing Au concentrations (ppb) in modern ocean island tholeiitic and alkali basalts, ocean-floor basalts, and low-Ti, high-Mg volcanics with the Mount Read basalts and high-Ti Crimson Creek basalts. Data for samples other than this study are from Gottfried et al. (1972), Keays and Scott (1976) and Hamlyn et al. (1985).

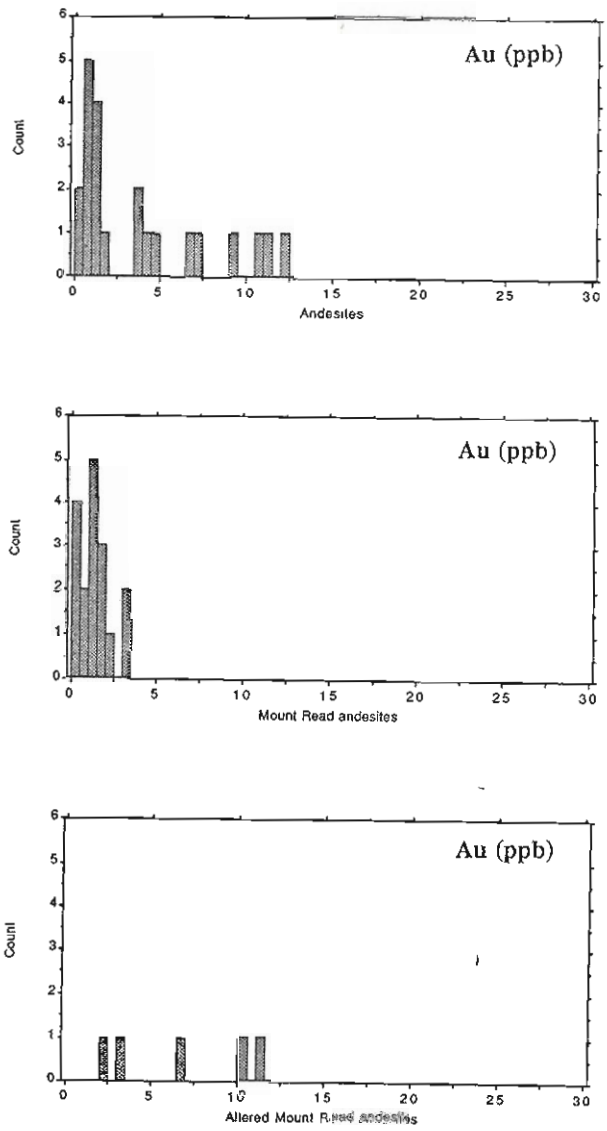

Figure 2 Frequency histograms comparing Au concentrations (ppb) of modern andesites with those for least altered and altered Mount Read andesites. Data for modern lavas principally from Gottfried et al. (1972).

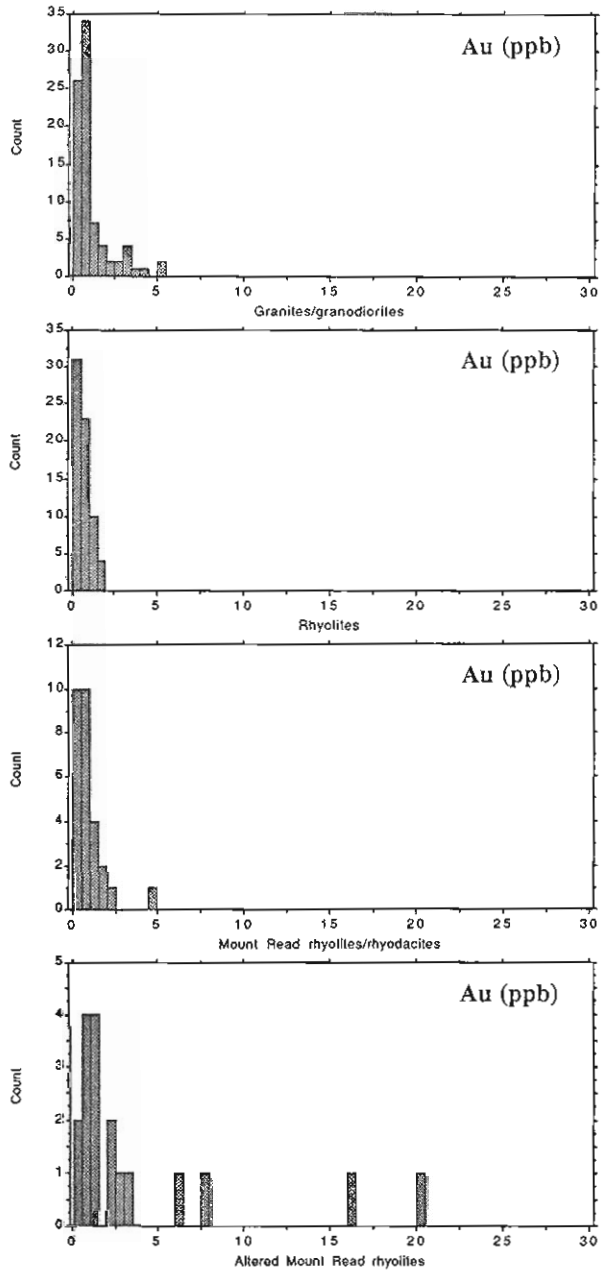

Figure 3 Frequency histograms comparing Au concentrations (ppb) of granites and granodiorites, and modern rhyolites with least altered and altered Mount Read rhyolites and rhyodacites. Data for the granites, granodiorites and modern rhyolites principally from Gottfried et al. (1972).

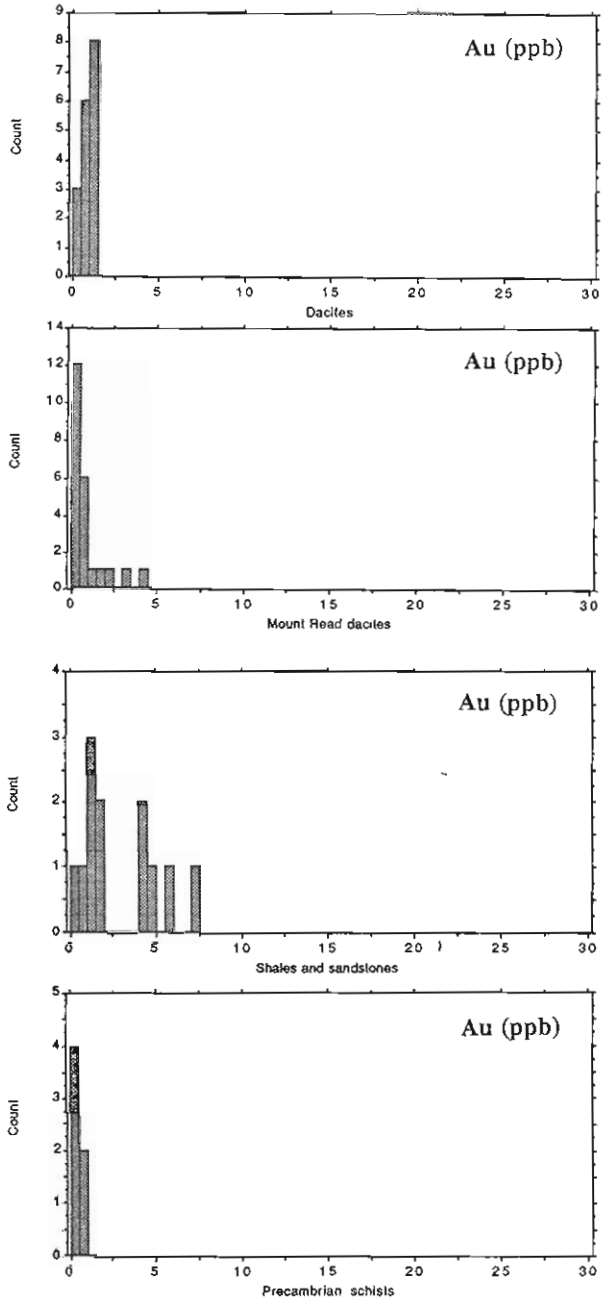

Figure 4 Frequency histograms comparing Au concentration data for modern dacites with the Mount Read dacites. Data for modern dacites from Gottfried et al. (1972). Histograms are also provided of the Au abundances for shales and sandstones interbedded with the Mount Read Volcanics, and for Precambrian schists from the Tyennan Block.

cover a similar range as fresh boninites from Papua Niugini, Cyprus and the Bonin Islands. These overlap values for basalts from the Que-Hellyer Sequence that are comparable with values for tholeiites and alkali basalts from intraplate oceanic island and continental settings, but generally a little higher than the majority of ocean-floor basalts (Fig. 1). In contrast, relatively Ti-rich basalts from the Crimson Creek Formation generally have markedly higher Au concentrations. Three samples (two from core and one outcrop sample) have Au contents in the range 10-23 ppb, whereas a second outcrop sample has considerably lower Au (0.1 ppb). Although this latter sample has a high TiO_2 content (>3 wt. %) which is typical of the Crimson Creek basalts, it has a much higher Zr/Nb (~52), and lower Cu content than the other three samples (Table 10). The higher Zr/Nb values are more typical of island arc volcanics, and the marked chemical differences between these samples collected from the Cleveland area indicate a complex relationship between these volcanics possibly involving tectonic juxtaposition.

The least altered MRV andesites, dacites and rhyodacites/rhyolites all have similar Au contents to modern fresh volcanics of similar composition (Figs. 2-4), whereas altered samples typically have elevated Au concentrations that are often associated with higher concentrations of other base metals. Epiclastic rocks have a similar range of Au contents to compositionally similar volcanics, whereas black shales interbedded with the MRV (Fig. 4) generally have slightly higher Au contents (0.9-7.3 ppb). Micaceous sandstones at the base of the Que-Hellyer Sequence have relatively low Au contents (~1 ppb).

Precambrian basement rocks which vary from greenschist to amphibolite facies grade assemblages (Turner, 1988), and include quartz-muscovite schists, dolomite, quartzite and garnet-mica schists, are strongly depleted in Au (<0.7 ppb).

The analyzed ultramafic rocks include serpentinized harzburgites, dunites, pyroxenites and associated chromitites. All have Au contents (Fig. 5) generally lower than those of unaltered peridotites (based principally on analyses of spinel and garnet lherzolite xenoliths), and also lower than values for harzburgites and dunites from ophiolites (Oshin and Crockett, 1982). A number of studies of chromite-rich rocks (e.g. Page *et al.*, 1982; Oshin and Crockett, 1982; Talkington and Watkinson, 1986) have shown that chromitites often have high concentrations of platinum group elements (PGE's) relative to the associated ultramafics. If the PGE's are concentrated in a sulphide phase (Talkington and Watkinson, 1986), enrichment in other precious metals (Au) might also be expected.

PGE analyses for the chromite-rich rocks have chondrite-normalized patterns similar to chromitites from ophiolites, except for a significant enrichment of Pt in the Tasmanian samples (Brown *et al.*, 1988). Even though the West Tasmanian chromitites contain minor laurite (Ru, Os, IrS_2), they have low Au contents.

CORRELATION OF GOLD WITH MAJOR AND TRACE ELEMENTS

Correlations of Au with major and trace elements for the total data set were examined in a series of computer plots. It was necessary to exclude the altered (Na_2O depleted) samples in order to study the primary geochemical variations with Au content. Figure 6 shows that the altered volcanics (<0.8 wt. % Na_2O) vary from 0.1 to 32ppb Au, however unaltered volcanics show no apparent relationship between Au and Na_2O contents. The general decrease in Au concentrations with increasing silica content observed in some data sets (Gottfried *et al.*, 1972; Tilling *et al.*, 1973; Crockett, 1978) is not as obvious in the western Tasmanian volcanics. The basaltic rocks clearly have a higher average Au concentration than the andesites and more silicic rocks, but there is little difference in the average values for the Mount Read andesites, dacites and rhyolites (Fig. 7).

No significant relationships were observed with any of the other major elements, however the trace elements showed some interesting patterns.

A weak correlation exists between Cu and Au, and S and Au (Figs. 8a,b), but no correlations are evident between Au and Pb or Zn (Figs. 8c,d). The Au-S correlation suggests the Au is concentrated in more S-enriched melts and probably occurs with pyrite in the rocks. The Au-Cu correlation suggests that minor amounts of chalcopyrite occur with the Au-pyrite grains. The Crimson Creek basalts are an exception to this trend, being enriched in both Cu and Au but depleted in S (Figs. 8a,b). This is interesting in view of reports of native Cu in Crimson Creek equivalent basalts from the Smithton Trough. In this case the Au may be included within the native Cu and unrelated to sulphide phases. More sampling is needed to resolve this possibility.

EFFECTS OF ALTERATION ON GOLD CONCENTRATIONS

The effects of different styles of alteration on the abundance and distribution of Au in the MRV have been assessed on several suites of samples. Rhyolites from the Jukes-Darwin area (JD2001, JD2002, Table 10) are characterized by a pronounced K-feldspar and hematitic alteration which is apparently related to the emplacement of Cambrian granitic magma. This style of alteration has not resulted in any significant increase in Au concentrations above the background values for the unaltered andesitic to rhyolitic volcanics. On the

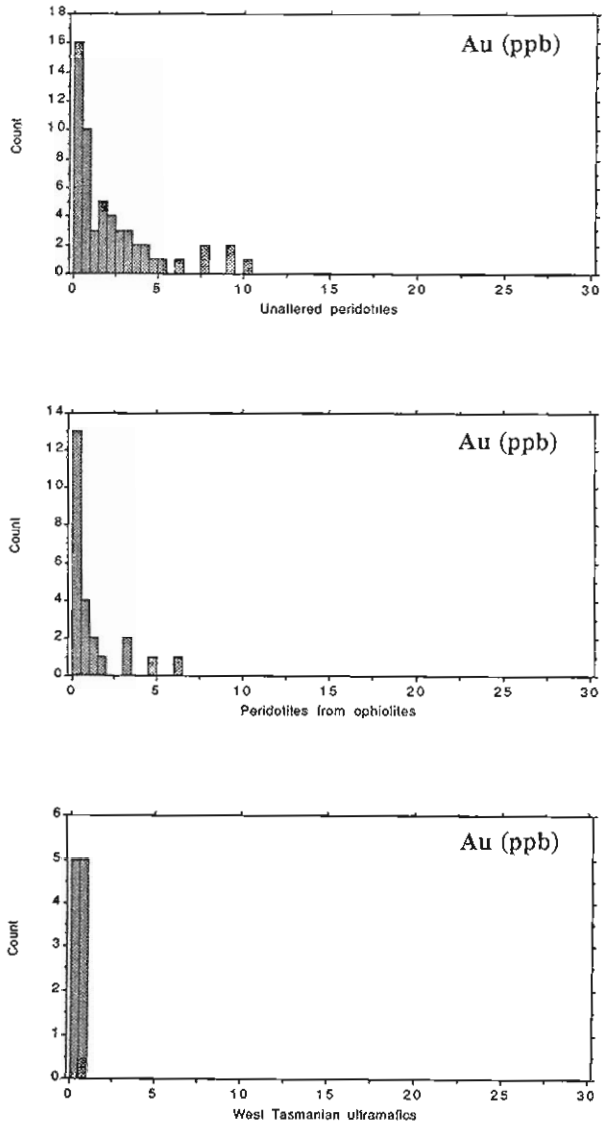

Figure 5 Frequency histograms comparing Au concentration data for unaltered spinel and garnet lherzolites, with harzburgites, dunites and pyroxenites from ophiolites and western Tasmania. Data for unaltered lherzolites from Ehmann et al. (1970), Basaltic Volcanism Study Project (1981), Mitchell and Keays (1981), Garuti et al. (1984), and ophiolites (Oshin and Crockett, 1982).

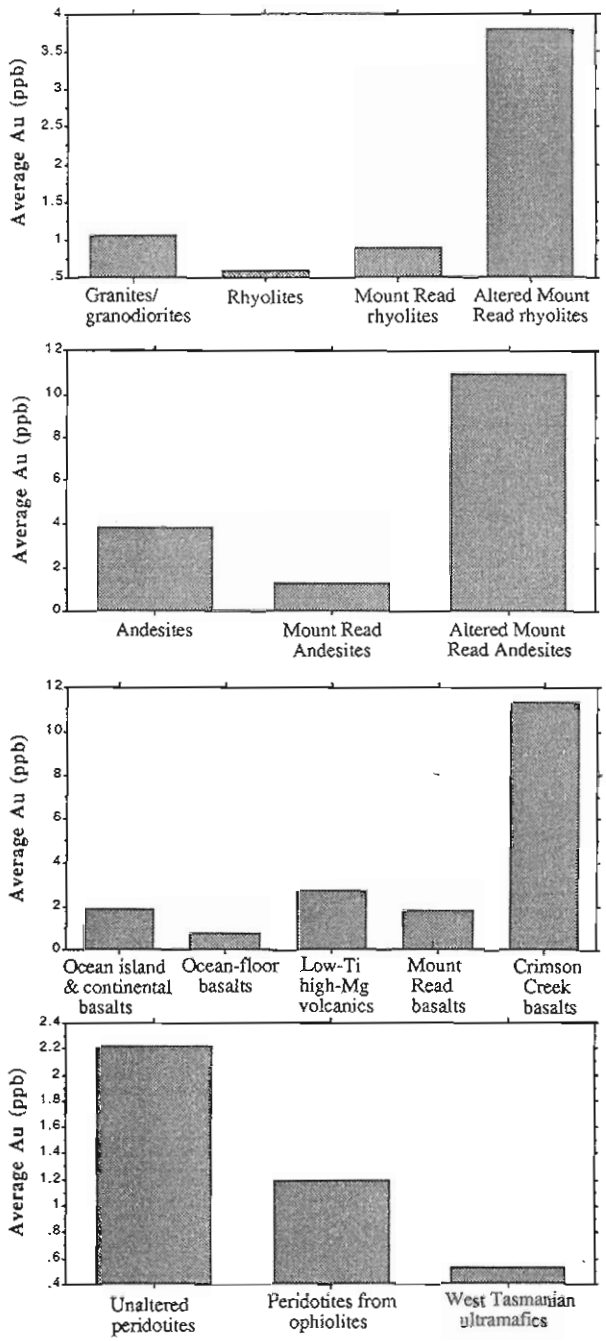

Figure 7 Bar graphs comparing the average Au abundances for various volcanic and ultramafic rock types with altered and relatively unaltered rocks of similar composition from western Tasmania.

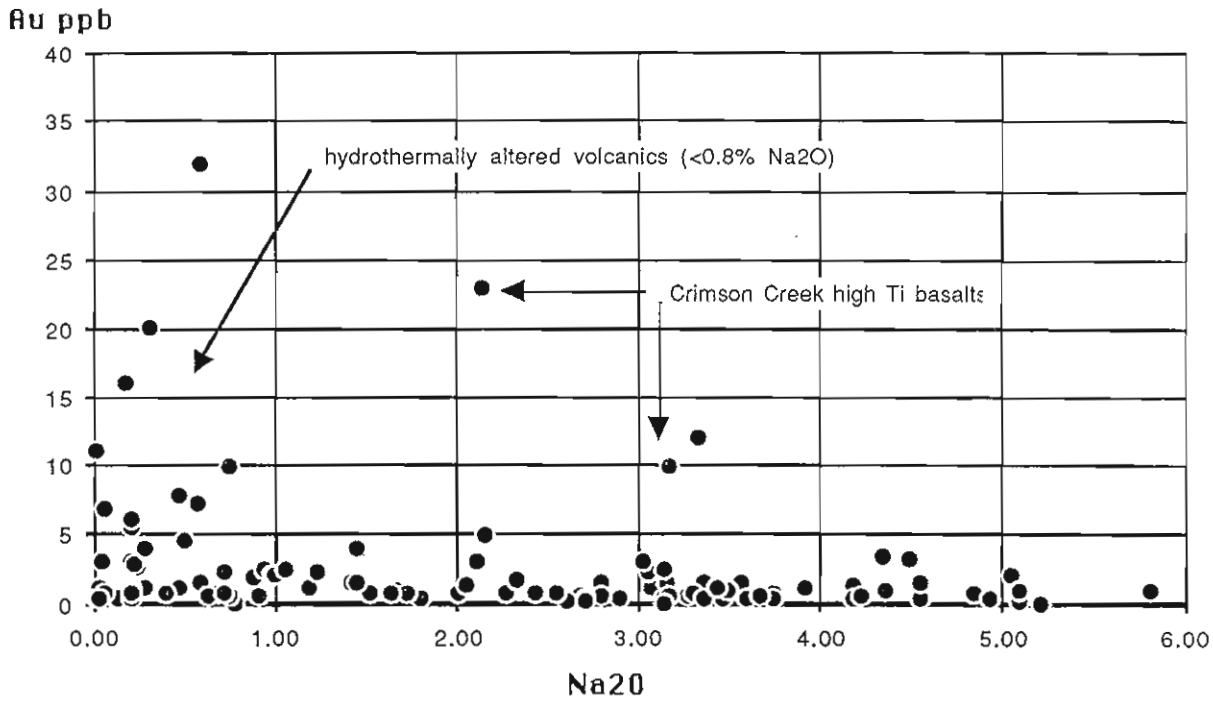

Figure 6 Plot of whole-rock Na_2O content versus Au for the whole data set which shows the enrichment of Au in the more altered Na_2O-depleted rocks.

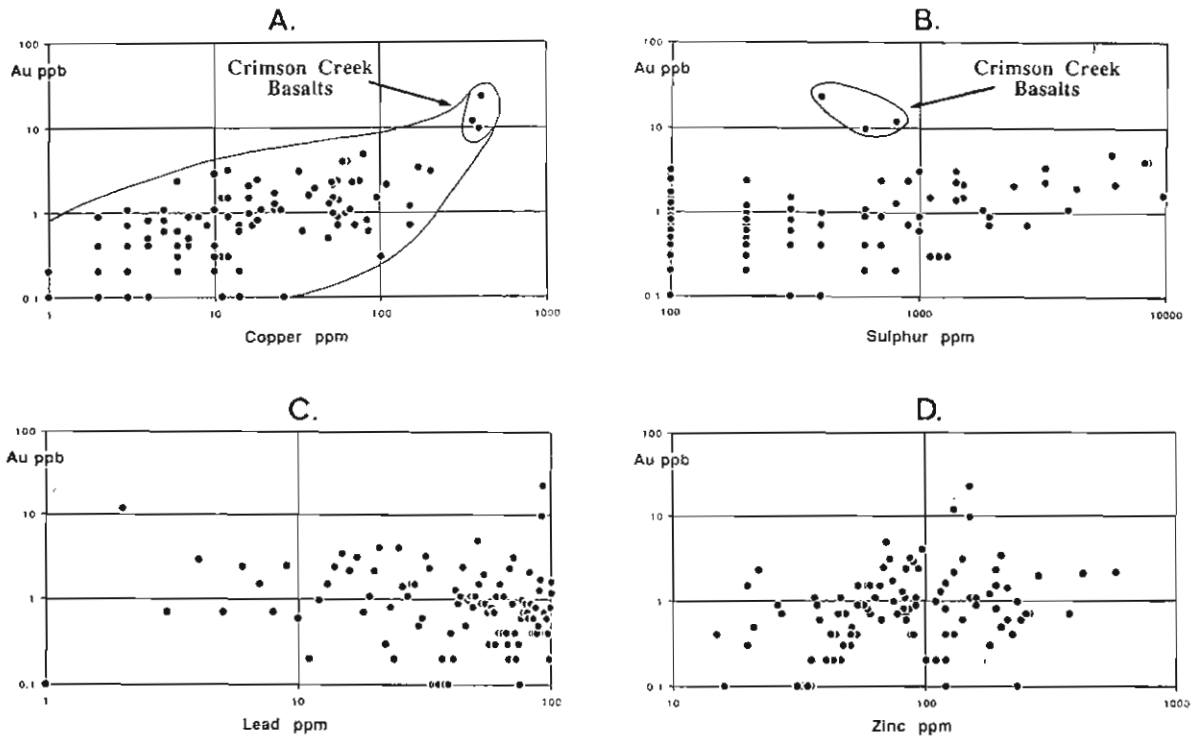

Figure 8 Relation of Au to Cu, S, Pb and Zn in the least altered data set. Note the weak positive correlations of Au with Cu and S, but lack of correlation with Pb and Zn.

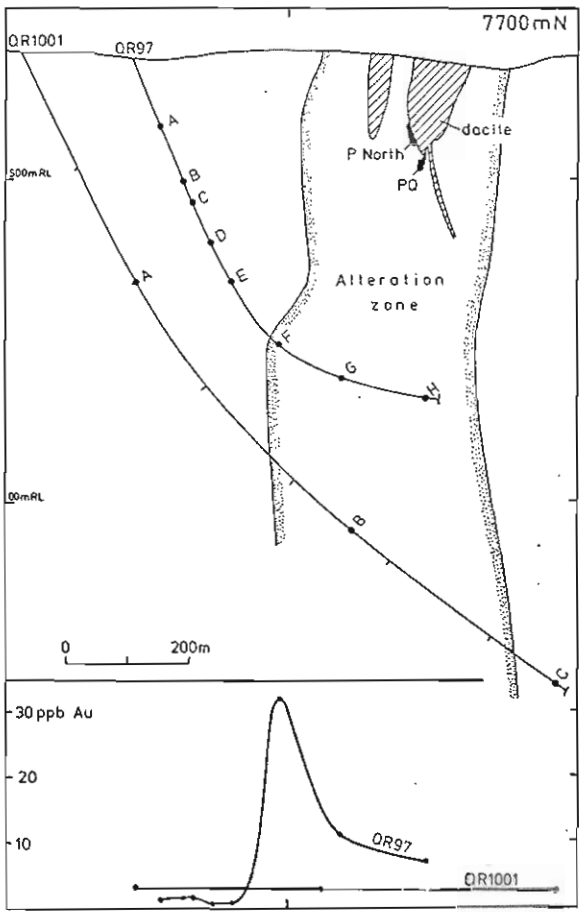

Figure 9 Section through the Que River massive sulphide deposit showing the position of the diamond drill hole QR97 and QR1001, and our samples from those holes relative to the alteration zone. The Au abundances for these core samples are plotted beneath.

other hand, extensive sericite and carbonate alteration of rhyolitic to andesitic volcanics at Howards Anomaly and Leech Hill is accompanied by higher Au and also usually higher base metal concentrations.

The effects of alteration on andesitic volcanics were also examined by sampling one of the deeper DDH at Que River which is collared in dacite (rhyolite), passes down through relatively unaltered andesite and eventually into the stringer zone beneath the Que River deposit (Fig. 9). Eight samples were selected at approximately 100m intervals. In addition, three samples were taken from a deeper hole (QR1001, Fig. 9); including a relatively unaltered andesite, an extensively altered andesite from the stringer zone, and another andesite from the other side of the stringer zone. The Au data for samples from QR97 (plotted at the bottom of Fig. 9) indicate normal background values in the unaltered dacite (rhyolite) and andesites. On approaching the stringer zone there is an interesting decrease in the Au contents of QR97/D and QR97/E, followed by a marked increase in Au at the margin of the stringer zone which decreases slightly towards the centre of the alteration zone.The depletion in Au concentrations at the outer edge of the stringer zone coincides with a bleached appearance of the volcanic in handspecimen and may reflect minor fluid activity and leaching adjacent to the principal zone of alteration and fluid activity. The relatively low Au content of QR1001/B which comes from the stringer zone in the deeper of these two holes may indicate that Au was not being deposited at that depth. Analysis of more closely spaced samples from both holes would be useful to clarify the nature of the zoning of Au concentrations within and adjacent to the stringer zone.

SURFACE LEACHING OF GOLD

An additional aspect of alteration relates to apparent differences in the Au concentrations between outcrop samples and those collected from DDH. The most notable differences exist between rhyolitic to dacitic samples collected from cuttings along the Pieman River Road and volcanics of similar composition collected from drill core in the Rosebery-Hercules area. Nearly all of the outcrop samples from the Pieman River Road had Au concentrations below the detection limit (0.1ppb), even though great care was taken to obtain the freshest material possible. Clearly the surface samples from this area have had virtually all of their Au leached by groundwater. In contrast, the outcrop samples of basalts from the Cleveland and Serpentine Hill areas do not appear to have been affected by this process.

EFFECTS OF METAMORPHISM ON AU DISTRIBUTION AND ABUNDANCE

Although our data base for the MRV and associated rocks do not indicate widespread anomalous Au concentrations in the footwall rocks to the VMS deposits, all of these rocks have experienced low-grade regional metamorphism. It is therefore important to establish whether the measured Au concentrations closely approximate original magmatic values or whether they have been modified by subsequent metamorphic events.

Considerable research on the greenstone belts of Canada and Western Australia has demonstrated the importance of metamorphic processes in the mobilization and redistribution of Au. During regional metamorphism at temperatures of 400-600°C, which results in the breakdown of greenschist facies to amphibolite facies assemblages, metamorphic degassing is widely regarded as the single most important process

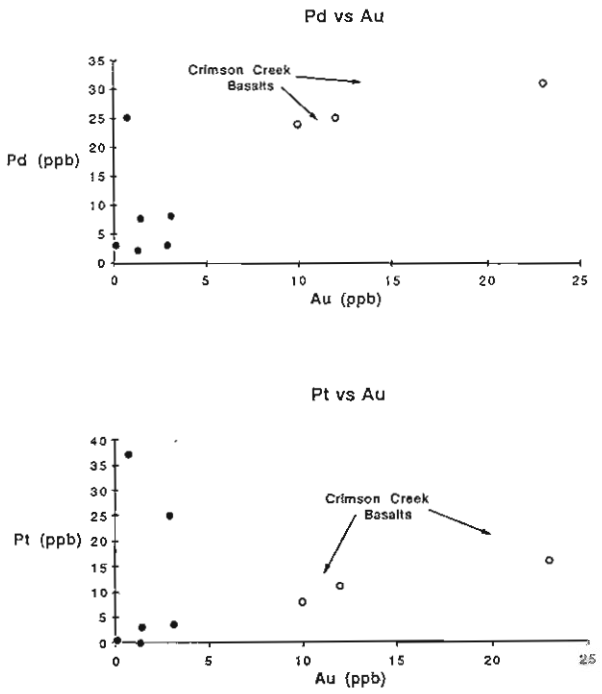

Figure 10 Plots of (a) Pd vs Au and (b) Pt vs Au for the western Tasmanian mafic volcanics.

in the leaching and transport of Au to form the Archean lode Au deposits (Fyfe and Kerrich, 1983). As might be expected, the breakdown of hydrous silicates such as chlorite to form biotite liberates considerable quantities of fluid along grain boundaries, and provides access of these fluids to Au in sulphide inclusions and in the silicates. Experimental work indicates that Au solubility increases markedly in Cl-bearing solutions at temperatures greater than 250°C. Therefore Au is likely to be very mobile at these higher metamorphic grades, particularly where the transfer of large volumes of fluid are involved. The very low Au concentrations in the Precambrian basement rocks in Tasmania may be the result of such metamorphic processes as peak metamorphic temperatures in some regions exceed 700°C (Turner, 1988). Alternatively, the low Au in these rocks may simply reflect a very mature and barren sedimentary precursor.

All of the western Tasmanian Cambrian volcanics have experienced low grade regional metamorphism ranging from prehnite-pumpellyite facies in the northern part of the MRV belt to greenschist facies elsewhere (Corbett and Solomon, 1988), with peak metamorphic temperatures probably less than 350°C. Locally, slightly higher temperatures were achieved in the southern part of the belt in response to the emplacement of the Devonian granitoids. Although Au mobility under amphibolite facies conditions is generally accepted, there is some dispute concerning the mobility of Au during greenschist facies metamorphism.

Significant loss of Au from the MRV and associated rocks during greenschist facies regional metamorphism seems unlikely in view of the close similarity of Au concentrations in the MRV and fresh modern volcanics of similar composition. Furthermore, the existence of a significant range of Au concentrations in the basaltic rock types would not be expected to survive if the Au was readily mobilized during the metamorphism. Serpentinization of the ultramafic rocks is also unlikely to have affected their Au concentrations. Studies of the precious metal concentrations of variably serpentinized dunites and harzburgites from the Thetford Mines ophiolite, Quebec, Canada (Oshin and Crockett, 1982) indicate that serpentinization had not significantly affected noble metal concentrations. Therefore, the low concentrations of Au in the West Tasmanian harzburgites, dunites and chromitites probably reflect original values.

Hamlyn *et al.* (1985) argued that fresh low-Ti lavas from the Bonin Islands and Papua Niugini have Au concentrations, Pd/Au and Ir/Au which reflect original magmatic compositions, whereas greenschist facies metamorphic equivalents from Victoria (generally characterized by much lower Au contents, and higher Pd/Au and Ir/Au) have been depleted in Au by seafloor alteration and metamorphic processes. This conclusion is based on the results of previous research which indicates that Ir and Pd are relatively immobile during seafloor alteration and metamorphism, whereas Au (and Pt) are relatively easily leached during seafloor alteration. Plots of Au versus Pd and Au versus Pt (Figs. 10a,b) for the West Tasmanian mafic rocks (Tables 2, 4 & 10; from Brown *et al.*, 1988 & this study) indicate a strong positive correlation of Au with Pd and Pt. The absence of any serious decoupling of Pd from the Pt and Au suggests that no significant loss or redistribution of Au (and Pt) occurred during the metamorphism.

One interesting aspect of the PGE data is that the Au/Pd values for the high-Ti Crimson Creek basalts are considerably higher than the values for fresh high-Mg andesites from the Bonin Islands. If, as we suspect, the Au/Pd values in both suites of rocks represent magmatic values, this has important implications for the melting relations of these basalts. Hamlyn *et al.* (1985) and Keays (1987) argued that the first-stage melts from a primitive peridotitic mantle are saturated in S at relatively low concentrations, implying that the depleted mantle residue contained a sulphide phase which buffered the S contents and precious metal concentrations of the melts. As the partition coefficients for Pd and Au between sulphide and melt are considered to be very large (~2000 and 250, respectively, Keays, 1987), the depleted mantle residue should be relatively enriched in PGE's and Au. Subsequent melting of such

a source to produce second-stage low-Ti high-Mg boninitic melts is considered to involve melting of this sulphide, thereby enriching these melts in precious metals relative to first-stage melts.

The high-Ti Crimson Creek basalts have major and trace element characteristics of melts generated from a primitive mantle source (first-stage melts), yet as noted above, they have considerably higher Au/Pd than most second-stage melts. This suggests the Crimson Creek basalts may not have been S-saturated when they were generated. The relatively high S contents of these basalts (400-800 ppm) compared with those of the low-Ti high-Mg lavas from the Bonin Islands (generally 20-120 ppm S, Hamlyn *et al.*, 1985) appears consistent with this interpretation.

SOURCE OF GOLD IN THE VMS DEPOSITS

If a special Au-rich source is necessary to provide the elevated Au contents in the Western Tasmanian VMS deposits our data suggests the choice of the most important geological unit is quite staightforwad. The immediate footwall rocks to the VMS deposits, the andesite, dacites and rhyolites of the Central Volcanic Complex and Western Sequence do not have anomalous Au concentrations, and although several of the interbedded black shales have slightly higher Au contents, volumetrically they are a relatively minor component of the stratigraphy. Similarly, if a layer of ophiolitic mafic-ultramafic rocks exists beneath the MRV belt as proposed by Berry and Crawford (1988), the low Au contents of the ultramafic rocks suggests that they were not a major contributor of Au to the VMS deposits. The low-Ti tholeiites and high-Mg andesitic rocks have higher Au than the ultramafic units, but only comparable with the Hellyer basalts and andesites.

The only rocks with anomalous Au concentrations that suggest they may be a suitable source for the Au are the basalts of the Crimson Creek Formation. These high-Ti basalts have Au concentrations up to 10 times those in the MRV, and they are generally higher than modern basalts of similar composition. The inferred distribution of the Crimson Creek Formation relative to the MRV also appears consistent with this model. In most recent tectonic reconstructions for western Tasmania (summarized in Fig. 11, after Corbett and Turner, 1988) the Crimson Creek Formation forms the basement on to which the MRV were erupted. Deep (possibly up to 6km) cone-shaped hydrothermal convection cells beneath an embryonic VMS deposit (Large, 1987) would have had access to the relatively Au, Cu and Zn-rich Crimson Creek basalts. However, the low Pb concentrations in these basalts (<6ppm) suggest that contributions of Pb from the overlying MRV belt may also have been necessary.

Clearly, in addition to source rock control, the composition and temperature of the hydrothermal fluids and the consequent solubility of the various metal species provide a powerful (and probably dominant) control on the final concentrations of base and precious metals in a specific massive sulphide deposit. These issues are addressed by Huston (1988), and in an accompanying report by Huston and Large (Exploration implications of the chemical model for gold deposition in volcanogenic massive sulphide systems).

One reservation regarding the role of the Crimson Creek basalts as the major source for the Au in the VMS deposits relates to the fact that all of our samples of these high-Ti basalts are from the Cleveland area. It could be argued that their higher Au concentrations may have been caused by fluids which emanated from nearby granitic intrusions. However, the Au contents of interbedded arkosic sediments are low (<2 ppb), and there is little evidence for the enrichment of Au in the skarn-type Sn deposits at Cleveland which are widely accepted as mineralization associated with the granitic rocks. The high Au contents also correlate with relatively high contents of Pt and Pd (Figs. 10a,b) that are not likely to be contributed by hydrothermal fluids derived from granites. We therefore consider that the high Au contents of these basalts closely reflect the original magmatic values, and the specific mantle source region for these basalts. It is intended to do a follow-up study on a suite of similar basalts from the Sorrell Peninsula and the Smithton area to confirm this conclusion.

EXPLORATION SIGNIFICANCE OF THE STUDY

Some important results which have emerged from this study and have significance are listed below:

1) The volcanics of the MRV belt contain sufficient Au to be the source of the Au in the VMS deposits (the mean values for the andesites and rhyolites are in the range 0.9-1.3 ppb). Large (1987) showed that only 0.2 ppb Au needs to be leached from approximately 60 km^3 of volcanics and basement rocks to produce a 20 mt deposit with an average grade of 2.5 g/t.

2) The early Cambrian ultramafic rocks have a mean Au content (~ 0.5 ppb) significantly less than the MRV and are therefore not likely to be a major source for the Au. The higher Au contents of their associated mafic rocks suggest they could have contributed some Au to the deposits if present in sufficient volume.

3) The high-Ti basalts of the early Cambrian Crimson Creek Formation are the most Au-enriched primary volcanics in the Dundas Trough (up to 23 ppb). These volcanics are thought to be associated with the first

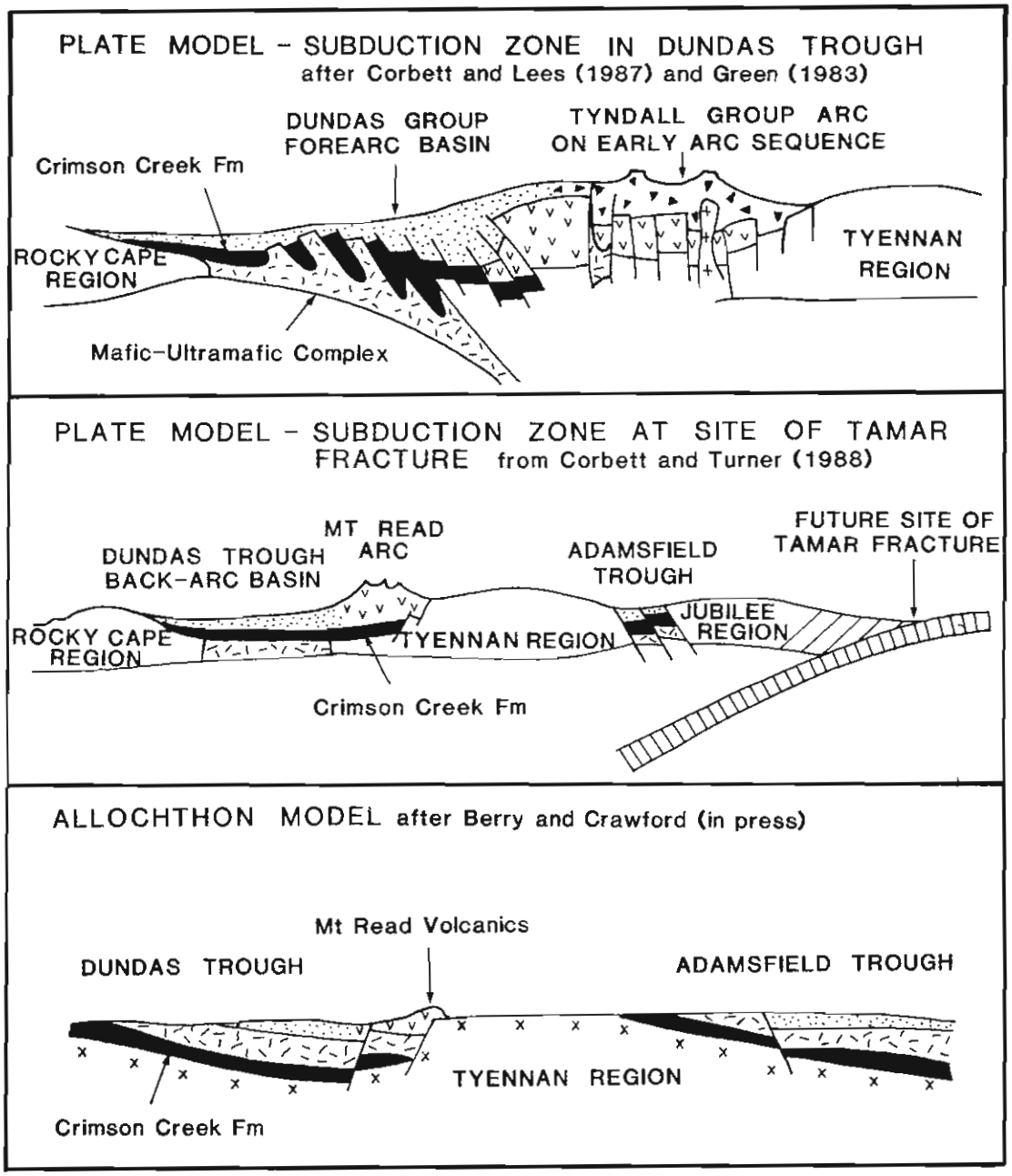

Figure 11 Summary of the more recent proposals for the Cambrian tectonic development of western Tasmania showing the implied relationship in each case between the MRV, Crimson Creek Formation, ultramafic-mafic complex rocks and the Precambrian basement (reproduced after Corbett, 1988).

rifting phase in the trough (Varne and Foden, 1987), and probably form a floor to the MRV.

4) The anomalous Au in the Crimson Creek high-Ti basalts indicates the potential for shear-related lode Au mineralization within or at the margins of the Crimson Creek equivalent lava sequences. The extensive Early Cambrian basalt-andesite sequences south of Macquarie Harbour (the Mainwaring Group) and in the Smithton Trough (Smithton basalts) are likely exploration targets.

5) Extensive leaching of trace quantities of Au from surface outcrops in the MRV is indicated from a comparison of Au analyses on surface and drill hole samples. Care is therefore required in exploration when comparing background and anomalous Au levels between surface and primary drill core samples.

ACKNOWLEDGMENTS

We are grateful to Keith Corbett, Mines Department of Tasmania, and the following individuals and companies (Doug Jack and Steve Richardson,Aberfoyle; Ian Gordon, EZ; Fergus Fitzgerald, Goldfields Exploration; David Hall, Shell Exploration) for access to drill core and assistance in sample selection. We thank Tony Brown for providing many of the mafic-ultramafic suite samples and relevant chemical data, and also Ron Berry and Tony Crawford for discussions on the MRV and tectonic development of Tasmania.

REFERENCES

Basaltic Volcanism Study Project (1981) *Basaltic Volcanism on the Terrestrial Planets.* Pergamon Press, New York, 1286pp.

Berry, R.F. and Crawford, A.J. (1988) The tectonic significance of Cambrian allochthonous mafic-ultramafic complexes in Tasmania. *Aust. J. Earth Sci.* (in press).

Brown, A.V., Page, N.J. and Love, A.H. (1988) Geology and platinum-group-element geochemistry of the Serpentine Hill Complex, Dundas Trough, western Tasmania. *Can . Mineral.* 26, 161-175.

Corbett, K.D. and Lees, T.C. (1987) Stratigraphic and structural relationships and evidence for Cambrian deformation at the western margin of the Mt Read Volcanics, Tasmania. *Aust. J. Earth Sci.* 34, 45-67.

Corbett, K.D. and Solomon, M. (1988) Cambrian Mt Read Volcanics and mineral deposits. In : C.F. Burrett and E. Martin (eds) The Geology and Mineral Resources of Tasmania. Geol. Soc. Aust. (Tasm. Div.), in press.

Corbett, K.D. and Turner, N.J. (1988) Early Palaeozoic deformation and tectonics. In : C.F. Burrett and E. Martin (eds) The Geology and Mineral Resources of *Tasmania.* Geol. Soc. Aust. (Tasm. Div.), in press.

Crawford, A.J. (1986) Chemistry of volcanics in the Mt. Read Arc. *AMIRA Progress Report* (April) - Controls on gold and silver grades in volcanogenic sulphide deposits (84/P210), 29-35.

Crawford, A.J. (1987) Geochemistry of the Mount Read Volcanics : internal correlations and tectonic implications. *AMIRA Second Annual Report* (August) - Controls on gold and silver grades in volcanogenic sulphide deposits (84/P210), 79-108.

Crawford, A.J. and Berry, R.F. (1988) Petrogenesis and tectonic implications of Late Proterozoic - Early Palaeozoic igneous rock associations in western Tasmania. *Aust. J. Earth Sci.* (in press).

Crockett, J.H. (1978) Gold. *In : Handbook of Geochemistry* II/5 (K.H. Wedepohl, ed.) Springer-Verlag, Berlin.

Ehmann, W.D., Baedecker, P.A. and McKown, D.M. (1970) Gold and iridium in meteorites and some selected rocks. *Geochim. Cosmochim. Acta* 34, 493-507.

Fyfe, W.S. and Kerrich, R. (1983) Gold : natural concentration processes. *In : Gold 82, The geology, geochemistry of gold deposits. Proc. Symposium Gold '82,* University of Zimbabwe, Geological Society of Zimbabwe, 99-127.

Garuti, G., Gorgoni, C. and Sighinolfi, G.P. (1984) Sulfide mineralogy and chalcophile and siderophile element abundances in the Irea-Verbano mantle peridotites (western Italian Alps). *Earth Planet. Sci. Lett.* 70, 69-87.

Gottfried, D., Rowe, J.J. and Tilling, R.I. (1972) Distribution of gold in igneous rocks. *U.S. Geol. Surv. Prof. Pap.* 727, 42pp.

Hamlyn, P.R., Keays, R.R., Cameron, W.E., Crawford, A.J. and Waldron, H.M. (1985) Precious metals in magnesian low-Ti lavas : implications for metallogenesis and sulfur saturation in primary magmas. *Geochim. Cosmochim. Acta* 49, 1797-1811.

Huston, D. and Large, R.R. (1988) A chemical model for the deposition of gold in volcanogenic massive sulphide systems. *Ore Geology Reviews* (in press).

Keays, R.R. (1987) Principles of mobilization (dissolution) of metals in mafic and ultramafic rocks - the role of immiscible magmatic sulphides in the generation of hydrothermal gold and volcanogenic massive sulphide deposits. *Ore Geology Reviews* 2, 47-63.

Keays, R.R. and Scott, R.B. Precious metals in ocean-ridge basalts : implications for basalts as source rocks for gold mineralization. *Econ. Geol.* 71, 705-720.

Large, R.R. (1987) Source and movement of gold and base metals in submarine volcanic systems : a discussion paper. *AMIRA Second Annual Report* (August) - Controls on gold and silver grades in volcanogenic sulphide deposits (84/P210), 170-182.

Large, R.R., Crawford, A.J. and Adrichem, S. (1986) Primary alteration chemistry of the Mount Read Volcanics. *AMIRA Progress Report* (November) - Controls on gold and silver grades in volcanogenic sulphide deposits (84/P210), 38-45.

Mitchell, R.H. and Keays, R.R. (1981) Abundance and distribution of gold, palladium and iridium in some spinel and garnet lherzolites : implications for the nature and origin of precious metal-rich intergranular components in the upper mantle. *Geochim. Cosmochim. Acta* 45, 2425-2442.

Oshin, I. O. and Crockett, J.H. (1982) Noble metals in Thetford Mines Ophiolites, Quebec, Canada. Part I : Distribution

of gold, iridium, and palladium in the ultramafic and gabbroic rocks. *Econ. Geol.* 77, 1556-1570.

Page, N.J., Cassard, D. and Haffty, J. (1982) Palladium, platinum, rhodium, ruthenium, and iridium in chromitites from the Massif du Sud and Tiebaghi Massif, New Caledonia. *Econ. Geol.* 77, 1571-1577.

Talkington, R.W. and Watkinson, D.H. (1986) Whole-rock platinum-group element trends in chromite-rich rocks in ophiolitic and stratiform igneous complexes. *Proc. Conf. Metallogeny of basic and ultrabasic rocks*, The Institution of Mining and Metallurgy (M.J. Gallagher *et al.*, eds), 427-440.

Tilling, R.I., Gottfried, D. and Rowe, J.J. (1973) Gold abundance in igneous rocks : bearing on gold mineralization. *Econ. Geol.* 68, 168-186.

Turner, N.J. (1988) The Precambrian rocks. In : C.F. Burrett and E. Martin (eds) The Geology and Mineral Resources of Tasmania. Geol. Soc. Aust. (Tasm. Div.), in press.

Varne, R. and Foden, J.D. (1987) Tectonic setting of Cambrian rifting, volcanism and ophiolite formation in western Tasmania. *Tectonophysics* 140, 275-295.

APPENDIX I

LOCALITIES, DESCRIPTIONS AND CHEMICAL DATA FOR SAMPLES USED IN THE GOLD SOURCE-ROCK STUDY

Location:- Pieman River Road - Outcrop samples collected from road cuttings.

PRR/B Dacite (<0.1ppb Au)
AMG Reference:- 383861mE 5381337mN
Petrography:- Phenocrysts of plagioclase in a recrystallized quartz-feldspar-rich groundmass with minor chlorite and epidote, and veins of epidote.

PRR/C Dacite (<0.1ppb Au)
AMG Reference:- 383168mE 5380693mN
Petrography:- Plagioclase phenocrysts (embayed and partly carbonated) in a finer groundmass of quartz, chlorite, feldspar and carbonate.

PRR/D Dacite (<0.1ppb Au)
AMG Reference:- 382178mE 5380223mN
Petrography:- Plagioclase phenocrysts (partly kaolinized/carbonated) in a groundmass of quartz, feldspar, chlorite and sericite.

PRR/E Dacite (0.2ppb Au)
AMG Reference:- 381733mE 5380099mN
Petrography:- Phenocrysts of quartz and plagioclase (minor carbonate alteration) in a fine recrystallized groundmass of quartz, feldspar, sericite and chlorite with a weak foliation.

PRR/F Rhyodacite (<0.1ppb Au)
AMG Reference:- 380842mE 5380099mN
Petrography:- Plagioclase phenocrysts in a fine groundmass of feldspar, quartz, chlorite and carbonate.

PRR/G Rhyodacite (0.1ppb Au)
AMG Reference:- 379802mE 5380296mN
Petrography:- Phenocrysts of quartz and plagioclase in a recrystallized groundmass composed of quartz, feldspar, chlorite and sericite (weakly foliated).

PRR/H Rhyolite (0.4ppb Au)
AMG Reference:- 379185mE 5380222mN
Petrography:- Plagioclase and quartz (embayed) phenocrysts in a quartz-feldspar-rich groundmass with a weak foliation defined by chlorite and sericite.

PRR/I Dacite (0.2ppb Au)
AMG Reference:- 378741mE 5379728mN
Petrography:- Epiclastic rock rich in plagioclase and quartz grains with a finer matrix of quartz, feldspar, chlorite, sericite and carbonate.

Geochemistry

PRR	B	C	D	E	F	G	H	I
SiO_2	67.96	65.12	64.86	67.68	72.61	70.85	69.08	66.02
TiO_2	0.58	0.57	0.61	0.28	0.25	0.35	0.29	0.46
Al_2O_3	14.41	14.24	15.39	16.01	13.33	14.09	13.41	14.00
Fe_2O_3	4.82	4.90	6.20	3.09	2.64	3.01	3.31	4.43
MnO	0.08	0.09	0.16	0.04	0.08	0.07	0.09	0.08
MgO	1.48	1.10	1.31	0.71	0.80	0.53	0.68	1.05
CaO	2.68	3.46	2.11	1.49	1.49	1.66	3.04	3.14
Na_2O	5.55	3.57	3.49	3.34	4.72	3.47	2.02	3.89
K_2O	1.06	2.41	2.56	4.05	2.73	3.35	3.29	2.54
P_2O_5	0.13	0.13	0.13	0.04	0.03	0.08	0.07	0.14
LOI	1.30	4.20	3.76	2.87	1.68	2.68	4.03	3.79
Total	100.05	99.79	100.58	99.60	100.36	100.14	99.31	99.54
Rb	32	100	102	157	71	133	146	127
Sr	169	113	107	106	134	113	114	163
Y	35	33	48	49	46	22	31	44
Zr	212	210	238	328	272	268	175	205
Nb	12	12	13	20	17	17	10	11
Cu	26	3	4	1	1	2	2	14
Zn	35	32	31	43	16	34	53	40
Pb	6	4	7	11	4	4	12	9
Mo	<0.5	<0.5	0.5	0.5	<0.5	0.5	<0.5	<0.5
S	<100	300	100	<100	<100	300	100	200
Ti/Zr	17	17	16	5	6	8	10	14

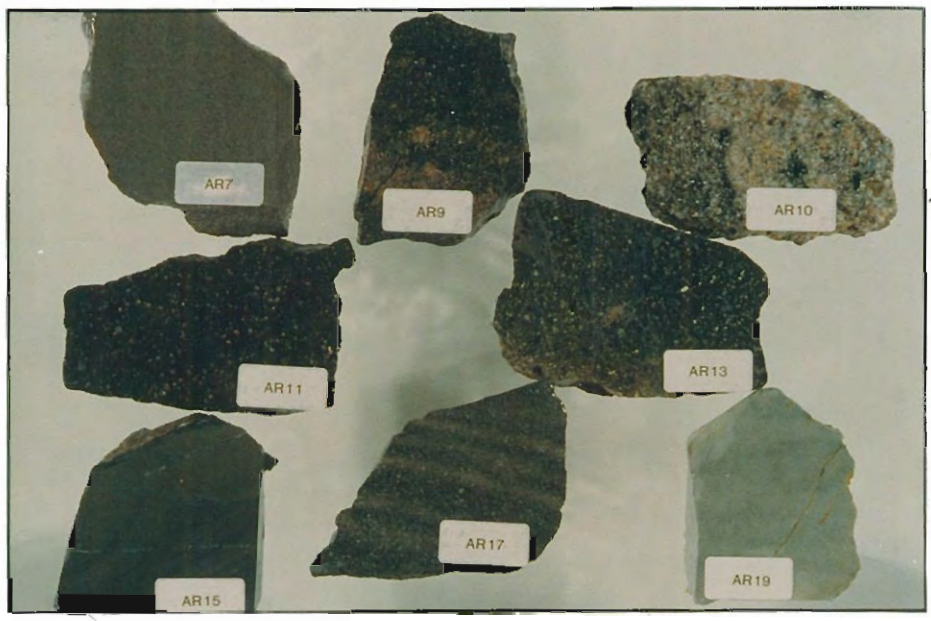
AR7
AR9
AR10
AR11
AR13
AR15
AR17
AR19

Location:- Hellyer
DDH:- MAC1 (Aberfoyle Exploration, Hellyer)
Collar AMG Reference:- 393096.2mE 5394851.9mN
MAC1/A Basalt (2.4ppb Au)
Sample Interval:- 173.4-202.6m
Petrography:- Extensively carbonated aphyric rock composed of interlocking plagioclase laths with interstitial chlorite, carbonate and quartz. Rare carbonate pseudomorphs after plagioclase, and some vesicles filled with quartz.

Location:- Hellyer
DDH:- MAC5 (Aberfoyle Exploration, Hellyer)
Collar AMG Reference:- 392965.7mE 5394957.9mN
MAC5/A Andesite (3.4ppb Au)
Sample Interval:- 216.7-239.9m
Petrography:- Plagioclase phenocrysts (partly carbonated) in a fine groundmass of plagioclase, chlorite, and carbonate.
MAC5/B Basalt (2.2ppb Au)
Sample Interval:- 201.8-216.7m
Petrography:- Aphyric fine-grained feldspar-rich rock extensively carbonated in patches with groundmass sericite, chlorite and clinozoisite.

Geochemistry

	MAC1/A	MAC5/A	MAC5/B
SiO_2	44.43	54.73	47.64
TiO_2	0.28	0.48	0.47
Al_2O_3	10.79	14.51	11.83
Fe_2O_3	8.26	7.65	8.64
MnO	0.18	0.12	0.27
MgO	9.01	4.53	5.90
CaO	9.73	5.83	9.28
Na_2O	0.78	4.02	0.85
K_2O	0.87	0.63	1.69
P_2O_5	0.12	0.21	0.28
LOI	15.27	7.11	13.13
Total	99.27	99.82	99.98
Rb	34	25	68
Sr	157	240	123
Y	12	14	19
Zr	42	69	107
Nb	2	4	6
Cu	55	170	110
Zn	190	200	130
Pb	6	12	8
Mo	<0.5	1.5	0.5
S	700	3200	1500
Ti/Zr	47	45	30

Location:- Hellyer
DDH:- MAC10 (Aberfoyle Exploration, Hellyer)
Collar AMG Reference:- 391835.4mE 5396974.3mN
MAC10/A Hellyer Basalt (3.1ppb Au)
Sample Interval:- 141.2-153.9m & 193.8-201.5m
Petrography:- Phenocrysts of clinopyroxene in a groundmass of interlocking plagioclase laths with interstitial clinopyroxene, sphene, carbonate and chlorite.
MAC10/B Andesite (FPA) (0.7ppb Au)
Sample Interval:- 332.9-347.2m
Petrography:- Euhedral plagioclase phenocrysts in a fine recrystallized groundmass of quartz and plagioclase and chlorite (possibly after glass).
MAC10/C Lower Basalt / Andesite (1.1ppb Au)
Sample Interval:- 378.2-393.4m
Petrography:- Occasional phenocrysts of plagioclase (partly carbonated) and some large segregations of recrystallized quartz in a fine groundmass of quartz and feldspar, chlorite, carbonate and minor sericite.
MAC10/D Andesite (2.2ppb Au)
Sample Interval:- 454.6-468.8m
Petrography:- Plagioclase phenocrysts (often in aggregates) in a fine groundmass of plagioclase laths, chlorite, quartz and sphene. Some larger aggregates of quartz and chlorite.
MAC10/E Micaceous sandstone (4.0ppb Au)
Sample Interval:- 482.1-489.4m & 515.5-519.2m
Petrography:- Abundant angular quartz grains with subordinate plagioclase and microcline in a matrix of quartz, muscovite and chlorite.

Geochemistry

	MAC 10/A	MAC 10/B	MAC 10/C	MAC 10/D	MAC 10/E
SiO_2	49.61	67.01	59.80	60.69	63.48
TiO_2	0.79	0.39	0.39	0.57	0.58
Al_2O_3	11.76	14.98	12.33	14.68	13.11
Fe_2O_3	7.90	4.96	6.05	6.96	5.18
MnO	0.25	0.12	0.15	0.14	0.08
MgO	7.83	1.80	5.35	3.03	2.63
CaO	9.13	1.53	5.90	2.83	3.82
Na_2O	1.94	6.18	3.73	4.84	1.35
K_2O	1.88	1.27	1.18	1.86	3.36
P_2O_5	0.73	0.14	0.18	0.17	0.11
LOI	7.30	2.29	4.44	3.70	6.05
Total	99.12	100.67	99.50	99.47	99.75
Rb	51	32	41	51	180
Sr	370	288	271	334	96
Y	31	36	27	30	33
Zr	333	228	147	150	170
Nb	12	15	11	11	19
Cu	200	9	66	52	63
Zn	140	260	150	570	97
Pb	23	58	87	109	44
Mo	3.5	0.5	1.5	3.0	4.0
S	1000	<100	600	6200	8500
Ti/Zr	15	11	17	24	22

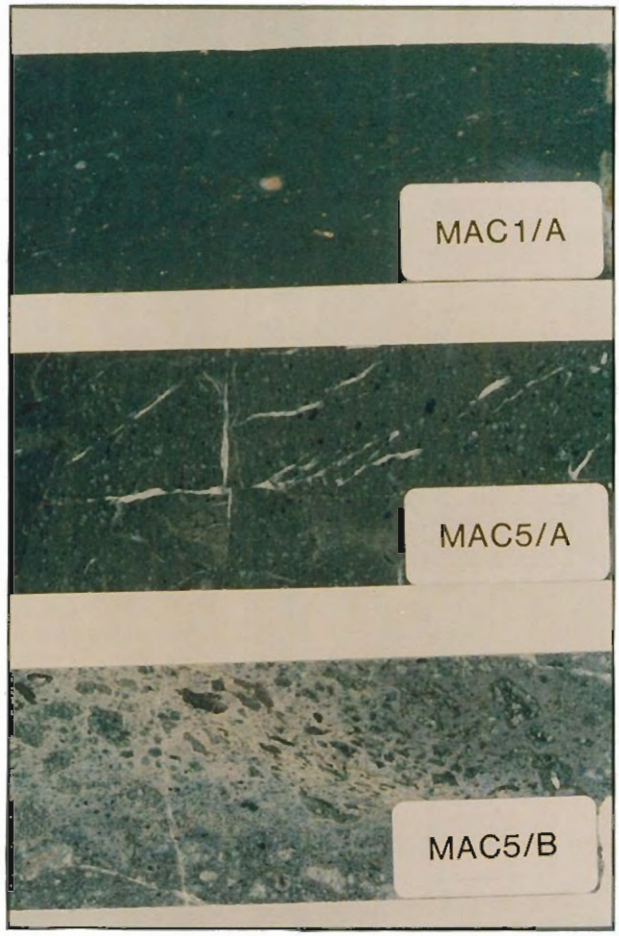
MAC1/A
MAC5/A
MAC5/B

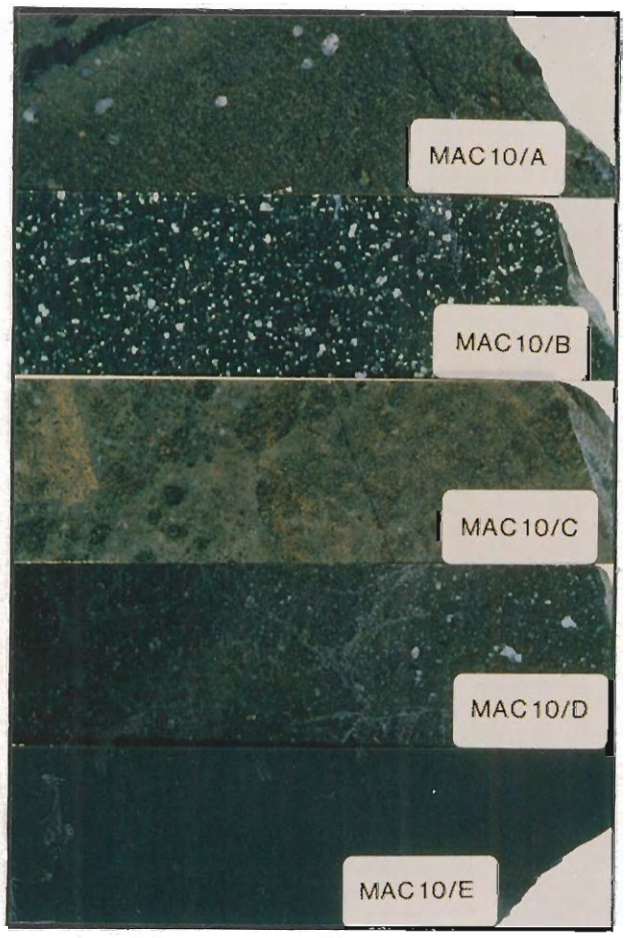
MAC10/A
MAC10/B
MAC10/C
MAC10/D
MAC10/E

Location:- 3km west of Hellyer
DDH:- HAT5 (Aberfoyle Exploration, Hellyer)
Collar AMG Reference:- 390232.9mE 5396192.9mN
HAT5/A Andesite (1.4ppb Au)
Sample Interval:- 259.1-298.6
Petrography:- Interlocking plagioclase laths with interstitial chlorite, quartz and granular sphene. Substantial carbonate alteration of feldspar.

Location:- 3.5km southwest of Hellyer
DDH:- HAT6 (Aberfoyle Exploration, Hellyer)
Collar AMG Reference:- 390717.3mE 5393692.3mN
HAT6/A Dacite (0.2ppb Au)
Sample Interval:- 192.5-199.5m
Petrography:- Porphyritic dacite with phenocrysts of plagioclase (partly carbonated) in a groundmass of fine tabular plagioclase crystals with interstitial chlorite, sphene and patchy sericitization.

Geochemistry

	HAT5/A	HAT6/A
SiO_2	54.31	66.00
TiO_2	0.42	0.44
Al_2O_3	12.42	15.65
Fe_2O_3	7.18	5.26
MnO	0.19	0.09
MgO	7.98	1.86
CaO	6.12	0.86
Na_2O	3.88	6.35
K_2O	0.18	0.65
P_2O_5	0.18	0.10
LOI	6.77	2.12
Total	99.63	99.38
Rb	7	27
Sr	228	112
Y	27	30
Zr	137	158
Nb	10	11
Cu	56	6
Zn	210	100
Pb	50	4
Mo	1.5	1.5
S	1400	<100
Ti/Zr	20	17

Location:- Hellyer
DDH:- HL55 (Aberfoyle Exploration, Hellyer)
Collar AMG Reference:- 393565.4mE 5396549.6mN
HL55/A Hellyer Basalt (0.3ppb Au)
Sample Interval:- 144.0-153.7m
Petrography:- Aggregates of clinopyroxene microphenocrysts set in a groundmass of plagioclase laths , interstitial clinopyroxene, minor chlorite, sphene and carbonate.
HL55/B Hellyer Basalt (0.8ppb Au)
Sample Interval:- 183.5-199.0m
Petrography:- Plagioclase (largely pseudomorphed by carbonate) and clinopyroxene phenocrysts in a groundmass of plagioclase, clinopyroxene, carbonate, actinolite, chlorite and sphene. Minor carbonate veining.

Location:- Hellyer
DDH:- HL30 (Aberfoyle Exploration, Hellyer)
Collar AMG Reference:- 393117.6mE 5396731.7mN
HL30/A Andesite (4.1ppb Au)
Sample Interval:- 469.6-484.4m
Petrography:- Porphyritic andesite with slightly kaolinized plagioclase phenocrysts in a groundmass composed of fine tabular plagioclase, chlorite, sphene and minor clinozoisite. Some carbonate segregations.

Geochemistry

	HL55/A	HL55/B	HL30/A
SiO_2	51.95	47.88	62.64
TiO_2	0.63	0.45	0.58
Al_2O_3	12.46	13.31	16.04
Fe_2O_3	8.78	8.53	6.35
MnO	0.15	0.18	0.09
MgO	9.57	10.74	2.73
CaO	8.77	10.08	2.27
Na_2O	2.81	1.42	5.98
K_2O	1.54	0.89	0.86
P_2O_5	0.30	0.16	0.10
LOI	3.69	6.28	2.66
Total	100.65	99.92	100.30
Rb	27	21	25
Sr	559	320	188
Y	25	17	23
Zr	155	67	115
Nb	10	5	8
Cu	100	83	59
Zn	50	86	97
Pb	2	3	16
Mo	<0.5	<0.5	<0.5
S	1100	200	8200
Ti/Zr	25	43	31

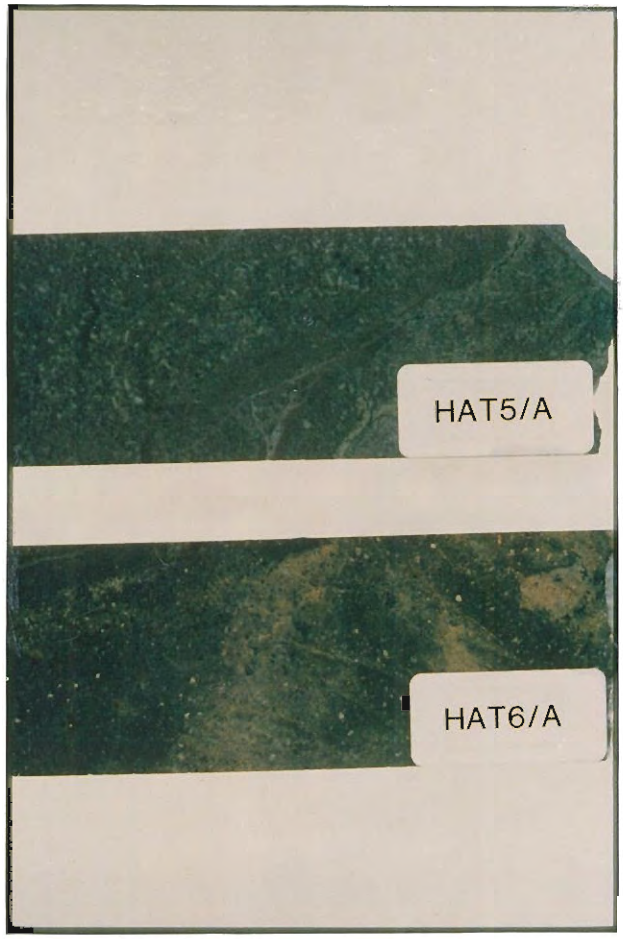
HAT5/A
HAT6/A

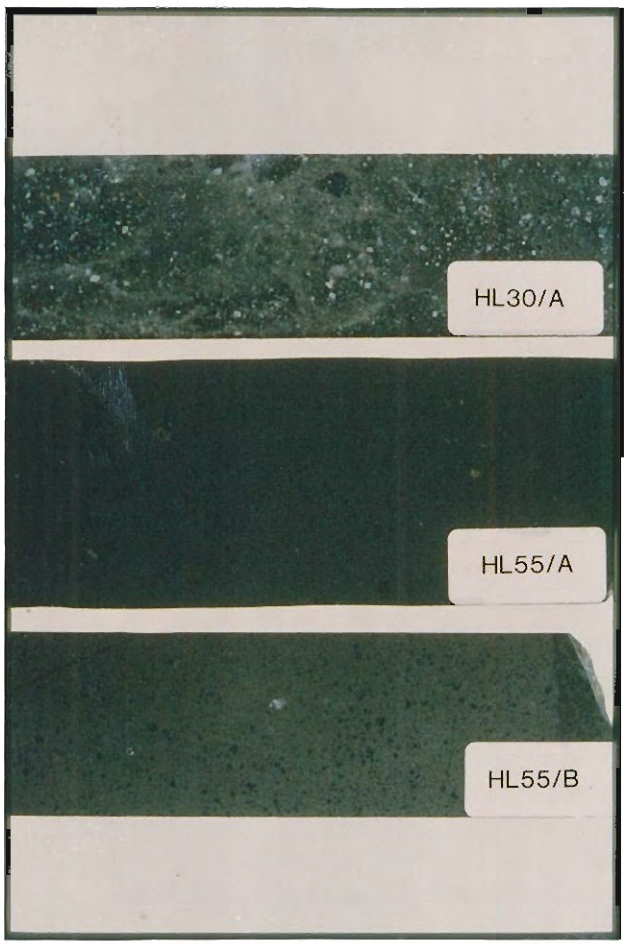
HL30/A
HL55/A
HL55/B

Location:- Mt Charter
DDH:- MC1 (Mines Department) = MC15 (Aberfoyle)
Collar AMG Reference:- 389040mE 5391170mN
MC1/A Black Shale (5.5ppb Au)
Sample Interval:- 3.5-5.7m
Petrography:- Very fine grained carbonaceous shale with dispersed angular quartz grains in a sericitic and chloritic matrix.
MC1/B Upper Basalt (0.6ppb Au)
Sample Interval:- 69.5-80.6m
Petrography:- Euhedral clinopyroxene phenocrysts, and less common plagioclase phenocrysts (partly carbonated) in a groundmass of interlocking plagioclase laths with interstitial clinopyroxene, and minor chlorite and actinolite.
MC1/C Andesite (0.2ppb Au)
Sample Interval:- 134.7-176.0m
Petrography:- Plagioclase phenocrysts and large recrystallized quartz aggregates in a fine groundmass of quartz, feldspar, chlorite, sericite and minor sphene.
MC1/D Lower Basalt (1.0ppb Au)
Sample Interval:- 253.0-265.0m
Petrography:- Phenocrysts of plagioclase (partly replaced by carbonate and epidote) and clinopyroxene in agroundmass of flow-aligned plagioclase laths with interstitial clinopyroxene, chlorite and actinolite.

Geochemistry

	MC1/A	MC1/B	MC1/C	MC1/D
SiO_2	71.32	46.34	69.67	53.66
TiO_2	0.62	0.57	0.38	1.01
Al_2O_3	12.62	17.32	14.63	16.16
Fe_2O_3	4.74	10.88	4.37	10.01
MnO	0.02	0.27	0.09	0.23
MgO	2.05	8.63	0.92	4.59
CaO	0.02	7.83	0.67	6.31
Na_2O	<0.20	2.70	4.99	3.48
K_2O	2.71	1.34	2.16	1.66
P_2O_5	0.04	0.53	0.08	0.37
LOI	5.62	3.63	1.38	2.57
Total	99.81	100.04	99.34	100.05
Rb	126	33	72	44
Sr	20	768	187	562
Y	25	29	36	29
Zr	130	137	223	142
Nb	12	10	14	12
Cu	78	85	6	61
Zn	59	84	46	230
Pb	43	5	4	52
Mo	4.5	<0.5	0.5	1.0
S	16000	100	600	100
Ti/Zr	30	26	10	44

Location:- Mt Charter
DDH:- MC2A (Mines Department) = MC17 (Aberfoyle)
Collar AMG Reference:- 388965mE 5390975mN
MC2A Lower Basalt (1.5ppb Au)
Sample Interval:- 352.5-373.5m
Petrography:- Aphyric rock with carbonated plagioclase laths and interstitial clinopyroxene. Abundant chlorite, actinolite and minor clinozoisite in the groundmass. Occasional veins and aggregates of recrystallized quartz.
MC2A/B Micaceous sandstone (1.2ppb Au)
Sample Interval :- 229.3-239.0
Petrography:- Fine grained clastic rock with angular quartz grains, and abundant sericite which imparts a weak foliation. Some carbonate segregations.

Geochemistry

	MC2A/A	MC2A/B
SiO_2	55.33	67.29
TiO_2	0.48	0.45
Al_2O_3	12.85	8.12
Fe_2O_3	7.20	4.77
MnO	0.25	0.13
MgO	6.28	4.28
CaO	6.91	5.84
Na_2O	3.35	<0.20
K_2O	1.01	1.34
P_2O_5	0.23	0.09
LOI	5.69	7.33
Total	99.58	99.64
Rb	25	57
Sr	347	40
Y	25	24
Zr	146	163
Nb	12	9
Cu	11	170
Zn	59	230
Pb	209	6
Mo	<0.5	<0.5
S	1500	500
Ti/Zr	21	18

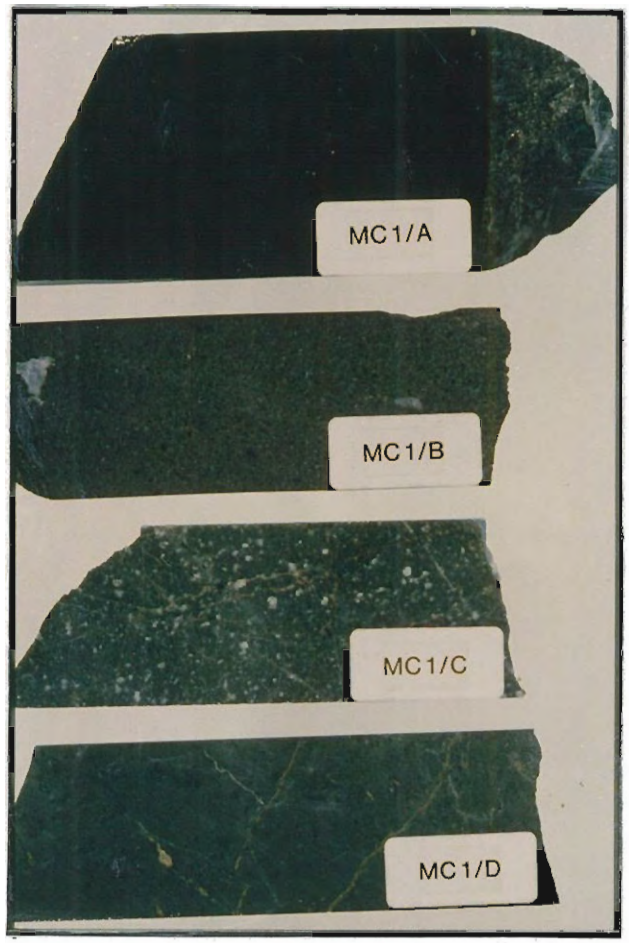
MC1/A
MC1/B
MC1/C
MC1/D

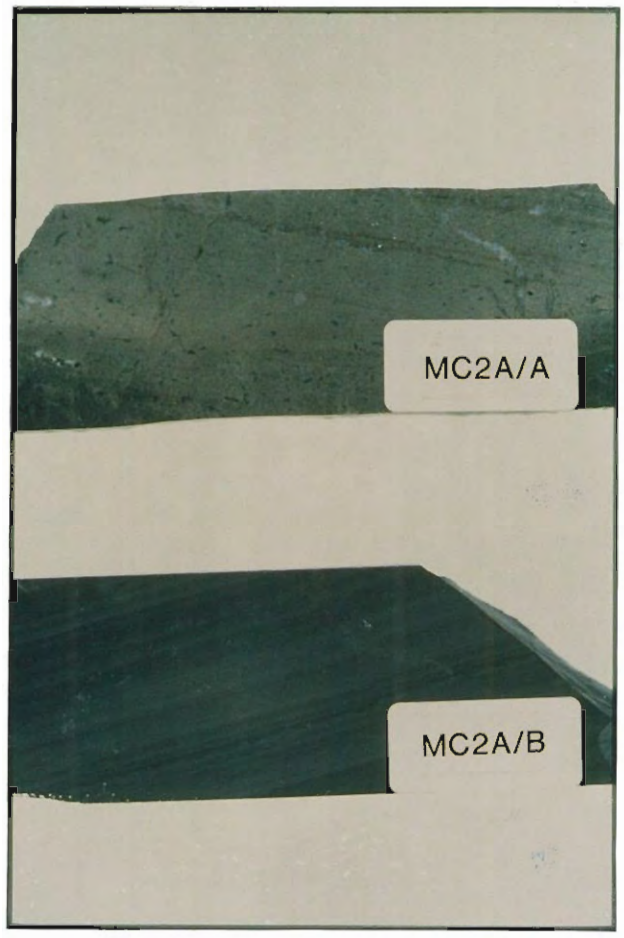
MC2A/A
MC2A/B

Location:- Que River
DDH:- QR97 (Aberfoyle, Que River)
Collar AMG Reference:- 391270.38mE 5394025.74mN
QR97/A Rhyolite (1.1ppb Au)
Sample Interval:- 112.5-118.2m
Petrography:- Equigranular fine-grained volcanic rich in quartz and plagioclase (partly kaolinized) with subordinate sericite, carbonate and chlorite. Weak foliation.
QR97/B Andesite breccia (1.5ppb Au)
Sample Interval:- 206.4-212.3m
Petrography:- Altered andesitic breccia composed of angular chlorite-rich (after glass) rock fragments with partly carbonated plagioclase phenocrysts in a fine-grained groundmass of feldspar, chlorite and quartz.
QR97/C Andesite (1.5ppb Au)
Sample Interval:- 241.4-247.6m
Petrography:- Plagioclase phenocrysts (partly carbonated) in a plagioclase-rich groundmass with interstitial chlorite, carbonate and quartz.
QR97/D Andesite (slightly bleached) (0.5ppb Au)
Sample Interval:- 310.4-316.4m
Petrography:- Plagioclase phenocrysts partially replaced by carbonate, clinozoisite and chlorite, and chlorite pseudomorphs after hornblende ? phenocrysts. The groundmass is composed of feldspar, quartz, chlorite, carbonate and minor clinozoisite.
QR97/E Andesite (slightly bleached) (0.6ppb Au)
Sample Interval:- 381.2-389.1m
Petrography:- Altered andesitic breccia similar to QR97/B
QR/97/F Andesite (within stringer zone) (32ppb Au)
Sample Interval:- 522.7-527.7m
Petrography:- Extensively altered porphyritic volcanic. Sericite and carbonate pseudomorphs after plagioclase phenocrysts in a sericite-quartz-rich groundmass with a weak foliation, accessory chlorite and opaques.
QR97/G Andesite (within stringer zone) (11ppb Au)
Sample Interval:- 611.3-619.1m
Petrography:- Extensively altered volcanic with carbonate pseudomorphs after plagioclase. Some ovoid pods of quartz in a groundmass rich in carbonate, sericite and quartz with dispersed opaques.
QR97/H Andesite (within stringer zone) (6.9ppb Au)
Sample Interval:- 752.1-759.8m
Petrography:- Highly altered and weakly mineralized volcanic. Ovoid pods of quartz and euhedral sulphides with carbonate pseudomorphs after plagioclase? phenocrysts. The groundmass is composed of recrystallized quartz, sericite, carbonate and chlorite. Some carbonate veining.

Geochemistry

	QR97 A	B	C	D	E	F	G	H
SiO_2	71.13	61.25	62.45	55.37	70.33	59.56	57.44	53.59
TiO_2	0.30	0.47	0.49	0.58	0.31	0.63	0.55	0.66
Al_2O_3	13.21	13.27	13.73	14.63	13.22	16.70	13.77	14.04
Fe_2O_3	2.30	5.46	5.91	8.66	2.25	7.08	7.15	7.59
MnO	0.04	0.11	0.11	0.16	0.04	0.16	0.46	0.42
MgO	0.34	1.42	1.48	5.36	0.42	3.76	5.36	5.42
CaO	3.44	5.69	5.69	5.82	3.38	1.87	1.21	3.49
Na_2O	2.95	3.12	2.99	2.52	3.12	0.55	0.01	0.05
K_2O	2.34	1.87	1.74	1.17	2.31	4.02	3.71	3.02
P_2O_5	0.07	0.13	0.14	0.14	0.08	0.15	0.15	0.16
LOI	4.13	7.74	5.99	4.79	5.43	4.95	10.11	9.37
Total	100.25	100.53	100.72	99.20	100.89	99.43	99.92	97.81
Rb	73	93	88	31	35	126	125	118
Sr	138	104	172	443	214	51	33	29
Y	34	31	24	19	20	28	26	25
Zr	192	134	106	64	81	125	124	115
Nb	13	10	8	3	6	9	10	11
Cu	23	96	52	48	34	71	165	71
Zn	160	190	60	200	210	160	1050	810
Pb	11	8	6	41	16	30	174	341
Mo	2.0	1.5	1.0	1.0	1.0	1.5	1.5	1.5
S	<100	<100	<100	<100	<100	30000	23000	28000
Ti/Zr	10	23	29	57	24	32	29	39

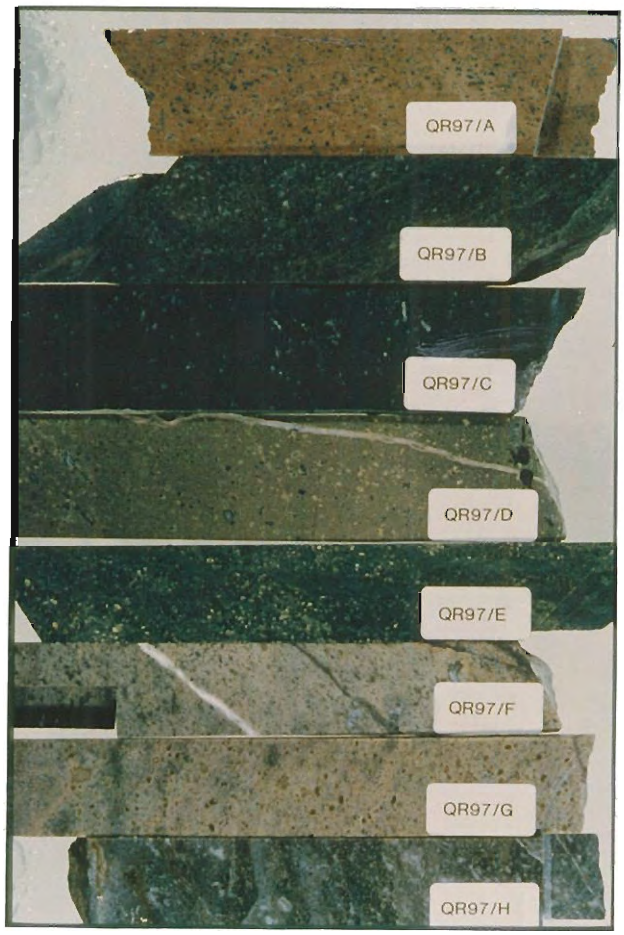
QR97/A
QR97/B
QR97/C
QR97/D
QR97/E
QR97/F
QR97/G
QR97/H

Location:- Que River
DDH:- QR1001/A (Aberfoyle, Que River)
Collar AMG Reference:- 391107.23mE 5394101.57mN
QR1001/A Andesite (relatively unaltered) (3.2ppb Au)
Sample Interval:- 398.0-401.0m
Petrography:- Fragments of porphyritic andesite characterized by plagioclase phenocrysts (minor carbonate alteration) in a groundmass of fine plagioclase laths with interstitial chlorite, carbonate and sphene. Some large elongate chlorite-rich aggregates rimmed by fine-grained quartz which may reflect original flattened pumice fragments.
QR1001/B Andesite (from stringer zone) (3.0ppb Au)
Sample Interval:- 926.7-930.7m
Petrography:- Carbonate pseudomorphs after plagioclase phenocrysts and ovoid patches of quartz in a carbonate-sericite-quartz-rich groundmass with fairly abundant dispersed sulphides. Some quartz-sericite veining.
QR1001/C Andesite (other side of alteration zone) (2.3ppb Au)
Sample Interval:- 1327.3-1330.0m
Petrography:- Extensively altered andesitic volcanic. Carbonate pseudomorphs after plagioclase phenocrysts in a fine groundmass rich in chlorite and carbonate. Vesicles rimmed by quartz and filled with carbonate.

Geochemistry

	QR1001/A	QR1001/B	QR1001/C
SiO_2	60.94	62.92	54.20
TiO_2	0.59	0.55	0.56
Al_2O_3	14.87	14.09	12.60
Fe_2O_3	7.14	8.22	7.20
MnO	0.12	0.20	0.12
MgO	2.98	3.54	9.64
CaO	3.40	0.75	3.90
Na_2O	4.33	0.04	1.14
K_2O	1.85	3.08	1.02
P_2O_5	0.16	0.13	0.18
LOI	3.71	6.06	9.44
Total	100.09	99.58	100.00
Rb	55	99	25
Sr	297	20	66
Y	28	23	20
Zr	134	121	104
Nb	10	8	7
Cu	12	220	68
Zn	86	400	190
Pb	8	34	7
Mo	1.0	2.0	1.0
S	<100	10000	3200
Ti/Zr	27	29	36


QR1001/A
QR1001/B
QR1001/C

Location:- 1.5km northeast Rosebery
DDH:- 80R (EZ, Rosebery)
Collar AMG Reference:- 379418.4mE 5375659.4mN
80R/A Rhyolitic ignimbrite (1.5ppb Au)
Sample Interval:- 103.3-114.9m
Petrography:- Fine-grained quartz-feldspar-rich volcanic clasts with plagioclase microphenocrysts, in a recrystallized matrix of quartz, feldspar , sericite carbonate and chlorite
80R/B Dacite (0.4ppb Au)
Sample Interval:- 383.0-390.8m
Petrography:- Plagioclase and quartz phenocrysts in a recrystallized groundmass of quartz, feldspar chlorite and carbonate.
80R/C Dacitic ignimbrite (fiamme-rich) (1.1ppb Au)
Sample Interval:- 444.2-474.5m
Petrography:- Large plagioclase phenocrysts (partly carbonated) in a fine-grained recrystallized groundmass of quartz, feldspar, sericite, chlorite and carbonate. Minor veins of quartz, chlorite and carbonate.
80R/D Rhyodacite (0.4ppb Au)
Sample Interval:- 805.8-821.6m
Petrography:- Epiclastic rich in angular quartz and plagioclase grains in a finer recrystallized quartz-feldspar-rich matrix with sericite, chlorite and carbonate.
80R/E Black shale (7.3ppb Au)
Sample Interval:- 829.5-845.0m
Petrography:- Very fine-grained carbonaceous shale with alternating graphite-rich and quartz-cabonate-rich layers.Significant pyrite in the latter.

Geochemistry

	80R/A	80R/B	80R/C	80R/D	80R/E
SiO_2	71.52	66.58	63.71	72.14	63.92
TiO_2	0.23	0.48	0.36	0.33	0.78
Al_2O_3	14.35	13.86	16.87	13.37	11.86
Fe_2O_3	2.52	4.22	4.67	2.53	7.81
MnO	0.06	0.12	0.09	0.07	0.07
MgO	0.58	1.31	1.27	0.63	2.26
CaO	1.42	3.26	2.19	2.69	3.82
Na_2O	1.39	3.46	3.32	3.05	0.53
K_2O	5.53	2.76	3.84	2.02	2.55
P_2O_5	0.03	0.14	0.07	0.08	0.18
LOI	2.64	4.07	3.73	2.87	5.48
Total	100.27	100.26	100.12	99.78	99.26
Rb	183	108	176	78	110
Sr	65	207	135	293	116
Y	45	26	55	29	31
Zr	284	199	312	193	132
Nb	18	10	20	10	13
Cu	16	7	5	6	86
Zn	20	44	46	87	170
Pb	4	10	9	14	93
Mo	2.5	<0.5	1.0	<0.5	4.5
S	300	100	300	400	25000
Ti/Zr	5	15	7	11	38

Location:- 1.5km east of Rosebery
DDH:- 85R (EZ, Rosebery)
Collar AMG Reference:- 379995.2mE 5374039.4mN
85R/A Rhyolite (0.3ppb Au)
Sample Interval:- 176.9-200.8ft
Petrography:- Plagioclase phenocrysts (partly carbonated) and subordinate quartz phenocrysts in a quartz-feldspar and carbonate-rich groundmass. Fractures filled with chlorite and sericite.
85R/B Dacite (0.2ppb Au)
Sample Interval:- 623.9-637.0ft
Petrography:- Even-grained rock of recrystallized quartz, feldspar, subordinate carbonate, sericite and chlorite. Occasional veins of quartz and carbonate.
85R/C Rhyolite (White Spur Formation) (2.3ppb Au)
Sample Interval:- 1575.3-1595.4ft
Petrography:- Broken, angular quartz and plagioclase phenocryts in a very fine-grained groundmass of quartz, feldspar, sericite, chlorite and carbonate with a weak foliation.

Geochemistry

	85R/A	85R/B	85R/C
SiO_2	72.14	65.64	71.37
TiO_2	0.27	0.50	0.40
Al_2O_3	13.73	14.29	13.12
Fe_2O_3	1.95	5.17	3.65
MnO	0.05	0.11	0.10
MgO	0.36	1.23	0.79
CaO	1.05	2.98	1.45
Na_2O	3.36	2.52	2.97
K_2O	4.08	3.93	3.26
P_2O_5	0.05	0.13	0.07
LOI	2.17	3.82	2.26
Total	99.21	100.32	99.44
Rb	151	178	305
Sr	131	140	234
Y	41	34	48
Zr	283	211	243
Nb	18	12	13
Cu	6	2	51
Zn	20	35	22
Pb	4	4	6
Mo	1.5	0.5	2.0
S	100	100	1400
Ti/Zr	6	15	10


80R/A
80R/B
80R/C
80R/D
80R/E

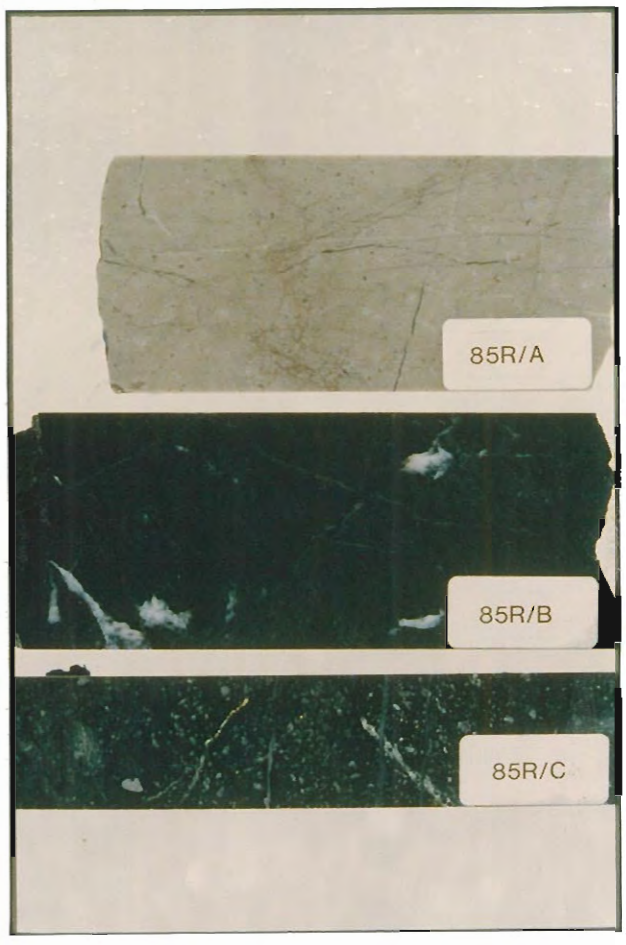
85R/A
85R/B
85R/C

Location:- 3.5km north of Rosebery
DDH:- BD269 (EZ, Rosebery)
Collar AMG Reference:- 377732.1mE 5377377.9mN
BD269/A Dacite (0.9ppb Au)
Sample Interval:- 91.6-110.6m
Petrography:- Plagioclase and quartz phenocrysts in a recrystallized groundmass of quartz, feldspar, sericite, carbonate and chlorite.
BD269/B Shale (1.5ppb Au)
Sample Interval:- 287.6-295.8m
Petrography:- Recrystallized and sheared epiclastic. Very fine-grained clasts rich in quartz, feldspar and carbonate in a similar recrystallized matrix that displays variable sericitization concentrated along clast boundaries.
BD269/C Dacite (3.1ppb Au)
Sample Interval:- 247.1-255.3m
Petrography:- Epiclastic comprising large clasts rich in fine quartz and feldspar in a fine-grained quartz-chlorite-sericite-rich matrix.

Geochemistry

	BD269/A	BD269/B	BD269/C
SiO_2	65.23	64.15	65.36
TiO_2	0.68	0.47	0.52
Al_2O_3	15.38	14.80	14.07
Fe_2O_3	4.84	4.49	4.56
MnO	0.15	0.05	0.25
MgO	1.50	2.60	1.93
CaO	1.86	2.78	3.60
Na_2O	5.61	0.54	2.90
K_2O	1.23	3.65	2.81
P_2O_5	0.13	0.09	0.10
LOI	3.64	6.50	4.30
Total	100.25	100.12	100.40
Rb	56	185	113
Sr	242	88	93
Y	46	32	33
Zr	294	219	154
Nb	11	13	9
Cu	2	32	32
Zn	57	54	72
Pb	9	28	32
Mo	1.0	1.0	9.5
S	600	5800	1400
Ti/Zr	14	14	21

Location:- 1km southwest of Rosebery
DDH:- BP272 (EZ, Rosebery)
Collar AMG Reference:- 377946.14mE 5372802.75mN
BP272/A Sheared epiclastic (1.1ppb Au)
Sample Interval:- 70.4-85.8m
Petrography:- Strongly foliated rock with alternating sericite-chlorite-rich and quartz-feldspar-carbonate-rich bands.
BP272/B Andesitic epiclastic (2.3ppb Au)
Sample Interval:- 93.6-108.6m
Petrography:- Epiclastic with abundant subangualr and fractured quartz grains, subordinate plagioclase grains and fine-grained volcanic rock fragments, in a fine matrix of quartz, chlorite, sericite and carbonate.
BP272/C Rhyolitic epiclastic (4.9 ppb Au)
Sample Interval:- 335.1-360.2m
Petrography:- Very fine-grained quartz-feldspar-rich rock with veins containing quartz, carbonate and pyrite.
BP272/D Black Shale (10ppb Au)
Sample Interval:- 244.4-260.8m
Petrography:- Carbonaceous black shale with occasional bands enriched in quartz and pyrite. Veins of quartz, carbonate and pyrite.

Geochemistry

	BP272/A	BP272/B	BP272/C	BP272/D
SiO_2	67.40	55.87	68.07	53.63
TiO_2	0.58	0.55	0.64	0.65
Al_2O_3	12.29	11.25	14.48	10.30
Fe_2O_3	6.00	6.14	4.74	7.31
MnO	0.11	0.18	0.04	0.16
MgO	1.59	2.13	1.75	4.66
CaO	3.34	10.40	1.58	7.45
Na_2O	1.13	0.64	2.07	0.65
K_2O	2.41	2.33	2.76	2.32
P_2O_5	0.20	0.11	0.13	0.17
LOI	4.46	10.71	3.46	12.24
Total	99.51	100.31	99.72	99.54
Rb	137	144	129	121
Sr	150	277	177	333
Y	29	27	28	24
Zr	210	201	286	116
Nb	9	9	14	11
Cu	19	16	79	76
Zn	83	120	70	75
Pb	19	30	17	18
Mo	1.0	2.0	2.5	2.5
S	4000	4300	6000	15000
Ti/Zr	17	18	14	38


BD269/A
BD269/B
BD269/C

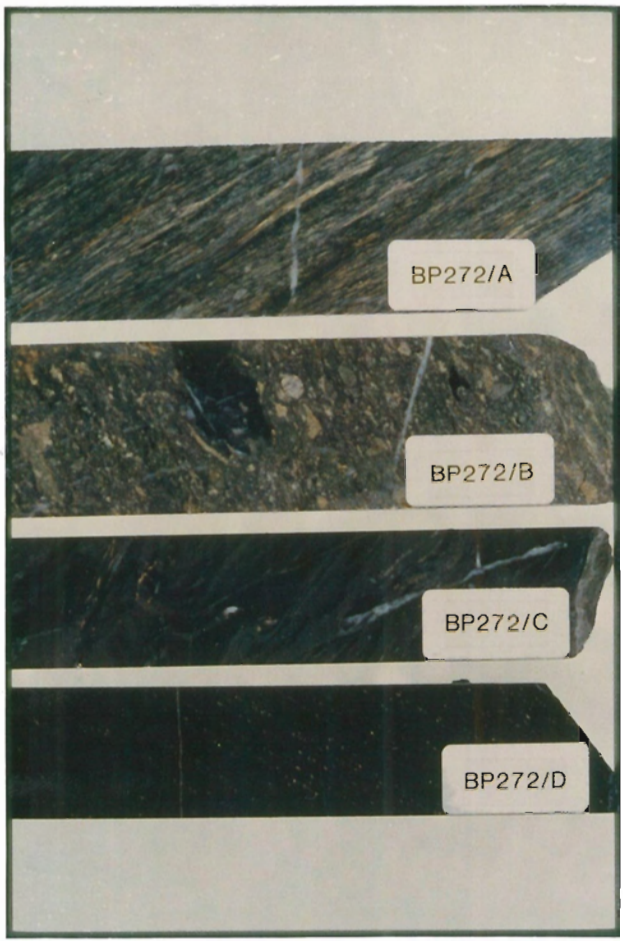
BP272/A
BP272/B
BP272/C
BP272/D

Location:- Approximately 1km southwest of Rosebery
DDH:- BP273 (EZ, Rosebery)
Collar AMG Reference:- 378123.5mE 5373101.6mN
BP273/A Rhyolite (1.5ppb Au)
Sample Interval:- 194.8-228.0m
Petrography:- Fine-grained quartz-feldspar-rich rock fragments with occasional plagioclase phenocrysts set in a recrystallized groundmass of quartz, feldspar, carbonate and sericite.
BP273/B Rhyolite (0.9ppb Au)
Sample Interval:- 136.2-161.3m
Petrography:- Phenocrysts of plagioclase and quartz in a very fine groundmass of quartz, feldspar, sericite and chlorite with a weak foliation.
BP273/C Rhyolite (2.0ppb Au)
Sample Interval:- 411.1-441.2m
Petrography:- Very fine-grained carbonaceous shale with occasional segregation bands rich in recrystallized quartz, and dispersed pyrite grains.

Geochemistry

	BP273/A	BP273/B	BP273/C
SiO_2	72.56	68.97	68.68
TiO_2	0.22	0.45	0.63
Al_2O_3	12.59	13.75	15.76
Fe_2O_3	3.50	3.97	3.86
MnO	0.08	0.10	0.06
MgO	1.75	1.15	1.96
CaO	0.84	2.32	0.35
Na_2O	2.71	4.23	0.85
K_2O	2.57	1.98	4.05
P_2O_5	0.03	0.10	0.09
LOI	2.77	3.32	3.27
Total	99.62	100.34	99.56
Rb	156	120	228
Sr	245	391	61
Y	40	34	42
Zr	147	181	252
Nb	11	10	20
Cu	12	7	40
Zn	54	37	280
Pb	22	13	12
Mo	0.5	1.5	1.5
S	1100	1000	4300
Ti/Zr	9	15	15

Location:- Approximately 3km of Hercules
DDH:- DP288 (EZ, Rosebery)
Collar AMG Reference:- 378422.9mE 5369126.2mN
DP288/A Rhyodacite (0.9ppb Au)
Sample Interval:- 126.3-134.5m
Petrography:- Phenocrysts of plagioclase (minor alteration to carbonate) in a quartz-feldspar-rich groundmass. Sericite and carbonate locally abundant in the groundmass defining a weak foliation.
DP288/B Rhyolite (0.7ppb Au)
Sample Interval:- 208.5-233.2m
Petrography:-
DP288/C Rhyolite (0.3ppb Au)
Sample Interval:- 249.5-266.7m
Petrography:- Partly carbonated plagioclase phenocrysts in a quartz-feldspar-rich groundmass with subordinate sericite, carbonate and 'pyrite. Occasional veins of quartz and carbonate.
DP288/D Altered Rhyolite (7.8ppb Au)
Sample Interval:- 350.0-370.0m
Petrography:- Abundant plagioclase phenocrysts in a fine groundmass of feldspar, quartz, carbonate, sericite, chlorite and minor pyrite.

Geochemistry

	DP288/A	DP288/B	DP288/C	DP288/D
SiO_2	73.12	70.91	72.78	73.12
TiO_2	0.24	0.43	0.27	0.30
Al_2O_3	12.21	13.47	13.05	13.07
Fe_2O_3	2.70	3.69	1.87	2.33
MnO	0.09	0.10	0.22	0.18
MgO	0.61	0.80	0.60	1.12
CaO	2.15	2.05	1.16	0.41
Na_2O	3.43	1.94	1.74	0.45
K_2O	2.36	3.22	5.13	6.55
P_2O_5	0.06	0.07	0.05	0.06
LOI	2.62	3.14	2.37	2.02
Total	99.59	99.82	99.24	99.61
Rb	90	137	231	323
Sr	103	68	73	48
Y	36	42	35	36
Zr	194	274	231	230
Nb	15	17	14	13
Cu	12	3	11	2
Zn	26	27	180	50
Pb	3	13	47	26
Mo	<0.5	4.5	<0.5	<0.5
S	700	2700	1300	2700
Ti/Zr	8	10	7	8

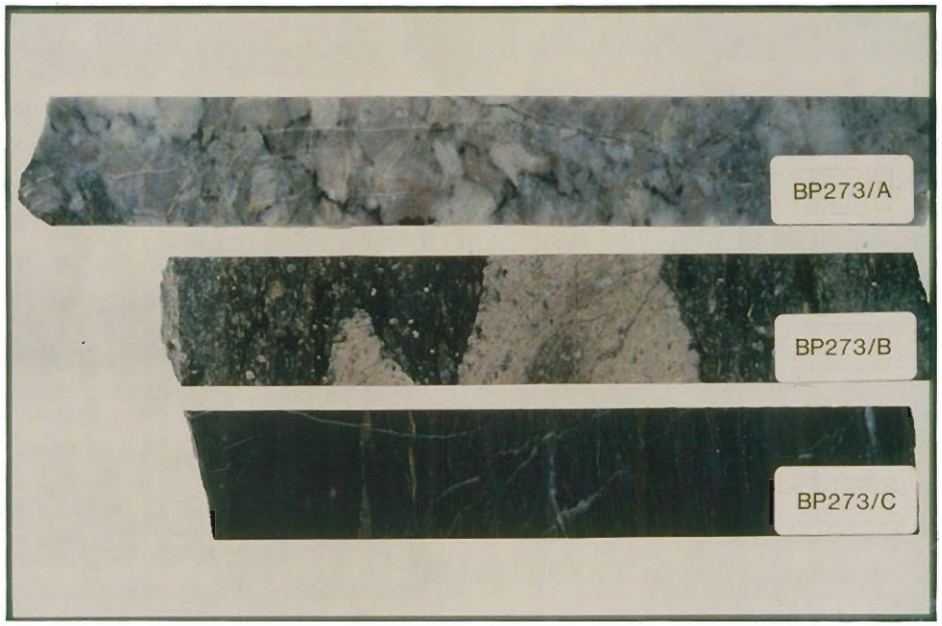
BP273/A
BP273/B
BP273/C


DP288/A
DP288/B
DP288/C
DP288/D

Location:- Robbies Creek (northwest of Mt Black)
DDH:- RED87-1 (Shell Exploration, Devonport)
Collar AMG Reference:- 379481mE 5377000mN
RED87-1/A Dacite (2.4ppb Au)
Sample Interval:- 120.2-132.6m
Petrography:- Abundant plagioclase phenocrysts (partially carbonated) in groundmass of tabular plagioclase crystals with interstitial quartz and carbonate. Veins of chlorite, carbonate and quartz.
RED87-1/B Dacite (0.5ppb Au)
Sample Interval:- 174.9-193.6m
Petrography:- Large plagioclase phenocrysts (partly carbonated and kaolinized) in a quartz-feldspar-rich groundmass with minor sericite and carbonate.
RED87-1/C Rhyolite (1.0ppb Au)
Sample Interval:- 242.9-262.0m
Petrography:- Even-grained rock composed of tabular plagioclase and intergrowths of quartz and alkali feldspar. Mild recrystallization with a weak foliation defined by sericite and chlorite. Skeletal aggregates of chlorite and Fe-oxide probably after biotite. Veins of quartz and carbonate.
RED87-1/D Rhyolite (1.1ppb Au)
Sample Interval:- 313.3-332.5m
Petrography:- Sparse plagioclase and quartz phenocrysts in a fine groundmass of quartz, feldspar, sericite and chlorite. Weak foliation and fractures filled by chlorite and quartz.
RED87-1/E Dacite (0.8ppb Au)
Sample Interval:- 357.9-370.3m
Petrography:- Large quartz phenocrysts (embayed) and subordinate pplagioclase phenocrysts in a quartz-feldspar-rich groundmass with some chlorite-rich patches. Veins zoned from quartz-chlorite-carbonate from margin to core.

Geochemistry

	RED 87-1/A	RED 87-1/B	RED 87-1/C	RED 87-1/D	RED 87-1/E
SiO_2	66.24	66.89	73.61	71.77	64.41
TiO_2	0.46	0.48	0.29	0.28	0.56
Al_2O_3	13.92	14.09	13.26	13.55	14.33
Fe_2O_3	4.64	4.83	1.98	4.34	7.72
MnO	0.09	0.07	0.07	0.09	0.17
MgO	1.15	1.15	0.51	0.97	1.93
CaO	3.13	2.63	1.35	1.11	2.06
Na_2O	2.26	3.45	2.13	1.88	3.40
K_2O	3.41	3.29	3.62	3.13	1.84
P_2O_5	0.11	0.12	0.02	0.05	0.13
LOI	4.14	3.33	2.49	2.65	3.51
Total	99.55	100.33	99.33	99.82	100.06
Rb	154	115	143	138	87
Sr	113	182	101	43	101
Y	29	30	33	41	33
Zr	203	199	244	262	189
Nb	11	11	15	17	11
Cu	6	4	16	3	4
Zn	94	51	110	36	82
Pb	5	8	5	5	6
Mo	1.5	<0.5	2.0	1.0	<0.5
S	900	200	400	600	300
Ti/Zr	14	15	7	7	18

Location:- 1km north of Hercules
DDH:- H955 (EZ, Rosebery)
Collar AMG Reference:- 376384.69mE 5367860.19mN
H955/A Rhyolite (0.8ppb Au)
Sample Interval:- 345.0-359.0ft
Petrography:- Plagioclase phenocrysts partly carbonated and altered to clinozoisite which also occurs as radial aggregates of prismatic crystals with quartz, chlorite and sphene. The groundmass is dominated by quartz and feldspar with subordinate sericite and carbonate.
H955/B Rhyolite (0.7ppb Au)
Sample Interval:- 1623.0-1643.0ft
Petrography:- Plagioclase phenocrysts (broken and partly carbonated) in a foliated groundmass of quartz, feldspar and sericite.

Geochemistry

	H955/A	H955/B
SiO_2	70.17	72.05
TiO_2	0.40	0.35
Al_2O_3	14.93	13.99
Fe_2O_3	2.78	2.34
MnO	0.08	0.33
MgO	0.78	2.08
CaO	1.64	0.45
Na_2O	3.69	2.21
K_2O	3.78	4.10
P_2O_5	0.05	0.04
LOI	1.16	2.31
Total	99.46	100.25
Rb	176	185
Sr	353	56
Y	39	33
Zr	281	246
Nb	14	12
Cu	4	3
Zn	59	77
Pb	17	7
Mo	1.0	<0.5
S	<100	1900
Ti/Zr	9	9


RED87-1/A
RED87-1/B
RED87-1/C
RED87-1/D
RED87-1/E

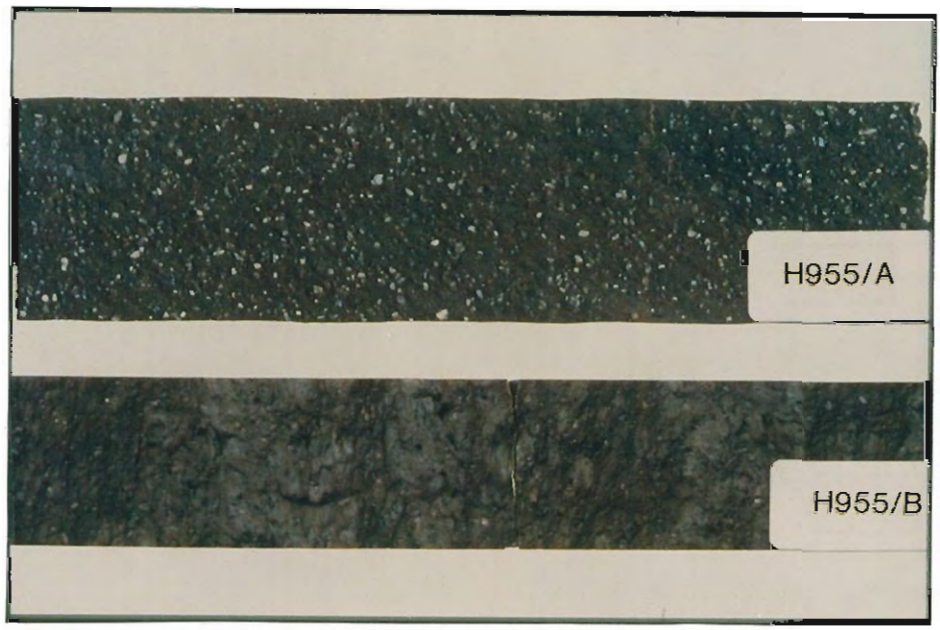
H955/A
H955/B

Location:- Mt Read
DDH:- MR1 (Mines Department)
Collar AMG Reference:- 377043mE 5362227mN
MR1/A Dacite (0.3ppb Au)
Sample Interval:- 86.8-102.0m
Petrography:- Plagioclase phenocrysts (partly kaolinized and carbonated) in a fine recrystallized groundmass of quartz, feldspar, chlorite and minor clinozoisite. Some quartz-chlorite-carbonate veins.
Location:- Mt Read
DDH:- RE1 (Goldfields Exploration Pty. Ltd.)
Collar AMG Reference:- 379900mE 5365425mN
RE1/A Andesite (1.3ppb Au)
Sample Interval:- 269.1-285.7m
Petrography:- Aphyric recrystallized volcanic composed of quartz, plagioclase, chlorite, carbonate and sericite. Occasional quartz-carbonate veins, and rare carbonate pseudomorphs after plagioclase phenocrysts.
RE1/B Basalt (0.9ppb Au)
Sample Interval:- 154.1-162.4m
Petrography:- Rare plagioclase phenocrysts altered to carbonate and sericite in a fine groundmass of plagioclase, clinozoisite, carbonate, chlorite, actinolite and sphene.
RE1/C Andesite (1.1ppb Au)
Sample Interval:- 227.6-244.3m
Petrography:- Plagioclase phenocrysts (partly carbonated) in a fine recrystallized groundmass of quartz, feldspar, sericite, carbonate and chlorite.

Geochemistry

	MR1/A	RE1/A	RE1/B	RE1/C
SiO_2	67.23	57.42	50.85	62.63
TiO_2	0.46	0.81	0.99	0.45
Al_2O_3	14.33	16.25	16.77	14.87
Fe_2O_3	3.55	8.89	9.98	5.04
MnO	0.08	0.15	0.20	0.13
MgO	0.86	1.57	5.74	2.65
CaO	3.53	4.19	8.02	3.84
Na_2O	3.62	4.02	2.59	2.77
K_2O	2.82	2.70	1.31	2.68
P_2O_5	0.12	0.32	0.16	0.06
LOI	3.21	4.41	3.89	4.46
Total	99.81	100.73	100.50	99.58
Rb	133	104	42	129
Sr	252	152	388	105
Y	40	44	28	36
Zr	230	166	81	229
Nb	13	6	2	13
Cu	10	49	55	25
Zn	47	115	160	91
Pb	19	15	27	7
Mo	0.5	1.0	0.5	<0.5
S	200	800	600	1800
Ti/Zr	13	30	75	12

Location:- Howards Road south of Mt Read (Western Sequence)
DDH:- WSP3 (Goldfields Exploration, Burnie)
Collar AMG Reference:- 378391.0mE 5362496.0mN
WSP3/A Dacite (0.2ppb Au)
Sample Interval:- 88.3-104.7m
Petrography:- Large plagioclase (partly carbonated) and quartz grains in a foliated sericite-chlorite-carbonate-rich matrix.
WSP3/B Rhyolite (0.8ppb Au)
Sample Interval:- 264.3-281.2m
Petrography:- Pyroclastic composed of probable pumice fragments with sparse phenocrysts of quartz and plagioclase in a fine-grained recrystallized quartz-feldspar-rich groundmass.
WSP3/C Basalt (1.2ppb Au)
Sample Interval:- 287.5-314.4m
Petrography:- Aphyric (dyke?) composed of interlocking laths of plagioclase with interstitial clinopyroxene, carbonate and sphene.
WSP3/D Andesite (1.6ppb Au)
Sample Interval:- 146.6-171.8m
Petrography:- Plagioclase phenocrysts (minor carbonation) in a heterogeneous groundmass of smaller plagioclase grains and a fine-grained foliated matrix of quartz, feldspar, sericite and chlorite.

Geochemistry

	WSP3/A	WSP3/B	WSP3/C	WSP3/D
SiO_2	66.46	71.41	47.90	60.71
TiO_2	0.50	0.27	0.73	0.68
Al_2O_3	13.62	13.28	16.08	15.07
Fe_2O_3	4.42	2.69	9.68	6.79
MnO	0.09	0.07	0.19	0.10
MgO	1.41	0.74	6.64	2.78
CaO	2.88	2.15	9.49	3.06
Na_2O	2.60	2.34	3.30	4.40
K_2O	3.79	3.40	1.75	3.03
P_2O_5	0.12	0.06	0.12	0.16
LOI	3.62	3.15	4.06	3.80
Total	99.51	99.56	99.94	100.58
Rb	143	194	57	108
Sr	151	67	376	233
Y	30	34	23	34
Zr	211	268	64	189
Nb	13	16	1	12
Cu	10	5	150	37
Zn	120	190	180	120
Pb	12	44	16	22
Mo	1.5	<0.5	<0.5	1.5
S	800	200	200	9700
Ti/Zr	15	6	71	22

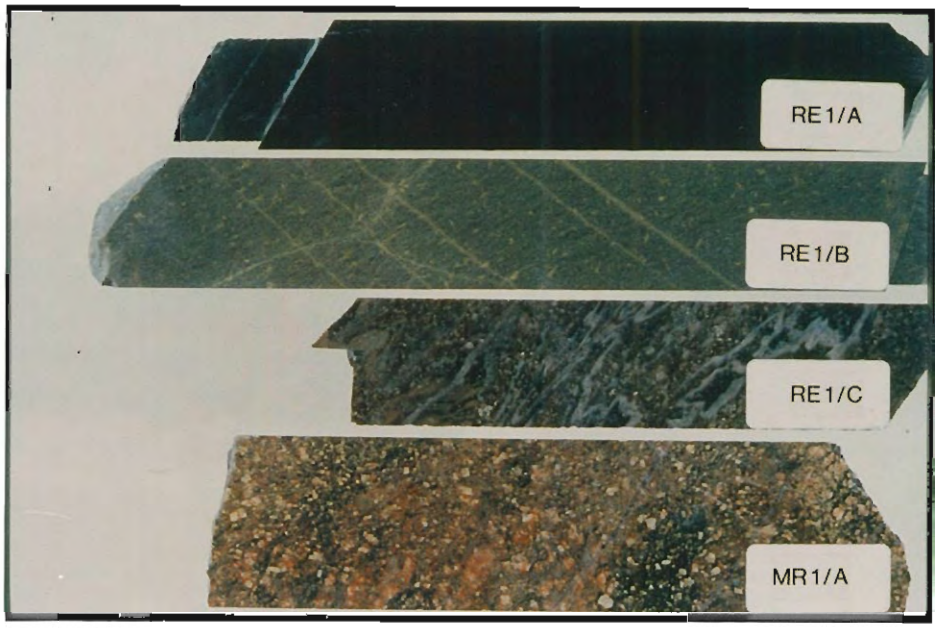
RE1/A
RE1/B
RE1/C
MR1/A

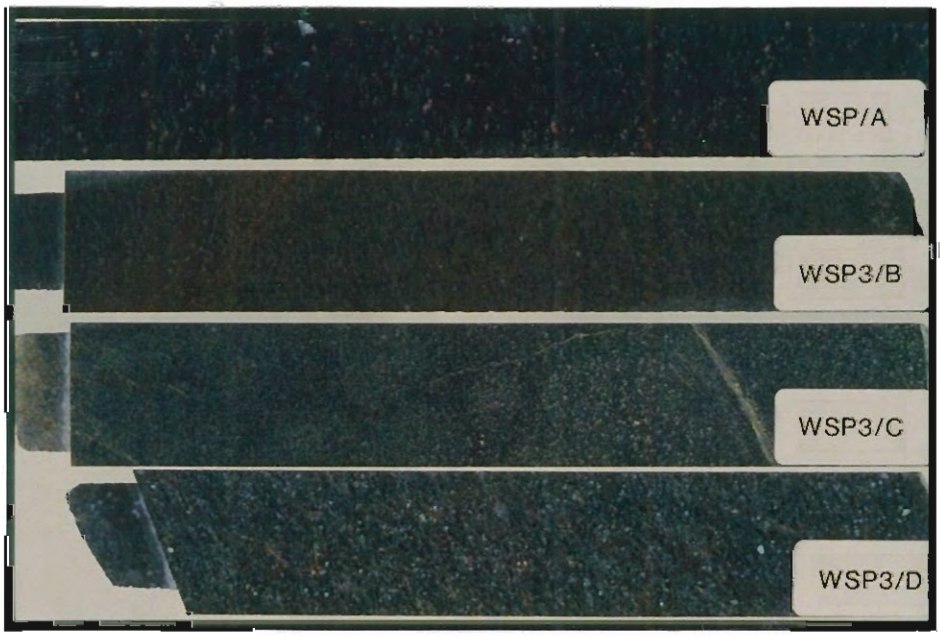
WSP/A
WSP3/B
WSP3/C
WSP3/D

Location:- Bradshaws Road
DDH:- BR1 (Mines Department)
Collar AMG Reference:- 374929.5mE 5350434mN
BR1/A Basalt (0.7ppb Au)
Sample Interval:- 36.5-57.5m
Petrography:- Phenocrysts of plagioclase in a groundmass of interlocking plagioclase laths with interstitial clinopyroxene, chlorite and actinolite. Minor carbonation of plagioclase. Some aggregates of clinozoisite, chlorite and carbonate.
BR1/B Tuff (0.9ppb Au)
Sample Interval:- 146.3-165.9m
Petrography:- Finegrained sericite-chlorite-rich rock with dispersed angular quartz grains and rare quartz-chlorite veins.
BR1/C Black Shale (0.4ppb Au)
Sample Interval:- 91.9-109.0m
Petrography:- Very fine-grained carbonaceous shale.
BR1/D Altered Rhyolitic tuff (<0.1ppb Au)
Sample Interval:- 313.0-325.8m
Petrography:- Angular quartz and plagioclase (partly sericitized) grains, and ragged chlorite pseudomorphs after biotite? in a fine quartz-feldspar-sericite-chlorite groundmass.
BR1/E Basalt (0.7 ppb Au)
Sample Interval:- 337.0-375.5
Petrography:- Interlocking plagioclase lathswith interstitial chlorite, carbonate and sphene. Vesicles filled with chlorite and carbonate.

Geochemistry

	BR1/A	BR1/B	BR1/C	BR1/D	BR1/E
SiO_2	48.45	74.32	75.12	71.59	48.98
TiO_2	0.94	0.36	0.27	0.45	0.85
Al_2O_3	17.15	13.08	12.21	12.77	15.21
Fe_2O_3	11.09	2.97	2.21	3.71	9.12
MnO	0.23	0.03	0.03	0.05	0.17
MgO	4.84	1.93	1.34	2.26	5.66
CaO	6.74	0.45	1.50	1.25	7.58
Na_2O	4.60	0.13	1.62	0.74	3.04
K_2O	0.83	4.03	2.86	3.19	1.04
P_2O_5	0.12	0.06	0.02	0.15	0.14
LOI	4.97	3.13	2.94	3.29	8.76
Total	99.96	100.49	100.12	99.45	100.55
Rb	33	227	180	188	62
Sr	358	15	116	26	99
Y	25	43	48	42	26
Zr	77	152	151	391	116
Nb	3	18	16	15	3
Cu	150	15	7	11	55
Zn	250	96	54	85	370
Pb	14	27	14	9	22
Mo	0.5	1.0	0.5	0.5	<0.5
S	200	1800	100	500	400
Ti/Zr	77	15	11	7	48

Location:- North of Mt Huxley
DDH:- HX1 (Goldfields Exploration, Burnie)
Collar AMG Reference:- 381385.8mE 5346903.5mN
HX1/A Rhyodacite (0.6ppb Au)
Sample Interval:- 91.8-107.2
Petrography:- Plagioclase phenocrysts (partly carbonated) in a groundmass of tabular plagioclase with interstitial quartz sericite, carbonate and chlorite. Minor carbonate veining, and occasional large chlorite pseudomorphs after hornblende or biotite.
HX1/B Altered Rhyolite (2.1ppb Au)
Sample Interval:- 268.8-286.3
Petrography:- Epiclastic rock with abundant quartz and subordinate plagioclase grains in a foliated matrix dominated by sericite and chlorite.
HX1/C Dacite (0.9ppb Au)
Sample Interval:- 182.5-197.9
Petrography:- Plagioclase and quartz phenocrysts in a fine-grained foliated groundmass of quartz, feldspar, chlorite, sericite and carbonate. Minor carbonate veining.
Location:- Southwest of Mt Sedgwick
DDH:- WS4
Collar AMG Reference:- 381385.8mE 5346903.5mN
WS4/A Andesite (1.0ppb Au)
Sample Interval:- 59.9-79.2m
Petrography:- Sheared hornblende andesite containing hornblende and plagioclase phenocrysts with subordinate broken quartz phenocrysts in a cataclastic groundmass rich in chlorite, feldspar and carbonate.

Geochemistry

	HX1/A	HX1/B	HX1/C	WS4/A
SiO_2	70.37	69.44	66.55	58.46
TiO_2	0.40	0.34	0.48	0.46
Al_2O_3	14.56	12.65	14.34	15.37
Fe_2O_3	3.99	5.89	5.29	7.80
MnO	0.06	0.28	0.12	0.13
MgO	1.18	1.51	2.20	4.72
CaO	0.42	0.77	1.33	3.19
Na_2O	3.60	0.95	3.37	4.96
K_2O	3.40	3.58	2.65	2.05
P_2O_5	0.09	0.09	0.11	0.28
LOI	1.97	3.77	3.43	3.20
Total	100.04	99.27	99.87	100.60
Rb	111	172	108	59
Sr	91	36	114	465
Y	40	36	27	24
Zr	302	279	199	134
Nb	13	12	12	7
Cu	14	16	8	52
Zn	67	420	91	75
Pb	4	131	82	8
Mo	1.0	2.0	1.0	<0.5
S	300	2400	1900	200
Ti/Zr	8	8	15	21

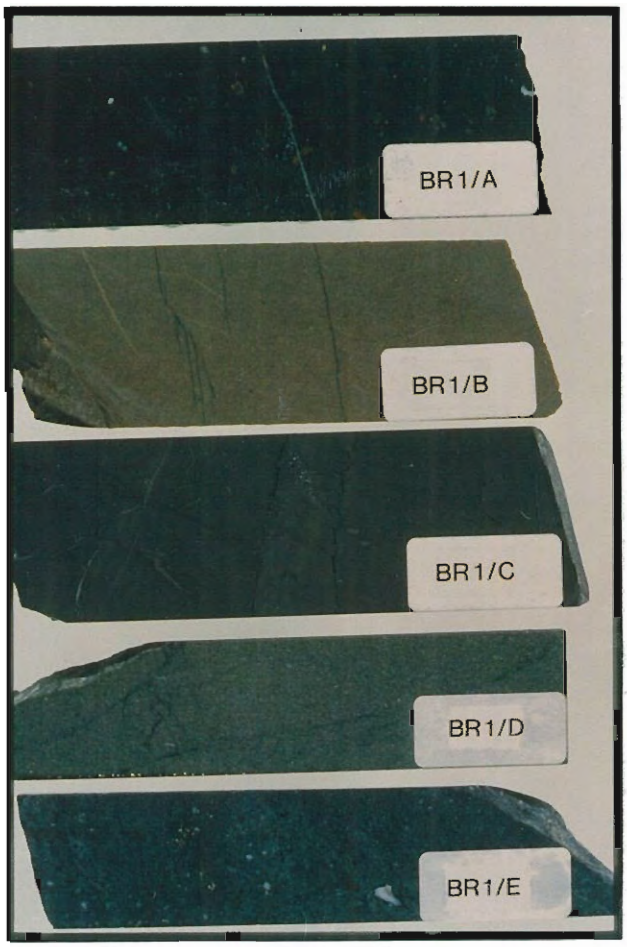
BR1/A
BR1/B
BR1/C
BR1/D
BR1/E

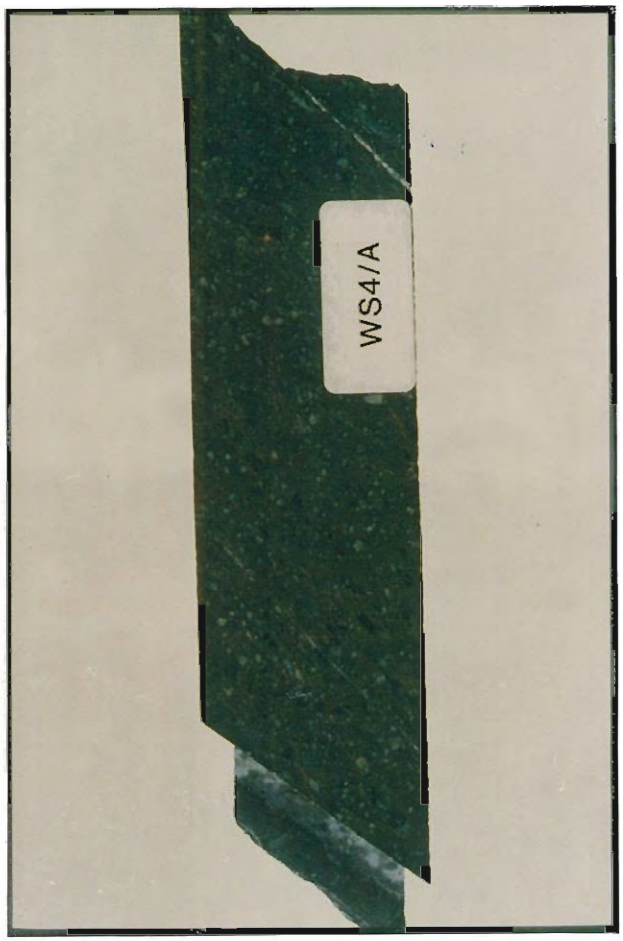
WS4/A


HX1/A
HX1/B
HX1/C

Location:- Anthony Road, southern section
Outcrop samples of Central Volcanic Sequence and Western Sequence rocks collected from roadcuttings.

AR7 Siltstone (0.4ppb Au)
AMG Reference:- 381360mE 5359010mN
Petrography:- Angular partially recrystallised quartz grains in a quartz-chlorite-sericite-rich matrix with minor epidote

AR9 Andesite (0.2ppb Au)
AMG Reference:- 381312mE 5358911mN
Petrography:-

AR10 Dacite (0.3ppb Au)
AMG Reference:- 380693mE 5356881mN
Petrography:- Phenocrysts of quartz (embayed) and plagioclase (partly kaolinised) in a fine grained, weakly foliated groundmass of chlorite, sericite, quartz and feldspar.

AR11 Andesite (<0.1ppb Au)
AMG Reference:- 380594mE 5356683mN
Petrography:- Phenocrysts of plagioclase, hornblende and clinopyroxene in a groundmass of interlocking laths of plagioclase with interstitial chlorite and carbonate.

AR13 Hornblende Andesite (0.6ppb Au)
AMG Reference:- 379827mE 5355297mN
Petrography:- Euhedral plagioclase and hornblende phenocrysts in a fine groundmass of quartz, plagioclase, chlorite, carbonate and minor clinozoisite.

AR15 Daciteepiclastic (0.7ppb Au)
AMG Reference:- 378861mE 5354381mN
Petrography:- Angular quartz and plagioclase grains in a fine quartz-chlorite-rich matrix with a weak foliation. Minor sericite and carbonate veining.

AR17 Andesite epiclastic (0.4ppb Au)
AMG Reference:- 378317mE 5352970mN
Petrography:- Angular grains of quartz and plagioclase (carbonate alteration) in a fine matrix of quartz, plagioclase, chlorite and carbonate.

AR18 Rhyolite epiclastic (0.6ppb Au)
AMG Reference:- 377871mE 5352228mN
Petrography:- Abundant angular quartz grains and subordinate plagioclase in a recrystallised quartz-chlorite-sericite matrix with a weak foliation.

AR19 Dacitic tuff (0.4ppb Au)
AMG Reference:- 375248mE 5350000mN
Petrography:- Recrystallised quartz-feldspar-rich matrix with dispersed, angular grains of quartz and feldspar.

Geochemistry

	AR7	AR9	AR10	AR11	AR13	AR15	AR17	AR18	AR19
SiO_2	85.61	63.30	68.38	59.16	55.25	64.98	63.76	74.21	67.06
TiO_2	0.32	0.72	0.35	0.56	0.50	0.58	0.86	0.29	0.66
Al_2O_3	5.04	16.47	16.97	15.65	16.27	14.56	16.03	12.88	16.13
Fe_2O_3	1.94	5.91	3.45	7.76	8.79	4.84	5.69	2.58	3.72
MnO	0.08	0.14	0.04	0.14	0.17	0.16	0.11	0.04	0.05
MgO	1.04	2.17	1.65	3.98	4.72	1.33	2.11	0.85	1.26
CaO	0.99	0.82	0.71	3.15	5.65	3.15	1.41	0.73	0.13
Na_2O	0.11	7.79	4.50	5.13	4.05	1.65	4.82	3.15	3.23
K_2O	1.44	0.87	2.75	2.91	0.29	3.90	2.73	3.84	3.71
P_2O_5	0.05	0.10	0.15	0.22	0.25	0.16	0.15	0.04	0.07
LOI	2.52	1.42	2.04	1.71	4.44	4.95	2.73	1.73	3.20
Total	99.14	99.71	100.99	100.37	100.38	100.26	100.40	100.34	99.22
Rb	56	20	111	73	10	218	102	169	177
Sr	31	257	506	316	1080	54	234	86	325
Y	26	28	36	27	25	43	38	45	54
Zr	282	211	137	178	136	278	263	193	311
Nb	8	12	6	9	7	17	16	16	18
Cu	2	3	12	14	84	3	4	5	3
Zn	15	110	180	120	240	45	89	38	130
Pb	4	27	11	8	16	8	8	7	18
Mo	<0.5	<0.5	<0.5	<0.5	<0.5	0.5	2.5	1.5	0.5
S	200	200	1200	<100	1000	900	600	200	300
Ti/Zr	7	21	15	19	23	13	20	9	13

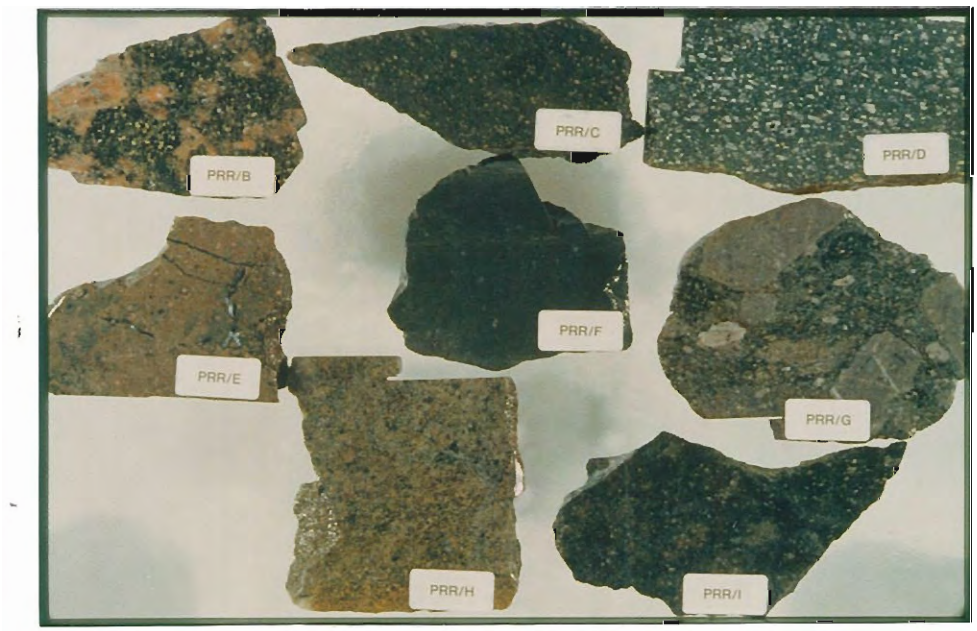
PRR/B
PRR/C
PRR/D
PRR/E
PRR/F
PRR/G
PRR/H
PRR/I

Location:- Leech Hill
DDH:- LH1 (Mines Department)
Collar AMG Reference:- 379365.5mE 5353632.7mN
LH1/A Rhyolite (least altered) (0.8ppb Au)
Sample Interval:- 181.0-193.6m
Petrography:- Even-grained quartz-feldspar-rich rock with xenoblastic texture. Some interstitial sericite, carbonate and chlorite.
LH1/B Rhyolite (slightly altered) (1.1ppb Au)
Sample Interval:- 258.6-264.0m
Petrography:- Similar to LH1/A but with a weak foliation.
LH1/C Rhyolite (altered) (1.2ppb Au)
Sample Interval:- 302.9-313.1
Petrography:- Occasional large plagioclase phenocrysts (largely pseudomorphed by carbonate) in a quartz-carbonate-sericite-rich groundmass.
LH1/D Rhyolite (extensively altered) (6.2ppb Au)
Sample Interval:- 420.7-435.2m
Petrography:- Very fine-grained quartz-feldspar-rich rock with layers rich in sericite defining a foliation. Some carbonate and pyrite.

Geochemistry

	LH1/A	LH1/B	LH1/C	LH1/D
SiO_2	64.84	67.61	75.43	68.06
TiO_2	0.49	0.47	0.31	0.35
Al_2O_3	13.85	13.36	11.29	12.31
Fe_2O_3	4.88	4.50	2.46	5.53
MnO	0.10	0.07	0.04	0.11
MgO	1.76	1.71	1.25	1.38
CaO	3.09	2.68	1.68	2.13
Na_2O	0.65	0.43	0.27	<0.20
K_2O	3.83	3.44	2.83	3.03
P_2O_5	0.17	0.11	0.04	0.11
LOI	5.88	5.51	4.03	6.41
Total	99.54	99.89	99.63	99.42
Rb	120	113	102	102
Sr	70	73	53	70
Y	34	33	29	30
Zr	221	212	149	207
Nb	11	10	16	10
Cu	11	8	9	120
Zn	95	64	130	56
Pb	13	13	29	32
Mo	1.5	1.0	2.5	0.5
S	300	1800	700	34000
Ti/Zr	14	14	13	11

Location:- Howards Anomaly
DDH:- HA8 (Aberfoyle Exploration, Burnie)
Collar AMG Reference:- 380615mE 5358620mN
HA8/A Altered Rhyolite (16ppb Au)
Sample Interval:- 190.7-231.5m
Petrography:- Large quartz phenocrysts (embayed) and subordinate plagioclase phenocrysts (almost completely kolinized and sericitized) in a very fine-grained groundmass of quartz, feldspar, sericite and disseminated opaques.
HA8/B Altered Rhyolite (20ppb Au)
Sample Interval:- 85.5-109.8m
Petrography:- Large, angular and broken quartz grains in a fine recrystallized quartz-feldspar-rich groundmass with sericite, chlorite and carbonate.

Geochemistry

	HA8/A	HA8/B
SiO_2	68.77	68.47
TiO_2	0.38	0.34
Al_2O_3	14.71	13.64
Fe_2O_3	4.07	5.06
MnO	0.08	0.09
MgO	0.48	0.41
CaO	0.61	0.45
Na_2O	0.16	0.28
K_2O	6.49	5.39
P_2O_5	0.31	0.12
LOI	3.47	4.04
Total	99.53	98.29
Rb	179	142
Sr	61	45
Y	19	16
Zr	158	123
Nb	12	10
Cu	230	76
Zn	2000	7400
Pb	418	1330
Mo	1.0	1.5
S	29000	38000
Ti/Zr	15	18

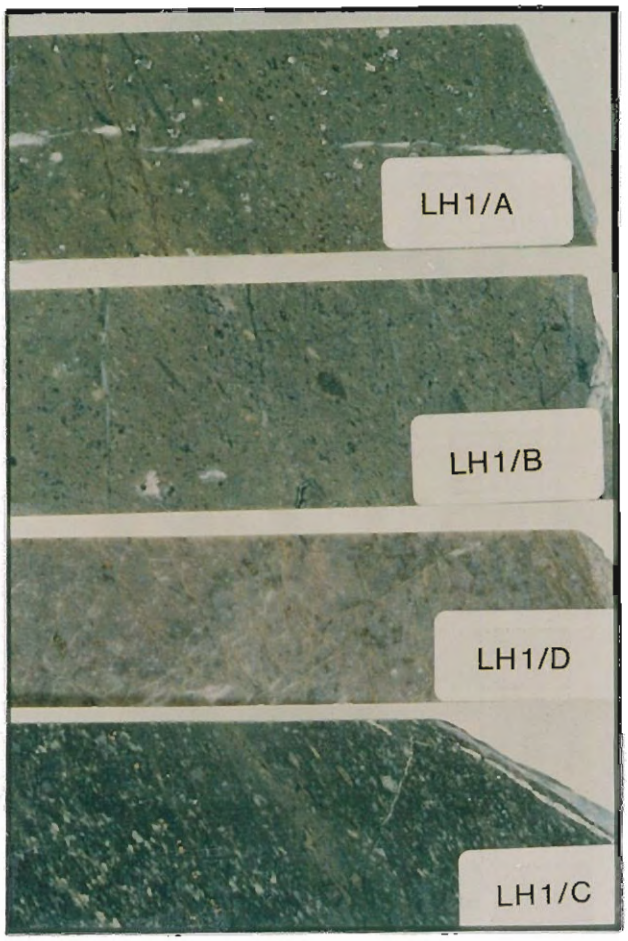
LH1/A
LH1/B
LH1/D
LH1/C


HA8/A
HA8/B

Location:- Jukes-Darwin area
DDH:- Z142001 (Ref. No. 5311-Mines Department)
Collar AMG Reference:- 3844mE 53230mN
JD2001/A Rhyolite (0.4ppb Au)
Sample Interval:- 60.2-65.4m
Petrography:- Occasional large plagioclase phenocrysts (extensively carbonated) in a fine groundmass of quartz, chlorite and sericite. Large quartz phenocrysts (partly carbonated) and fractured in a groundmass of quartz, feldspar and sericite.
JD2001/B Altered Rhyolite (0.6ppb Au)
Sample Interval:- 95.8-101.6m
Petrography:- Large, broken quartz grains (embayed) in a very fine groundmass of quartz, carbonate, sericite and chlorite.
JD2001/C Altered Rhyolite (1.2ppb)
Sample Interval:- 237.5-267.5m
Petrography:- Equigranular k-feldspar (partially sericitized) and quartz-rich rock with xenoblastic texture. Minor pyrite.
JD2001/D Altered Rhyolite (0.9 ppb Au)
Sample Interval:- 303.6-325.8m (N.B. Hematite veining and pyrite avoided where possible).
Petrography:- Equigranular k-feldspar (partially sericitized) and quartz-rich rock with xenoblastic texture. Minor pyrite.

Geochemistry

	JD2001/A	JD2001/B	JD2001/C	JD2001/D
SiO_2	73.69	66.37	70.76	73.98
TiO_2	0.31	0.45	0.33	0.30
Al_2O_3	12.84	14.40	12.40	12.86
Fe_2O_3	2.56	3.47	8.97	3.31
MnO	0.07	0.22	0.28	0.08
MgO	0.44	0.72	0.87	0.38
CaO	1.29	3.37	0.07	0.06
Na_2O	2.80	0.59	<0.20	<0.20
K_2O	2.93	4.48	4.07	8.05
P_2O_5	0.04	0.08	0.04	0.04
LOI	2.71	5.60	2.96	1.64
Total	99.68	99.75	100.75	100.70
Rb	116	168	196	239
Sr	90	96	13	72
Y	41	37	35	37
Zr	279	261	267	267
Nb	15	15	13	13
Cu	3	6	77	27
Zn	50	140	180	49
Pb	9	19	9	7
Mo	0.5	<0.5	<0.5	1.0
S	100	<100	1200	1000
Ti/Zr	7	11	8	7

Location:- Jukes Darwin area
DDH:- Z142002 (Ref. No. 5312-Mines Department)
Collar AMG Reference:- 3843mE 53234mN
JD2002/A Altered Rhyolite (2.6ppb Au)
Sample Interval:- 68.6-81.0m
Petrography:- Large quartz phenocrysts (embayed) in a foliated fine-grained groundmass rich in quartz, feldspar and sericite.
JD2002/B Altered Rhyolite (3.1ppb Au)
Sample Interval:- 111.5-121.5m
Petrography:- Strongly foliated quartz-chlorite-sericite schist with trails of fine opaques parallel to the foliation and patches of carbonate.
JD2002/C Altered Rhyolite (0.8ppb Au)
Sample Interval:- 170.9-217.0m
Petrography:- Euigranular K-feldspar and quartz-rich rock.Some kaolinization and sericitization of feldspar and a weak foliation. Occasional Fe-oxide (hematite) veins.

Geochemistry

	JD2002/A	JD2002/B	JD2002/C
SiO_2	70.72	68.53	72.93
TiO_2	0.37	0.50	0.30
Al_2O_3	12.52	12.71	12.86
Fe_2O_3	7.96	4.94	4.12
MnO	0.33	0.32	0.11
MgO	0.39	1.29	0.46
CaO	0.43	2.21	0.05
Na_2O	0.23	<0.20	<0.20
K_2O	4.91	4.26	7.07
P_2O_5	0.05	0.10	0.04
LOI	2.38	5.60	1.90
Total	100.29	100.46	99.84
Rb	193	177	239
Sr	35	53	37
Y	38	38	58
Zr	265	235	276
Nb	14	11	13
Cu	10	50	9
Zn	440	87	42
Pb	55	10	6
Mo	0.5	1.0	1.5
S	100	4500	1100
Ti/Zr	9	14	21


JD2001/A
JD2001/B
JD2001/C
JD2001/D


JD2002/A
JD2002/B
JD2002/C

Location:- Luina
DDH:- LD86-1 (Shell Exploration, Devenport)
Collar AMG Reference:- 364200mE 5404760mN

LD86-1/A Argillite (1.3ppb Au)
Sample Interval:- 27.0-33.1m
Petrography:- Angular grains of quartz, plagioclase and microcline with some large muscovite and biotite crystals in a finer matrix of the same minerals plus carbonate and chlorite. Rare quartz-chlorite veins.

LD86-1/B Argillite (1.7ppb Au)
Sample Interval:- 44.1-56.4m
Petrography:- Similar to LD86-1/A.

LD86-1/C Chert (0.6ppb Au)
Sample Interval:- 106.0-113.0m
Petrography:- Very fine-grained aggregate of quartz, chlorite and sericite with occasional quartz-carbonate veins.

LD86-1/D Basalt (10ppb Au)
Sample Interval:- 131.0-143.8m
Petrography:- Rare plagioclase and clinopyroxene phenocrysts in a groundmass of interlocking plagioclase laths with interstitial clinopyroxene (partially altered to actinolite), chlorite and carbonate.

LD86-1/E Basalt (23ppb Au)
Sample Interval:- 275.8-288.7m
Petrography:- Similar to LD86-1/D with chlorite and actinolite filling fractures.

Geochemistry

	LD86 -1/A	LD86 -1/B	LD86 -1/C	LD86 -1/D	LD86 -1/E
SiO_2	66.24	65.12	78.40	47.14	47.31
TiO_2	0.61	0.61	0.43	2.50	2.50
Al_2O_3	12.62	12.24	8.46	12.76	13.04
Fe_2O_3	4.87	4.87	4.69	15.16	15.78
MnO	0.15	0.11	0.48	0.25	0.25
MgO	2.48	2.57	1.78	6.02	5.91
CaO	3.00	4.31	0.40	8.63	10.70
Na_2O	1.95	2.21	0.72	3.07	2.10
K_2O	2.99	2.51	1.92	0.89	0.59
P_2O_5	0.16	0.19	0.09	0.30	0.27
LOI	4.47	5.07	2.06	3.32	1.74
Total	99.54	99.81	99.43	100.04	100.19
Rb	130	98	80	30	18
Sr	142	156	62	357	197
Y	32	36	17	41	42
Zr	193	212	96	172	172
Nb	12	12	11	14	15
Cu	23	23	47	390	400
Zn	81	74	80	150	150
Pb	43	20	14	4	3
Mo	2.0	<0.5	<0.5	0.5	0.5
S	<100	100	100	600	400
Ti/Zr	20	18	27	90	89

Location:- Cattley Range
DDH:- CRD86-1 (Shell Exploration, Devenport)
Collar AMG Reference:- 403025mE 5405958mN

CRD86-1/A Black shale (4.0ppb Au)
Sample Interval:- 63.8-67.8m
Petrography:- Finely laminated carbonaceous shale with significant carbonate.

CRD86-1/B Rhyolite (0.5ppb Au)
Sample Interval:- 114.9-127.7m
Petrography:- Aphyric, recrystallized, fine-grained quartz-feldspar-rich aggregate with minor carbonate and chlorite, and some relatively large carbonate segregations.

Geochemistry

	CRD86-1/A	CRD86-1/B
SiO_2	61.60	68.88
TiO_2	0.82	0.33
Al_2O_3	12.52	13.04
Fe_2O_3	7.11	4.11
MnO	0.19	0.25
MgO	2.32	0.70
CaO	3.42	2.73
Na_2O	0.26	0.85
K_2O	3.11	3.38
P_2O_5	0.23	0.08
LOI	8.02	5.07
Total	99.60	99.42
Rb	131	149
Sr	40	29
Y	26	47
Zr	125	252
Nb	12	14
Cu	59	7
Zn	220	21
Pb	41	2
Mo	0.5	<0.5
S	2800	<100
Ti/Zr	43	8

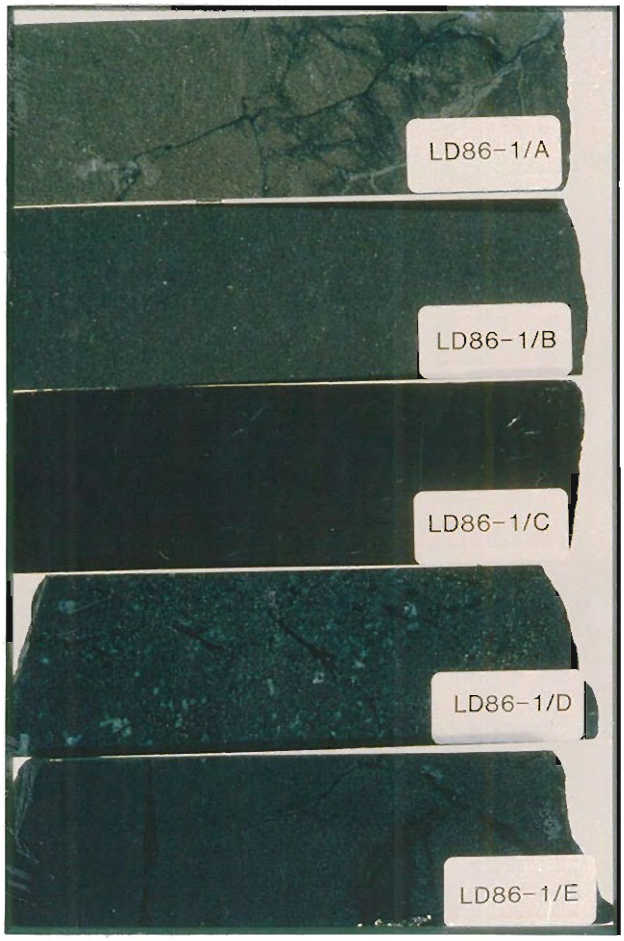
LD86-1/A
LD86-1/B
LD86-1/C
LD86-1/D
LD86-1/E

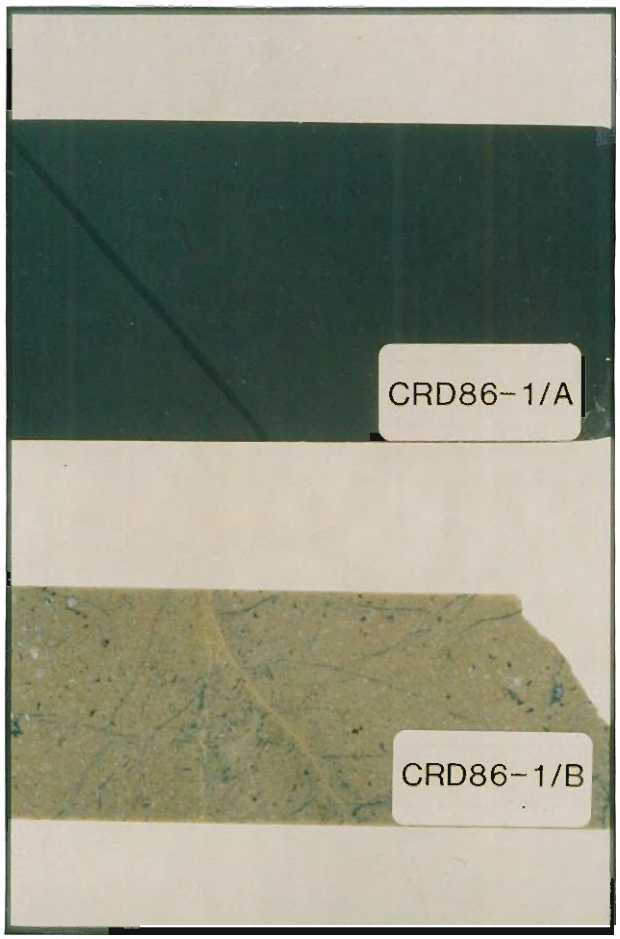
CRD86-1/A
CRD86-1/B

Location:- 2.5km north of Rosebery
DDH:- 71R (EZ, Rosebery)
Collar AMG Reference:- 378834.37mE 5376395.6mN
71R/A Rhyolite (1.1ppb Au)
Sample Interval:- 219.0-239.0ft
Petrography:- Equigranular recrystallized quartz-feldspar-rich assemblage withminor sericite and chlorite which impart a weak foliation.Occasional carbonate veins.
71R/B Black shale (4.5ppb Au)
Sample Interval:- 1620.0-1677.0ft
Petrography:-
71R/C Rhyodacite (0.4ppb Au)
Sample Interval:- 1990.0-2030.0ft
Petrography:- Pyroclastic with angular, broken quartz plagioblase and K-feldspar phenocrysts in a fine recrystallized groundmass of quartz, feldspar, sericite and chlorite.

Geochemistry

	71R/A	71R/B	71R/C
SiO_2	73.64	65.87	72.41
TiO_2	0.22	0.82	0.33
Al_2O_3	12.18	12.50	14.20
Fe_2O_3	7.07	5.56	3.17
MnO	0.11	0.05	0.07
MgO	0.87	2.79	0.64
CaO	0.03	2.56	1.44
Na_2O	0.03	0.47	4.12
K_2O	3.42	2.83	1.92
P_2O_5	0.01	0.11	0.05
LOI	2.28	6.01	2.00
Total	99.86	99.65	100.35
Rb	164	136	79
Sr	6	97	326
Y	40	30	137
Zr	202	146	201
Nb	14	15	11
Cu	10	56	10
Zn	63	210	120
Pb	5	37	27
Mo	0.5	4.5	1.0
S	100	11000	700
Au(ppb)	1.1	4.5	0.4
Ti/Zr	7	36	10

Location:- Lake Selina
DDH:- LS12 (Aberfoyle Exploration, Burnie)
Collar AMG Reference:- 385421mE 5363530mN
LS12/A Murchison Granite (0.4ppb Au)
Sample Interval:- 302.8-318.6m
Petrography:- Coarse-grained equigranular assemblage of quartz and plagioclase. Some alteration of plagioclase to clays and clinozoisite. Some large aggregates of epidote associated with Fe-oxides. Occasional veins of carbonate and epidote.

Location:- Elliot Bay
Samples collected from boulders on beach.
AMG Reference:- 38570mE 52390mN
EB1 Porphyry (0.8ppb Au)

EB2 Porphyry (0.4ppb Au)

Geochemistry

	LS12/A	EB1	EB2
SiO_2	66.67	74.14	72.34
TiO_2	0.43	0.27	0.40
Al_2O_3	15.79	12.52	13.04
Fe_2O_3	5.21	2.60	3.69
MnO	0.09	0.04	0.06
MgO	1.79	0.32	0.56
CaO	0.86	1.20	0.94
Na_2O	6.54	2.51	2.67
K_2O	0.66	4.89	5.06
P_2O_5	0.11	0.04	0.06
LOI	2.15	0.90	1.14
Total	100.30	99.43	99.96
Rb	153	232	195
Sr	330	85	109
Y	30	40	36
Zr	183	187	298
Nb	11	19	17
Cu	2	18	10
Zn	220	120	42
Pb	28	12	18
Mo	<0.5	3.0	2.5
S	100	100	<100

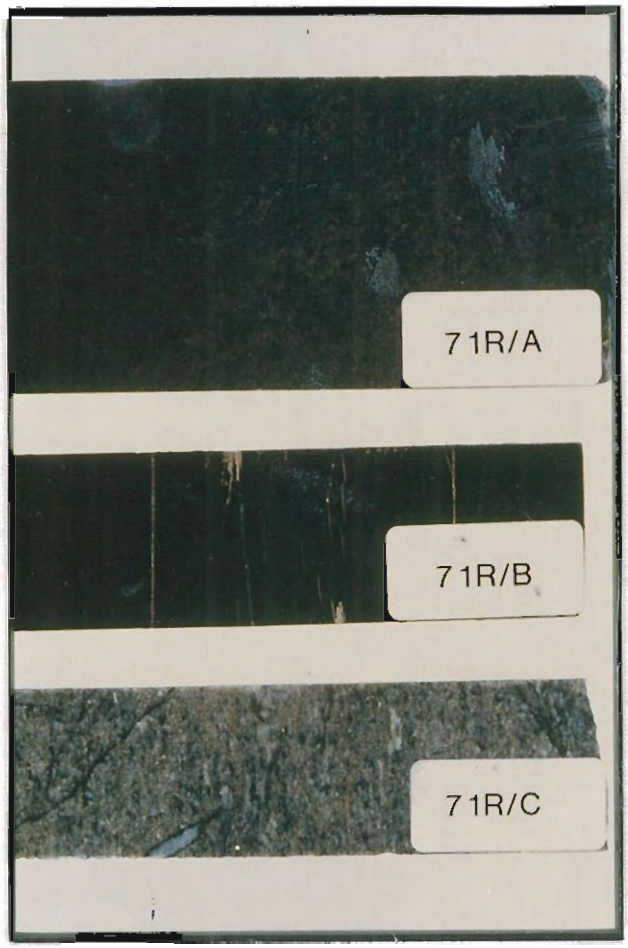
71R/A
71R/B
71R/C

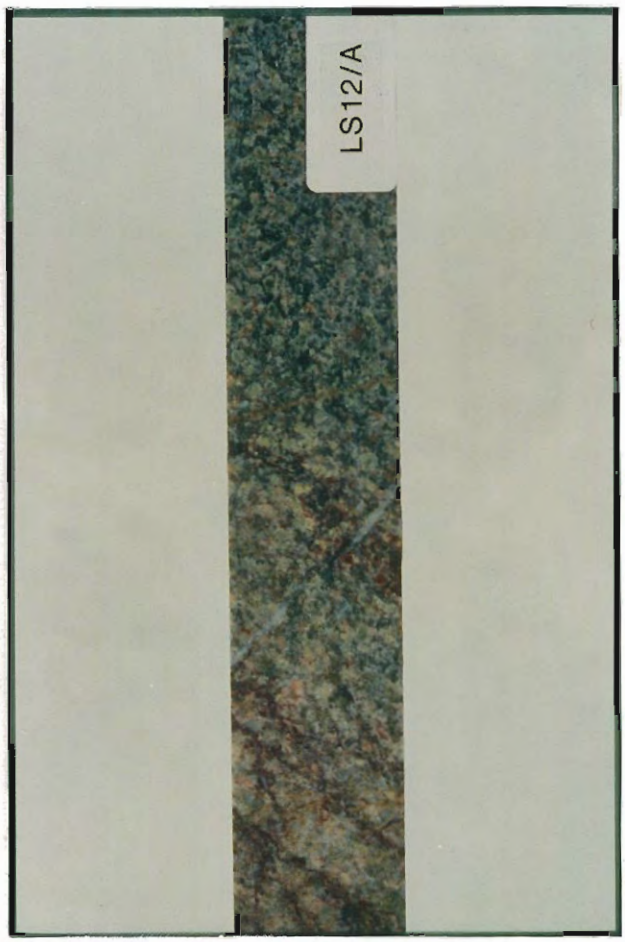
LS12/A

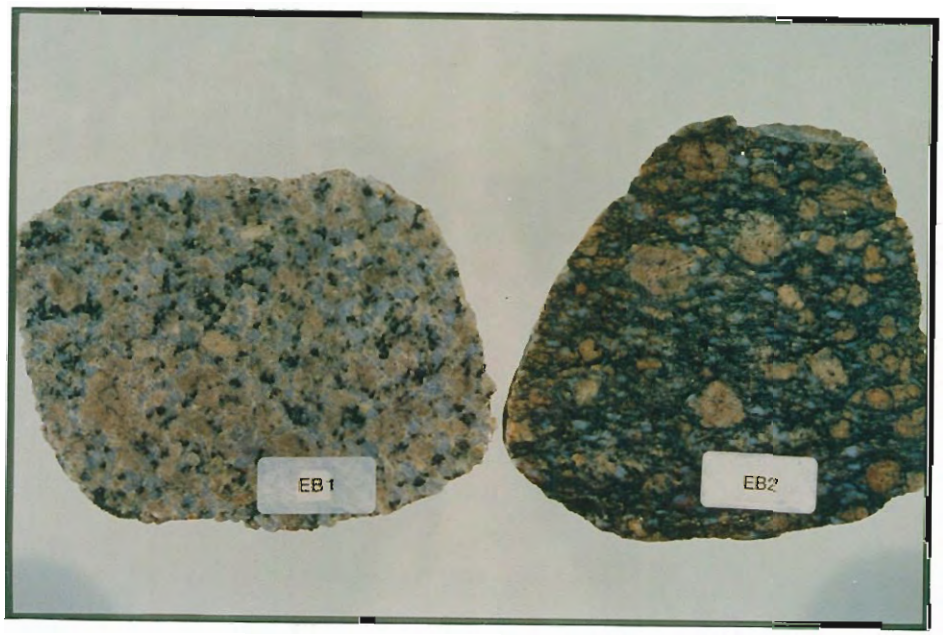
EB1
EB2

Location:- Heazlewood Complex
DDH:- TDH1 (Ref. No. 5955-Mines Department)
Collar AMG Reference:-
TDH1/A Serpentinized harzburgite (0.3ppb Au)
Sample Interval:- 230-250ft
Petrography:- Thoroughly serpentinized olivine-rich assemblage with minor orthopyroxene pseudomorphed by bastite.
TDH1/B Serpentinized harzburgite (0.3ppb Au)
Sample Interval:- 323-343ft
Petrography:- Abundant serpentinized olivine (with chromite inclusions), some which is enclosed in large optically continuous orthopyroxene. The boundaries between pseudomorphed olivine and orthopyroxene are marked by narrow clinopyroxene reaction rims. Intercumulus plagioclase has been altered to hydrogrossular.
TDH1/C Serpentinized dunite (0.3ppb Au)
Sample Interval:- 55-75ft
Petrography:- Serpentinized olivine-rich rock. Only a trace of bastite after orthopyroxene.
TDH1/D Pyroxenite (0.7ppb Au)
Sample Interval:- 380-397ft
Petrography:- Orthopyroxene-rich cumulate with minor clinopyroxene and plagioclase (partly altered to hydrogrossular).

Geochemistry

	TDH1/A	TDH1/B	TDH1/C	TDH1/D
SiO_2	36.87	37.79	34.61	51.04
TiO_2	0.04	0.05	0.04	0.05
Al_2O_3	1.56	2.57	0.59	4.42
Fe_2O_3	8.82	9.77	13.03	7.23
MnO	0.15	0.15	0.17	0.15
MgO	36.69	35.63	37.56	25.42
CaO	0.66	1.18	0.03	7.88
Na_2O	<0.20	<0.20	<0.20	<0.20
K_2O	*0.01*	*0.02*	*<0.01*	*0.02*
P_2O_5	<0.03	<0.03	<0.03	<0.03
LOI	14.58	12.93	14.42	3.25
Total	99.38	100.09	100.45	99.46
Rb	<2	<2	<2	2
Sr	<2	<2	<2	6
Y	<2	<2	<2	2
Zr	<1	<1	<1	1
Nb	<1	<1	<1	<1
Cu	9	7	4	23
Zn	69	57	69	57
Pb	<2	<2	<2	2
Mo	<0.5	<0.5	<0.5	<0.5
S	100	100	<100	<100

Location:- Lyell Highway from King William saddle to the Collingwood River.
Outcrop samples of Precambrian metamorphic basement rocks.
PC2 Quartz-muscovite-graphite schist (0.6ppb Au)
AMG Reference:- 424630mE 5325630mN
PC3 Dolomite (0.2ppb Au)
AMG Reference:- 422750mE 5325500mN
PC4 Quartz-muscovite-chlorite schist (0.2ppb Au)
AMG Reference:- 421130mE 5325500mN
PC6 Muscovite-bearing quartzite (0.2ppb Au)
AMG Reference:- 415550mE 5326900mN
PC10 Garnet-mica schist (0.4ppb Au)
AMG Reference:- 406250mE 5335750mN
PC12 Quartz-muscovite-chlorite scist (0.5ppb Au)
AMG Reference:- 425250mE 5326000mN

Geochemistry

	PC2	PC3	PC4	PC6	PC10	PC12
SiO_2	75.24	6.55	74.95	88.86	80.12	74.97
TiO_2	0.58	<0.01	0.33	0.12	0.40	0.81
Al_2O_3	10.59	0.97	12.90	5.93	9.52	10.94
Fe_2O_3	3.78	0.16	2.63	0.89	3.56	5.07
MnO	0.03	<0.01	<0.01	0.01	0.05	0.07
MgO	1.81	19.73	1.16	0.80	0.70	1.80
CaO	0.04	29.51	0.18	<0.01	0.96	0.08
Na_2O	<0.20	<0.20	<0.20	<0.20	2.74	<0.20
K_2O	3.30	0.05	6.43	2.49	1.16	3.45
P_2O_5	0.04	0.01	0.05	0.01	0.04	0.07
LOI	4.71	42.59	1.85	1.01	0.55	2.73
Total	100.12	99.57	100.52	100.12	99.80	99.99
Rb	108	3	142	57	68	121
Sr	16	64	8	3	61	38
Y	27	2	47	17	36	31
Zr	246	2	271	170	325	311
Nb	13	<1	13	5	12	16
Cu	21	3	3	2	3	26
Zn	62	8	18	<1	35	41
Pb	9	2	7	2	15	4
Mo	1.5	<0.5	0.5	1.5	2.5	0.5
S	7100	<100	<100	<100	<100	<100
Ti/Zr	15		7	4	7	16

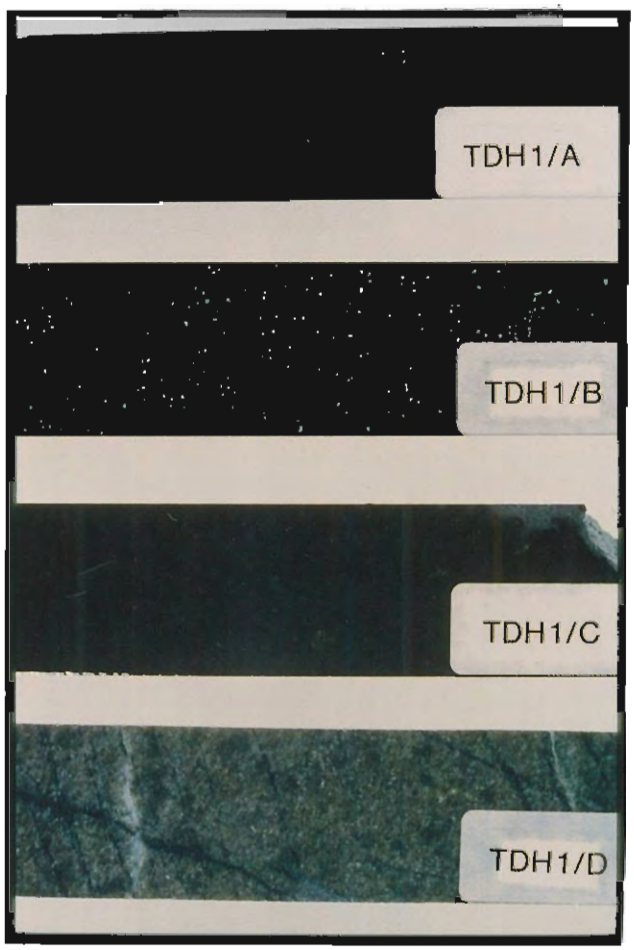
TDH1/A
TDH1/B
TDH1/C
TDH1/D

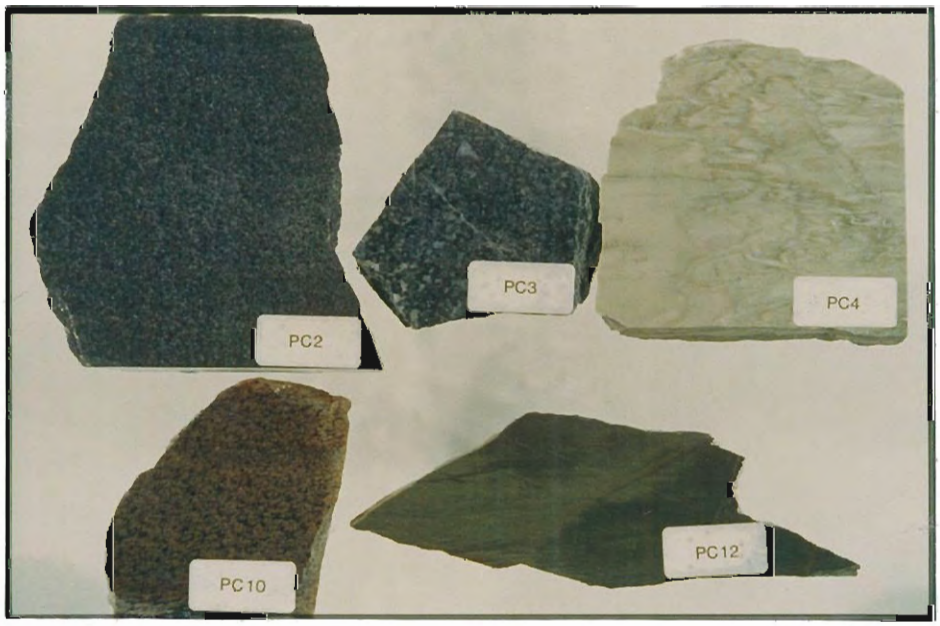
PC2
PC3
PC4
PC10
PC12

Locations:- Serpentine Hill, Cleveland and Stonehenge areas.
Samples of basaltic, gabbroic and ultramafic rocks provided by Dr A.V. Brown (Mines Department of Tasmania).

85-0014 High-Ti Tholeiite (0.1ppb Au)
AMG Reference:- 3719000mE 54025000mN

48302 High-Ti Tholeiite (12ppb Au)
DDH C800 - 108.5m

85-0023 High-Mg Andesite (0.7ppb Au)
AMG Reference:- 3634000mE 5408000mN

85-0028 High-Mg Andesite (2.9ppb Au)
AMG Reference:- 3569000mE 54597000mN

85-0032 Low-Ti Tholeiite (0.7ppb Au)
AMG Reference:- 3693000mE 54675000mN

85-0034 Low-Ti Tholeiite (2.4ppb Au)
AMG Reference:- 3702000mE 54664000mN

60919 Low-Ti Tholeiite (1.5ppb Au)
AMG Reference:- 3608100mE 54074500mN

85-0107 Low-Ti Gabbro (0.7ppb Au)
AMG Reference:- 3680000mE 54673000mN

85-0127 Low-Ti Gabbro (2.5ppb Au)
AMG Reference:- 3680000mE 54673000mN

85-0139 Serpentinized Dunite (0.4ppb Au)
AMG Reference:- 3614000mE 34869000mN

85-0140 Serpentinized Dunite (0.5ppb Au)
AMG Reference:- 3681000mE 54775000mN

85-0154 Pyroxenite (0.8ppb Au)
AMG Reference:- 3700000mE 54763000mN

85-0155 Pyroxenite (0.3ppb Au)
AMG Reference:- 3698000mE 54761000mN
85-0219 Chromitite in serpentinized dunite (0.8ppb Au)
AMG Reference:- 3683000mE 54675000mN

85-0228 Chromitite in serpentinized dunite (0.8ppb Au)
AMG Reference:- 3683000mE 54675000mN

Geochemistry

	0014	48302	0023	0028	0032	0034	60919	0107
SiO_2	49.01	45.35	51.20	51.13	57.10	57.30	49.56	48.09
TiO_2	3.36	2.56	0.07	0.04	0.28	0.42	0.25	0.04
Al_2O_3	14.52	13.29	8.40	4.56	12.90	12.90	14.73	13.35
Fe_2O_3	14.86	17.39	9.96	10.56	13.34	9.21	10.59	13.35
MnO	0.27	0.25	0.17	0.33	0.13	0.14	0.18	0.20
MgO	5.24	6.25	17.10	17.65	4.40	4.60	10.49	12.42
CaO	7.84	10.58	4.60	9.69	7.60	4.40	11.72	11.68
Na_2O	3.12	3.31	0.36	0.21	1.60	2.90	1.44	0.70
K_2O	0.19	0.20	0.06	0.19	0.19	0.19	0.56	0.11
P_2O_5	0.52	0.30	0.01	0.12	0.04	0.05	0.04	0.14
LOI	1.64	2.30	8.29	5.10	2.80	8.06	1.71	2.89
Total	100.57	101.78	100.22	99.58	100.38	100.17	101.27	100.48
Sc	54		26	21	47	44		44
V	440	415	97	98	260	230	21	130
Cr	130	92	860	2900	24	139		670
Ni	44	65	687	570	58	70	172	165
Rb	10	7	<4	13	6	6	7	165
Sr	200	620	10	32	49	64	36	180
Y	59	46	7	5	8	9	14	4
Zr	260	162	6	5	8	9	14	4
Nb	5	15	<4	<3	<4	<4	2	<2
Cu	11	360	70	10	17	75	53	14
Zn	230	130	84	89	48	84	66	60
Pb	16	6	14	5	3	9	9	2
Mo	2.0	0.5	<0.5	<0.5	0.5	<0.5	<0.5	<0.5
S	400	800	<100	<100	100	200	<100	<100
Ti/Zr	78.4	95.1	79.9	48.0	217.3	197.0	99.9	

	0127	0139	0140	0154	0155	0219	0228
SiO_2	49.75	38.60	35.77	54.67	50.48		
TiO_2	0.05	0.01	0.02	0.01	0.02		
Al_2O_3	13.56	0.08	0.08	1.04	2.98		
Fe_2O_3	11.03	7.08	6.29	7.61	7.78		
MnO	0.20	0.09	0.08	0.17	0.16		
MgO	12.23	45.70	41.53	33.17	30.76		
CaO	10.87	0.02	0.02	1.72	2.91		
Na_2O	1.04	0.01	0.03	0.05	0.03		
K_2O	0.18	0.01	0.01	0.01	0.02		
P_2O_5	<0.01	0.01	0.01	0.01	0.01		
LOI	1.90	8.42	15.80	1.91	3.90		
Total	100.81	99.65	99.56	100.37	99.05		
Cr		1940	1758	4862	4605		
Ni		2660	2521	626	724		
Rb	6	<4	<4	<4	<4		
Sr	140	<4	<4	<4	<4		
Y	4	<4	<4	<4	<4		
Zr	<1	<4	<4	<4	<4		
Nb	<1	<4	<4	<4	<4		
Cu	18	2	2	3	3	3	360
Zn	68	23	34	52	36	230	130
Pb	<2	2	2	2	<2	2	7
Mo	<0.5	1.0	<0.5	<0.5	<0.5	1.0	0.5
S	<100	200	100	<100	<100	<100	<100

GOLD DISTRIBUTION AND GENESIS IN AUSTRALIAN VOLCANOGENIC MASSIVE SULFIDE DEPOSITS, AND SIGNIFICANCE FOR GOLD TRANSPORT MODELS

Ross R. Large, David L. Huston, Peter J. McGoldrick, Peter A. Ruxton and Garry McArthur

INTRODUCTION

The volcanogenic massive sulfide deposits of Australia contain significant grades of gold in addition to base metals and silver. The twenty-one deposits listed in Table 1, and located in figure 1, show a range of ore grades from 0.2 ppm Au to 4.75 ppm Au with an overall Australian mean of 1.6 ppm. The major gold production has come from two provinces;

a) The Mount Read Volcanic belt of western Tasmania where four deposits have an average grade exceeding 2 ppm Au (Rosebery, Hercules, Que River and Hellyer), and together with Mt. Lyell these deposits contain a combined resource of 156.3 tonnes of gold (Fig. 2).

b) The Rockhampton district of eastern Queensland where two deposits have an average grade exceeding 2 ppm Au. The Mt. Morgan deposit, which averages 4.75 ppm has produced 237.5 tonnes of gold, more than half the total gold content of all Australian VMS deposits (Fig. 2).

The purpose of this paper is to describe the distribution and zonation of gold relative to base metals in a number of deposits from the major gold bearing VMS provinces in Australia, and to discuss the factors which control the transport and deposition of gold in volcanic hydrothermal systems.

Other recent studies of gold in Canadian massive sulfides (eg. Knuckey et al., 1982, Knuckey and Watkins 1982 and Hannington and Scott, 1987), gold in Kuroko deposits (eg. Yamada et al., 1988), and gold in active sea floor chimneys (Hannington et al., 1986) are briefly discussed as a comparison to the Australian deposits.

SUMMARY AND CONCLUSIONS

1. Volcanogenic massive sulfide deposits in Australia exhibit a range in average gold content from 0.2 ppm to 4.75 ppm Au, with an overall mean of 1.6 ppm.

2. The Mount Morgan Cu-Au deposit in Eastern Queensland had been the major producer (237.5 tonnes of Au), followed by the deposits in the Mt. Read Volcanics of Western Tasmania (Rosebery, Hercules, Que River, Hellyer and Mt. Lyell) which together have a premining resource of 156.3 tonnes of Au.

3. From a study of 21 Australian deposits, and by comparison with Canadian Archean and Kuroko deposits, it is apparent that massive sulfides which average greater than 10% Zn generally, but not always, contain gold grades greater than 1 ppm Au. In such deposits the gold grade increases with increasing zinc grade and is concentrated along with Pb, Ag, Ba and As toward the hanging wall of the deposit. Examples which show the hanging wall zinc-gold association are Rosebery, Que River, Hellyer and most Kuroko deposits.

4. Massive sulfides which average less than 10% Zn, commonly exhibit low gold grades. However, these deposits may display a positive correlation between copper and gold, in which case the gold is concentrated in the footwall stringer zone and lower portion of the massive sulfide associated with high copper grades. Examples of deposits which show this footwall gold-copper association are Mt. Chalmers, Mt. Morgan, Mt. Lyell and many other stringer dominated deposits.

5. Thermodynamic studies on the controls of gold transport and deposition indicate that the two gold associations described above may relate directly to the gold transporting mechanism. The footwall gold-copper association reflects gold transport as the $AuCl_2^-$ complex by high temperature (>300°C), low pH (<4.5) moderate to high fO_2 and high salinity fluids (> seawater). The hanging wall gold-zinc association reflects gold transport as the $Au(HS)_2^-$ complex by lower temperature (200-250°C), moderate pH (4.5-6) and moderate fO_2 fluids.

6. A process of gold refining, where cooling hydrothermal solutions leach gold (plus zinc and lead) from the lower parts of the sulfide body and reprecipitate the gold at the top of the body, associated with dropping temperature and increasing SO_4/H_2S ratio, is proposed

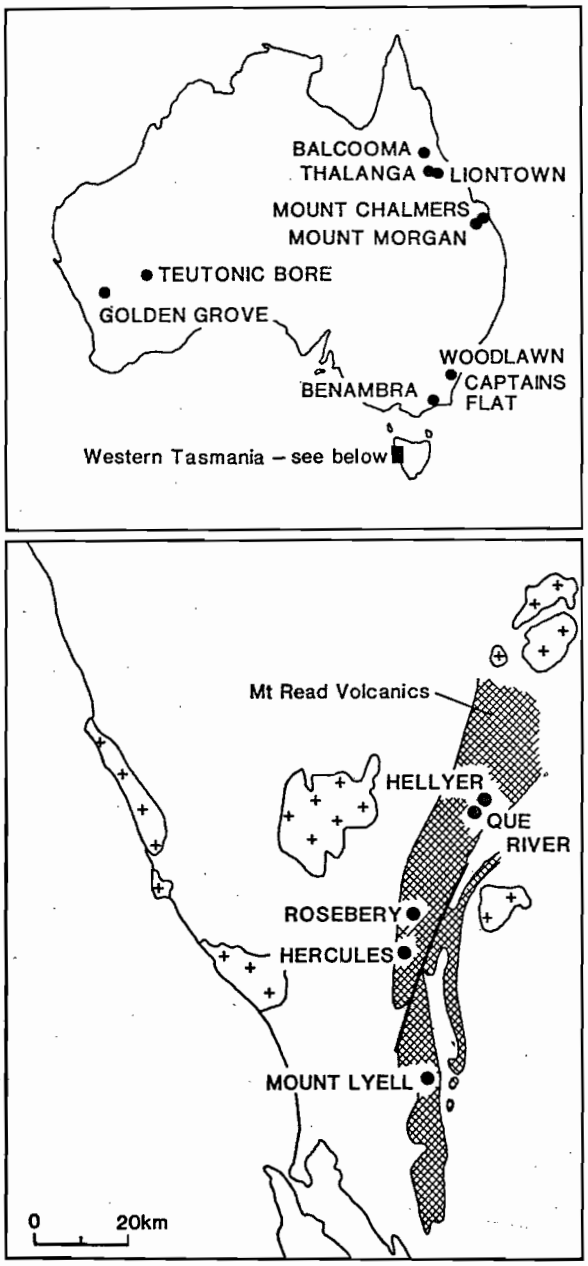

Figure 1 Locations of the major volcanogenic massive sulfide deposits in Australia.

as the mechanism which leads to gold enrichment at the top of zinc-rich deposits. This process is common in barite-rich Palaeozoic deposits but rare in Archean deposits, due to lower SO_4/H_2S fluid ratios in the latter.

7. By analogy with massive sulfides, other deposits which exhibit a gold- copper association, such as porphyry related gold-copper ores, acid-sulfate epithermal deposits, and Proterozoic magnetite-gold deposits, are considered to form by the transport and deposition of gold from chloride complexes.

DEPOSITS IN THE MOUNT READ VOLCANICS

The Mount Read Volcanics is an arcuate belt of Cambrian volcanics about 220 km long and 5 to 15 km wide. The oldest part of the volcanic belt, the Central Volcanic Complex, is the host to five major massive sulfide deposits at Mt. Lyell, Hercules, Rosebery, Que River and Hellyer, plus a large number of smaller deposits.

The polymetallic deposits at Rosebery, Hercules, Que River and Hellyer are particularly enriched in lead and zinc in addition to gold and silver (Table 1). Compared with Canadian Archean massive sulfides (Fig. 3) and the Japanese Kuroko deposits, the Tasmanian ores standout in terms of overall tonnage and grade.

Gold at Rosebery: In 1985 Rosebery ranked eleventh on the Australian gold production list, with an annual output of 1.25 tonnes. The Rosebery deposit is a folded massive sulfide sheet composed of banded galena-sphalerite- pyrite ore overlain by a barite-rich zone and underlain by discrete lenses of pyrite-chalcopyrite (Brathwaite, 1974, Green *et al.*, 1981). Recent studies by Huston and Large (1987) have shown that gold is concentrated in the massive galena-sphalerite-pyrite mineralization where average grades generally exceed 3 ppm and may reach over 25 ppm (Fig. 4a, b). The gold grades in the banded galena-sphalerite ore are fairly homogenous and tend to increase upwards and decrease laterally. Significant gold also extends into the overlying barite zone with values typically of 2 to 5 ppm but generally with a more erratic pattern than within the Pb-Zn ore. The footwall chalcopyrite pyrite lenses are commonly depleted in gold with values of 1-3 ppm, and averaging less than 1.5 ppm (Table 2).

The gold occurs as discrete electrum grains (fineness 320 to 970) from 5 to 40 microns across and is commonly associated with pyrite (Huston & Large, in prep.).

Gold at Hellyer: The Hellyer massive sulfide averages 2.3 ppm Au, and like Rosebery, the gold is concentrated toward the stratigraphic hangingwall of the deposit. The deposit is composed of a single, faulted, elongate massive sulfide body overlying a well developed pyrite footwall alteration pipe (Fig 4b and McArthur, 1986). A central sub-vertical spine of copper mineralisation carrying less than 2 ppm Au extends from the stringer zone up through the massive sulfide body (Fig. 4d). Gold values of 5-10 ppm are concentrated at the top of the massive sulfide and extend laterally down the sides of the sulfide mound adjacent to, and on the western side, of the copper spine. This distribution pattern suggests that gold deposition did not accompany syngenetic sulfide accumulation on the upper surface of the mound, but may have involved a later stage of

TABLE 1: Tonnage and grade data for Australian volcanogenic massive sulfide deposits.

	Age	M. tonnes	Au ppm	Ag ppm	Cu %	Pb %	Zn %	Status
WESTERN TASMANIA								
Rosebery	Cambrian	19.4	2.9	155	0.7	5.0	16.2	Current mine
Hercules	Cambrian	2.6	2.7	159	0.4	5.2	16.7	Past producer
Que River	Cambrian	3.1	3.4	200	0.6	7.5	13.5	Current mine
Hellyer	Cambrian	19	2.3	160	0.4	7.0	13.0	Current mine
Mt. Lyell								
The Blow	Cambrian	5.6	2.0	61	1.3	N.R.	N.R.	Past producer
Prince Lyell*		87.6	0.3	2	2.0	0.01	0.04	Current mine
North Lyell		5.1	0.4	33	5.3	N.R.	N.R.	Past producer
QUEENSLAND								
Thalanga	Cambrian	7.5	0.5	83	3.0	3.0	9.0	Feasibility
Liontown	Cambrian	2.0	2.0	100	1.0	2.0	10.0	Prospect
Balcooma	Cambrian	5.0	0.3	23	2.8	1.5	3.0	Feasibility
Mt. Morgan	Devonian	50.0	4.7	6	0.7	0.05	0.1	Past producer
Mt. Chalmers	Permian	3.6	2.0	14	1.8	0.1	0.8	Past producer
NEW SOUTH WALES								
Woodlawn**	Silurian	6.3	N.R.	89	1.7	5.5	14.4	Current mine
Captains Flat	Silurian	4.2	1.7	56	0.7	6.0	10.0	Past producer
VICTORIA								
Wilga	Silurian	4.6	N.R.	32	3.6	N.R.	5.8	Feasibility
Currawong	Silurian	9.5	1.3	38	1.6	0.9	4.3	Feasibility
WESTERN AUSTRALIA								
Gossan Hill	Archean	16.7	0.3	21	3.1	0.2	1.5	Feasibility
Scuddles	Archean	26.1	0.9	59	1.2	0.5	6.9	Feasibility
Teutonic Bore	Archean	2.2	0.2	148	3.5	0.8	11.1	Past Producer

N.R. = No reliable data available.
* = Prince Lyell ore types grouped together.
** = The massive sulfide ore only.

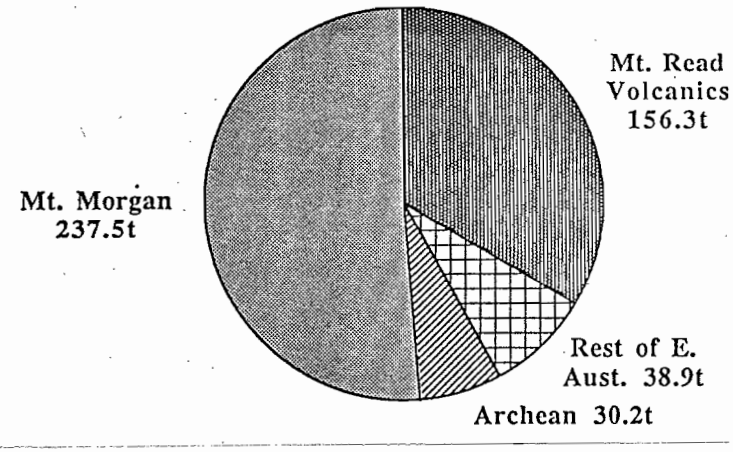

Figure 2 Pre mining tonnes of gold in Australian massive sulfide districts. Note that Mt Morgan and the deposits in the Mt Read Volcanics contain the major VMS-gold resource. As a comparison, the Kalgoorlie Golden Mile has a total resource of 1,200 tonnes of gold (Groves et al., 1986) compared to 463 tonnes from Australian VMS deposits.

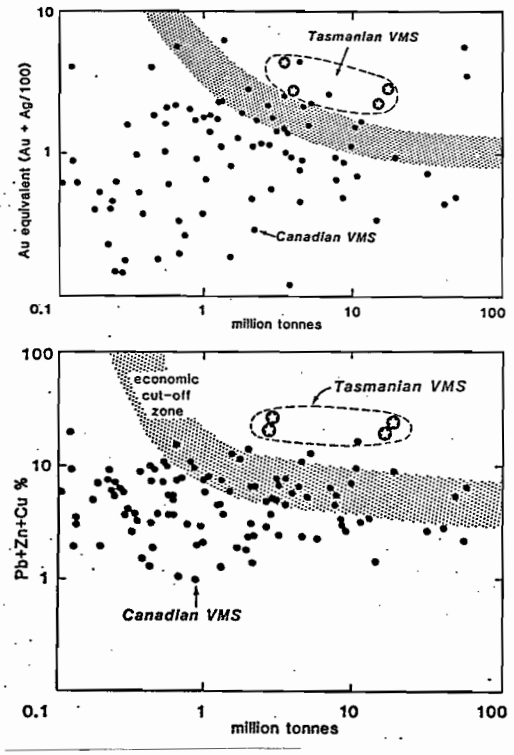

Figure 3 Grade VS tonnage plots comparing the four polymetallic VMS deposits from Tasmania with Canadian Archean VMS deposits (data from Franklin & Thorpe, 1982). The stippled zone represents the likely economic cut-off zone under Australian conditions for an underground polymetallic mine.

gold emplacement in the outer parts of the mound, accompanying and surrounding the copper spine mineralization. The upper and outer zone of gold enrichment is also accompanied by enrichment of lead, zinc, silver, barium and arsenic. The highest gold grades are found in a thin silica-rich layer that caps the barite zone over the central part of the deposit. Free gold or electrum is very rare and the majority of gold appears to be locked-up in pyrite and arsenopyrite (C.S.I.R.O. reference).

Gold at Que River: The Que River massive sulfide consists of two major ore lenses which have been folded in a complex upright syncline sheared along its western limb. The upper-most ore lens (PQ-P-north system) is lead-zinc- rich with high gold (3-5 ppm) whilst the lower lens (S lens) is lead-zinc poor and copper-rich with negligible gold (0.1-1 ppm). On the 7550 mN section (Fig. 4e, f) the PQ-Pnorth lens is deformed into a W-fold structure with the highest gold grades (10-30 ppm) concentrated along the trace of the axial surfaces of the fold, and overlapping the high grade lead-zinc zone (with >30% Pb + Zn). Significant copper occurs in the keel of the syncline below the Au-Zn-Pb zone (Fig. 4f). A pre-folding reconstruction of the ore deposit outlined by Large et al. (in press) indicates that gold grades increase toward the top of the massive sulfide along with lead and zinc, while copper is concentrated in the lower part of the massive sulfide, and overlies a low grade pyrite-rich stockwork zone.

TABLE 2: Summary of gold and base metal zonation in some Australian massive sulfides.

	ROSEBERY		HELLYER		MT. CHALMERS		SCUDDLES	
		Au* ppm		Au* ppm		Au* ppm		Au* ppm
Hanging wall	barite, minor Pb-Zn	2-5	silica-pyrite-cap	5-10	barite-Pb-Zn	2-3	massive Zn-Py	~1
	massive Pb-Zn-Ag-py	3-10	barite-Pb-Zn	3-5	massive Cu-py	2-10	massive Zn-Cu	1-5
			massive Pb-Zn-Ag-py	2-3				
Cu-py	massive	1-3	massive py low Pb-Zn	1-2			massive Cu-py-po	~0.5
	dissem. py	<1	Pb-Zn>Cu stringers	0.5-1	Cu-py stringers	0.5-5	stringer Cu-py-po	0.01-1
Footwall								

* Typical range of gold values in the respective zones.

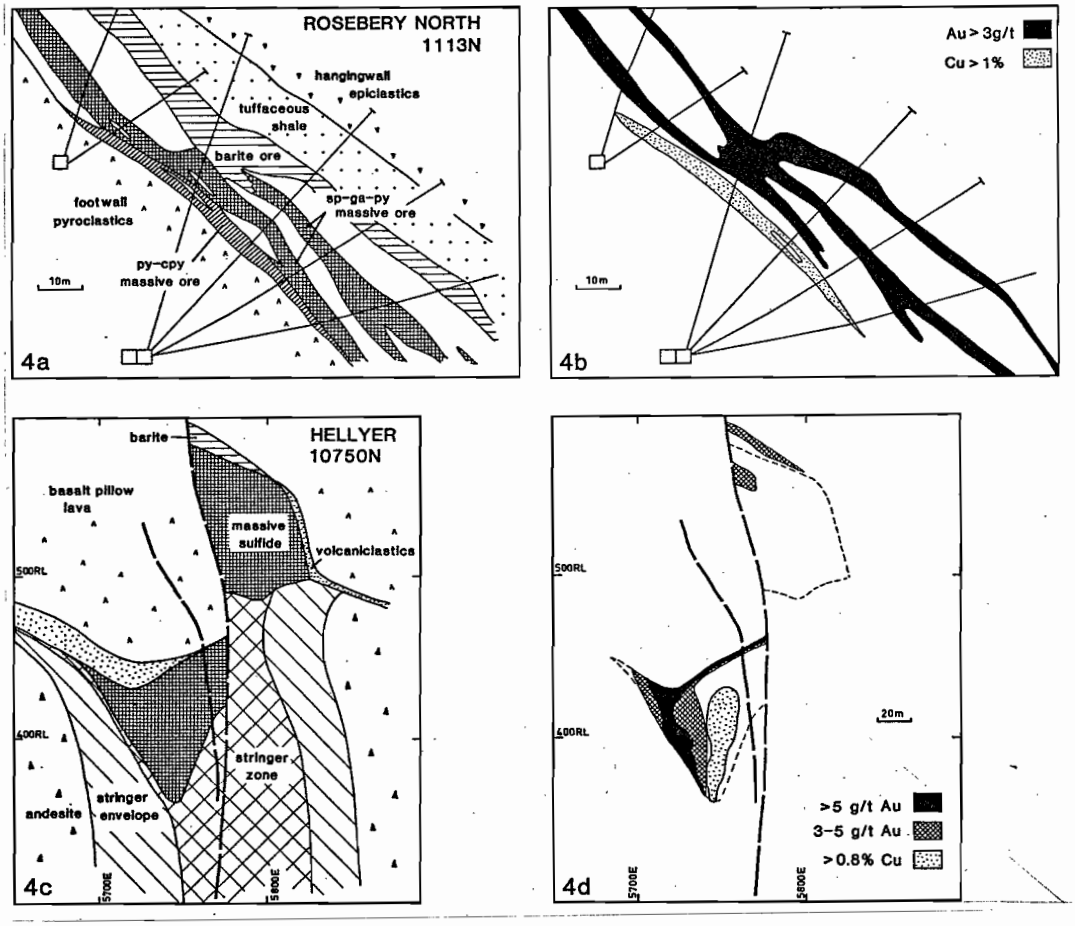

Figure 4a-d Typical geological cross sections, and gold-copper distribution sections for Rosebery North and Hellyer.

The association of gold with zinc at Que River is well illustrated in figure 5. Here the drill hole assay data for the 7550N section has been plotted on a gold versus zinc diagram, along with the average ore grades for other Australian massive sulfides. It is apparent from this relationship that at values of less than about 7% zinc, gold grades are typically less than 1 ppm, and there is no obvious correlation between zinc and gold; this corresponds with the lower massive and stringer parts of the deposits. However, above 7% Zn there is an exponential increase in gold grade with increasing zinc grade, rising from about 1 ppm gold at 10% Zn to over 10 ppm gold above 20% Zn. A similar increase in gold grades with zinc grades is recorded in the massive sulfide ore at Rosebery and Hellyer.

The gold occurs as electrum (fineness 550 to 820) and grainsize is related to the degree of recrystallization associated with deformation (Large *et al.*, 1988). Strongly recrystallized galena zones contain gold grains from 50 to 400 μm, less recrystallized sphalerite contains gold from 20 to 200 μm, whereas the relatively undeformed pyrite contains very fine gold (<10 μm).

***Gold at Mt. Lyell*:** Since mining began in 1895 the Mt. Lyell deposits have produced over 40 tonnes of gold from about 100 million tonnes of ore. The principal deposits of West Lyell and Prince Lyell consist of disseminated and stockwork pyrite-chalcopyrite mineralization containing from 0.2 to 0.6 ppm Au. Carswell (in Large *et al.*, 1988) reports a positive correlation between gold and copper in these deposits, with the highest copper grade sections of the orebody containing the best gold values. The Cu:Au ratio is consistently about 40,000:1. The Blow deposit, a massive pyrite lens to the east and stratigraphically above the major disseminated ore deposits (Walshe & Solomon, 1981), contained the best gold grades, averaging 2 ppm, with a lower Cu:Au ratio (about 10,000:1) than the other ores. Unlike the other Tasmanian massive sulfides, the Mt. Lyell deposits contain very little lead and zinc, averaging less than 0.1% Zn, and they show no correlation between gold and zinc.

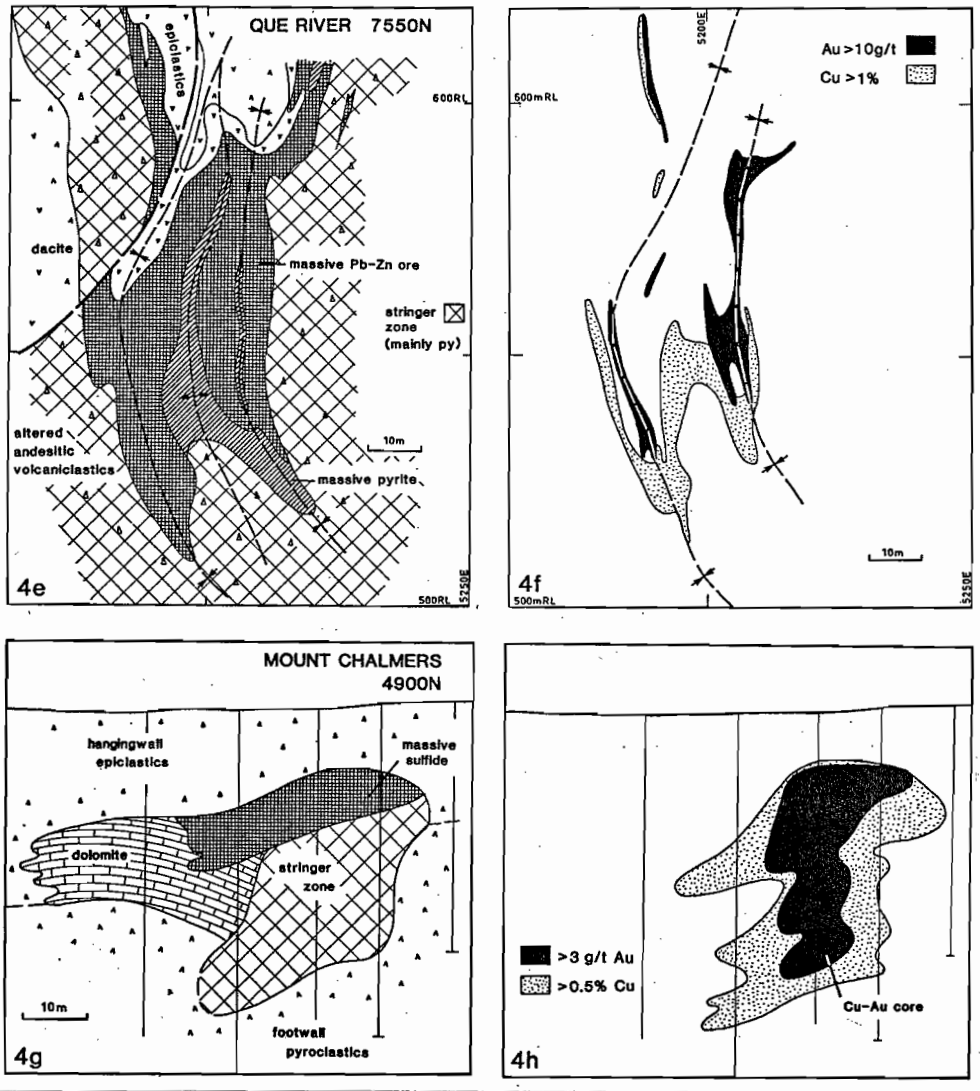

Figure 4e-h Typical geological cross sections, and gold-copper distribution sections for Que River and Mt Chalmers.

DEPOSITS IN THE ROCKHAMPTON AREA, QUEENSLAND

Gold at Mount Chalmers: The Mt. Chalmers massive sulfide lies within a belt of Permian volcanics, 27 km northeast of Rockhampton (Fig. 1). Previous studies (eg. Large & Both, 1980) have demonstrated that the best gold grades were located in the central part of the stringer pyrite-chalcopyrite zone, and extended into the overlying copper-rich massive sulfide (Fig. 4g, e). Zinc, lead and silver were concentrated toward the top of the massive sulfide, overlying the gold-copper zone, and extended laterally down the interpreted sea floor palaeoslope. There is a positive correlation between gold and copper throughout the ore deposit, with an average Cu:Au ratio of about 10,000:1, similar to the Blow deposit at Mt. Lyell.

Gold at Mt. Morgan: The Mt. Morgan deposit is a copper-gold bearing massive sulfide which occurs in a sequence of Devonian felsic volcanics, 36 km south-southwest of Rockhampton (Fig. 1). Taube (1986) reports that the deposit averaged 4.75 g/t Au (Table 1) with total production of 238 tonnes, and as such has been the major producer of VMS gold in Australia (Fig. 2). The deposit consists of a cross cutting body of massive pyrite ore (the Main Pipe orebody) and an adjacent siliceous stockwork zone (the sugarloaf orebody). Minor bedded lead-zinc-bearing sulfides occur lateral to the upper-most part of the massive pyrite orebody (Taube, 1986). The highest values of primary gold occurred in the central core of the massive sulfide pipe, where average grades of 14 ppm Au and 2% Cu were recorded (Frets, 1974). Lower gold-copper grades plus minor zinc occurred laterally outwards and upwards

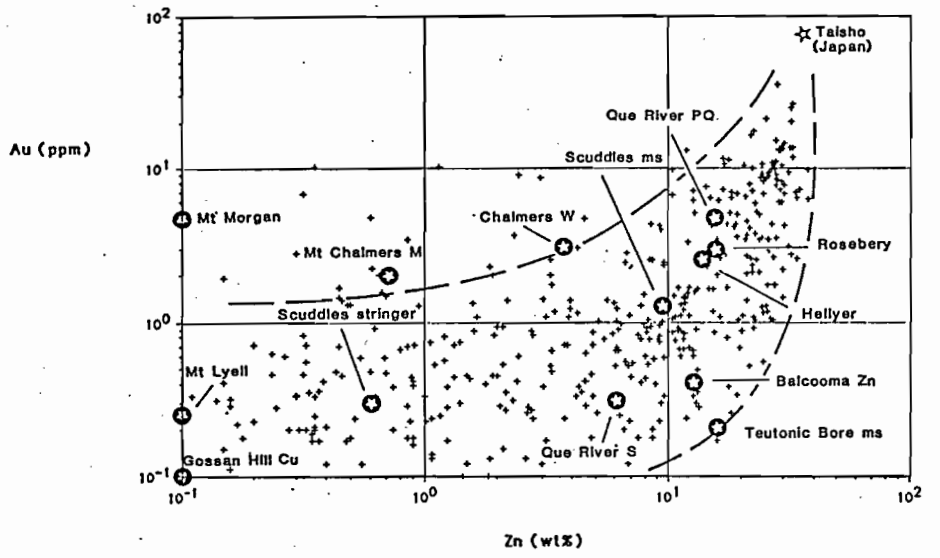

Figure 5 Gold versus zinc plot for drill hole assays at Que River section 7550N(+). Average ore grades for other Australian VMS deposits are also shown, and the high grade Au-Zn Kuroko deposit (Taisho). Note the two patterns in the data. Below 7% there is no obvious correlation between gold and zinc. Above 7%, the gold grades increase exponentially with increasing zinc.

from the central core. The native gold and chalcopyrite mineralization are associated with a network of quartz-pyrite veinlets which form the lower stockwork zone in the sugarloaf orebody and extend upwards into the massive sulfide orebody. Although some features of this deposit (eg. the lack of significant bedded sulfides, and the overprint stockwork vein system) are not typical of volcanogenic massive sulfide ores, the bulk of the evidence strongly supports a volcanogenic origin for this deposit (Taube, 1986).

WESTERN AUSTRALIAN ARCHEAN MASSIVE SULFIDES

Compared with the Canadian Archean province, the Australian Archean contains very few VMS deposits. Of the three major deposits listed in Table 1, only Scuddles contains significant gold (averaging 0.9 ppm) whilst the silver-rich Teutonic Bore deposit contains negligible gold (averaging 0.2 ppm). Recent studies on the Scuddles deposit (Ruxton, 1987) indicate that the gold is spread throughout the massive sulfide zone at levels of about 0.5 to 1 ppm, however, enrichment of up to 5 ppm Au occurs in the central part of the massive sulfide lens (Table 2). Unlike the polymetallic deposits in the Mount Read Volcanics, the best gold grades do not correspond to the highest zinc grades at the stratigraphic top of the lens. However, there is a general linear correlation between gold and copper throughout both the stringer zone (where Cu:Au ~ 7,000:1) and the massive sulfide (where Cu:Au ~ 700:1) in a similar pattern to the Mt. Chalmers deposit.

TWO ASSOCIATIONS OF GOLD IN MASSIVE SULFIDES

Based on the gold distribution patterns outlined above for Australian deposits it is apparent that there are two distinct spatial and mineralogical associations of gold and base metals in VMS deposits.

1) A gold-zinc (-lead-silver-barite) association which is typical of lead- zinc rich deposits, with gold concentrated toward the stratigraphic hangingwall of the deposit. Examples are Rosebery, Hellyer and Que River.

2) A gold-copper association in which gold is concentrated in the central and lower portions of the massive sulfide and extends down the core of the stringer zone. Examples are Mt. Lyell, Mt. Chalmers and Mt. Morgan.

Some deposits show both associations, although one generally dominates at the expense of the other. For example, at Rosebery the majority of the gold occurs with zinc-rich and baritic ore at the top of the deposit, however minor gold is concentrated in small patches within the footwall chalcopyrite-pyrite lens (Huston & Large, in prep).

Several conclusions that emerge from figure 5 and the observations outlined above on the individual deposits, are given below:

1) Massive sulfides which average greater than 10% Zn will generally (but not always) contain gold grades of greater than 1 ppm Au, above which the gold increases with zinc and becomes concentrated (along with Pb, Ba, As) toward the hangingwall of the deposit.

2) Massive sulfides which average less than 10% Zn

TABLE 3: List of chemical parameters and related mineralogies which favour high or low gold grades in zinc-rich zones and copper-rich zones of VMS deposits.

Gold Content	Zinc Ores ($Au(HS)_2^-$ transport)	Copper Ores ($AuCl_2^-$ transport)
	Zn > 15%	Cu ≥ 2%
High gold 3-20 ppm	high fO_2 : py-barite>hematite moderate pH : carbonate stable moderate T : 150-250°C high αS_2 : low FeS in ZnS	high fO_2 : py>magnetite low pH : sericite>kaolinite high T : >300°C high salinity : =5 wt% NaCl
	Zn < 10%	Cu ≤ 2%
Low gold <1 ppm	low fO_2 : pyrite>pyrrhotite low pH : sericite/chlorite moderate T: 150-250"C	low fO_2 : pyrite>pyrrhotite high pH : carbonate stable low salinity < 5 wt% NaCl low αS_2 : high FeS in ZnS

TABLE 4: Typical ore fluid conditions for a variety of gold-bearing ore types.

	VMS Cu[1]	VMS Pb/Zn[1]	Epithermal Au/Ag[2]	Porphyry Cu[4]	Archean lode Au[3]
Temperature (°C)	280-380	200-300	200-300	350-800	250-350
pH	3.5-5.5		4.5-7	3-6	5.5-7
Salinity (wt%)	3-10	3-6	0-3	25-60	0-2
$a_{H2S(m)}$	$10^{-2.5}$ to $10^{-3.5}$		$10^{-1.5}$ to $10^{-2.5}$	$10^{-1.5}$ to $10^{2.5}$	10^{-2} to 10^{-3}
Fe-S-O minerals	py ± po	py	py ± hem	py ± mag	py-po

* Conditions for adularia-sericite type.

References:

1. Pisutha-Arnond & Ohmoto (1983), Large & Both (1981), Large (1977).
2. Heald, Foley & Hayba (1987), Hayba et al. (1986).
3. Ho (1987), Neill (1987), Phillips & Groves (1983), Kerrich & Hodder (1982).

will commonly show low gold grades. However, these deposits may display a positive correlation between copper and gold, leading to the possibility of high gold grades in the stringer zone and lower massive ores associated with high copper grades (eg. Mt. Chalmers and Mt. Morgan).

COMPARISON WITH OTHER MASSIVE SULFIDE PROVINCES

The two gold associations outlined above have also been recorded in other VMS provinces. For example, in the Noranda district of the Canadian Archean, the Millenbach deposit displays a classic copper-gold association (Knuckey *et al.*, 1982) whilst the nearby Corbett deposit displays the gold-zinc association (Knuckey & Watkins, 1982). In the Kuroko district of Japan, the majority of deposits conform closely to the gold-zinc association (eg. Shimazaki, 1974), with gold concentrated in the upper part of the black-ore along with zinc, lead, silver and barite. However, a recent discovery of high grade gold ore at the Nurukawa deposit, in the Hokuroko district, has features of the gold-copper association. Yamada *et al.* (1987) report grades of 15 to 30 ppm Au in the central core of a copper-bearing stockwork system, with a strong correlation between copper and gold throughout the system.

Studies of the gold content of recent sulfide chimneys at sea-floor spreading centres in the eastern Pacific by Hannington (*et al.*, 1986) have revealed that high gold values at the top of the Axial seamount deposit average 4.9 ppm Au, and are associated with a silica-barite-sphalerite assemblage plus minor lead sulfosalts. Other chimney and mound deposits in the Guaymas Basin, along the Juan de Fuca Ridge and Galagagos rift contain lower gold values averaging 0.1 to 0.7 ppm, but generaly show a correlation of gold with Zn, Pb, As, Sb, Ba and Ag (Hannington *et al.*, 1986). All these Recent deposits exhibit the gold-zinc association, with a general lack of correlation between gold and copper. However, the sample population is very small, and the deeper portions of the sulfide systems (where the Au-Cu association is to be expected) have yet to be sampled.

TRANSPORT MODELS FOR GOLD

Gold is considered to be transported in hydrothermal solutions as either thio-complexes (Seward, 1973) or as chloro-complexes (Helgeson, 1969; Henley, 1971), although other complexes such as thio-arsenates and tellurium species may play some role (eg. Seward, 1984). Thermodynamic data only exists for the species $Au(HS)_2^-$, $Au_2(HS)_2S^{2-}$ (Seward, 1973) and $AuCl_2^-$ (Helgeson, 1969). Cole & Drumond (1986) and Wood *et al.* (1987) suggested that the stability of gold chloride complexes may be four to six orders of magnitude greater than predicted by Helgeson (1969), however based on the geological evidence (see below) and other experimental studies (eg. Rytuba & Dickinson 1977; Nikolaev 1972; Henley, pers. comm., 1987; Seward, pers.comm. 1988) the estimate by Helgeson is considered to be the best data available.

For the pH and temperature range considered appropriate for massive sulfide deposition (eg. Large, 1977; Ohmoto *et al.*, 1983 and Table 4) the two relevant equations describing gold transport are:

$$4\ Au(HS)_2^- + 2H_2O + 4H^+ \Leftrightarrow 4Au^\circ + 8H_2S + O_2 \quad \ldots (1)$$

$$4\ AuCl_2^- + 2H_2O \Leftrightarrow 4\ Au^\circ + 4H^+ + 8Cl^- + O_2 \quad \ldots (2)$$

Previous studies by Seward (1973, 1984), Henley (1985, 1986), Phillips and Groves (1983, 1984), Cathles (1986), and Neil (1987) suggest that the thio-complex $Au(HS)_2^-$ is the most important species involved in gold transport and deposition for epithermal gold-silver deposits and Archean greenstone lodes. However, for the higher salinity, lower pH, massive sulfide systems the role of the $AuCl_2^-$ complex cannot be easily dismissed and, as will be shown subsequently, this complex is considered to play a critical role in the development of gold-bearing massive sulfide ores.

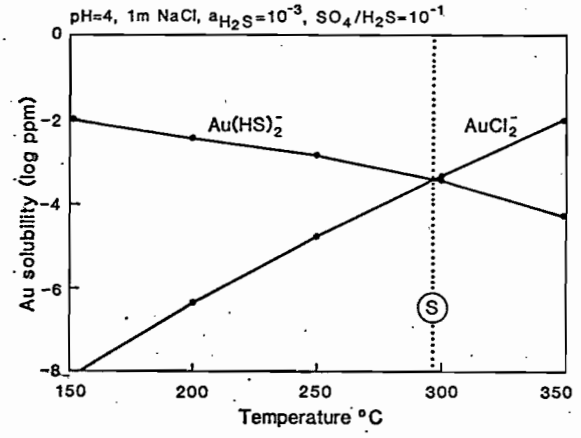

Figure 6 Variation of gold solubility with temperature for the thio-complex and the chloro-complex. Under these conditions the switchover line (S) is at 290°C, with the $AuCl_2^-$ complex more stable above 290°C.

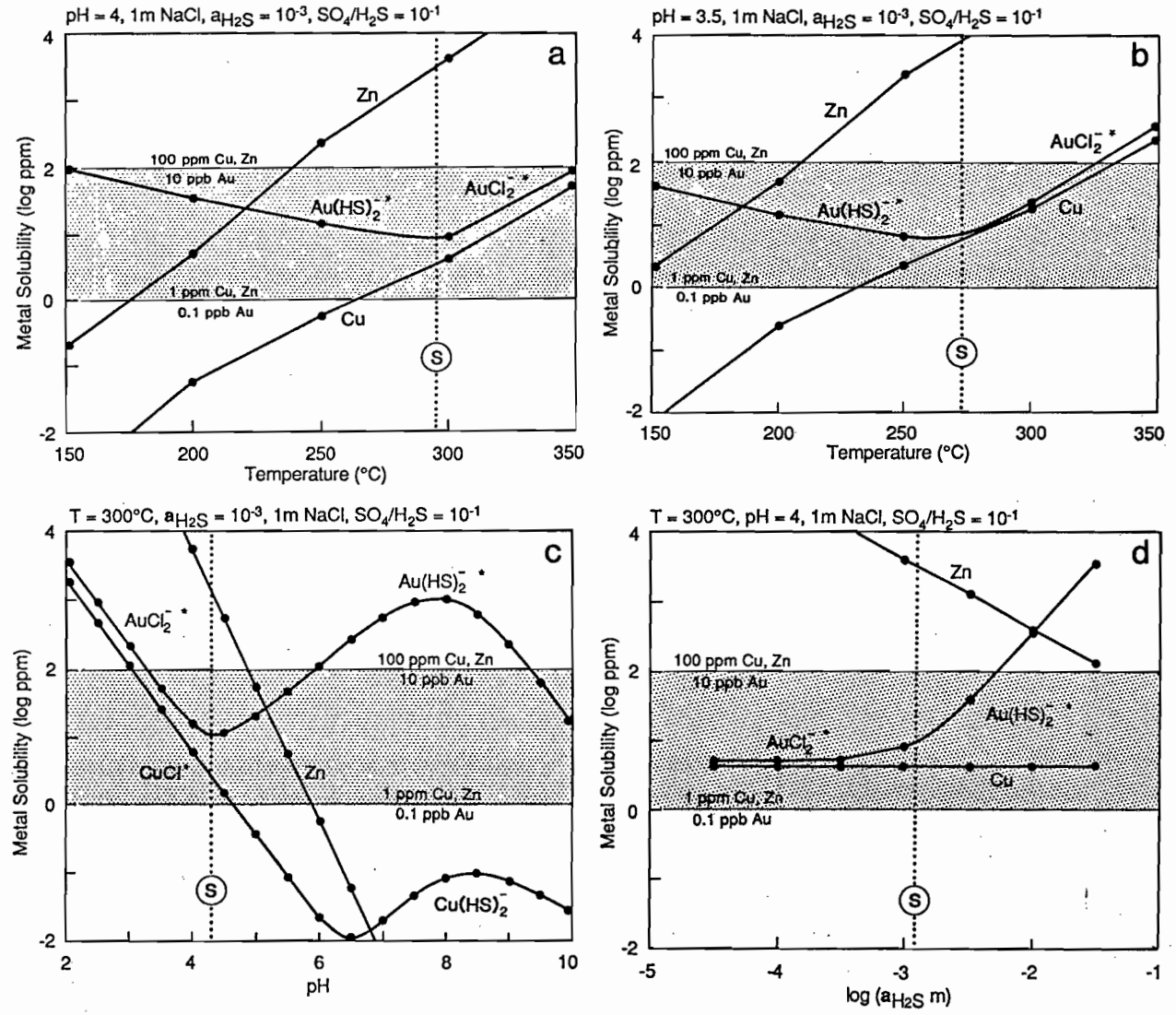

Figure 7 Series of plots showing the variation of gold solubility with temperature, pH and log aH_2S. The solubility of copper and zinc (as chloride complexes) is also shown. The switchover line between $Au(HS)_2^-$ predominance and $AuCl_2^-$ predominance is marked (S). The stippled zone represents the probable range in metal content of gold and base metal ore fluids. Note that gold solubilities have been multiplied by 10^4 compared to base metal solubilities as this is their common ratio in the earth's crust, i.e. Cu/Au ~ 10^4 ~ Zn/Au.

The Switchover from Gold Chloride to Gold Bisulphide Transport

The equilibrium between the $AuCl_2^-$ and $Au(HS)_2^-$ complex in a reduced hydrothermal system (SO_4^{2-}/H_2S < 1) is controlled by the equation;

$$AuCl_2^- + 2H_2S \quad \Leftrightarrow \quad Au(HS)_2^- + 2H^+ + 2Cl^- \qquad (1)$$

Therefore:

$$a(AuCl_2^-)/a(Au(HS)_2^-) = [K_1/K_2]\,[(a_{H^+})^2\,(aCl^-)^2)/(aH_2S)^2] \qquad (2)$$

where K_1 is the equilibrium constant of equation 1, and K_2 is the equilibrium constant of equation 2. Thus, the relative importance of these two complexes in a hydrothermal fluid is controlled by temperature, pH, salinity and the activity of H_2S. Calculations based on this thermodynamic relationship (eg. Figs. 6 and 7) show that gold transport as the $AuCl_2^-$ complex is favoured in relatively high temperature fluids (>300°C) with low

pH (<4.5), low aH_2S ($<10^{-2.5}$ m), high salinity (>seawater) and moderate to high fO_2 (pyrite or magnetite ± hematite stable). On the other hand, gold transport as the $Au(HS)_2^-$ complex is favoured by lower temperature fluids (150-300°C) with moderate to alkaline pH (>4.5), high aH_2S ($>10^{-2.5}$ m), low salinity (<seawater) and moderate fO_2 (pyrite field only) (see also Huston & Large, in press).

From figure 6 it is apparent that for the given conditions (pH=4, $aH_2S=10^{-3}$, 1m NaCl, $SO_4/H_2S=10^{-1}$) the switchover from $AuCl_2^-$ transport to $Au(HS)_2^-$ occurs at about 290°C. At 350°C the $AuCl_2^-$ complex is about 100x more abundant than the $Au(HS)_2^-$ complex, while at 200°C the $Au(HS)_2^-$ complex is 10,000x more abundant than the $AuCl_2^-$ complex. If the pH of the fluid is changed from 4 to 3.5 (Fig. 7a, 7b) the switchover is reduced from 290°C to 272°C. Figure 9 contains a series of solubility plots for gold, copper and zinc constructed by utilising the thermodynamic data in appendix 1, activity coefficients calculated from data

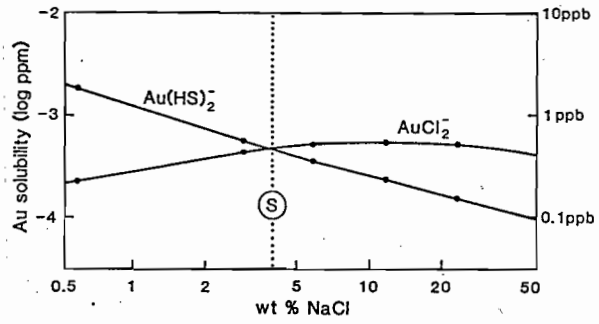

Figure 8 The effect of salinity on the solubility of the $Au(HS)_2^-$ complex and the $AuCl_2^-$ complex, for pH = 4, log aH_2S = -3 and 300 °C.

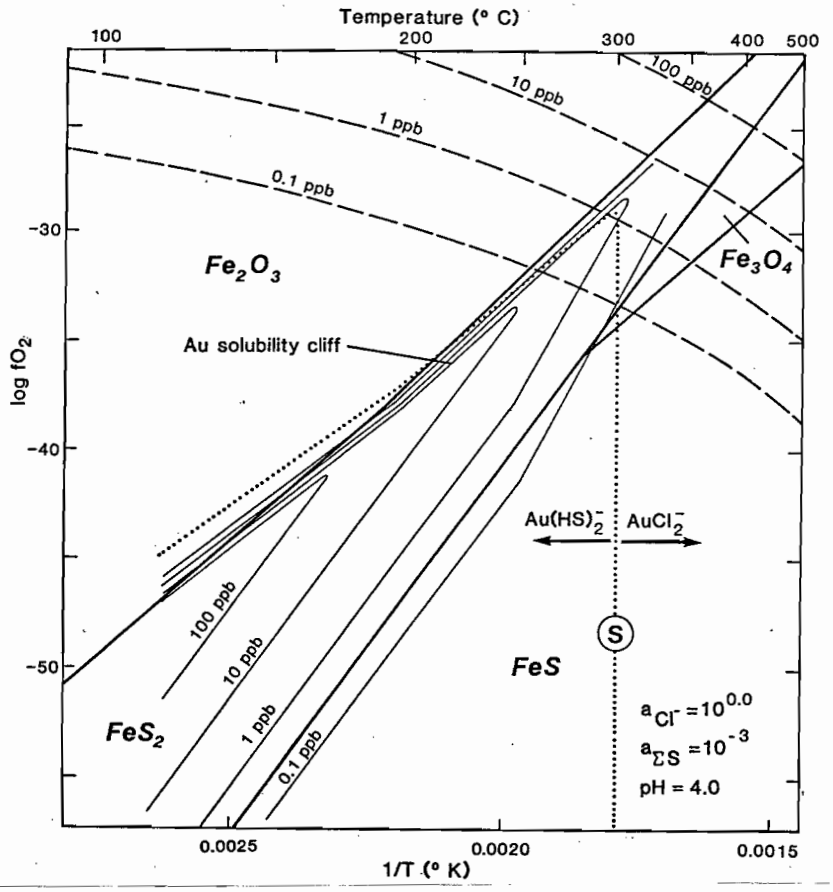

Figure 9 A log fO_2 versus temperature diagram showing solubility contours for $Au(HS)_2^-$ and $AuCl_2^-$.

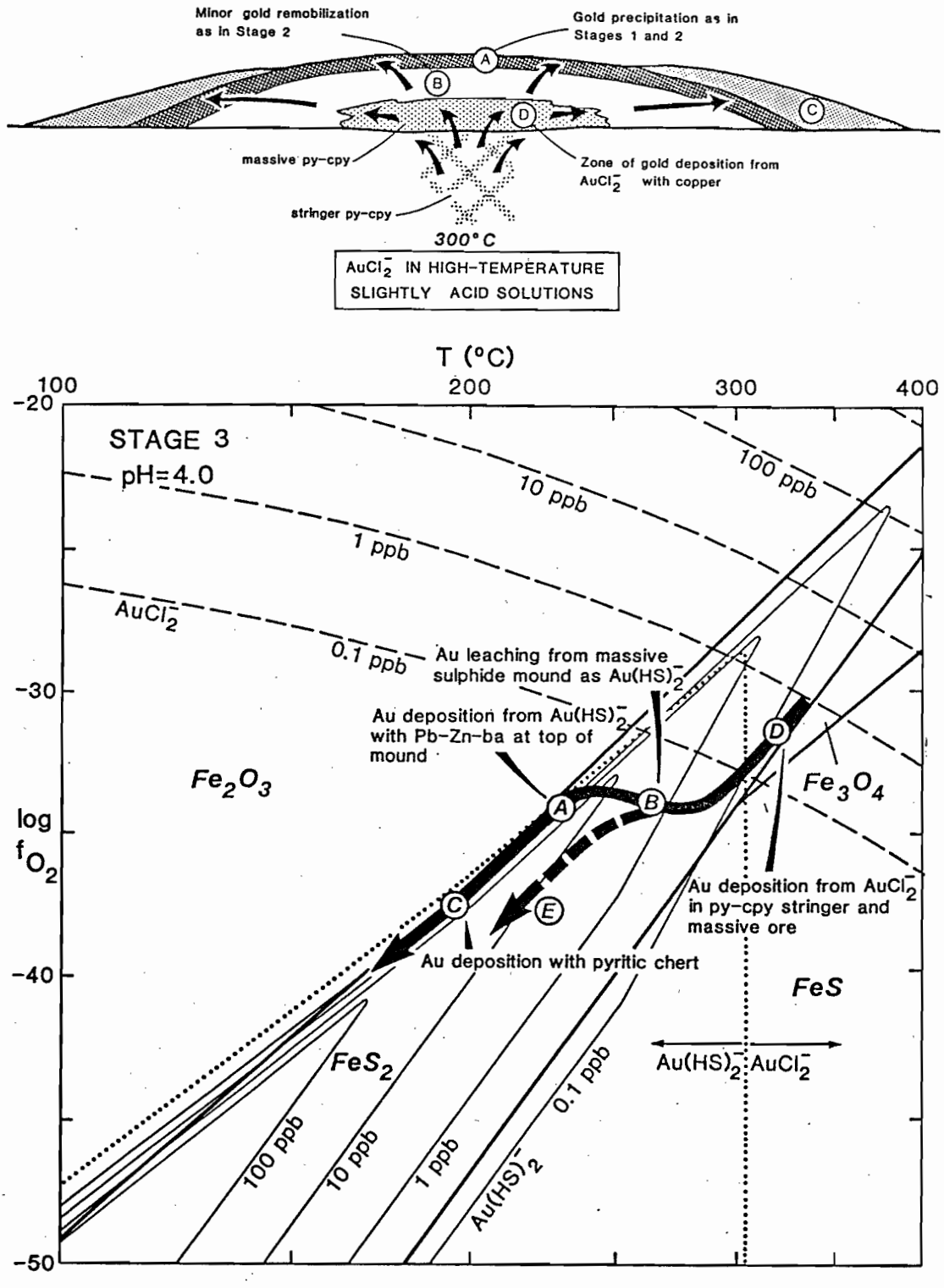

Figure 10 Stage 3 of the model proposed by Huston & Large (in press) to explain the precipitation of gold in massive sulfide deposits. Path BE represents Archean fluids which do not cross the solubility cliff.

by Barrett & Anderson (in press), and a computer program developed by Brian Harrold (Australian National University). The relative solubilities of the $AuCl_2^-$ and $Au(HS)_2^-$ complexes compared to total copper and zinc chloride solubility are depicted for varying temperature, pH, aH_2S and salinity, with the gold complex switchover lines clearly marked. These diagrams show that for high temperatures and low pH where $AuCl_2^-$ predominates, both gold and copper show very similar solubility characteristics (with a Cu:Au ratio of about 10,000:1 at saturation). This indicates that copper and gold can be transported and deposited together at temperatures above 270-300°C under a regime of dropping temperature or increasing pH. At lower temperatures (175 to 250°C) $Au(HS)_2^-$ predominates and approaches the zone of zinc saturation, providing a field of zinc-gold transport and deposition (where Zn:Au~ 10,000:1) at low temperatures and moderate to neutral pH.

Effect of Salinity on Gold Transport

Previous studies by Cathles (1986) and Henley (1985) indicate that gold solubility in hydrothermal systems decreases with increasing salinity. They conclude that high salinity solutions are favourable for base metal transport but not gold transport. However, our calculations suggest that for moderate to high temperature and low pH fluids, typical of massive sulfide systems, gold solubility decreases over the range 0.5 to 4 wt% NaCl but then shows a marginal increase from 4 to 15 wt% NaCl as $AuCl_2^-$ becomes the dominant species (Fig. 8).

The decrease in $Au(HS)_2^-$ solubility with increasing salinity is caused by the effect of ionic strength on the activity coefficient of the $Au(HS)_2^-$ species, whilst the gradual increase in $AuCl_2^-$ solubility and flattening off above 4 wt% NaCl is controlled by iron pairing of NaCl° under high salinity, high temperature conditions.

TEMPERATURE - fO_2 CONTROL ON GOLD TRANSPORT

Gold solubility contours for $AuCl_2^-$ and $Au(HS)_2^-$ have been plotted in temperature -fO_2 space in figure 9 (after Huston & Large, in press), in order to relate the major areas of gold transport and deposition to the dominant iron minerals; pyrite, pyrrhotite, magnetite and hematite. $AuCl_2^-$ is most soluble at high temperatures and high fO_2 and is independent of the iron sulfide or oxide minerals present. However, $Au(HS)_2^-$ is most stable at lower temperatures, forming a solubility window within the pyrite field. $Au(HS)_2^-$ solubility decreases rapidly adjacent to the pyrite-hematite boundary where a "solubility cliff" is defined by the contours. Gold solubility in this region is controlled by the reaction,

$$4\ Au(HS)_2^- + 2H_2O + 15O_2 \Leftrightarrow 4\ Au^\circ + 8\ SO_4^{2-} + 12H^+$$

Under these conditions rapid gold deposition is favoured by increasing fO_2, decreasing temperature and increasing pH, i.e. the changes which accompany the mixing of a reduced hydrothermal fluid with seawater. The position of this solubility cliff has important implications for the deposition of gold in moderate to low temperature and oxidised systems where SO_4^{2-}/H_2S = 0.1 to 1.0.

Consideration of Activity Coefficients

Previous calculations of gold solubility by Huston & Large (in press, fig. 7) did not take into account the effect of activity coefficients. In this study activity coefficients calculated using data from Helgeson (1969), and Barrett & Anderson (in press) are shown to have caused only a minor change in the gold solubility contours. For example, a solution of pH = 4.0, 1mNaCl and log a_{H2S} = -3, the switchover from $AuCl_2^-$ to $Au(HS)_2^-$ was calculated at to take place at 260°C when ignoring activity coefficients (Huston & Large, in press, fig. 7), but changed to 290°C, when activity coefficients were considered (Fig. 7a).

GEOLOGIC THERMODYNAMIC MODEL

Previous studies on the mineralogy, zonation and sulfide paragenesis of massive sulfide deposits have led to the development of a variety of chemical models to explain sulfide deposition and orebody evolution (eg. Sato, 1973; Large, 1977; Solomon & Walshe, 1979; Lyndon, 1981; Eldridge *et al.*, 1983 and Ohmoto *et al.*, 1983). Typical ore fluid conditions revealed by these studies are shown in Table 4. In all studies, it has been concluded that copper mineralization in the footwall of the deposits resulted from higher temperature fluids compared to the overlying lead-zinc mineralization. Fluid inclusion studies, although far from definitive (eg. Large & Both, 1980; Pisutha-Arnond & Ohmoto, 1983 and Bryndzia *et al.*, 1983) suggest that the fluids responsible for Cu mineralization are commonly more saline than those related to Pb-Zn mineralisation (Table 4). In addition, the presence of kaolinite alteration in some copper-gold-rich stringer zones (eg. Mt. Chalmers, McLeod 1985; Nurukawa, Yamada *et al.*, 1987) indicates low fluid pH of about 3.5 to 4.5 accompanying Cu mineralization.

These data, in conjunction with our current geological and geochemical studies, has formed the basis for the development of a geologic- thermodynamic model (Huston & Large, in press) to describe the

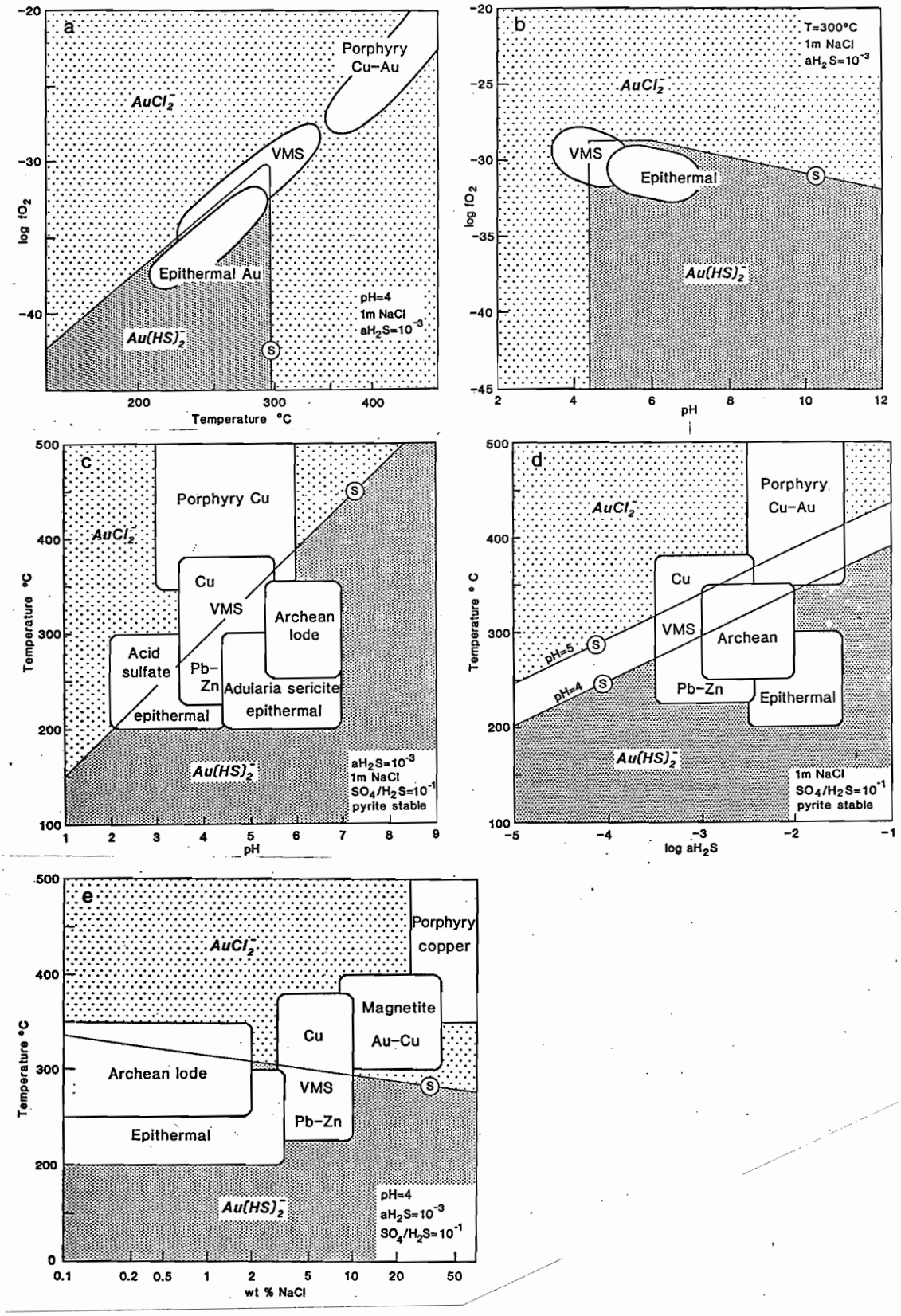

Figure 11 Series of diagrams outlining the fields of $AuCl_2^-$ predominance and $Au(HS)_2^-$ predominance for a spectrum of hydrothermal systems. The fields and boxes represent the probable chemical contraints on the ore fluids for each deposit type (from Table 4).

evolution of gold-bearing massive sulfide ores, and to account for the two distinct associations of gold with zinc and gold with copper. Stage 3 of the model, which is the main stage of high temperature mineralization, is depicted in figure 10. Fluids at 300-350°C pass up the hydrothermal pipe carrying gold and base metals as chloride complexes (point D, Fig. 10). Copper and gold are deposited in the stringer zone and lower part of the sulfide mound due to decreasing temperature (and/or increasing pH). At point B, the fluid has crossed the switchover and is capable of leaching gold as $Au(HS)_2^-$ from the sulfide mound, along with zinc and lead (following the model by Eldridge *et al.*, 1983). This leads to a gold and lead-zinc depleted zone in the lower part of the massive sulfide. As the fluid moves to the top of the sulfide mound and cools to point A, the $Au(HS)_2^-$ solubility cliff is crossed, and all gold is dumped from solution, resulting in a gold-rich zone at the stratigraphic top of the deposit.

This model accounts for the formation of a gold-copper association in the lower parts of massive sulfides, related to the high temperature, low pH, phase of mineralisation, and a gold-zinc association in the upper parts related to a moderate to low temperature phase of gold remobilisation and reprecipitation (i.e. gold refining). The exponential relationship between gold and zinc depicted for Que River in Fig. 5 is considered to be a result of the refining of both zinc and gold in the upper part of the massive sulfide. The Archean Scuddles deposit, which is relatively zinc-rich but gold-poor, does not display the enrichment of gold towards the stratigraphic top. Buffering of the SO_4^{2-}/H_2S ratio in the ore fluids by mixing with seawater at the top of the sulfide mound may be an important process which controls the degree of gold refining. For example, if the ore fluid is buffered to a low SO_4^{2-}/H_2S ratio (say about 0.01 to 0.1) as it moves to the top of the mound, then it will follow the path BE on figure 10. Under these circumstances the fluid will not cross the solubility cliff and therefore no major gold refining process will occur. The presence of barite in the tops of many massive sulfides indicates a high fluid SO_4^{2-}/H_2S ratio which generally corresponds with zones of gold enrichment (eg. Rosebery and Hellyer). However, the Archean massive sulfide deposits, which lack hanging wall barite, probably developed under low SO_4^{2-}/H_2S conditions (Large, 1977) which may account for the general lack of hanging wall gold concentration in these ores (eg. Scuddles). In these cases gold transported as the thio-complex would not re-precipitate at the top of the sulfide mound.

Hannington *et al.* (1986) report that high gold grades (up to 4.9 ppm Au) in Recent seafloor chimneys and sulfide mounds along the East Pacific Rise may be concentrated from early low grade copper-iron sulfides (averaging 0.2 ppm Au) by late low temperature (<250°C) solutions ascending through the mound. This process is somewhat similar to the refining process outlined above for the ancient massive sulfides. Hannington & Scott (1987) also record that for a given massive sulfide district, the average FeS content of orebody sphalerite (and therefore the fS_2 of the fluid) shows a rough correlation with the average gold grade of the deposit. For example, Recent chimney deposits with an average of less than 5 mole % FeS in sphalerite contain relatively high gold values, while deposits with more than 5 mole % FeS in ZnS contain low gold values. Such differences are considered to relate to decreasing fluid temperature and increasing fS_2 (Hannington & Scott, 1987) and will be strongly affected by variations of the SO_4^{2-}/H_2S related to mixing of the ore fluid with seawater. Further work is needed to evaluate the detailed relationship between FeS content of sphalerite and gold grade, through a particular massive sulfide lens. However, care will be needed to ensure that later metamorphic recrystallization of the sphalerites has not caused a change in their FeS content.

Based on the geologic-thermodynamic model discussed above and outlined in detail by Huston and Large (in press), the interpreted conditions and related mineralogies which favour high gold grades within massive sulfide ores are listed in Table 3. Gold-rich zinc ores are found in refined deposits which show barite ± hematite tops, carbonate gangue and low FeS content of sphalerite. Gold-rich copper ores on the other hand are found in the lower zones of deposits with pyrite ± magnetite assemblages, sericite ± kaolinite gangue and high FeS content of sphalerite.

SIGNIFICANCE FOR OTHER GOLD DEPOSITS

The premise that relatively high temperature, saline, low pH ore- fluids, transport gold principally as the chloride complex and give rise to ores with a gold-copper association, has important implications for the development of transport/deposition models for other types of gold deposits. Combining data on the likely chemistry of the major types of gold ore-fluids (Table 4) with a set of diagrams showing the stability fields for both the $AuCl_2^-$ and $Au(HS)_2^-$ complexes (Fig. 11), it is possible to speculate on a range of transport models which cover the spectrum of ore types; including epithermal Au-Ag, Archean lode Au and porphyry Cu-Au.

Epithermal deposits: Seward (1973, 1984), Henley (1984, 1985) and Cathles (1986) provide strong evidence that the moderate temperature, low salinity, high aH_2S fluids typical of geothermal and epithermal systems carry gold as the $Au(HS)_2^-$ complex. Gold chloride complexes are considered to be insignificant under these conditions. Although epithermal ore fluids typical of

adularia-sericite type deposits (Table 4) plot well within the $Au(HS)_2^-$ dominant field in figure 11, fluids associated with acid-sulfate type deposits (eg. Hayba et al., 1986; Heald et al., 1987) are of lower pH (2-4.5, kaolinite ± alunite stable) and of higher, but erratic, salinity (5-24 wt% NaCl) and plot partly within the $AuCl_2^-$ dominant field (Fig 11c). This observation is supported by the association of copper with gold in many acid-sulfate deposits (eg. Goldfield, Summitville and Red Mountain, Mosier *et al.*, 1986), indicating co-transport and deposition of gold and copper from chloride complexes, in a similar manner to that proposed for gold-copper massive sulfide ores.

Based on thermodynamic considerations of gold and silver transport Drummond & Cole (1986) and Shikazono & Shimizu (1987) suggest that the Ag/Au ratio in epithermal ores, or their contained electrum, can be used to deduce the likely gold transport mechanism. Ores with Ag/Au>1 are considered to precipitate from higher temperature AuCl bearing fluids, while ores with Ag/Au<1 are indicative of lower temperature $Au(HS)2^-$ bearing fluids. These conclusions only partly agree with our studies, in that the Cu-Au bearing acid sulfate deposits commonly display high Ag/Au ratios (eg. Summitville and El Indio) however the more typical adularia-sericite deposits show a complete range of Ag/Au ratios from 0.1 to over 100. We consider that the Cu/Au ratio is a more reliable indicator of the gold- transport mechanism, than the Ag/Au ratio

Porphyry related deposits: Fluid inclusion studies of porphyry copper-gold deposits (e.g. Nash, 1976) indicate that fluids associated with the main mineralizing event are commonly high temperature (350 to 800°C) and hypersaline (25-60 wt% NaCl). Under these conditions both gold and copper would be transported as chloride complexes (Fig. 11e), however, at temperatures above say 500°C it is possible that the neutral species $AuCl^\circ$ may become more important (eg. Wood *et al.*, 1987). The association of gold-rich porphyry deposits with magnetite-K feldspar alteration assemblages (Sillitoe, 1979) is in keeping with an increase in the solubility of AuCl associated with more oxidized (magnetite ± hematite) fluid conditions (Fig. 11a).

Archean lode deposits: The low salinity, neutral to alkaline and H_2S, CO_2 enriched fluids typical of syn-metamorphic Archean gold environments are considered to transport gold as the thio-complex (Phillips & Groves, 1983; Neal, 1987), and are seen to plot well within the $Au(HS)_2^-$ field in figure 11c, d. However fluids of this nature are probably not responsible for all Archean gold deposits. For example, deposits which show a gold-copper association, such as the Au-Cu-Ag-Mo Peal Lake Porphyry at the McIntyre Mine, Timmins Ontario (Burrows & Spooner, 1986) provide evidence for the possiblity of $AuCl_2^-$ transport from an Archean magmatic fluid of high temperature and low pH.

Proterozoic magnetite-gold-copper deposits: Recent studies of magnetite- rich gold-copper hydrothermal deposits in the Proterozoic of northern Australia, such as at Tennant Creek (Wedekind *et al.*, 1988 and Wedekind *et al.*, this volume), Starra and Trough Tank (Davidson *et al.*, this volume) suggest that these ores precipitated from high temperature (300-400°C), oxidized, high salinity (10-40 e.g. wt% NaCl) fluids. Under these conditions gold and copper were most probably transported together as chloride complexes (Fig 11e) and deposited together under conditions of decreasing temperature, decreasing fO_2 and/or increasing pH.

CONCLUSIONS

1. Volcanogenic massive sulphide deposits in Australia have variable average gold grades from 0.2 to 4.7 ppm Au, with a mean of 1.6 ppm. Two major districts, the Mt. Read Volcanics in western Tasmania and the Rockhampton district in eastern Queensland account for about 85% (ie. 394 tonnes) of the gold resource in Australian massive sulfide deposits.

2. There are two distinct spatial and mineralogical association of gold in the VMS deposits studied:
— a gold-zinc association (with lead and silver) which typically occurs throught the massive and layered ores, with gold concentrated toward the stratigraphic hanging wall of the deposit (eg. Rosebery, Hellyer, Que River, also most Kuroko Deposits and Corbett in the Noranda district).
— a gold-copper association which typically occurs in the footwall stringer and lower massive ore zones of some deposits, particularly those with a high Cu/Zn ratio (eg. Mt. Chalmers, Mt. Morgan, Scuddles, Millenbach and some stockwork Kuroko ores).

3. The two gold associations are considered to relate directly to different gold transport mechanisms. The gold-copper association reflects gold tranpsort as the $AuCl_2^-$ complex from high temperature (>300°C) low pH (<4.5) moderate to high fO_2 and high salinity fluids. The gold-zinc association reflects gold transport as the $Au(HS)_2^-$ complex from lower temperature (200-250°C), moderate pH (4.5-6) and moderate fO_2 fluids.

4. A process of gold refining, where cooling hydrothermal fluids leach gold (plus lead and zinc) from the lower parts of the sulfide lens and dump the gold (plus galena, sphalerite barite and sulfosalts) at the top of the lens associated with dropping temperature and

an increasing SO_4^{2-}/H_2S ratio is envisaged as the major process contributing to gold enrichment at the top of zinc-rich VMS deposits.

5. Other deposits which exhibit a gold-copper association, such as porphyry related gold-copper ores, acid-sulfate epithermal deposits and Proterozoic magnetite-gold deposits are considered to form by the transport and depostion of gold from chloride complexes. Gold ores which show no correlation with copper such as adularia-sericite epithermal deposits and Archean gold lode deposits are related to gold transport and deposition from thio-complexes.

ACKNOWLEDGEMENTS

We wish to thank all members of the University of Tasmania, Ore Deposit Research Team, particularly Khin Zaw, Steven Hunns, Ian Gordon, Sharon Adrichem, Garry Davidson, Richard Wedekind and John Pemberton for fruitful discussions throughout the course of this research. Financial support from the Australian Mineral Industry Research Association and the Australian

Research Grants Committee is gratefully acknowledged, and in particular those companies (Aberfoyle Resources and E.Z. West Coast Mines) who provided access to their deposits. We are particularly grateful to June Pongratz for her drafting skills and Julie Beattie for her typing skills.

REFERENCES

Barrett, T.J. and Anderson, G.M., in press. The solubility of sphalerite and galena in 1-5 m NaCl solutions to 300°C: *Geochim. Cosmochim. Acta.*

Bowers, T.S., Jackson, K.J., and Helgeson, H.C., 1984. Equilibrium activity diagrams for coexisting minerals and aqueous species at pressures and temperatures to 5 kb and 600°C: Springer-Verlag, Berlin, 397 p.

Boyle, R.W., 1979. The geochemistry of gold and its deposits: *Geol. Surv Can. Bull.* 280, 584 p.

Brathwaite, R.L., 1974. The geology and origin of the Rosebery ore deposit: *Econ. Geol.*, v. 69, p. 1086-1101.

Bryndzia, T.L., Scott, S.D., and Farr, J.E., 1983. Mineralogy, geochemistry and mineral chemistry of siliceous ore and altered footwall rocks in Uwamuki 2 and 4 Deposits, Kosaka Mine, Hokuroho District Japan, *in* Ohmoto, H. and Skinner, B.J., eds., The Kuroko and related volcanigenic massive sulfide deposits: *Econ. Geol. Mon.* 5 p.507-522.

Burrows, D.R., and Spooner, E.T.C., 1986. The McIntyre Cu-Au deposit, Timmins, Ontario, Canada: *in* Macdonald, A.J., ed., *Proceedings of Gold '86, and International Symposium on the Geology of Gold*: Toronto 1986, p.23-39.

Cathles, L.M., 1986. The geologic solubility of gold from 200-350°C, and its implications for gold-base metal ratios in vein and stratiform deposits: *in* Clark, L.A., ed., *Gold in the Western Shield*: C.I.M. Spec. Vol. 38, p.187-211.

Cole, D.R., and Drummond, S.E., 1986. The effect of transport and boiling on Ag/Au ratios in hydrothermal solutions: a preliminary assessment and implications for the formation of epithermal precious-metal ore deposits: *J. Geochem. Explor.*, v. 25, p. 45-80.

Davidson, G., Large, R.R., Cary, G., and Osborne, R., this volume. The BIF- hosted Starra and Trough Tank Au-Cu mineralization: *in* Keays et al. eds., *Bicentennial gold 88*: Econ. Geol. Monograph.

Eldridge, C.S., Barton, P.B., and Ohmoto, H., 1983. Mineral textures and their bearing on the formation of the Kuroko orebodies, *in* Ohmoto, H., and Skinner, B. J., eds., *The Kuroko and related volcanogenic massive sulfide deposits*: Econ. Geol. Mon. 5, p. 241-281.

Franklin, J.M., Lydon, J.W., and Sangster, D.F., 1981. Volcanic-associated massive sulfide deposits: *Econ. Geol. 75th Anniv. Vol.*, p. 485-627.

Franklin, J.M. and Thorpe, R.I., 1982. Comparative metallogeny of the Superior, Slave and Churchill Provinces: *in* Hutchinson, R.W., Spence, L.D., and Franklin, J.M., ed: *Precambrian Sulfide Deposits*: Geol. Assoc. Canada, Spec Paper 25, p. 3-90.

Frets, D.C., 1974. Rock relations and mineralization at Mt. Morgan: Australian Inst. Mining & Metallurgy Southern and Central Queensland Conf., 1974, Brisbane Papers, p.425-440.

Green, G.R., Solomon, M., and Walshe, J.L., 1981. The formation of the volcanic-hosted massive sulfide ore deposit at Rosebery, Tasmania: *Econ. Geol.*, v. 76, p. 304-338.

Grip, E., and Wirstam, A., 1970. The Boliden sulfide deposit: *Sver. Geol. Unders.*, Ser. C, no. 651, v. 64, no. 8, 68 p.

Groves, D.I., Phillips, G.N., Ho, S.E., Hendersbn, C.A., Clarke, M.E., and Woad, M.E. Controls on distribution of Archean hydrothermal deposits in Western Australia, *in* Foster, R. P., ed., *Gold '82: The geology and genesis of gold deposits*: Geol. Soc. Zimbabwe Spec. Pub. 1, p. 689-711.

Hannington, M.D., Peter, J.M., and Scott, S.D., 1986. Gold in seafloor polymetallic sulfide deposits: *Econ. Geol.*, v. 81, p. 1867-1883.

Hannington, M.D., and Scott, S.D., in press. Sulfidation equilibria as guides to gold mineralization in volcanogenic massive sulfides, submitted to Econ. Geol.

Hayba, D.O., Bethke, P.M., Heald, P., and Foley, N.K., 1985. Geologic, mineralogic and geochemical characteristics of volcanic-hosted eqipthermal precious-metal deposits: *in* Berger, B.R., and Bethke, P.M., ed., Geology and geochemistry of epithermal systems: *Reviews in Econ. Geol.*, V.2, p.129-168.

Heald, P., Foley, N.K., and Hayba, D.O., 1987. Comparative anatomy of volcanic-hosted epithermal deposits: acid-sulfate and adularia- sericite types: *Econ. Geol.*, v. 82, p. 1-26.

Helgeson, H.C., 1969. Thermodynamics of hydrothermal systems at elevated temperatures and pressures: *Am. Jour. Sci.*, v. 267, p. 729-804.

Henley, R.W., 1973. The solubility of gold in hydrothermal chloride solutions: *Chem. Geol.*, v. 11, p. 622-635.

Henley, R.W., 1984. Chemical structure of geothermal systems, *in* Henley, R.W., Truesdell, A.H., and Barton, P.B., eds., *Fluid-mineral equilibria in hydrothermal systems: Reviews in Econ. Geol.*, v. 1, p. 9-27.

Henley, R.W., 1985. The geothermal framework of epithermal deposits: *in* Berger, B.R. and Bethke, P.M., eds., *Geology and geochemistry of epithermal systems: Reviews in Econ. Geol.*, V.2, p.1-24.

Henley, R.W., and Brown, K.L., 1985. A practical guide to the thermodynamics of geothermal fluids and hydrothermal ore deposits, *in* Berger, B.R., and Bethke, P.M., eds., *Geology and geochemistry of epithermal systems: Reviews in Econ. Geol.*, v.2, p.25-42.

Huston, D.L., and Large, R.R., 1987. Precious metals in the Rosebery north- end orebody, Tasmania, Australia: *Proc. Pacific Rim Congress* 87, p.199- 203.

Huston, D.L., and Large, R.R., sub. to Econ. Geol. The distibution, mineralogy and geochemistry of gold and silver in the north-end orebody, Rosebery mine, Tasmania.

Huston, D.L. and Large, R.R., in press. A chemical model for the concentration of gold in volcanogenic massive sulfide deposits: Ore Geology Reviews.

Knuckey, M.J., Comba, C.D.A., and Riverin, G., 1982. Structure, metal zoning and alteration at the Millenbach deposit, Noranda, Quebec, *in* Hutchison, R.W., Spence, C.D., and Franklin, J.M., eds., *Precambrian sulfide deposits:* Geol. Ass. Can. Special Paper 25, p. 255-295.

Knuckey, M.J., and Watkins, J.J., 1982. The geology of the Corbet massive sulfide deposit, Noranda district, Quebec, Canada, *in* Hutchinson, R.W., Spence, C.D., and Franklin, J.M., eds., *Precambrian sulfide deposits:* Geol. Ass. Can. Special Paper 25, p. 296-317.

Large, R. R., 1977, Chemical evolution and zonation of massive sulfid deposits in volcanic terrains: *Econ. Geol.*, v. 72, p. 549-572.

Large, R. R., and Both, R. A., 1980, The volcanogenic sulfide ores at Mount Chalmers, Eastern Queensland: *Econ. Geol.*, v. 75, p. 992-1009.

Large, R.R., McGoldrick, P.J., Berry, R.F. and Young, C.H., in press. A tightly folded gold-rich massive sulfide deposit: Que River Mine, Tasmania: Econ. Geol.

Large, R. R., Carswell, J., Creelman, R., Huston, D. L., McArthur, G., McGoldrick, P., Purvis, G., Ramsden, T., and Wallace, D., in press, Gold in western Tasmania, in Mineral resources of Australia: *Aus. Inst. Min. Metall. Bicentennial Vol.*

Large, R.R., and Huston, D.L., 1985. The relationship of gold to base metals in some volcanogenic ore systems (abstract), in Research trends in gold exploration: *Bur. Min. Res. Aus. Record* 1985/34, p. 31-36.

McArthur, G.J., 1986. The Hellyer massive sulfide deposit, *in* Large, R.R., ed., *The Mt. Read Volcanics and associated ore deposits*: Geol. Soc. Aust., Tasmanian Division, p. 11-20.

McLeod, R.L., 1985. Preliminary observations of kaolinite in a volcanogenic massive sulfide deposit of Permian age: *Tschermaks Miner. Petrogr. Mitt.*, v. 34, p261-269.

Mosier, D.L., Menzie, W.D., and Kleinhample, F.J., 1986. Geologic and grade-tonnage information on Tertiary epithermal precious and base- metal vein distrincts associated with volcanic rocks: *U.S.G.S., Bull.* 1666 39p.

Nash, J.T., 1976, Fluid-inclusion petrology—data from porphyry copper deposits and applications to exploration: *U.S. Geol. Surv. Professional Pap.* 907-D, 16 p.

Neall, F.B., 1987. Sulphidation of iron-rich rocks as a precipitation mechanism for Large Archean gold deposits in Western Australia: thermodynamic confirmation: *in* Ho, S.E., and Groves, D.I. eds., *Recent Advances in Understanding Precambrian gold deposits:* University of Western Australia Spec. Pub. No.11, p.265-270.

Nikolaeva, N.M., Yarenburg, A.M., and Antiniva, V.A., 1972. Temperature dependence of the standard potential of halide complexes of gold: Izuest. *Sib. Otd. Akad. Nawk. S.S.S.R., Ser. Khim.*, 6:126-129 (in Russian).

Ohmoto, H., Mizukami, M., Drummond, S.E., Eldridge, C.S., Pisutha-Arnond, V., and Lenaugh, T.C., 1983. Chemical processes of Kuroko formation, *in* Ohmoto, H., and Skinner, B.J., eds., *The Kuroko and related volcanogenic massive sulfide deposits*: Econ. Geol. Mon. 5, p. 570-604.

Phillips, G.N., and Groves, D.I., 1983. The nature of Archean gold-bearing fluids as deduced from gold deposits in Western Australia: *J. Geol. Soc. Aus.*, v.30, p.25-40.

Pisutha-Arnond, V., and Ohmoto, H., 1983. Thermal history, and chemical and isotopic composition of the ore-forming fluids responsible for the Kuroko massive sulfide deposits in the Hokuroko district in Japan, *in* Ohmoto, H. and Skinner, B.J., eds., *The Kuroko and related volcanogenic massive sulfide deposits*: Econ. Geol. Mon. 5, p.523-558.

Ruaya, J.R., and Seward, T.M., 1986, The stability of chlorozinc (II) complexes in hydrothermal solutions up to 350 C: *Geochim. Cosmochim. Acta*, v. 50, p. 651-661.

Rytuba, J.J., and Dickson, F.W., 1977. Reaction of pyrite + pyrrhotie + quartz + gold with NaCl-H O solutions, 300-500°C, 500 to 1500 bars and genetic implications. *In*: Problems of Ore Deposition, 4th A.I.G.D. Symposium, Varnia, 1974, Vol.11, Bulgarian Acad. Sci., Sofia.

Ruxton, P.A., 1987. Gold-base metal relationships at Scuddles, W.A. Unpubl. University of Tasmania report to AMIRA, August, 1987, p.131-149.

Sato, T., 1973, A chloride complex model for Kuroko mineralisation: *Geochem. Jour.*, v. 7, p. 245-270.

Seward, T. M., 1973, Thio complexes of gold in hydrothermal ore solutions: *Geochimica et Cosmochimica Acta*, v. 37, p. 379-399.

Seward, T. M., 1984, The transport and deposition of gold in hydrothermal systems, in Foster, R. P., Gold '82: The geology, geochemistry and genesis of gold deposits: *Geol. Soc. of Zimbabwe Spec. Pub.* 1, p. 165- 181.

Sillitoe, R. H., 1979, Some thoughts on gold-rich porphyry copper deposits: *Mineralium Deposita*, v. 14, p. 161-174.

Shikazono, N., and Shimizu, M., 1987. The Ag/Au ratio of native gold and eletrum and the geochemical environment of gold vein deposits in Japan: *Mineralium Deposita*, V.22, p.309-314.

Shimazaki, Y., Ores of Kuroko-type deposits, *in* Ishihara, S., ed., *Geology of Kuroko deposits*: Min. Geol. Spec. Issue No. 6, p. 311-322.

Solomon, M., and Walshe, J. L., 1979, The formation of massive sulfide deposits on the sea floor: *Econ. Geol.*, v. 74, p. 797-813.

Taube, A., 1986. The Mount Morgan gold-copper mine and environment, Queensland: A volcanogenic massive sulfide deposit associated with penecontemporaneous faulting: *Econ. Geol.*, V.81, p.1322-1340.

Wedekind, R., Large, R.R., and Williams, B.T., this volume. Geological controls on high grade gold mineralization at Tennant Creek: *in* Keays, et al., eds., *Bicentennial Gold 88:* Econ. Geol. Mon.

Wedekind, R., Large, R.R., Zaw, K., Horvath, H., and Gulson, B.L., 1988. The composition and sources of ore depositing fluids in the Tennant Creek Goldfield: *in* Abstracts Vol., *Bicentennial Gold 88*, May 1988, Melbourne.

Wood, S.A., Crear, D.A., and Borcsik, M.P., 1987. Solubility of the assemblage pyrite-pyrrhotite-magnetite-sphalerite-galena-gold-stibnite-bismuthinite-argentite-molybdenite in H_2O-NaCl-CO_2 solutions from 200 to 350°C: *Econ. Geol.*, V.82, p.1864-1887.

Yamada, R., Suyama, T., and Ogushi, O., 1987, Gold-bearing siliceous ore of the Nurukawa kuroko deposit, Akita prefecture, Japan: *Mining Geology*, v. 37, p.109-118.

EXPLORATION IMPLICATIONS OF THE CHEMICAL MODEL FOR GOLD DEPOSITION IN VOLCANOGENIC MASSIVE SULFIDE SYSTEMS

David L. Huston

INTRODUCTION

Huston & Large (in press) and Large *et al.* (this volume) presented a chemical model to describe the behaviour of gold in volcanogenic massive sulfide deposits. They argued that gold has two distinct associations in these deposits: (1) copper-gold, and (2) zinc-lead-silver-gold. In the former gold was transported as a chlorocomplex at high temperatures and deposited by decreases in temperature and $f(O_2)$, or by an increase in pH. In the latter case gold was transported as a thiocomplex at lower temperature and deposited by either oxidation of reduced sulfur or coprecipitation in sulfides (predominantly pyrite and arsenopyrite) upon exhalation onto the sea floor. A third minor association is in distal pyritic mineralization in which metastable polysulfide ions that form at the sea floor by partial oxidation complex gold and transport it furthur out to form this mineralization.

At least three chemical processes are at work when gold is concentrated in these deposits. These processes operate under different conditions and in different parts of the system. Using this information, predictions of gold behaviour may be made that have implications both to exploration and ore treatment. This communication treats the results and implications of that model in a non-chemical and, hopefully, more understandable way.

SUMMARY

1. An understanding of the processes that control the transport and deposition of gold in volcanogenic massive sulfide deposits helps in defining targets within the systems that form the deposit. Chemical modelling indicates that pH and temperature are the primary controls on gold grades in these systems. Extreme pH (either alkaline (>5) or acid (<4)) in the depositing hydrothermal fluids promotes the formation of gold-rich massive sulfide deposits. Conversely, fluids of intermediate pH (4-5) will produce deposits of intermediate or low gold tenor. Temperature has a lesser affect on the potential gold grades, but it affects the likely association and possibly the metallurgical recovery of the gold. Gold-rich deposits of the copper-gold association form from higher temperature fluids (>300°C) of low pH, while gold-rich deposits of the zinc-lead-silver-gold association form from low temperature fluids (<300°C) of high pH. Conditions that may promote extreme pH's in the fluids include unusual lithologies in the footwall leaching zone or a magmatic input into the mineralising system.

2. Due to differences in the mechanism of precipitation, gold and base metals do not necessarily precipitate together. Because of this characteristic, the following environments may produce gold-rich deposits in volcanogenic systems external to the massive sulfide: (1) epigenetic mineralization near the base of the footwall leaching zone where gold complexing switches over from a chloro-complex to a thio-complex, (2) the very edges of footwall alteration zones in porous rocks where seawater in the rocks interacts with upwelling hydrothermal fluids, (3) pyritic cherts at the top or along the edges of the massive sulfide mound, and (4) exhalative cherts associated with Archean massive sulfides external to the ore forming environment.

3. Due to the chemistry of gold deposition, undeformed deposits of the copper-gold association show have better gold recoveries than undeformed deposits of the zinc-lead-silver-gold association. Different types of gold mineralization in the zinc-lead-silver-gold association may also have different gold recoveries. For instance, baritic ores near the top of the pile might have better recoveries than non-baritic ores furthur down into the pile.

IMPLICATIONS FOR EXPLORATION

An important aspect in understanding the geochemistry of gold in volcanogenic massive sulfide deposits is the concept of switchover from one complex to another. This is controlled by the following reaction:

$$AuCl_2^- + 2H_2S = Au(HS)_2^- + 2Cl^- + 2H^+ \quad ...(1)$$

The switchover occurs at conditions when $a(AuCl_2^-) = a(Au(HS)_2^-)$, and is dependant on $a(Cl^-)$, $a(H_2S)$, temperature and pH. As $a(H_2S)$ and $a(Cl^-)$ are relatively fixed in volcanogenic massive sulfide deposits, the gold switchover is largely dependant on temperature and pH. High pH and low temperature favor thiocomplexes and the zinc-lead-silver-gold association, while low pH and high temperature favor chlorocomplexes and the copper-gold association. Given these chemical constraints, one might ask the following questions.

WHY ARE SOME VOLCANOGENIC MASSIVE SULFIDE DEPOSITS SO GOLD-POOR?

Most Australian volcanogenic massive sulfide deposits have relatively low gold grades of less than 1 g/t (e.g. Balcooma, Surveyor, Thalanga, Woodlawn, Gossan Hill, Scuddles and Benambra). Canadian Precambrian deposits average 0.71 g/t (Pemberton, 1987) while most Kuroko deposits contain less than 1 g/t (Ruxton, 1986). Worldwide volcanogenic massive sulfide deposits contain much less that 1 g/t gold; deposits exceeding this grade are much less common and, consequently, represent an anomaly.

A further characteristic of most volcanogenic massive sulfide deposits is that the fluids that deposited metals were in equilibrium with either sericite or chlorite. Feldspar or kaolinite minerals are rarely present in the stockwork zones of these deposits, although they often occur in alteration external to the central stockwork zone (cf. Shirozu (1974) and Iijima (1974)). The presence of sericite or chlorite and lack of feldspar or kaolinite indicates that most volcanogenic massive sulfide deposits formed between a pH of 3.5 and a pH of 5.

A characteristic of the gold switchover is that is occurs at conditions that allow the lowest gold solubility. Our calculations (Huston & Large, in press) indicate that under conditions of volcanogenic massive sulfide formation, this switchover occurs at a pH of between 3.5 and 4.5, depending on temperature. Many volcanogenic massive sulfide deposits may have formed from fluids of this pH, so the fluids could not carry enough gold to produce high grade deposits.

THEN WHY ARE SOME DEPOSITS GOLD-RICH?

The gold grades in these deposits are controlled by pH and temperature. Low pH fluids (3.5-4) at high temperatures (> 300°C) will produce gold-rich deposits of the copper-gold association (i.e. Mt. Chalmers (2.3 g/t Au), Mt. Morgan (4.87 g/t) and Nurukawa (>15 g/t)), while higher pH fluids (5-5.5) at lower temperature (< 300°C) will produce gold-rich deposits of the zinc-lead-silver-gold association (e.g. Rosebery (2.9 g/t), Que River (3.5 g/t) and Hellyer (2.3 g/t)).

Mt. Chalmers and Nurukawa both contain kaolinite which is intimately associated with the copper-gold mineralization. At Mt. Chalmers, kaolinite is observed as a gangue in the massive sulfide lens and in the footwall alteration zone where it is associated and deposited synchronously with veinlet and disseminated chalcopyrite (McLeod, 1985). In the Nurukawa deposit kaolin minerals are present in gold-rich stockwork mineralization (Yamada *et al.*, 1987). The gangue mineralogy intimately associated with base metal mineralization indicates that the depositional fluids had an unusually low pH of between 3 and 4. Modelling by Huston & Large (in press) indicates that these conditions promote high gold solubilities as chlorocomplexes at temperatures of about 300°C.

The Rosebery, Que River and Hellyer deposits are characterized by the presence of large quantities of carbonate gangue. Rosebery also contains albite as a ubiquitous gangue in the barite lens. This suggests that these gold-rich deposits were precipitated from solutions of relatively high pH (>5) at 250°C which allows high gold solubilities as a thiocomplex.

Large (1986) suggested that gold grades increase exponentially with zinc grades in the zinc-lead-silver-gold association and cited Que River as an example. However, such a relationship is not expected from geochemical modelling; zinc solubility decreases with pH while gold solubility as a thiocomplex increases with pH. This exponential increase is not noted at Rosebery (Huston & Large, 1986) or Hellyer (MacArthur, 1986), and gold-rich, (relatively) zinc-poor deposits occur at Greens Creek, Alaska (3.2 m.t. @ 4.2% Pb, 10.8% Zn, 867 g/t Ag and 5.5 g/t Au; Bundtzen and Green, 1987) and the Westmin district of British Columbia (H-W (14 m.t. @ 0.3% Pb, 5.3% Zn, 2.2% Cu, 34 g/t Ag and 2.4 g/t Au), Lynx (0.9 m.t. @ 1.0% Pb, 7.4% Zn, 1.4% Cu, 97 g/t Ag and 2.1 g/t Au) and Myra (0.6 m.t. @ 1.5% Pb, 7.6% Zn, 0.9% Cu, 192 g/t Ag and 3.4 g/t Au)) (Hannington, 1987). In the H-W mine gold has a mineral association (pyrite-sphalerite-chalcopyrite-galena-barite) that indicates that it is of the zinc-lead-silver-copper association. The Surveyor deposit of northern Queensland is zinc-rich but gold-poor (0.5 m.t. @ 7% Pb, 20% Zn, 0.8% Cu, 150 g/t Ag and 1 g/t Au) (Noranda prospectus, 1985).

The coincidence of high gold and zinc values, which is exemplified at Que River, and present to a lesser extent at Rosebery and Hellyer, is more likely due to the coincidental occurrence of processes that deposit the metals in the same part of the deposit. Gold precipitation is caused by oxidation and sulfide precipitation whereas zinc (and lead and silver) deposition is caused by quenching of the hydrothermal fluids. Both of these processes occur at the top of the massive sulfide mound where seawater mixes with the hydrothermal fluid.

WHICH GEOLOGICAL ENVIRONMENTS PROMOTE THE FORMATION OF GOLD-RICH HYDROTHERMAL SOLUTIONS?

Low level gold analyses by Stolz & Large (this volume) indicated that the Mt. Read volcanics and surrounding lithologies do not contain unusually high background gold values, although high-Ti basalts from the Crimson Creek Formation are gold enriched. As the background Mt Read values indicate that these rocks can provide adequate gold to produce a 20 m.t. orebody at 2.5 g/t Au, an enriched source rock is not required (Stolz & Large, this volume). Rather, the chemistry of the ore forming fluids probably controlled the gold tenor of the ores.

Evidence from alteration zones, which are fluid buffered, indicates that gold-rich deposits are formed from fluids of unusually low pH in the copper-gold association or from fluids of unusually high pH in the zinc-lead-silver-gold association.

The most probable control on the pH of the fluids is the lithology of the source area for the metals. In this zone of leaching, the mineralogy of the rocks probably controlled the pH of the fluids due to a low water to rock ratio. Reed (1982) calculated that a seawater derived hydrothermal fluid at 300°C in contact with rhyolite would have a pH of 5.1; this pH would not promote high gold grades in a volcanogenic massive sulfide deposit. However, if some anomalous rock (e.g. quartzite, shale or carbonate) were present in the leaching zone, the pH may be buffered to a pH more conducive to the formation of gold-rich deposits of either copper-gold or zinc-lead-silver-gold association. This has not been addressed in the literature and deserves some investigation.

Another factor that may produce a fluid of acid pH (and a gold-rich deposit of the copper-gold association) is the presence of a magmatic component in the hydrothermal fluid. Holland (1972) found that the pH of a quenched experimental fluid in equilibrium with a granite at 800 C to be between 1.4 and 2.2. This indicates that a fluid exsohed from a magma may have a very acid pH. If magmatically derived water was introduced into a volcanogenic circulation cell, the resultant fluid may have a pH suitable for transporting gold as a chlorocomplex. The Mt. Chalmers deposit contains salinities up to 13.7 wt. % NaCl with a mean of 10.3 wt. % (Large and Both, 1980). This is significantly higher that deposits of the Kuroko district (3.6-6 wt. % NaCl; Pisutha-Arnond and Ohmoto, 1983) and seawater (3.5 wt. % NaCl). This is consistant with an introduction of additonal chloride into the system, possibly from a magmatic source. Additonal fluid inclusion and stable isotope studies on this deposit may shed some light on this hypothesis.

ARE THERE INSTANCES WHERE GOLD PRECIPITATION WOULD NOT OCCUR WITH BASE METAL PRECIPITATION?

In Proterozoic and Phanerozoic deposits, the majority of gold is expected to precipitate with base metals. More specifically, in deposits of the gold-copper association gold and copper have to precipitate concurrently. If pyrite is stable and both metals are saturated, the ratio should be constant. If pyrrhotite, magnetite or hematite was the stable iron mineral, copper and gold may still precipitate together but with a widely variable ratio.

In the zinc-lead-silver gold association, however, zinc and gold do not have to precipitate together. Because seawater was oxidizing during the Proterozoic and Phanerozoic, oxidation of the hydrothermal fluids occured and gold precipitated with zinc. However, during the Archean, seawater may have been more reduced, and the oxidation associated with seawater/ hydrothermal fluid mixing may not have occurredto the same extent (cf. Large, 1977). Consequently, in the Archean, gold and zinc may not have been deposited together — gold may not have been precipitated in the deposit at all.

ARE THERE ANY OTHER GOLD TARGETS IN THE VOLCANOGENIC ORE-FORMING SYSTEM?

Large (1987) has suggested that in the footwall leaching zone, gold may be precipitated if switchover from chlorocomplexing to thiocomplexing occurs at depth due to decreasing temperature in the upward convecting zone. This is the first conceptural exploration target: epigenetic copper-gold mineralization towards the base of the footwall leaching zone (Fig. 1).

The second target is illustrated by the precious metal zone at Que River (McGoldrick & Large, 1987). Gold enrichment in the lateral parts of the footwall alteration zone is expected in deposits of the zinc-lead-silver-gold association. At the edges of the alteration zone, the hydrothermal fluids mix with cool seawater within porous volcanics leading to oxidation only in porous volcanic footwall system in a matter analogous to the top of the massive sulfide mound, and gold precipitation must occur. Gold enrichment therefore may be common along the edges of alteration pipes or zones feeding deposits of the zinc-lead-silver-gold association.

A third target in these systems may be cherts containing colloform pyrite: distal pyrite mineralization at Rosebery and the glassy chert that caps Hellyer. Huston & Large (in press) ascribed this mineralization to the formation of gold polysulfide complexes that are later precipitated with pyrite. The formation of polysulfide ions is a kinetic process that may only occur during

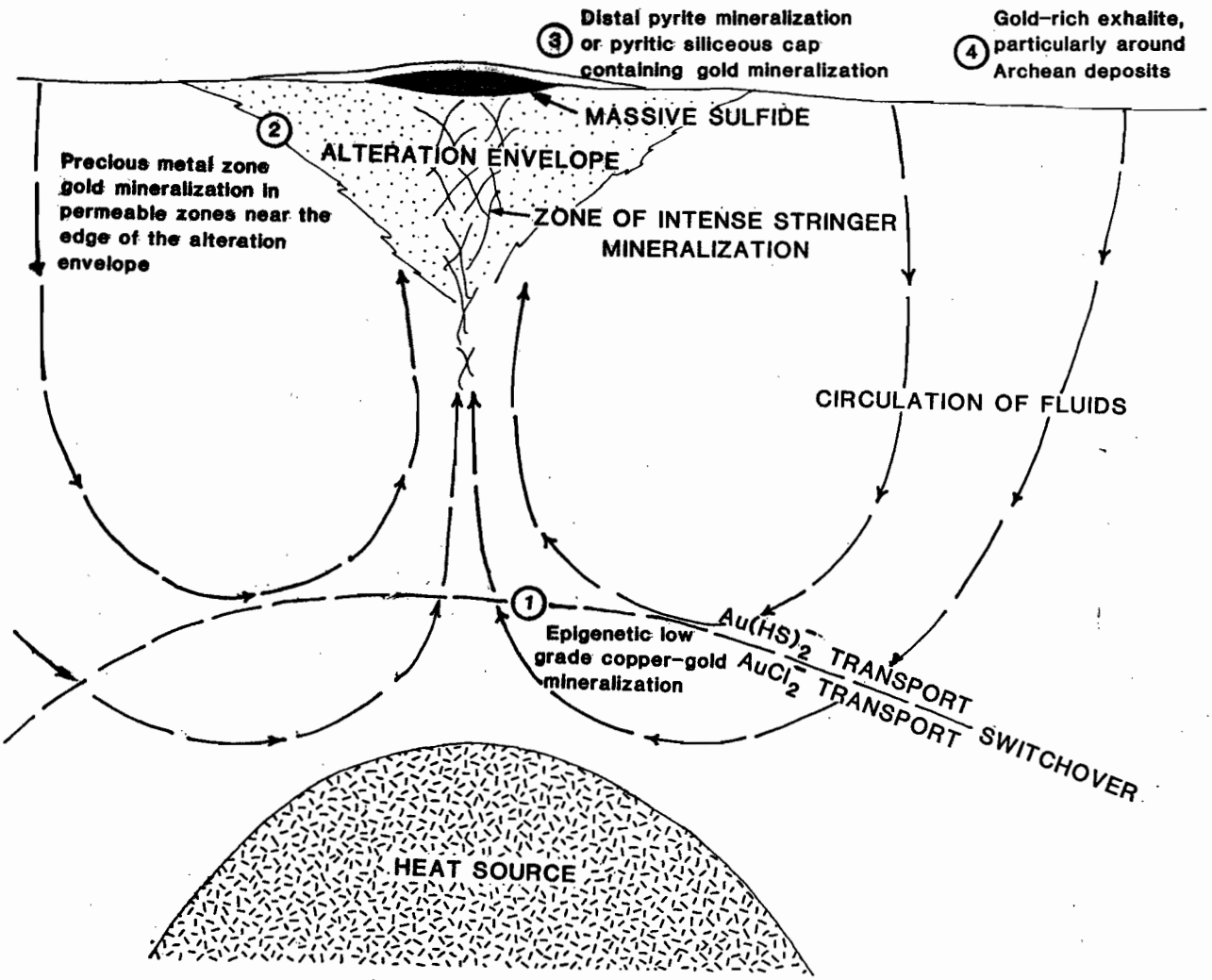

Figure 1 Possible zones of gold deposition external to the massive sulfide in volcanogenic systems.

seawater/hydrothermal fluid mixing. Therefore it will only occur close to deposits of the zinc-lead-silver-gold association.

A fourth gold target is cherts and exhalites associated with Archean deposits. If an Archean deposit was deposited from near neutral solutions, gold may have stayed in solution during zinc deposition and escaped the immediate ore forming environment. The possibility exists that this gold may be deposited later in exhalites removed from the deposit.

METALLURGICAL IMPLICATIONS

The mineral associations and textures of electrum have important ramifications for metallurgical recoveries of gold. Table 1 summarizes some implications of the gold model on gold recovery.

Table 1: Predicted gold recoveries for various ore types, volcanogenic massive sulfide deposits.

Association	Ore type	Predicted recovery
Cu-Au high	Massive pyrite-chalcopyrite	Moderate to
Zn-Pb-Ag-Au	Massive sphalerite-galena-pyrite	Low to moderate
	Barite-rich mineralization	Moderate
	Distal pyrite mineralization/silica cap	Moderate

Geochemical modelling by Huston & Large (in press) has indicated that deposits of the copper-gold association should have moderate to high recoveries while deposits of the zinc-lead-silver-gold association will have only low to moderate recoveries (Table 1). The deposition of gold and sulfide occurs independently in deposits of the copper-gold association as gold is carried as chloro-complex, so gold will be coarser grained and more free of enclosing sulfide grains. Conversely, as sulfide precipitation causes a decrease in H_2O, which in turn, causes gold to precipitate from a thio-complex, gold may coprecipitate in sulfides (predominantly pyrite and arsenopyrite) in deposits of the zinc-lead-silver-gold associotion. As a result, in sphalerite galena-pyrite ores, much or most of the gold will occur as submicroscopic grains encased in pyrite or arsenopyrite as at Rosebery, Que River and Hellyer (Huston & Large, 1986; and Large *et al.* in press).

In baritic ore, however, gold has a distinctly different metal, mineral and textural association. At Rosebery, electrum from the barite lens is associated with chalcopyrite and galena, or it may occur freely (Huston & Large, 1986). In the barite zone, gold may not have been precipitated by coprecipitation, but rather by oxidation of reduced sulfur. This process should yield free electrum and higher recoveries. Gold deposited near the the top of deposits showing the zinc-lead-silver-gold association may be more ameanable to metalurgical recovery, especially if barite is present as a gangue mineral.

The occurrence of coarser grained electrum in distal pyrite mineralization at Rosebery suggests that this type of mineralization may be more ameanable to metallurgical treatment. The pyritic cap at Hellyer may also contain coarser grained electrum.

These inferences are based solely on geological observation and geochemical modelling. They have not been tested metallurgically, and thus may only be used as a guide.

CONCLUSIONS

The gold model predicts that gold-rich volcanogenic massive sulfide deposits are deposited from high temperature (>300°C), acid (pH = 3.5 to 4) and saline fluids for the copper-gold association and low temperature (<300°C), near neutral fluids (pH = 5 to 5.5) for the zinc-lead-silver-gold association. Gold-poor volcanogenic massive sulfide deposits will be deposited from fluids of intermediate pH (4 to 5).

The lithology of the footwall leaching zone (as opposed to the footwall alteration zone) may control the pH of fluids and, consequently, the gold grades. Unusual rock units (e.g. quartzites, shales or carbonates) may produce fluid pHs that allow gold transport. The input of acidic magmatic fluids may allow the transport of gold as a chlorocomplex to form gold-rich volcanogenic massive sulfide deposits of the copper-gold association.

Archean deposits may show the zinc-lead-silver-gold association only under unusual conditions as the seawater may have been too reduced to allow gold precipitation from a thiocomplex.

Gold exploration targets in volcanogenic systems outside the deposit itself include: (1) epigenetic mineralization of the copper-gold association deep in the footwall leaching zone, (2) precious metal zone mineralization (e.g. Que River) which should occur at the lateral edge of all deposits showing the zinc-lead-silver-gold association, (3) distal pyrite mineralization and pyritic cherts around deposits of the zinc-lead-silver-gold association, and (4) exhalative cherts and other exhalites at stratigraphic horizons containing Archean deposits.

Gold in pyrite-chalcopyrite ore should be more ameanable to metallurgical treatment, but sphalerite-galena-pyrite ore should produce lower gold recoveries.

Baritic ore and distal pyrite mineralization should have better gold recoveries than sphalerite-galena-pyrite ore.

REFERENCES

Bundtzen, T.K., and Green, C.B., 1987, Exploration 1986: Alaska: Mining Engineering, v. 39, p. 328-329.

Hannington, M.D., 1987, Physical and chemical controls on the occurrence and distribution of gold in volcanogenic massive sulfide deposits: modern and ancient: Unpub. Ph.D. proposal, University of Toronto, 69 p.

Holland, H.D., 1972, Granites, solutions, and base metal deposits: *Econ. Geol.*, v. 67, p. 281-301.

Huston, D.L., and Large, R.R., 1986, The distribution, mineralogy and geochemistry of precious metals in the north-end orebody, Rosebery mine, Tasmania: Unpub. report, University of Tasmania, 132 p.

Huston, D.L., and Large, R.R., in press, A chemical model for the concentration of gold in volcanogenic massive sulphide deposits: *Ore Geology Reviews.*

Iijima, A., 1974, Clay and zeolitic alteration zones surrounding Kuroko deposits in the Hokuroko distict, Northern Akita, as submarine hydrothermal-diagenetic alteration products, *in* Ishihara, S., ed., Geology of kuroko deposits: *Mining Geology Special Issue 6*, p. 267-290.

Large, R.R., 1977, Chemical evolution and zonation of massive sulfide deposits in volcanic terrains: *Econ. Geol.*, v. 72, p. 549-572.

Large, R.R., 1987, Source and movement of gold in submarine volcanic environments–a discussion paper, *in* Controls on gold and silver grades in volcanogenic sulphide deposits (84/P210): Unpub. AMIRA report, University of Tasmania, p. 169-181.

Large, R.R., and Both, R.A., 1980, The volcanogenic sulfide ores at Mount Chalmers, eastern Queensland: *Econ. Geol.*, v. 75, p. 992-1009.

Large, R. R., Huston, D. L., McGoldrick, P.J., Ruxton, P. A. and McArthur, G., 1988. Gold distribution and genesis in Australian volcanogenic massive sulphide deposits, and significance for gold transport models. This volume.

McArthur, G.J., 1986, The Hellyer massive sulphide deposit (abstract), *in* Large, R.R., ed., The Mt. Read volcanics and associated ore deposits: Geol. Soc. Aus., Tasmanian Division, p. 11-20.

McGoldrick, P., and Large, R.R., 1987, Final report on the footwall precious metal zone, Que River, *in* Controls on gold ans silver grades in volcanogenic sulphide deposits (84/P210): Unpub. AMIRA report, University of Tasmania, p.9-41.

McLeod, R.L., 1985, Preliminary observations of kaolinite in a volcanogenic massive sulphide deposit of Permian age: *Tschermaks Miner. Petrogr. Mitt.*, v. 34, p. 261-269.

Pemberton, J., 1987, World data base, part 2–the Canadian Precambrian deposits (with emphasis on precious metal distribution): Unpub. AMIRA report, University of Tasmania, 58 p.

Pisutha-Arnmond, V., and Ohmoto, H., 1983, Thermal history, and chemical and isotopic composition of the ore-forming fluids responsible for the kuroko massive sulfide deposits in the Hokuroko district in Japan, *in* Ohmoto, H. and Skinner, B.J., eds., The kuroko and related volcanogenic massive sulfide deposts: *Econ. Geol. Mon. 5*, p. 523-558.

Reed, M.H., 19 . Calculation of multicomponent chemical equilibria and reaction processes in systems involving minerals, gases and an aqueous phase: *Geochim. Cosmochim. Acta,* v. 46, p. 513-528.

Ruxton, P., 1986, World data base, part 1–the kuroko deposits: Unpub. AMIRA report, University of Tasmania, 27 p.

Shirozu, H., 1974, Clay minerals in alterd wall rocks of the Kuroko-type deposits, *in* Ishihara, S., ed., Geology of kuroko deposits: *Mining Geology Special Issue 6*, p. 303-310.

Stolz, A.J., and Large, R.R., this volume, The source of gold in the western Tasmanian volcanogenic massive sulphide deposits.

Yamada, R., Suyama, T., and Ogushi, O., 1987, Gold-bearing siliceous ore of the Nurukawa kuroko deposit, Akita prefecture, Japan: *Mining Geology*, v. 37, p. 109-118 (in Japanese).

EXPLORATION MODELS FOR GOLD-BEARING DEPOSITS IN THE MOUNT READ VOLCANICS

Ross R. Large

INTRODUCTION

The ultimate objective of this three year research program has been to determine the geological and geochemical parameters which control the concentration of precious metals in volcanogenic sulphide deposits and to apply these parameters to the development of exploration models which can be used in the search for new gold-base metal ores in Australia.

In this paper five exploration models for gold-bearing volcanogenic deposits are presented. The models are based principally on our detailed research in the Mount Read Volcanics, but also incorporate important evidence from the Queensland massive sulphide deposits (Mt. Chalmers, Balcooma) and the Archean deposits (Scuddles and Teutonic Bore), that have formed part of this study.

SUMMARY AND CONCLUSIONS

1. Five distinct styles of gold mineralisation have been defined within submarine volcanic settings such as the Mt. Read Volcanics (MRV).
- sea floor Zn-Au (Pb-Ag-Cu-Ba) polymetallic massive sulphides
- sea floor Cu-Au massive sulphides and associated stockworks
- footwall Au-base metal-adularia veins and disseminated stockwork systems
- deep level Cu-Au-pyrite-chlorite disseminated and stockwork zones
- magnetite-hematite-pyrite ± Cu ± Au vein and replacement systems associated with granitic intrusives.

2. The sea floor massive sulphides represent the best exploration target for high grade gold and base metal mineralisation.

3. Zinc-barite-rich massive sulphide deposits (eg. Rosebery, Que River, Hellyer) have mean gold grades of 2-4 g/t with the best grades concentrated toward the stratigraphic hangingwall of the deposit.

4. Copper-rich massive sulphides (eg. Mt. Chalmers) exhibit a concentration of gold (with copper) in the footwall stringer zone and lower massive sulphide ore.

5. Gold-base metal-adularia mineralisation has been recognised in the footwall stringer system of the Que River deposit. This style of mineralisation may represent a submarine version of an epithermal stockwork feeding a seafloor massive sulphide.

6. The key factors contributing to the gold-lead-zinc rich nature of deposits in the Mt. Read Volcanics are considered to be:
- *Tectonic Environment* - the Central Volcanic Complex (CVC) has developed as a series of coalescing volcanic centres along a narrow rift structure. High heat flow associated with rifting created long-lived convective hydrothermal systems.
- *Source Rocks* - the Cambrian volcanics represent an adequate source for gold and base metals. Anomalously high gold values in the Crimson Creek high-Ti basalts (stratigraphically below the CVC) may have been a significant factor.
- *Chemistry of fluids* - the hydrothermal fluids were buffered by the volcanics to allow maximum transport of gold and base metal complexes. Switchover of gold transport from $AuCl_2$ to $Au(HS)_2$ within the developing sulphide mounds provided a mechanism for gold-zinc refining and upgrading of the outer and upper zones of the orebodies.

7. Many of the volcanic centres in the CVC show a bimodal suite with mineralisation concentrated at the contact between one suite and the other (eg. rhyolite-dacite, andesite-dacite or andesite-basalt contacts).

8. The Tyndall Group represents a graben fill sequence of epiclastics and volcanics overlying the CVC. Significant mineralisation (eg. Henty Prospect) is concentrated along the unconformable or faulted contact between the Tyndall Group and the CVC.

9. Lead isotope data suggests that the major episodes of massive sulphide mineralisation show an age progression from south to north along the belt. Both the geological and lead isotope data suggest a series of cycles of volcanism and mineralisation during the rifting and volcanic development of the MRV.

10. Intrusion of Cambrian granites and granitic porphyries along the eastern margin of the Mount Read Volcanics was probably the final phase of magmatic activity in the Cambrian. A complex series of alteration zones are related to the granitic intrusives (pink K-feldspar-hematite → chlorite-magnetite → pyrite-sericite) which are outlined by a semi-continuous belt of magnetic anomalies extending from Mt. Darwin to the Murchison Gorge. Minor Au-Cu prospects are located within some of the magnetic zones.

11. Folding and shearing of the massive sulphide ores in the Devonian has played an important role in increasing the grainsize of free gold and electrum leading to improved metallurgical recoveries. Relatively coarse and easily liberated gold is associated with the soft annealed sulphides such as galena, chalcopyrite, tetrahedrite and to a lesser extent sphalerite, while fine grained gold (which is difficult to liberate) is confined to the hard sulphides pyrite and arsenopyrite. The little-deformed, arsenic-rich ores at Hellyer contain very fine gold which presents a major metallurgical challenge.

12. Post-deformation, Late Devonian gold mineralisation associated with granite emplacement is confined along the Henty Fault and other major faults. Several styles of mineralisation have been reported along the Henty Fault Zone in the Sterling Valley and at the Henty Prospect. Evidence to date suggests the possibility of an early phase of Cambrian mineralisation was focused along the fault (when it acted as one of the major rift faults) followed by a later overprint of Devonian mineralisation related to granite intrusion.

13. The exploration models presented here for gold-bearing VMS deposits in the Mount Read Volcanics are applicable for massive sulphide exploration in all post-Archean volcanic terranes.

It will be argued in this paper that the tectonic setting, volcanic chemistry, hydrothermal processes, and types of ore bodies are not unique to the Mt. Read Volcanics. However a number of coincident geological events have occurred in the MRV which contribute to the exceptional quality of the orebodies in this region.

TECTONIC ENVIRONMENT OF THE MRV

The AMIRA supported study by Tony Crawford (see Crawford 1986 and 1987) on the chemistry of the Mt. Read Volcanics indicates that the Central Volcanic Complex is a high-K calc-alkaline orogenic andesite-dacite-rhyolite suite similar to other orogenic volcanic suites erupted through fairly thick continental crust along continental margins in North and South America.

Currently there is widespread disagreement regarding the tectonic development of the Cambrian Dundas Trough and the MRV (e.g. Corbett and Lees, 1987; Varne and Foden, 1987; Crawford and Berry, 1988). At the recent G.S.A. Symposium on the tectonics of Western Tasmania (Turner, 1988) at least six different models were proposed for the origin of the Cambrian volcanic sequences. However, most workers generally consider that some combination of subduction and rifting are the two important elements. Continental rifting in the Early Cambrian most probably produced the flood tholeiites of the Crimson Creek Formation, and later subduction-related rifting gave rise to the MRV.

The major lines of evidence for rifting during the development of the MRV are:

1. The narrow elongate nature of the volcanic belt; a Central Volcanic Complex is flanked by a marginal volcano-sedimentary Western Sequence on the western side, and an epiclastic dominated sequence (Tyndall Group) on the eastern side.

2. A series of major longitudinal faults (eg. the Great Lyell Fault, Henty Fault, Rosebery Fault, Copper Creek Fault) may represent the original rift faults. However, many of these faults show later transcurrent and thrust movement related to later phases of deformation from the Late Cambrian to Late Devonian (Berry, in press).

3. The basalt dyke swarm along the north side of the Henty Fault is chemically similar to basalts associated with rifting in recent arc settings (Crawford, 1987).

4. The Tyndall Group and overlying Owen Conglomerate are confined to narrow elongate basins between the major longitudinal faults (GLF and HFZ) and the Precambrian margin. These younger sequences are probably filling graben structures related to the final phases of rifting and uplift along the margin of the Precambrian block.

5. The narrow elongate Cambrian granites (Murchison and Darwin granites) and associated granitic porphyries have intruded along the eastern side of the MRV for its whole length from Elliott Bay to Black Bluff, and

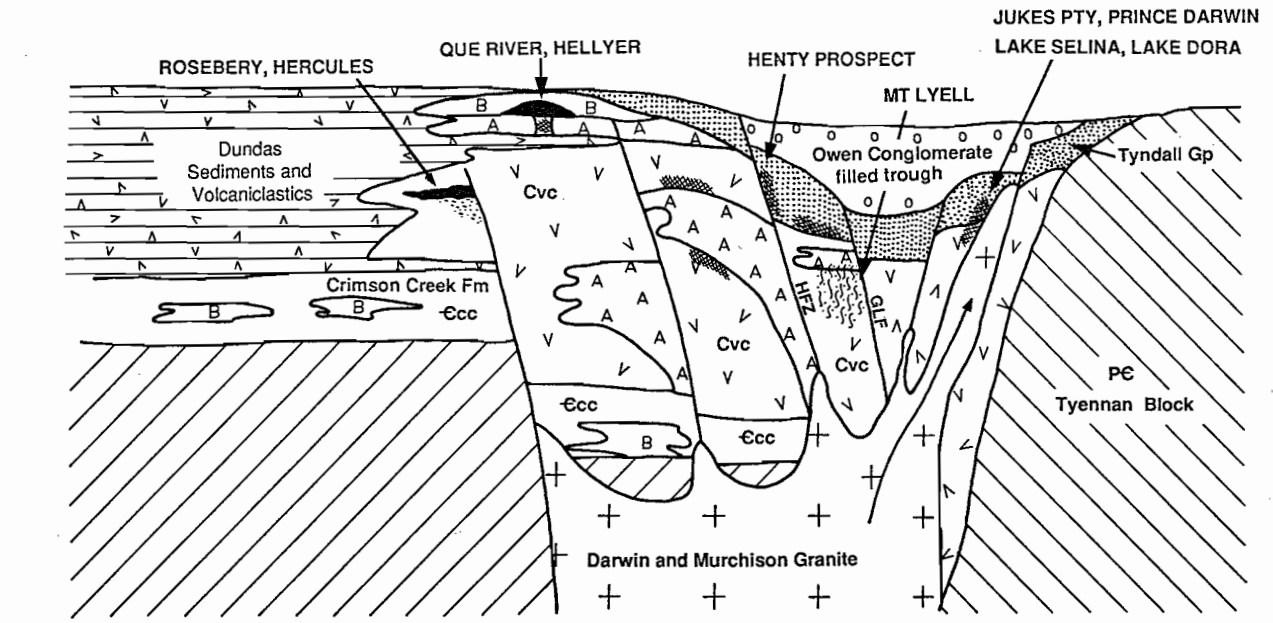

Figure 1 The rift model for the MRV: diagrammatic cross section (early Ordovician) showing the interpreted setting of the major mineral deposits (modified from Large et al., 1987).

probably represent a late stage (post Tyndall Group) magmatic event confined to the eastern marginal faults of the rift.

6. Gravity and magnetic studies by Leaman (1986a, 1988) indicate that the subsurface rock distribution in western Tasmania is best interpreted by a rift model involving 50 to 60 km of extension during the Cambrian.

Rifting during the formation of the MRV is considered to be a key element leading to the formation of the massive sulphide ores (fig. 1). Cathles (1985) points out that rift environments generate far greater heat flow than other tectonic settings. Such high heat flow is important in the movement of large qualities of hydrothermal fluid and the leaching of metals from vast volumes of rock. These processes are critical in the development of large and high grade massive sulphide ore deposits.

CENTRES IN THE CENTRAL VOLCANIC COMPLEX

The Mount Read Volcanics are made up of a series of overlapping volcanic centres aligned north-south along the belt (fig. 2). Using a combination of the recent mapping by the Mines Department (Corbett & McNeil, 1988) and whole rock/REE analyses from this AMIRA project it is possible to loosely define the major centres as follows.

	Postulated Volcanic Centres	Volcanic Suite
1	Que-Hellyer	dacite-andesite-basalt
2	Mt. Block	rhyolite-(?)
3	Pinnacles-Chester	rhyolite-andesite
4	Tullah	andesite-rhyolite
5	Rosebery-Hercules	rhyolite-dacite
6	Henty-Tyndal	andesite-rhyolite
7	Mt. Lyell	andesite-rhyolite
8	Lynchford	basalt-andesite
9	Jukes-Darwin	rhyolite

Most of the volcanic centres, and especially those associated with major ore deposits show a bimodal volcanic suite (fig. 3 and Large *et al.*, 1986). The volcanic centres are composed dominantly of massive lavas and pyroclastics. The orebodies commonly occur at the contact between volcanic suites (eg. dacite-andesite at Que River, basalt-andesite at Hellyer, rhyolite-andesite at Mt. Lyell). It appears that a change in the composition of the erupting volcanoes may accompany the period of hydrothermal circulation and ore formation. The orebodies are typically hosted by epiclastics or sedimentary horizons between the major volcanic episodes.

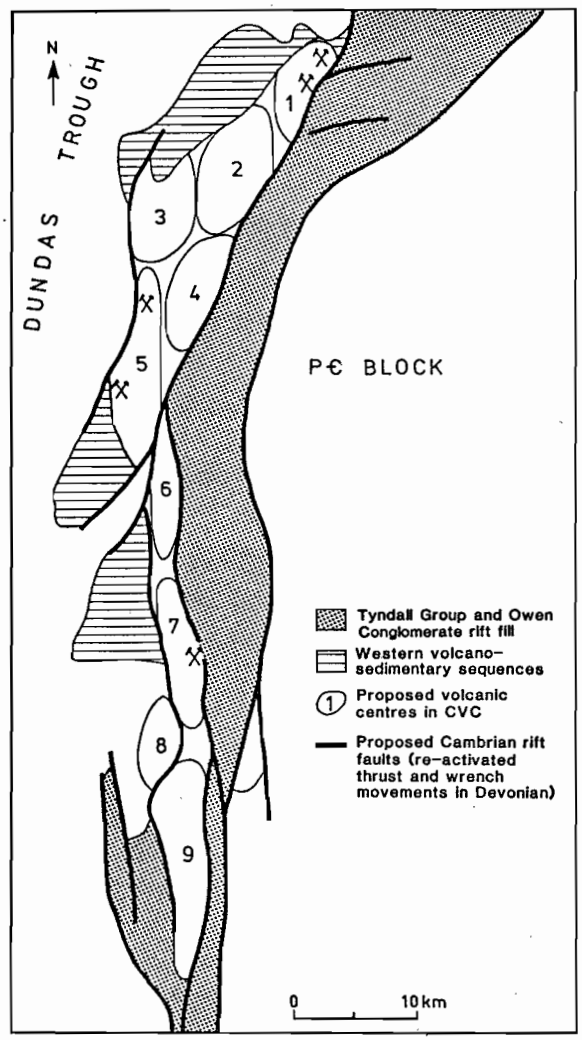

Figure 2 Postulated volcanic centres and major rift faults in the Mount Read Volcanics. 1 = Que-Hellyer, 2 = Mt. Block, 3 = Chester-Pinnacles, 4 = Tullah, 5 = Rosebery-Hercules, 6 = Henty-Tyndall, 7 = Mt. Lyell, 8 = Lynchford, 9 = Jukes-Darwin Complex.

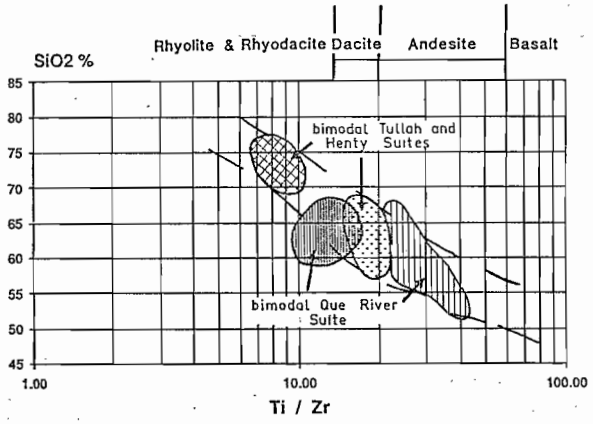

Figure 3 Ti/Zr vs SiO_2 diagram showing the bimodal volcanic suites from Que River (dacite and andesite) and Tullah and Henty-Tyndall centres (rhyolite and hb-andesite).

Crawford (1988) points out that bimodal lava suites similar to that Que-Hellyer centre are typical of large caldera complexes in recent arcs, and that there may be a relation between the caldera forming event and mineralisation at Que River and Hellyer. Green et al. (1981) previously suggested the possibility of a caldera collapse event preceding mineralisation at Rosebery and Hercules and this was more recently supported by Lees (1987).

In summary the development of volcanic centres erupting a bimodal suite of high-K calcalkaline volcanics along the centre of a major rift structure, are the critical elements of the volcanic environment hosting the VMS deposits in the MRV. The ores typically occur within an epiclastic horizon at the contact of the bimodal volcanic suite or in a mixed zone containing the suite.

Corbett and Lees (1987) suggest that the Henty Fault may separate two different arc sequences (northern arc and southern arc) which were originally quite separate and later juxtaposed by movements on the fault. However, the primary chemistry of the CVC north and south of the Henty Fault is very similar, in fact identical. In addition Crawford (1987) showed that the chemistry and REE pattern of hornblende andesites south of the fault in the Henty-Tyndal and Lyell areas are very similar to those of the andesites of the Que River sequence. Corbett (1986) indicated that an additional difference between the southern and northern CVC's is the fact that pink K-feldspar rich rhyolites and granite are confined to the southern CVC. However, the high K_2O nature of southern CVC rhyolites has been clearly shown to be due to alteration associated with Cambrian granite intrusion and porphyry-Cu style mineralisation (Hunns 1986, 1987) and therefore **is not** a primary volcanic feature of the southern lavas.

TYNDALL GROUP

The Tyndall Group is a rift fill sequence dominated by epiclastics and pyroclastics with minor lavas and intrusives which are compositionally identical to the central volcanic complex. The Comstock Tuff, which forms the base of the Tyndall Group in the Lyell and Henty-Tyndal areas, unconformably overlies the CVC. The contact between the Tyndall Group and the CVC appears to be an important locus for mineralisation. For example, base metal and gold-silver mineralisation is located close this contact at Howards Anomaly, the Tyndall prospect and the Henty Au prospect (fig. 4).

VARIATION IN AGE OF MAJOR MINERALISATION IN THE MRV

Lead isotope studies by Gulson, Large & Porritt (1987) indicate the possibility that the massive sulphide deposits may become progressively younger passing

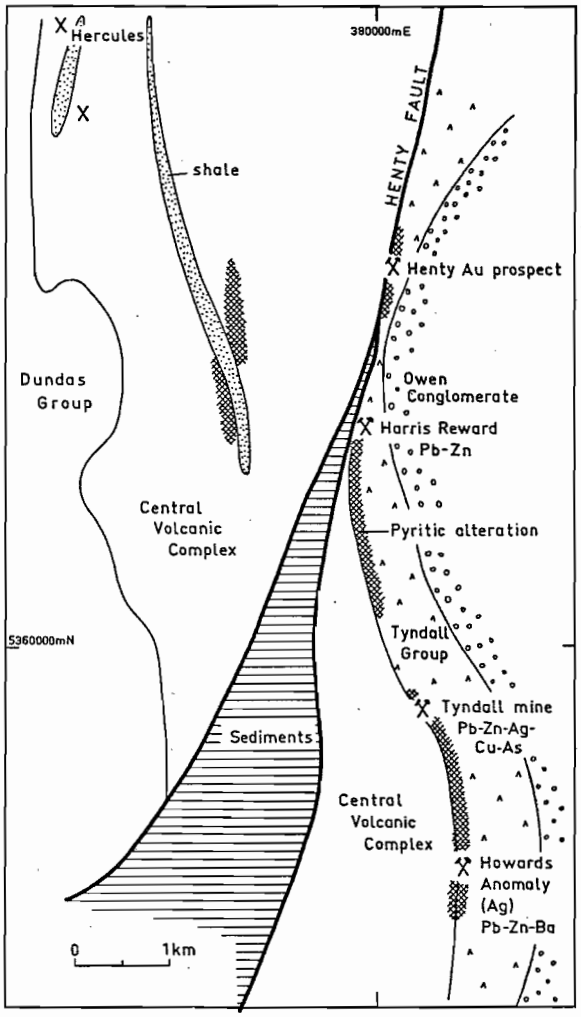

Figure 4 Relationship of pyrite alteration and mineral prospects to the contact of the Tyndall Group and the Central Volcanic Complex in the Henty-Tyndall area.

north along the volcanic belt. The small massive sulphide lenses at Voyager 19 Elliott Bay (Large et al., 1987) have the least radiogenic lead (206/204 = 18.10) whilst the Rosebery deposits are next (206/204 = 18.27) and the Que River and Hellyer deposits have the most radiogenic lead (206/204 = 18.34). As shown in figure 5, these data may be interpreted to indicate that the Elliott Bay VMS formed in the Middle Cambrian while the Que River-Hellyer ores formed in the Late Cambrian. Rifting, volcanism, and ore formation may have therefore commenced originally at the southern end of the MRV. Volcanic centres may have developed progressively northward along the propagation of the rift through the Middle to Late Cambrian. The time span of 110 myrs seems excessive for the development of the volcanic rift, suggesting that the lead isotope data may only be interpreted in relative rather than absolute terms. Certainly, more lead isotope work needs to be carried out to test this hypothesis. However, whatever the outcome, conclusive evidence is available in the geology to indicate that there were a series of massive sulphide forming events rather than just one event, during the buildup of the MRV. In other words, the crucial conditions that led to the formation of the high grade massive sulphide ores were repeated several times through the history of the MRV. For this reason no volcanic stratigraphy in the MRV can be totally excluded from exploration — although some volcanic centres can be considered to have more potential than others.

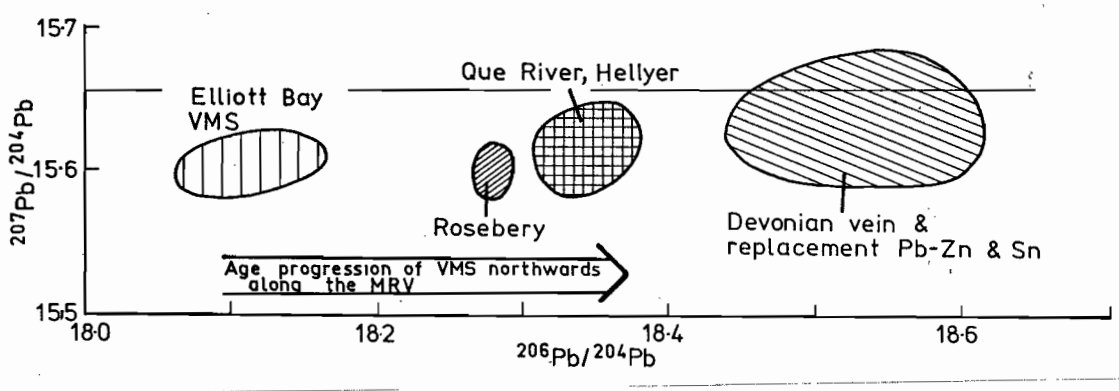

Figure 5 Lead isotope plot of Mt. Read VMS deposits indicating a progression in $^{206}Pb/^{204}Pb$ values passing northwards along the belt. This change may relate to a northward development of the rift and related mineralising process.

CAMBRIAN GRANITES AND MINERALISATION

Cambrian granites and related granitic porphyries extend along the eastern margin of the MRV intruding into the CVC and the Tyndall Group. A series of overlapping alteration zones extend outwards from the granites into the volcanic pile. Work by Steven Hunns (1986, 1987) in the Lake Selina area showed the following zonation:

1) Pink K-feldspar alteration within the granite and the adjacent porphyries and volcanics.
2) Chlorite-rich alteration, commonly accompanied by magnetite over-printing the K-feldspar and extending further from the granites.
3) Sericite-pyrite ± magnetite alteration overprinting the early K-feldspar and chlorite phases and forming extensive linear halo zones possibly parallel to the granite or porphyry contacts.

Minor copper mineralisation (0.1-0.2% Cu) and rare anomalous molybdenum are associated with the chlorite-magnetite alteration. Hunns compared the alteration and mineralisation to a very low-grade porphyry copper system.

Similar alteration zones with magnetite-cpy-py mineralisation extend from the halo of the Darwin Granite, along the Jukes-Darwin ridge to Lake Dora, Lake Selina and into the Murchison Gorge. Although Polya *et al.* (1986b) and Eastoe *et al.* (1987) considered these alteration zones to be the roots to the massive sulphide alteration systems, this AMIRA research has conclusively demonstrated that the K-feldspar-chlorite-magnetite mineralisation is much later than the VMS's and post dates the Tyndall Group. At Lake Selina the pyrite-magnetite zone is devoid of gold, but in a similar alteration system at Jukes Pty. significant Cu-Au grades occur in quartz stockworks penetrating a zone of intense K-feldspar–hematite–chlorite alteration. Further research is required to evaluate the gold potential of these magnetic K-feldspar-chlorite alteration systems.

BROAD MAGNETITE FEATURES IN THE MRV

The 1981-1982 Mines Department aeromagnetic data has revealed some important features concerning the structure and mineralisation in the MRV and the Dundas Trough (see figs. 6, 7). Some of the relevant points are listed below:

- The major polymetallic massive sulphide ores are non-magnetic, although Mt. Lyell has a weak magnetic response.
- The footwall alteration zones represent areas of anomalously low magnetics (Leaman 1986b).
- The rhyolite and dacite volcanics in the CVC are generally non-magnetic. Hornblende andesite lava breccias and intrusives south of the Henty Fault around the Henty-Tyndall volcanic centre and the Mt. Lyell volcanic centre are weakly magnetic. However, the andesites and basalts in the Que-Hellyer volcanic centre are virtually non-magnetic.
- The zone of intense magnetic anomalies extending along the eastern side of the MRV from Mt. Darwin to the Murchison Gorge is related to magnetite-chlorite ± pyrite mineralisation over-printing pink K-feldspar alteration associated with intrusion of Cambrian granites into the CVC and the Tyndall Group (fig. 7).
- A broad regional magnetic low occurs west of the Henty Fault over andesite-rhyolite volcanics in the Tullah area. The significance of this feature is not certain. It may relate to shallow intrusion of the Devonian Granite orto a broad zone of Cambrian hydrothermal alteration.

EXPLORATION MODELS

The five types of gold-bearing volcanogenic mineralisation defined during the research program are:

1) Zn-Au (Pb-Ag-Cu-Ba) polymetallic massive sulphides.
2) Cu-Au massive sulphides.
3) Au-base metal-adularia vein and disseminated stockwork systems.
4) Cu-Au-pyrite-chlorite deep level disseminated and stockwork systems.
5) Magnetite-hematite-pyrite ± Cu ± Au vein systems.

The critical features of the exploration model for each of these types are given in figures 8 to 12. These models do not only apply to the MRV but are based on our studies of many VMS deposits; including those in Queensland, Western Australia (Ruxton, 1986, 1987), Japan (Ruxton 1986) and Canada (Pemberton, 1987).

Why are the Tasmanian Polymetallic Ores Rich in Gold?

The high gold values of the Tasmanian VMS deposits are not unique. Some zinc-rich Kuroko ores also contain comparable grades (Ruxton, 1986) as do a few of the Canadian deposits (Pemberton, 1987). However, the key elements that have combined to generate the rich Tasmanian deposits are considered to be:

1) Favourable tectonic environment - rift related volcanic centres allow high heat flow creating long lived high temperature convection systems. A deep submarine environment was generated by continued rifting and possible caldera development.
2) An adequate metal supply of Au, Ag, Pb, Zn, Fe, S within the volcanic pile available for leaching by the

Figure 6: Magnetics image of Western Tasmania (courtesy of Carpentaria Exploration Company). ➟

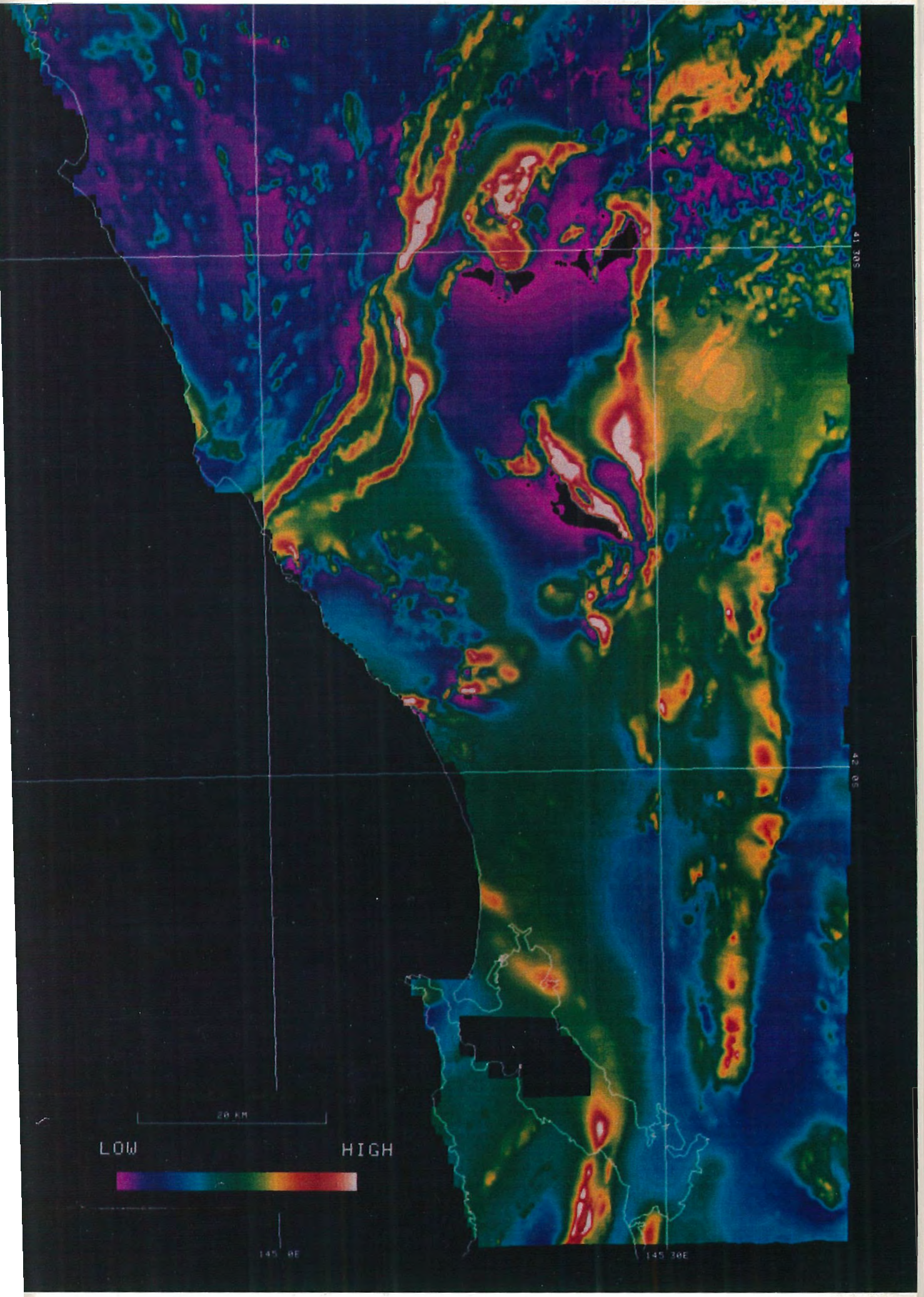
41 30S
42 0S
20 KM
LOW
HIGH
145 0E
145 30E

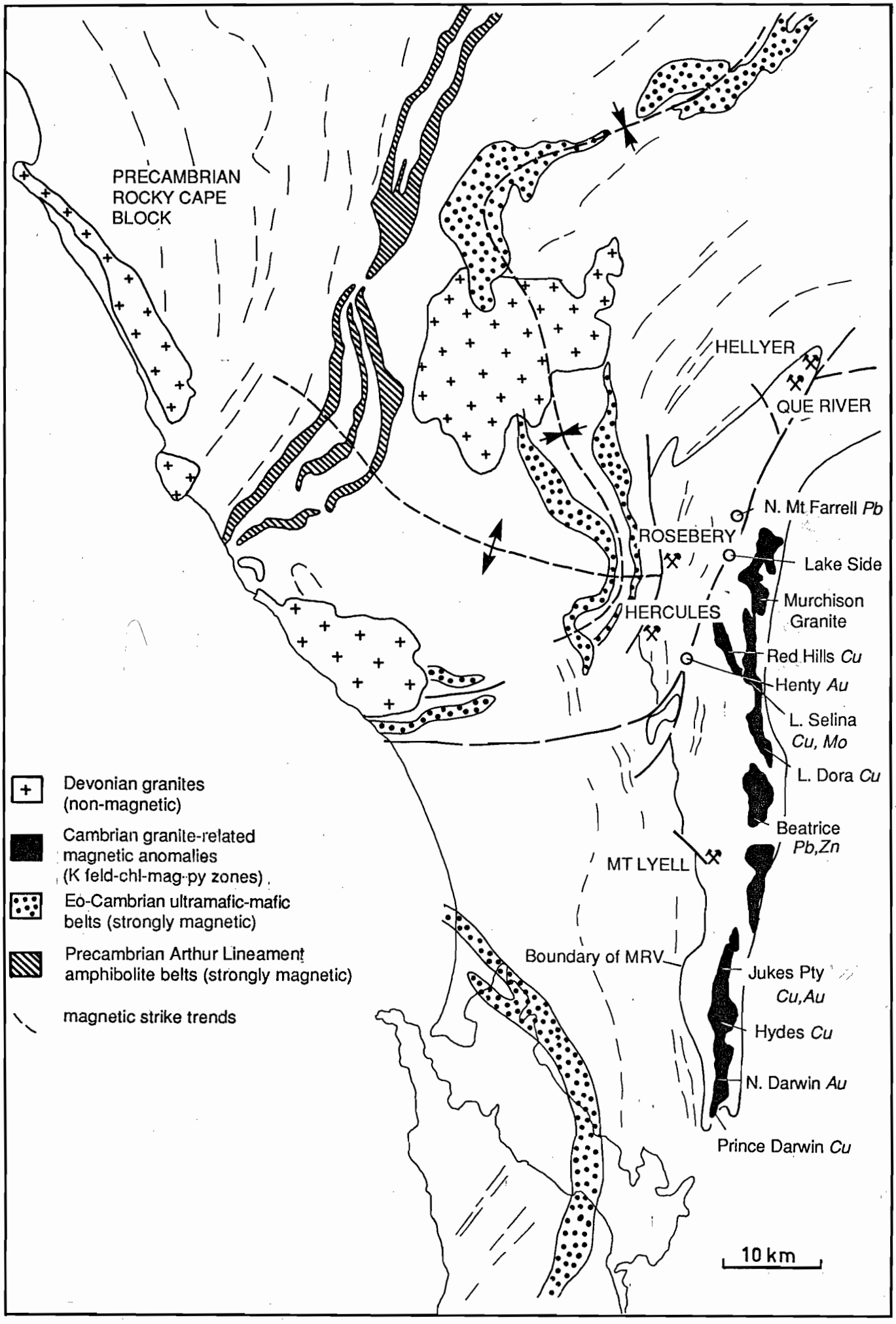

Figure 7 *Interpretation of magnetic image shown in figure 6.*

MODEL 1: Zn-Au-(Pb-Ag-Ba) polymetallic VMS

TARGET

- high priority
- typical grades 15% Zn, 3 g/t Au, 8% Pb, 160 g/t Ag, 0.4% Cu
- typical tonnage 2-20 mt
- examples — Rosebery, Que River, Hellyer (Tas.)

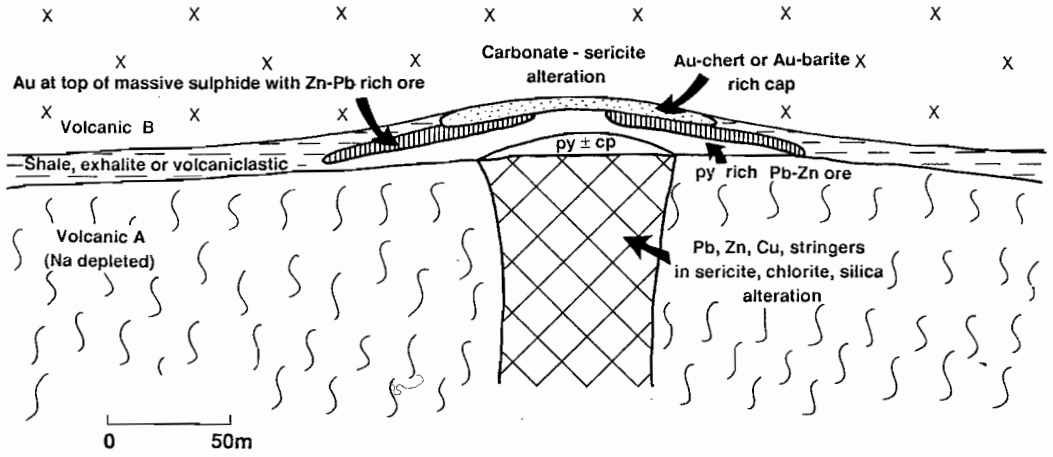

GEOPHYSICAL PARAMETERS

- non-magnetic
- moderate to poor conductor depending on cpy, py content
- high density contrast

GEOCHEMICAL PARAMETERS

- zoning from FW to HW : Fe → Cu → Pb, Zn, Ag, Au → Ba
- higher silver 100-300 g/t
- good Ba-Zn-Au correlation
- zinc ratio 60 to 80
- variable As (250 ppm - 5% in gold ores)

ENVIRONMENT

- Proterozoic to Recent calc-alkaline volcanic piles
- continental margin setting with eruption through thick continental crust
- subduction related tectonics but with VMS within local rift structures
- compositional variation from rhyolite-andesite basalt
- deep submarine volcanic setting in the rift
- target ores are distal from the hydrothermal heat engine, usually within upper-most or lateral primary volcanic stratigraphy
- underlain by massive pyroclastics or lavas

ORE FLUID CONDITIONS

- moderate temperature 200-250°C
- neutral to alkaline pH 5-6
- variable fO_2 reaching high values at top of ore (pyrite field)
- long-term hydrothermal system promotes mound refining
- moderate salinity <4 wt%
- moderate to high aH_2S
- switchover from $AuCl_2$ to $Au(HS)_2$ at base of sulphide mound

CAUSE OF GOLD DEPOSITION

- increasing SO_4/H_2S ratio as fluid moves to top of mound
- dropping temperature

Figure 9

MODEL 2: Cu-Au-rich VMS

TARGET

- high priority
- typical grades. 2-5 g/t Au, 1-2% Cu
- typical tonnage 3-50 mt
- Examples Mt Chalmers (Qld), Mt Morgan (Qld)

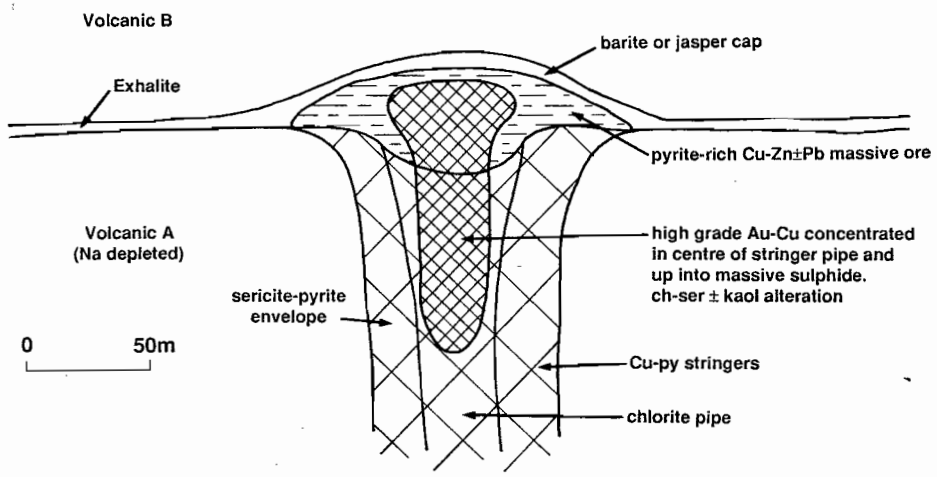

GEOPHYSICAL PARAMETERS

- commonly non-magnetic but magnetite or pyrrhotite zones within the stringer may cause a weak magnetic signature
- strongly conductive due to high cpy and py and low sp, gal content

GEOCHEMICAL PARAMETERS

- zoning from FW to HW of Fe → Cu Au → Pb, Zn → Ba
- low silver 5-50 g/t
- good Cu~Au correlation.
- low As, Sb, Hg.
- anomalous Bi, Se, Te.

ENVIRONMENT

- Proterozoic to Recent calc alkaline volcanic piles
- usually rift setting
- felsic volcanics predominate over mafic (Cu-rich VMS in mafic piles are commonly gold-poor)
- proximal to hydrothermal heat engine
- shallow to moderate depth submarine volcanic setting
- lower in volcanic stratigraphy than model 1
- underlain by massive lavas

ORE FLUID CONDITIONS

- high T; ≥ 300°C
- low pH — 2 to 4.5
- moderate to high fO_2 (po → py barite)
- $AuCl_2$ transport.

CAUSE OF GOLD DEPOSITION

- dropping T
- increasing pH

References: Large & Both (1980), Huston & Large (1987), Large *et al.* (this volume)

Figure 10

MODEL 3: Gold-base metal-adularia vein and disseminated stockwork zones

TARGET

- moderate priority
- typical grades - 0.5-4 g/t Au, 10-300 g/t Ag, 5% Pb+Zn, <0.2% Cu
- typical tonnage - unknown
- examples - Que River footwall PMZ, Red Hills (Tas.), Voyager 24, Elliott Bay (Tas.)

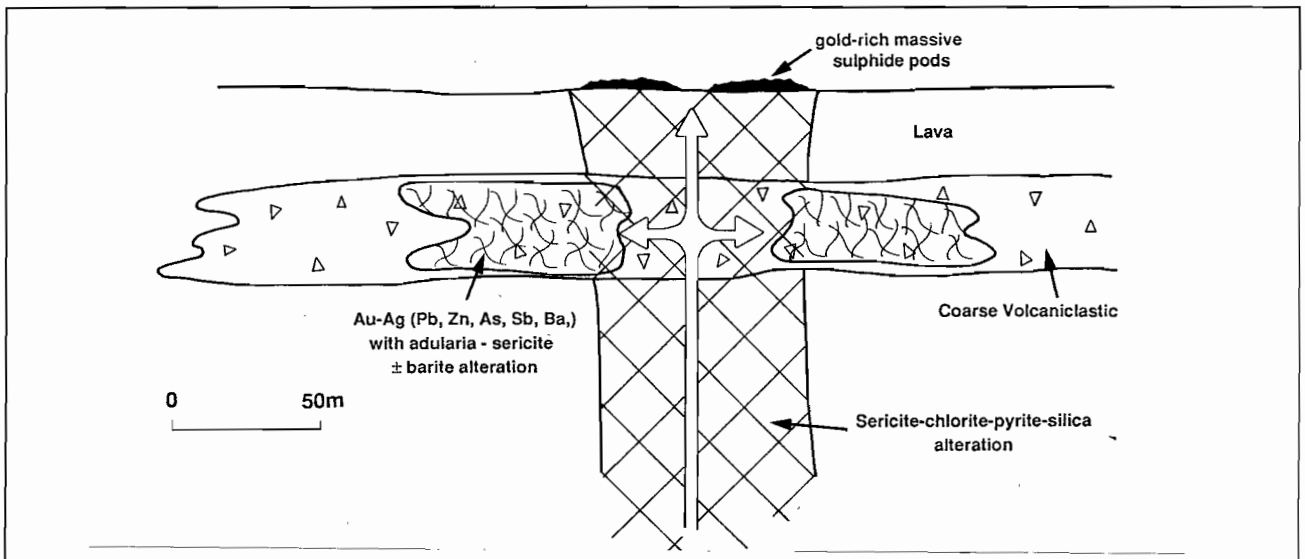

GEOPHYSICAL PARAMETERS

- non magnetic
- low conductivity

GEOCHEMICAL PARAMETERS

- zoning laterally away from pipe Fe, Cu → Zn, Pb → Au, As, Sb, Ba
- higher Au/Pb+Zn ratio than VMS
- good Au ~ Zn and Au ~ Ba correlations
- anomalous As and Sb, lacking Cu and Bi

ENVIRONMENT

- same environment as Model 1, with one important difference:
- coarse porous volcaniclastic horizon in footwall volcanics provides a permeable zone for the lateral subsurface flow of hydrothermal solutions away from the central feeder zone
- submarine equivalent of an epithermal system

ORE FLUID CONDITIONS

- hydrothermal fluids move outward from main footwall pipe along permeable volcaniclastic horizon
- cooling and mixing with seawater creates a unique fluid composition
  - low T: 150-200°C
  - neutral-alkaline pH (adularia stable)
  - moderate to high fO_2 (barite stable)
  - low Fe content of sphalerite (high fS_2)
  - $Au(HS)_2$ transport

CAUSE OF GOLD DEPOSITION

- mixing with seawater
- increasing SO_4/H_2S
- possibility of boiling (not confirmed)

References: McGoldrick & Large (1986), McGoldrick & Large (1987), Jenkins (this volume)

Figure 11 MODEL 4: large tonnage disseminate and stockwork replacement Cu-Au deposit

TARGET

- moderate priority
- typical grades - 1-2% Cu, 0.2-1 g/t Au
- typical tonnage 1-100 mt
- example - Prince Lyell orebody (Tas.)

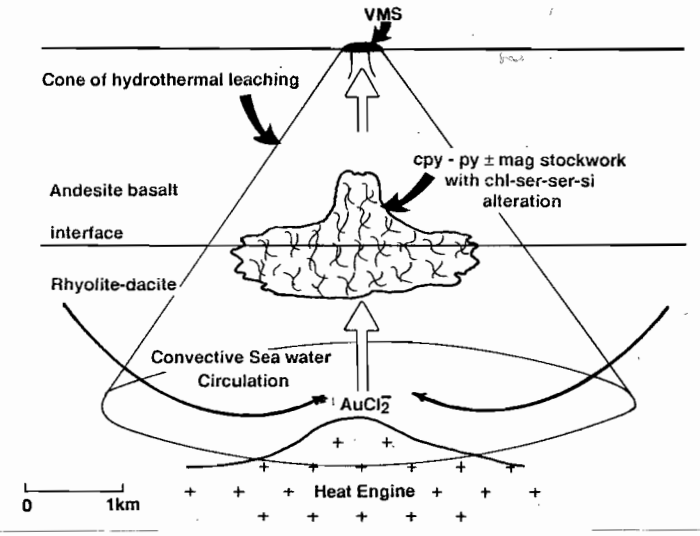

GEOPHYSICAL PARAMETERS

- weakly magnetic
- moderate conductivity
- high chargeability

GEOCHEMICAL PARAMETERS

- no distict zoning
- very low Pb and Zn, low zinc ratios (<50), i.e. Pb > Zn
- low As, Sb
- anomalous Mo, Bi, Co

ENVIRONMENT

- calc-alkaline volcanic pile in rift setting
- subaerial or submarine volcanics
- deep within volcanic pile within 1 to 3 km of granitic heat engine
- located preferentially at the contact between footwall felsic volcanics and hangingwall mafic volcanics
- cross cutting replacement or stratabound nature

ORE FLUID CONDITIONS

- deep circulating fluids in lower portion of hydrothermal cone transport gold as $AuCl_2$
- high temperature >300°C
- low pH 2-5
- buffered by footwall rhyolites to low pH, high fO_2 (pyrite stable ± magnetite)

CAUSE OF GOLD DEPOSITION

- interaction of rhylolite buffered fluid with andesite-basalt volcanics causes increase in pH, aH_2S and decrease in fO_2
- deposition of gold occurs if saturation of $AuCl_2$ is reached (due to increasing pH and decreasing fO_2) before switchover to the soluble $Au(HS)_2$ species

References: Walshe & Solomon (1981), Large (1987)

Figure 12

MODEL 5: Magnetite-hematite-pyrite ± copper ± gold vein system

TARGET

- low priority
- typical grades - 0.1-2% Cu, 0.5-2 g/t Au
- examples - Jukes Pty, Lake Selina (Tas.)

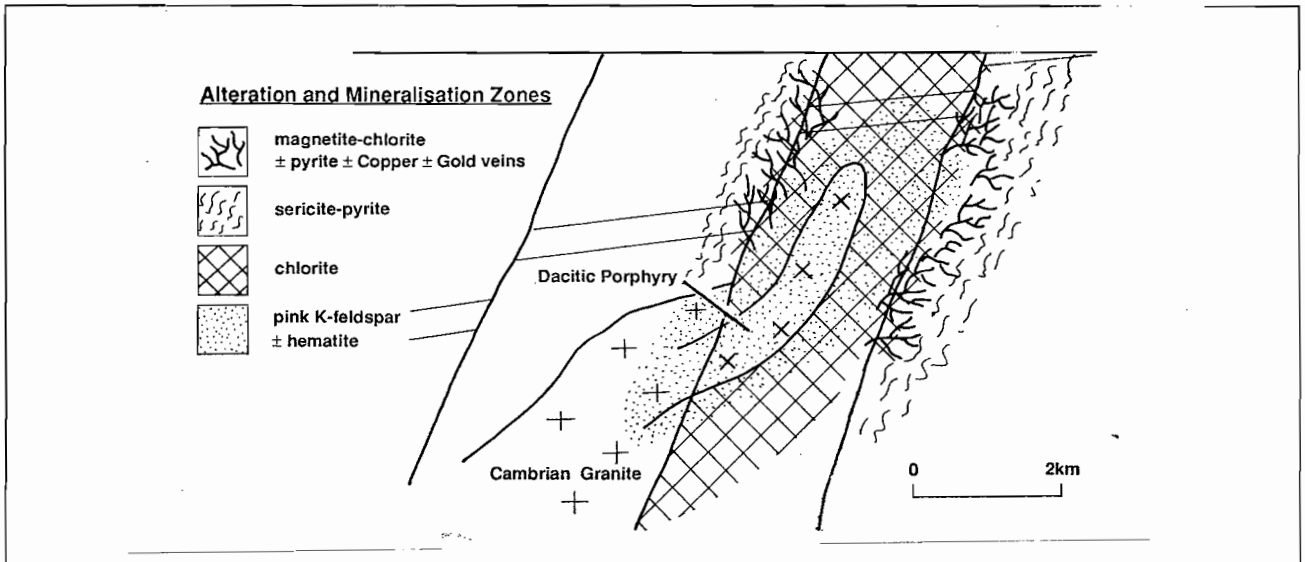

GEOPHYSICAL PARAMETERS

- strong magnetic anomaly
- commonly coincident IP and magnetics

GEOCHEMICAL PARAMETERS

- lateral and vertical zoning of alteration assemblages K feldspar-hematite → chlorite → sericite
- good Au-Cu correlation (when Au is present)
- very low Pb & Zn
- anomalous Mo, deficient As
- variable zinc ratio from 10 to 100, unlike the VMS pattern

ENVIRONMENT

- related to late-stage granite intrusion and granitic porphyries, co-magmatic with the volcanic host rocks
- located within both the CVC and Tyndall Group along the eastern margin of the MRV
- subvolcanic replacement origin with alteration zonation surrounding the granite and related granitic porphyries. Series of overprinting alteration zones from K feldspar → chlorite → sericite + pyrite. Magnetite ± cpy ± Au mineralisation extends from the chlorite zone through to the sericite-pyrite zone

ORE FLUID CONDITIONS

- high temperature (magmatic ± seawater) fluids - probably >400°C
- high fO_2 indicated by extensive hematite and later magnetite
- gold transport as $AuCl_2$ complex

CAUSES OF GOLD DEPOSITION

- dropping temperature
- dropping fO_2

References: Eastoe *et al.* (1987), Hunns (1986, 1987)

hydrothermal fluids. Background gold values of 0.5-1.5 ppb are sufficient for the source of the gold in the deposits. However, an anomalous supply of gold in the Early Cambrian Crimson Creek tholeiitic basalts may have been a contributing factor (Stolz & Large, this volume).

3) The chemistry of the hydrothermal fluid was buffered by the volcanics to allow the critical conditions of high transport of gold with the base metals (see Huston, this volume for details).

4) The long lived hydrothermal systems of moderate temperature (200-300°C near the seafloor) provided the conditions for zone refining of the sulphide deposits with gold concentrated in the outer layers of the sulphide mound.

Hydrothermal Alteration Associated with Gold-VMS Ores

The gold-rich VMS deposits exhibit normal footwall alteration patterns of silicification, sericitisation and chloritisation. The lateral extent of the alteration system appears to vary proportionally with the porosity of the footwall volcanics. The best geochemical indicator of footwall alteration is Na_2O depletion (see fig. 13).

Carbonate alteration is common around most of the Tasmanian VMS deposits, and may be an indicator for a gold-rich system. Huston (this volume) argues that carbonate alteration is indicative of higher fluid pH and therefore an effective high gold transport system (as $Au(HS)_2$ is more soluble in neutral to alkaline fluids). Low temperature K-feldspar (adularia?) alteration is present in the gold enriched footwall systems described in Exploration Model 3 (fig. 10). This type of alteration has also been recognised by Green (1986) at Hercules and may be more common than previously suspected.

Deformation and Recrystallisation: An Important Metallurgical Consideration

The grainsize of gold and electrum within VMS deposits parlty relates to the method of deposition of the gold (see Huston & Khin Zaw, this volume) but also to the degree of later deformation and recrystallisation of the sulphide minerals. In moderately deformed ores which have suffered sulphide annealing, such as Rosebery and Que River, most of the gold has been coarsened-up to allow metallurgical liberation. However, in the weakly deformed arsenic-rich ores at Hellyer the gold is too fine grained to achieve good recoveries (McArthur, 1986). Studies by the C.S.I.R.O. at Que River indicate that the coarse gold occurs with the softer annealed sulphides (galena ,sphalerite and tetrahedrite) while relatively fine gold is confined to undeformed pyrite grains. Khin Zaw (this volume) shows that metasomatic alteration at the southern end of Rosebery has resulted in very coarse grained gold within pyrrhotite-rich ores.

DEVONIAN GOLD MINERALISATION IN THE MRV

Significant gold mineralisation of probable Devonian age occurs along the Henty Fault Zone (fig. 7). Based on geochemical and textural evidence, Gordon (1986) defined two styles of gold mineralisation in the Sterling Valley area:

1) Pyrite-sphalerite-pyrrhotite veins with low arsenic content (<100 ppm As). Other minor elements are Cu-Bi-Pb. Gangue minerals are quartz, chlorite and carbonate.

2) Pyrrhotite-arsenopyrite-chalcopyrite-stannite veins with a high arsenic content (100 ppm to 10% As). Other minor elements are Pb-Zn, and the dominant gangue minerals are quartz, sericite, chlorite and tourmaline.

Gordon considered that Type 1 veins were pre-deformation and possibly Cambrian whilst Type 2 veins were definitely post-deformation and Devonian granite related.

In the 1988 March Quarterly Report on the Henty Prospect by Little River Goldfields, four styles of mineralisation are reported:

1) Massive pyrite; Au-As-Ag-Bi
2) Silica-carbonate veins; Au-Ag-Bi
3) Base metal zones; Au-Pb-Zn
4) Copper zones; Au-Cu.

These occur within a narrow mineralised zone adjacent to, and on the eastern side of, the Henty Fault within a sequence of quartz-feldspar phyric volcaniclastics belonging to the Tyndall Group. The high As and Bi values are indicative of Devonian mineralisation. Zinc ratio values (Huston & Large, 1987) calculated from data given by Reid & Meares (1981, fig. 11) indicate values of 11 and 33 which are totally unlike Cambrian massive sulphides but could be either Cambrian or Devonian vein systems. Lead isotope data on lead-rich samples reported by Gulson & Porritt (1985, Table 5) indicate a Cambrian age for these lead samples (fig. 14). Insufficient data are available to draw any conclusions, although a model which involves the over-printing of original Cambrian mineralisation within the base of the Tyndall Group, adjacent to the Henty rift fault, by later Devonian mineralisation introduced during granitic intrusion, remains a possibility. A third phase of mineralisation during the Early Ordovician or Middle Devonian thrust events should not be excluded.

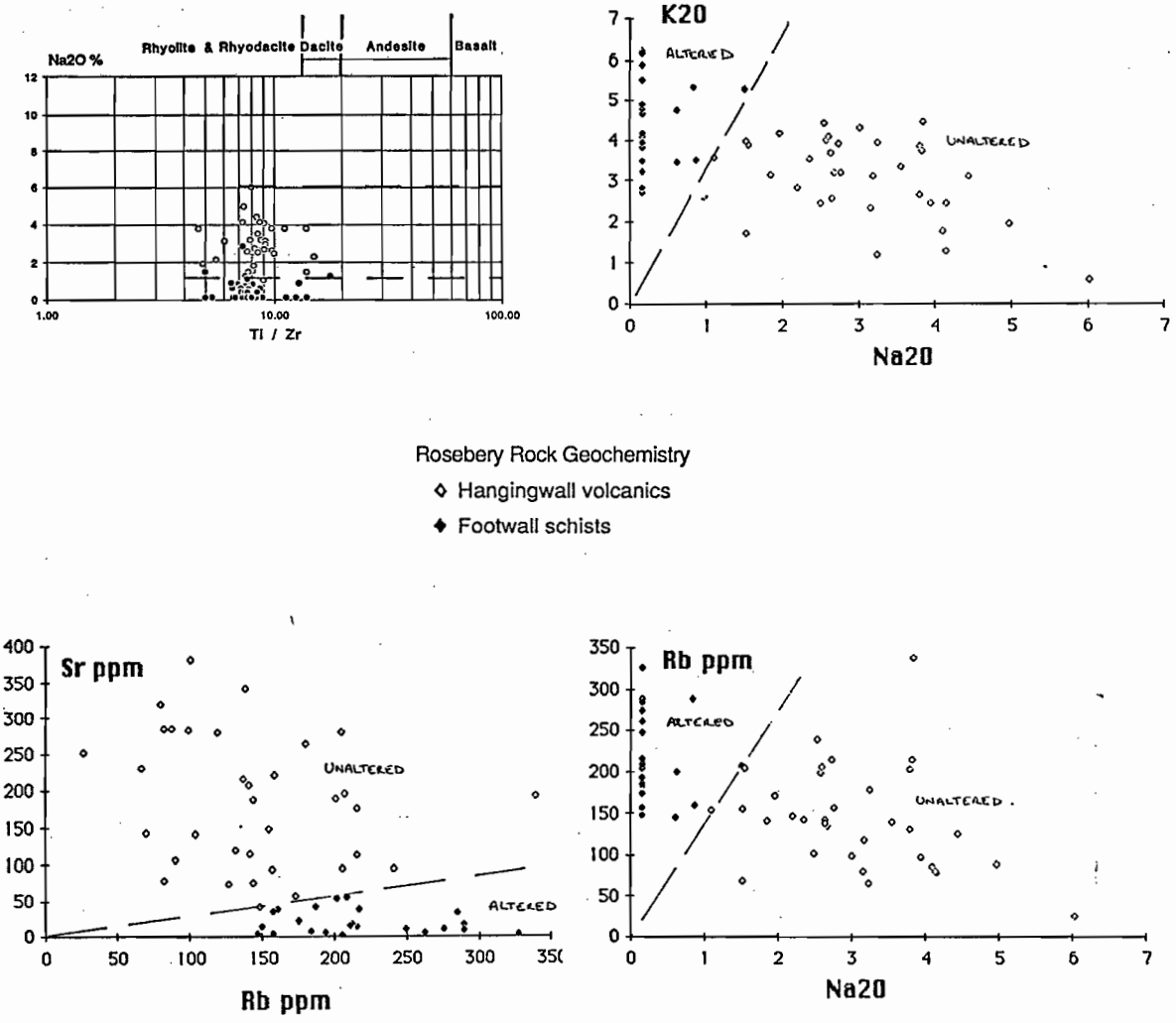

Figure 13 Series of plots which allow the discrimination of footwall altered volcanics from hangingwall volcanics at Rosebery (data from Naschwitz, 1985). Note that the altered rocks are depleted in Na_2O and Sr, and enriched in K_2O and Rb (see also Large et al., 1986).

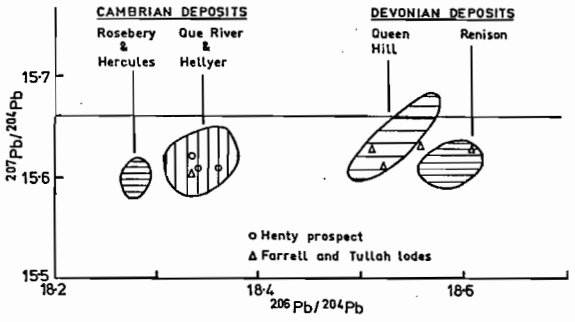

Figure 14: Pb isotope data on lead-rich samples from the Henty Prospect and the Farrel-Tullah lodes compared to other Cambrian VMS and Devonian tin deposits.

WHY THE LOW GOLD CONTENT OF ARCHEAN VMS DEPOSITS?

The Archean VMS deposits in Canada and Western Australia generally contain low gold grades averaging around 0.7 ppm (Pemberton, 1987). It is unlikely that these lower grades are related to a lack of gold in the source rock greenstone belts, as these same greenstones have given rise to major Archean lode gold deposits. The low gold grades are attributed to the chemical conditions prevailing at the site of deposition (Large *et al.*, this volume). The Archean oceans were more reduced than Proterozoic and Paleozoic oceans with a much lower SO_4/H_2S ratio. Consequently, the gold-bearing hydrothermal solution did not become sufficiently oxidised to reach the critical gold solubility cliff (see fig. 15) as they moved onto the seafloor. The gold refining process that was crucial to the development of high grades in the Paleozoic deposits did not take place in the Archean with the result that the deposits

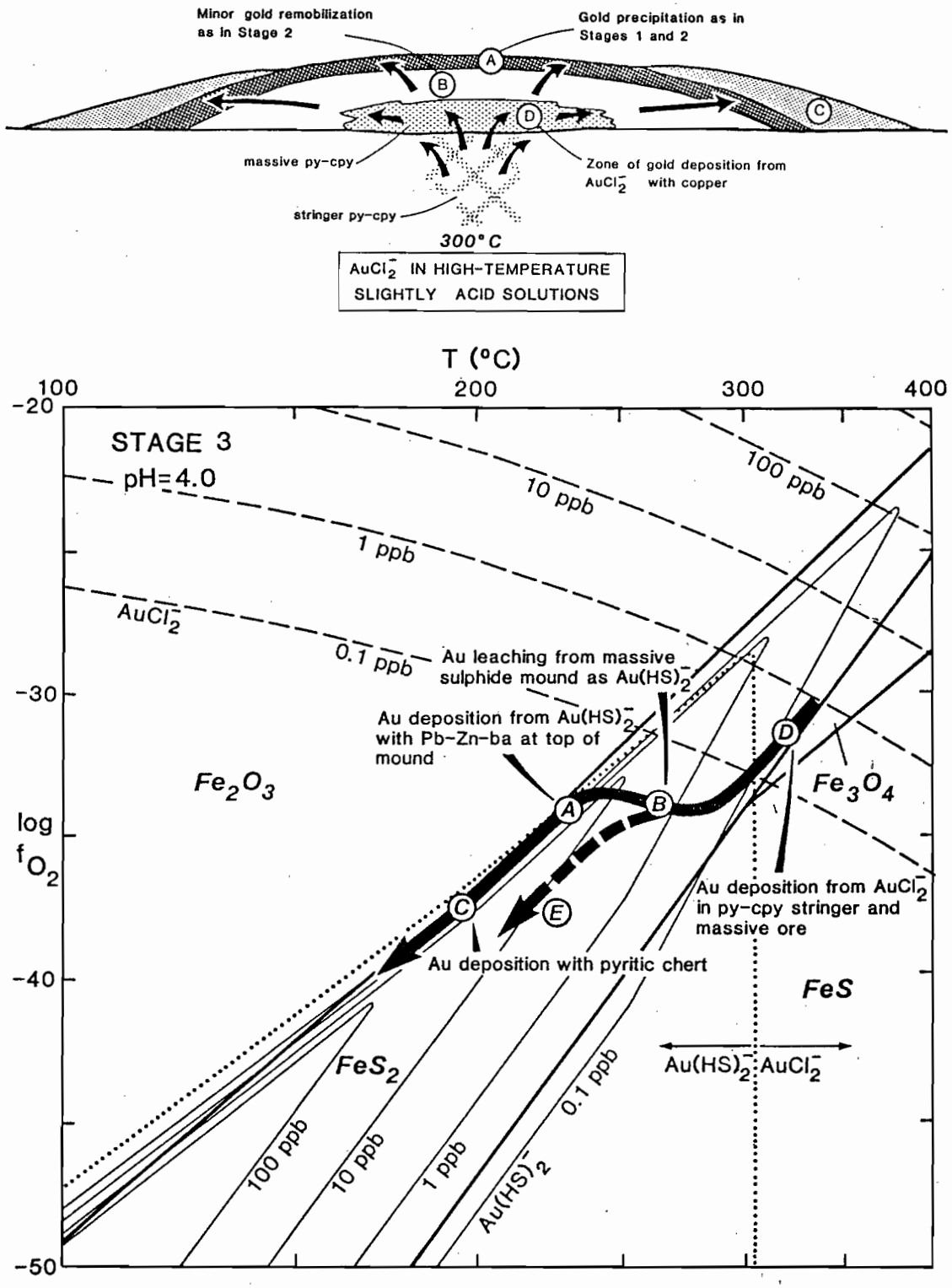

Figure 15 Thermodynamic-geologic model to explain zone refining and gold enrichment at the top of massive sulphide deposits (from Huston & Large, 1987). Note that Archean fluids follow the path BE as they move through the sulphide mound leading to minimal gold enrichment.

remained low grade (<1 ppm Au) and excess soluble gold was lost from the deposit to be precipitated in distal pyritic chert horizons (exhalites).

The massive ore at Scuddles averages 1.2 ppm Au (Ruxton, 1987) and is above the Archean average. However, the gold is concentrated in the central zinc-copper ore and shows no preferential enrichment toward the top of the deposit. Within the massive ore there is a good correlation between gold and copper but no correlation between gold and zinc (Ruxton, 1987, fig. 6). These observations confirm that gold-zinc refining was not a significant process during the formation of the Scuddles VMS deposit.

REFERENCES

Berry, R.F., in press. The history of movement on the Henty Fault Zone, Western Tasmania: an analysis of fault striations: *Aust. J. Earth Sci.* (1988).

Cathles, L.M., Guber, A.L., Lenagh, T.C. and Dudas, F.O., 1983. Kuroko-type massive sulphide deposits of Japan: products of an aborted island arc rift. Econ. Geol. Mon. 5, p. 96-114.

Corbett, K.D., and McNeil, A.W., 1988. Map 6. Geological compilation map of the Mount Read Volcanics and associated rocks Hellyer to South Darwin Peak. Geol. Surv. Tas. - Dept. of Mines, MRV Project.

Corbett, K.D., and Lees, T.C., 1987. Stratigraphic and structural relationship and evidence for Cambrian deformation at the western margin of the Mt. Read Volcanics, Tasmania. *Aust. J. Earth Sci.*, V.34, No. 1, p.45-68.

Corbett, K.D., 1986. The geological setting of mineralisation in the Mt. Read Volcanics: *in* Large, R.R. (ed.). The Mount Read and Associated Ore Deposits: A Symposium; Geol. Soc. Aust. Tas. Div. Burnie, November 1986, p. 1-10.

Crawford, A.J., 1986. Chemistry of volcanic rocks in the Mt. Read Arc: *in* Controls on gold and silver grades in volcanogenic sulphide deposits (84/P210): University of Tasmania unpubl. progress report to AMIRA, April 1986, p. 29-35.

Crawford, A.J., 1987. Geochemistry of the Mount Read Volcanics: internal correlations and tectonic implications: *in* Controls on gold and silver grades in volcanogenic sulphide deposits (84/P210): Univeristy of Tasmania. Unpubl. progress report to AMIRA, August 1987, p. 79-108.

Eastoe, C.J., Solomon, M., and Walshe, J.L., 1987. District-scale alteration associated with massive sulfide deposits in the Mount Read Volcanics, Western Tasmania: *Econ. Geol.*, V.82, p.1239-1258.

Gordon, I., 1986. Sterling Valley project: in Controls on gold and silver grades in volcanogenic sulphide deposits (84/P210): University of Tasmania. Unpubl. progress report to AMIRA, November 1986, p. 29-37.

Green, G.R., Solomon, M., and Walshe, J.L., 1981. The formation of the volcanic-hosted massive sulfide ore deposit at Rosebery, Tasmania: *Econ. Geol.*, V.76, p. 304-338.

Green, G.R., 1986. Stable isotope and alteration investigations of the Mount Read Volcanics, *in* Large, R.R. (ed.) The Mount Read and Associated Ore Deposits: A Symposium; Geol. Soc. Aust. Tas. Div. Burnie, November 1986, p. 39-42.

Gulson, B.L., Large, R.R. and Porritt, P.M., 1987. Base metal exploration in the Mount Read Volcanics, Western Tasmania: Pt. III. Application of lead isotopes at Elliott Bay. *Econ. Geol.*, V.82, p. 308-327.

Hunns, S., 1986. Lake Selina Prospect: in Controls on gold and silver grades in volcanogenic sulphide deposits (84/P210): Univeristy of Tasmania. Unpubl. progress report to AMIRA, November 1986, p. 29-37.

Hunns, S., 1987. Mineralisation in the Tyndall Group - the Lake Selina prospect: in Controls on gold and silver grades in volcanogenic sulphide deposits (84/P210): Univeristy of Tasmania. Unpubl. progress report to AMIRA, August 1987, p. 70-78.

Huston, D.L. and Large, R.R., 1986. The distribution, mineralogy and geochemistry of precious metals in the North-end orebody, Rosebery Mine, Tasmania: University of Tasmania Unpubl. report to E.Z. Co., April 1986, 132p.

Huston, D.L., and Large, R.R., 1987. A chemical model for the concentration of gold in volcanogenic massive sulphide deposits: University of Tasmania report to AMIRA, July 1987, 36p (to be published in Ore Geology Reviews).

Large, R.R., 1987. Source and movement of gold in submarine volcanic environments - A discussion paper: *in* Controls on gold and silver grades in volcanogenic sulphide deposits (84/P210): University of Tasmania. Unpubl. progress report to AMIRA, August 1987, p. 169-181.

Large, R.R., and Both, R.A., 1980. The volcanogenic sulfide ores at Mount Chalmers, Eastern Queensland. Econ. Geol., V.75, p. 992-1009.

Large, R.R., Hermann, W., and Corbett, K.D., 1987. Base metal exploration in the Mount Read Volcanics, Western Tasmania: Pt. I, Geology and exploration, Elliott Bay: Econ. Geol. V.82, p. 267-290.

Large, R.R., and McGoldrick, P.M., 1986. Structure and metal distribution in the PQ-P north lens system, Que River Mine: *in* Controls on gold and silver grades in volcanogenic sulphide deposits (84/P210): Univeristy of Tasmania. Unpubl. progress report to AMIRA, April 1986, p. 3-17.

Leaman, D.E., 1986a. Regional structural interpretation of gravity-magnetic data in Western Tasmania: *in* Large, R.R. (ed.) The Mount Read and Associated Ore Deposits: A Symposium; Geol. Soc. Aust. Tas. Div. Burnie November 1986, p. 61-64.

Leaman, D.E., 1986b. Gravity-magnetic signatures of mineralisation in the Mount Read Volcanics: *in* Large, R.R. (ed.) The Mount Read and Associated Ore Deposits: A Symposium; Geol. Soc. Aust. Tas. Div. Burnie November 1986, p. 65-66.

Leaman, D.E., 1988. Late Precambian and Early Palaeozoic basin evolution of Western Tasmania: in Turner (ed.), The geology and evolution of the latest Precambrian to Cambrian rocks in the Western Tasmanian Terrane: Abstr. Volume, Geol. Soc. Aust. Tas. Div., April 1986, p. 19-22.

Lees, T.C., 1987. Geology and mineralisation of the Rosebery-Hercules area, Tasmania: Unpubl. M.Sc. Thesis, University of Tasmania.

Little River Goldfields, 1988. Quarterly report to the Stock Exchange, March 1988.

McArthur, G.J., 1986. The Hellyer massive sulphide deposit: in Large, R.R. (ed.) The Mount Read and Associated Ore Deposits: A Symposium, Geol. Soc. Aust. Tas. Div. Burnie November 1986, p. 11-20.

McGoldrick, P.J., and Large, R.R., 1986. Preliminary report on the footwall precious metal zone, Que River, in controls on gold and silver grades in volcanogenic sulphide deposits (84/P210): Univeristy of Tasmania. Unpubl. progress report to AMIRA, November 1986, p. 7-16.

McGoldrick, P.J., and Large, R.R., 1987. Final report on the footwall precious metal zone, Que River, *in* Controls on gold and silver grades in volcanogenic sulphide deposits (84/P210): Univeristy of Tasmania. Unpubl. progress report to AMIRA, August 1987, p. 9-45.

Pemberton, John, 1987. World VMS Data Base Part 2: The Canadian Precambrian deposits (with emphasis on precious metal distribution): University of Tasmania report to AMIRA, August 1987, 58p.

Polya, D.A., Solomon, M., Eastoe, C.J., and Walshe, J.L., 1986. The Murchison Gorge, Tasmania - A possible cross section through a Cambrian massive sulfide system: *Econ. Geol.*, V.81, p. 1341-1355.

Reid, K.O., and Meares, R.M.D., 1981. Exploration for volcanic-hosted sulfide deposits in Western Tasmania: *Econ. Geol.*, V.76, p. 350-364.

Ruxton, P.A., 1986a. Golden Grove and Teutonic Bore, Western Australia: *in* Controls on gold and silver grades in volcanogenic sulphide deposits (84/P210): Univeristy of Tasmania. Unpubl. progress report to AMIRA, November 1986, p. 46-83.

Ruxton, P.A., 1986b. World VMS Data Base Part 1: The Kuroko deposits: University of Tasmania report to AMIRA, November 1986, 27p.

Ruxton, P.A., 1987. Gold-base metal relationships at Scuddles, W.A., *in* Controls on gold and silver grades in volcanogenic sulphide deposits (84/P210): University of Tasmania. Unpubl. progress report to AMIRA, August 1987, p. 131-149.

Turner, N.J. (ed.), 1988. The geology and evolution of the latest Cambrian to Cambrian rocks in the Western Tasmanian Terrane (abstr. volume) Symposium, Geol. Soc. Aust. Tas. Div., April 1988, 31p.

Walshe, J.L., and Solomon, M., 1981. An investigation into the environment of formation of the volcanic-hosted Mt. Lyell copper deposits using geology, mineralogy, stable isotopes and a six-component chlorite solid solution model: Econ. Geol., V.76, p. 246-284.

Zaw, K., 1987. F lens metal zonation , Rosebery: *in* Controls on gold and silver grades in volcanogenic sulphide deposits (84/P210): Univeristy of Tasmania. Unpubl. progress report to AMIRA, August 1987, p. 46-69.

DIRECTIONS FOR FUTURE RESEARCH INTO ORE DEPOSITS AND EXPLORATION

Ross R. Large

Following the recent policy statement by the Federal Government concerning higher education in Australia it is apparent that there will be major changes in research funding and research priorities within universities. The Geology Department is one of the most active research departments in this University, and geological research will be placed high on the University's overall research profile. In order to attract continued research funding from the Government and maintain a steady growth of geological research we will be seeking to gain Special Research Centre status in the field of Ore Deposits and Mineral Exploration. We consider that we have a very good case, because of our location (mining is critical to the economic future of Tasmania), proven reputation, excellent equipment facilities and strong ties with industry. It is my opinion that the Australian mining and exploration industry would be well served with three major Ore Deposit Centres of Research, located at the University of Tasmania, University of Western Australia and James Cook University.

Types of Research Projects

Under the umbrella of an Ore Deposit Research Centre at the University of Tasmania I would like to see the following types of research projects.

1) AMIRA funded research involving a group of sponsors on applied problems relevant to the mining and exploration industry.
2) Contract research to individual sponsors on topics specific to that company with results remaining confidential for an agreed period.
3) Collaborative research with other organizations such as the Tasmanian Department of Mines, the C.S.I.R.O. or the B.M.R. (plus AMIRA or Tasuni Research) in areas where a range of expertise or equipment is required to tackle the problem.
4) Basic research to be funded by the Australian Research Council and the University in fields where industry may not wish to contribute, but which could have a longer term benefit in understanding geological processes related to ore deposit environments.

Workshops and Refresher Courses

It is also planned that the Ore Deposit Research Centre would run regular workshops and refresher courses for professional geologists. At least two courses would be run each year on advanced theory and techniques relating to new developments in ore genesis studies, regional geological studies, and their application to exploration. Examples that could currently be run by the Ore Deposit Research Team are;

1) Exploration models and case studies for ore deposits of western Tasmania (3 days).

2) Application of isotopes to ore genesis and mineral exploration (2 days).

3) Application of techniques in structural geology to mapping and mineral exploration (2 days).

4) Massive sulphide deposits - environment, form, mineralogy, textures, genesis and important exploration criteria (3-4 days).

5) Fluid inclusion studies in ore genesis and their potential for exploration (2 days).

6) Characteristics of, and exploration models for, Proterozoic copper-gold deposits (3 days).

7) Primary and alteration geochemistry of volcanic rocks and their relationship to tectonic environments and mineralisation (4 days).

Some courses will have a limit of fifteen participants because of limited equipment in the Geology Department (especially microscopes). Major sponsors would be able to send geologists to these courses for a nominal charge (accommodation and meals only) whereas non sponsors will pay a full tuition charge. Interstate or overseas specialists will be brought in for specific workshops when required. Some of the workshops may be organised in conjunction with the A.M.F. when interstate meetings are required.

Postgraduate Courses: An M.Sc. course in Ore Deposit Studies would be offered to our on-going graduates, recent interstate and overseas graduates, and company geologists who wish to gain a higher qualification. This would be a combined course-work and research M.Sc. Research will be for 18 months (full time or external studies) on a particular ore deposit or mineralised region. Course-work would involve attending at least four Ore Deposit Research workshops in a two year period with completion of related assignments for each workshop.

Proposed Research Projects for 1989 and Beyond

Currently the Geology Department is seeking the opinion of industry on funding the following research projects.

Project 1: Relationship of faulting to mineralisation in western Tasmania (Principal investigators: Dr. Ron Berry and Dr. Ross Large) - budget $70,000 per year for three years.

Project 2: Geochemical finger-printing of gold - a new exploration tool (Principal investigators: Dr. Soey Sie (C.S.I.R.O.), Dr. Ross Large and Dr. Ramsay Ford).

Project 3: Ore deposits and volcanic processes in the Mt. Windsor Volcanics, Qld (Principal investigators: Dr. Ross Large, Dr. Joe Stolz, Dr. Tony Crawford).

Project 4: Petrology and geochemistry of ultramafic complexes and their significance for PGE exploration (Principal investigators: Professor David Green, Dr. Chris Ballhaus, Dr. Tony Crawford).

It is hoped that one or some of these projects will be funded by AMIRA while the others will be funded by contracts to individual companies or through Tasuni Research (the University research company).

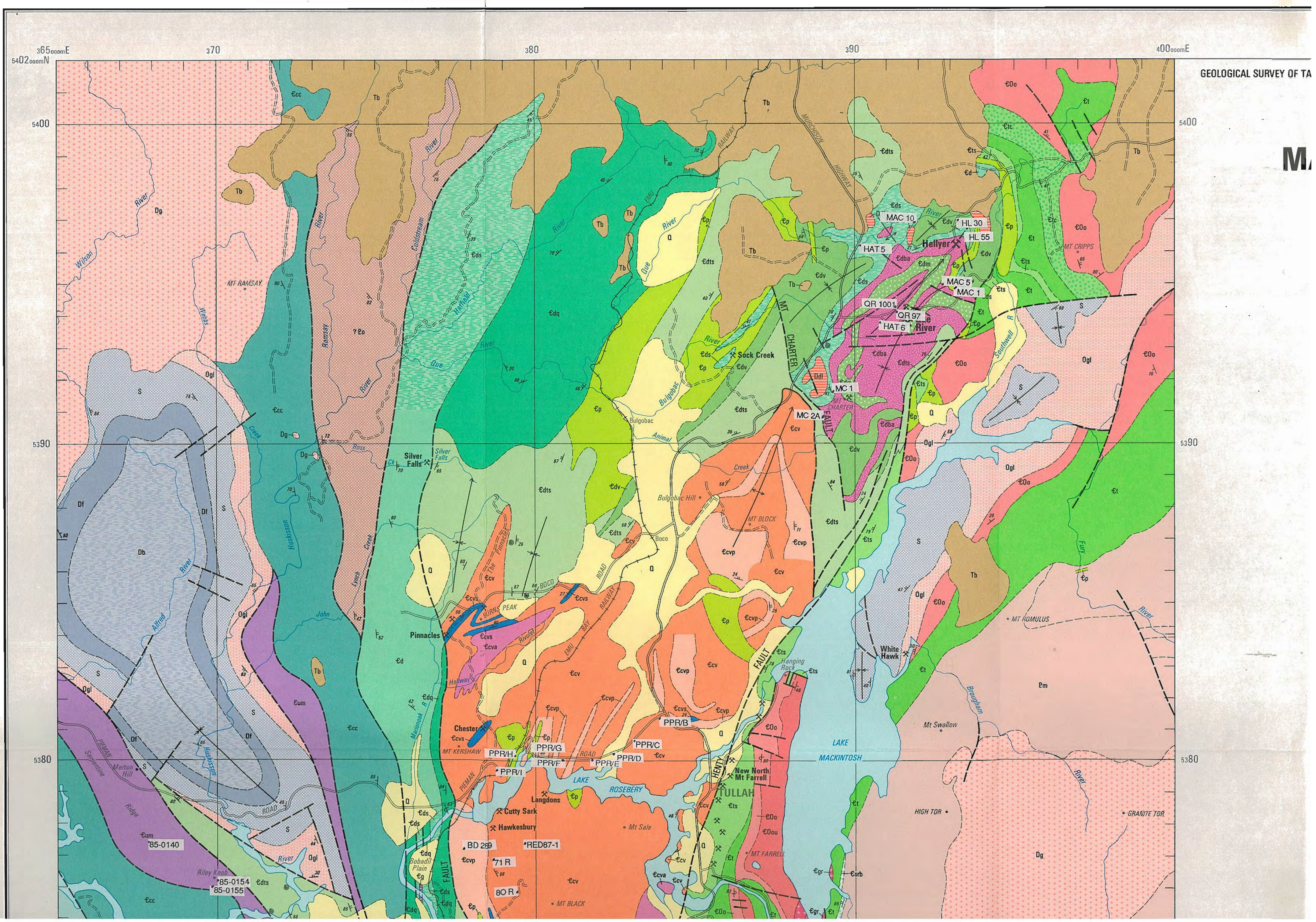

GEOLOGICAL SURVEY OF TA
MT RAMSAY
Silver Falls
Pinnacles
BIRNS PEAK
MT KERSHAW
Chester
Langdons
Cutty Sark
Hawkesbury
LAKE ROSEBERY
LAKE MACKINTOSH
MT BLOCK
Bulgobac Hill
Sock Creek
Hellyer
MT CRIPPS
MT ROMULUS
White Hawk
Mt Swallow
HIGH TOR
GRANITE TOR
Mt Sale
MT BLACK
MT FARRELL
New North Mt Farrell
Riley Knob
Merton Hill
Hanging Rock
MT CHARTER FAULT
HENTY FAULT
MURCHISON HIGHWAY
EMU BAY RAILWAY

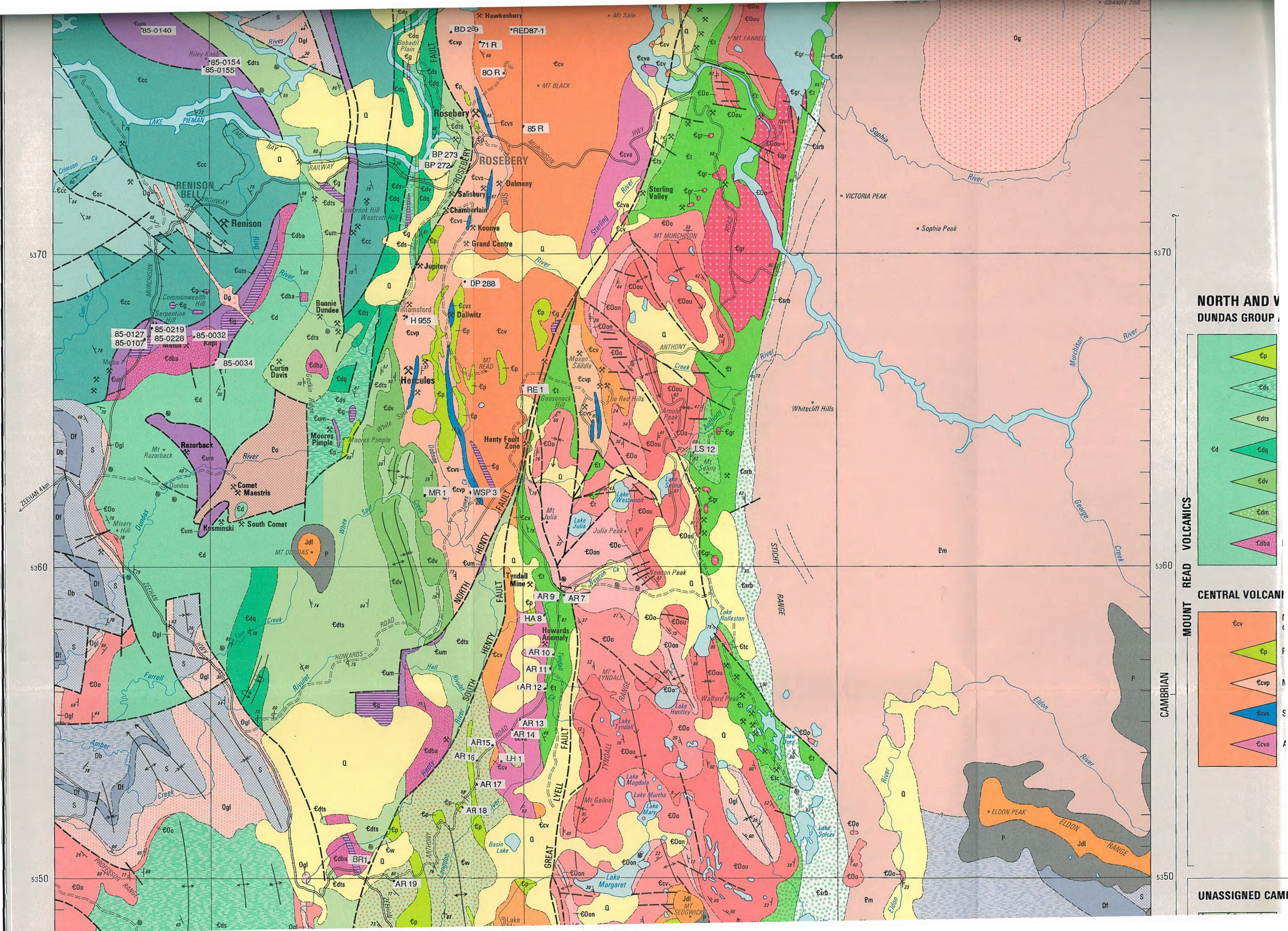
Hawkesbury
Mt Sale
BD 289
RED87-1
71 R
80 R
MT BLACK
MT FARRELL
85-0140
Riley Knob
85-0154
85-0155
Bobadil Plain
FAULT
LAKE PIEMAN
River
Rosebery
85 R
MURCHISON
HWY
BP 273
BP 272
ROSEBERY
Dalmeny
Salisbury
Chamberlain
Koonya
Grand Centre
Jupiter
Colebrook Hill
Westcott Hill
RENISON BELL
HIGHWAY
Renison
RAILWAY
Crimson Ck
Sterling Valley
Sterling River
MT MURCHISON
ROAD
VICTORIA PEAK
Sophia Peak
Sophia River
GRANITE TOR
5370
DP 288
Commonwealth Hill
Serpentine Hill
Bonnie Dundee
Williamsford
H 955
Dallwitz
85-0127
85-0107
85-0219
85-0228
85-0032
Kapi
Melba
85-0034
Curtin Davis
Hercules
MT READ
RE 1
Gooseneck Hill
Moxon Saddle
The Red Hills
ANTHONY
Creek
Arnold Peak
Whitecliff Hills
Murchison River
Razorback
Mt Razorback
Dundas
Comet Maestris
Moores Pimple
White Spur
Henty Fault Zone
LS 12
Mt Selina
Lake Selina
Misery Hill
Kosminski
South Comet
MR 1
WSP 3
Lake Westwood
Mt Julia
Lake Julia
Julia Peak
MT DUNDAS
STICHT
RANGE
George Creek
ZEEHAN 4 km
5360
NORTH
HENTY
FAULT
Tyndall Mine
AR 9
AR 7
HA 8
Howards Anomaly
AR 10
AR 11
AR 12
Newton Ck
Newton Peak
Lake Rolleston
HOWARDS ROAD
Hall Rivulet
Farrell
SOUTH
MT TYNDALL
Walford Peak
Lake Huntley
Lake Tyndall
Eldon River
AR 13
AR 14
AR 15
AR 16
LH 1
AR 17
AR 18
Lake Dora
Amber Creek
Henty River
TYNDALL RANGE
Lake Magdala
Lake Martha
Lake Mary
Mt Geikie
GREAT
LYELL
FAULT
Lake Spicer
ELDON PEAK
ELDON RANGE
Basin Lake
BR1
AR 19
ANTHONY
Lake Margaret
MT SEDGWICK
Eldon River
5350
PROFESSOR RANGE
CAMBRIAN
MOUNT READ VOLCANICS
NORTH AND W
DUNDAS GROUP
CENTRAL VOLCANI
UNASSIGNED CAMI

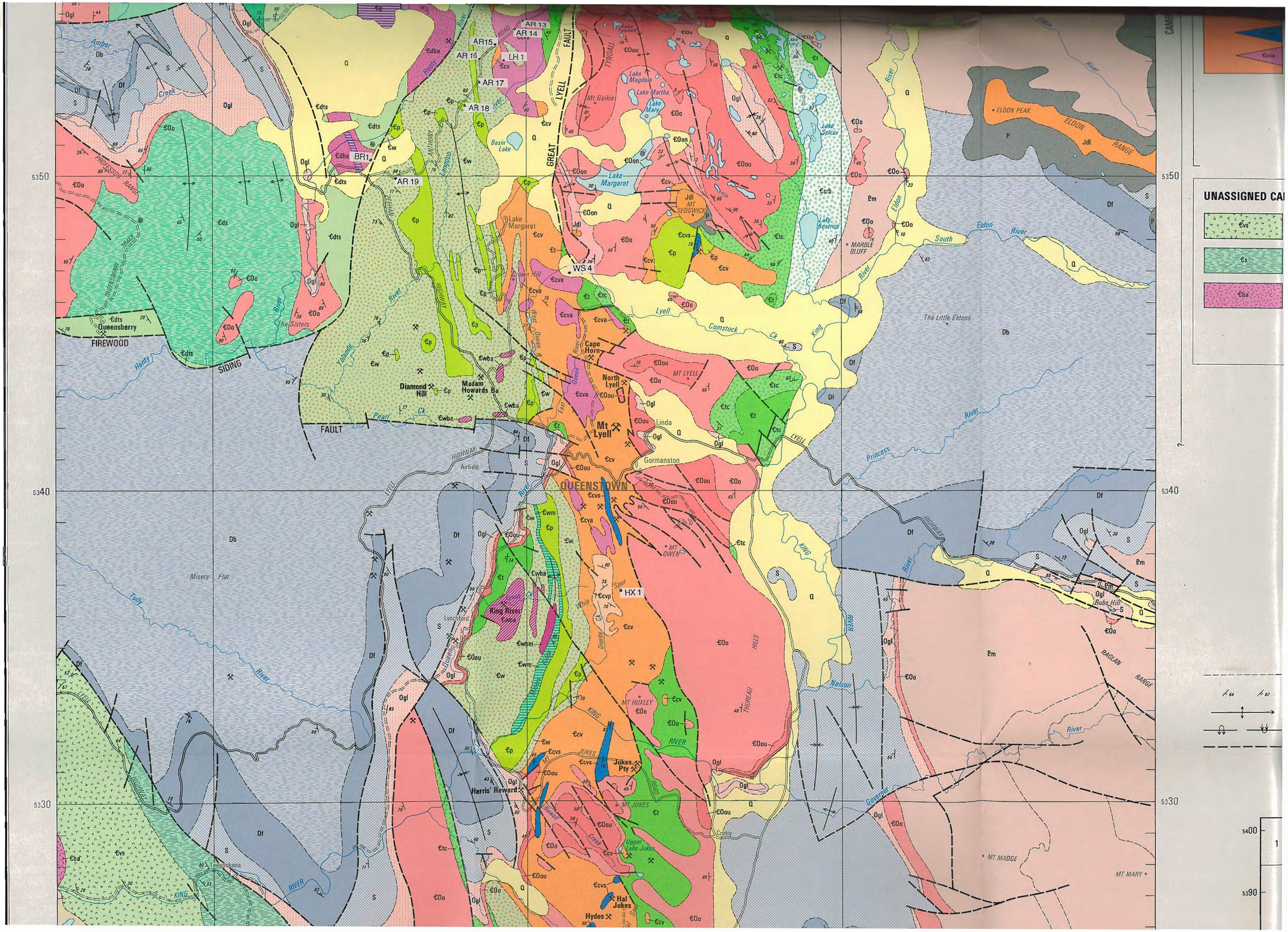
UNASSIGNED CA
QUEENSTOWN
Mt Lyell
North Lyell
Cape Horn
Gormanston
Linda
MT LYELL
MT OWEN
MT SEDGWICK
MT GEIKIE
MT HUXLEY
MT JUKES
Upper Lake Jukes
Hal Jukes
Hydes
Jukes Pty
Harris' Reward
King River
Lynchford
Crotty
Diamond Hill
Madam Howards Ba
Queensberry
FIREWOOD
SIDING
FAULT
GREAT LYELL FAULT
Lake Margaret
Lake Magdala
Lake Martha
Lake Mary
Lake Spicer
Lake Beatrice
Basin Lake
MARBLE BLUFF
ELDON PEAK
ELDON RANGE
The Little Eldons
MT MADGE
MT MARY
RAGLAN RANGE
THUREAU HILLS
Bubs Hill
Misery Flat
Airfield
HIGHWAY
PROFESSOR RANGE
QUEENSBERRY TRACK
The Sisters
King River
Lyell
Comstock Ck
Eldon River
South Eldon River
Princess River
Nelson River
Governor River
Tully River
Henty River
Yolande River
Queen River
Pearl Ck
Whip Spur
Newall Creek
Amber Creek
AR 13
AR 14
AR15
AR 16
AR 17
AR 18
AR 19
LH 1
BR1
WS 4
HX 1
5350
5340
5330
5400
5390

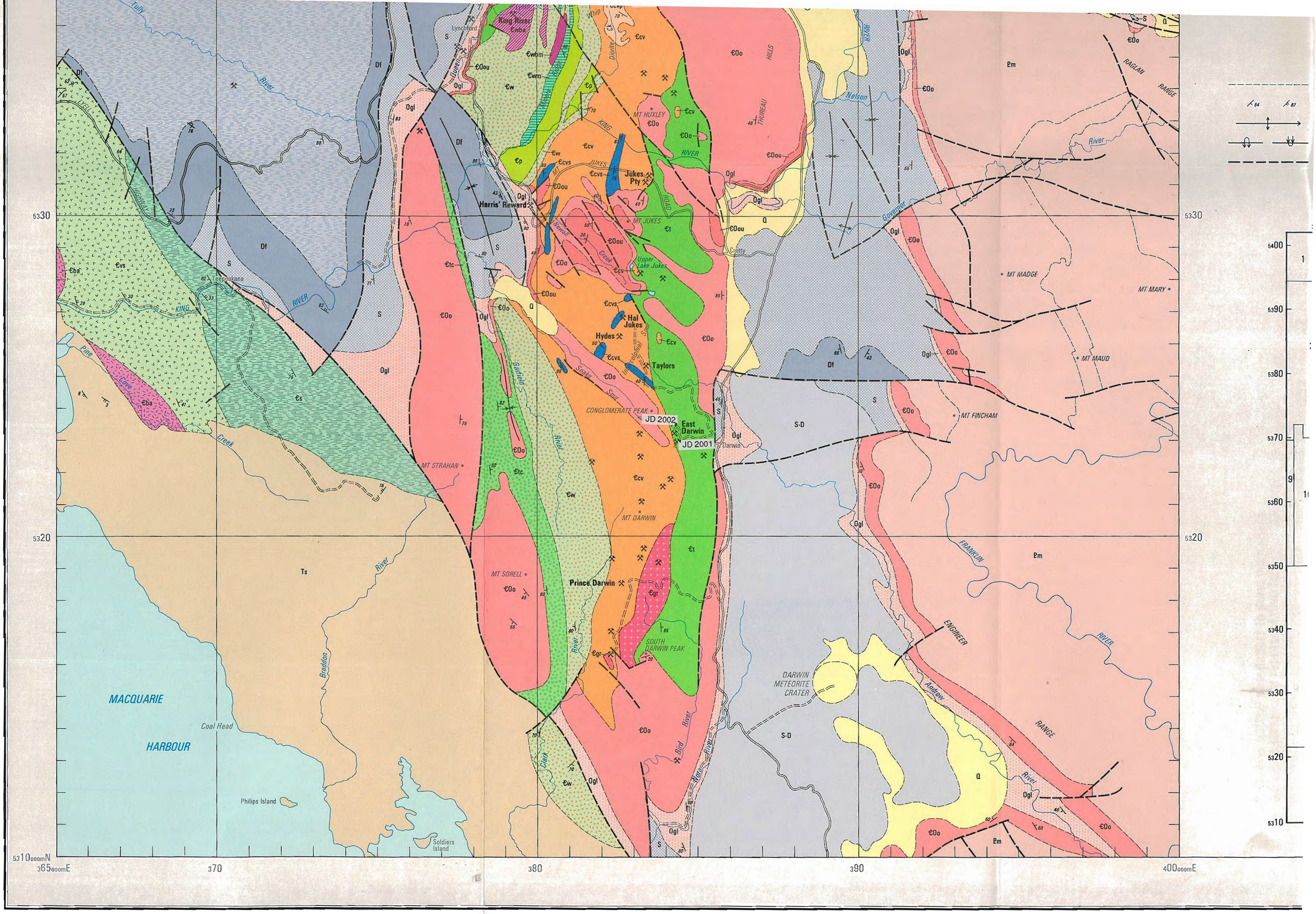

King River
Lynchford
Harris' Reward
MT HUXLEY
THUREAU HILLS
Nelson
Governor
RAGLAN RANGE
MT JUKES
Jukes Pty
Upper Lake Jukes
Hal Jukes
Hydes
Taylors
Teepookana
KING RIVER
LYELL
MT STRAHAN
CONGLOMERATE PEAK
JD 2002
JD 2001
East Darwin
Darwin
MT MADGE
MT MARY
MT MAUD
MT FINCHAM
MT DARWIN
MT SORELL
Prince Darwin
SOUTH DARWIN PEAK
Garfield River
FRANKLIN RIVER
ENGINEER
DARWIN METEORITE CRATER
Andrew River
RANGE
MACQUARIE HARBOUR
Coal Head
Philips Island
Soldiers Island
Pine Cove
Braddon River
Bird River
Nora River
Clark
Tully River
Snake Spur
Creek
5330
5320
5310000mN
365000mE
370
380
390
400000mE
5400
5390
5380
5370
5360
5350
5340
5330
5320
5310